observers in a blinded fashion from 3-slice SA (segments 1–16) and from LA (segment 17, apical tip) images. Multi-slice SA sets were used as reference standard. Transmurality of hyper-enhancement (HE) was graded for standardized myocardial segments on a scale from 0 (no HE) to 5 (75–100% HE).

Results: Of 131 segments with myocardial defects on multi-slice DE, selective 3-slice SA in conjunction with LA depicted 125 (sensitivity = 95.4%). The specificity of 3-slice SA + LA to detect affected segments was 99.1%. 3-slice SA + LA graded correctly 93.7% of all segments, and 77.9% of segments with myocardial defects. 98.5% of "viable" (grade 0–3) and 92.3% of "non-viable" (grade 4) defects were correctly identified. Fig. 1 shows a set of conventional multi-slice SA images (upper 3 rows) of a 46 year old male with chronic inferior STEMI and the corresponding selective 3-slice SA + LA set (lower row; from left to right: basal SA, mid-cavity SA, apical SA, vertical LA view).

Conclusions: In patients with STEMI, selective 3-slice SA in conjunction with LA DE imaging identifies viable and non-viable myocardial segments as defined by conventional multi-slice DE imaging with high accuracy. Selective 3-slice SA + LA DE imaging is a reliable approach to simplify and standardize segmental viability reporting in this group of patients.

457. Acute Infarct Size Assessed by Contrat-enhanced Cardiac Magnetic Resonance Imaging is Related to Increased Risk of a Reduced Ejection Fraction in Humans After 7 Months

Andre Schmidt, MD, PhD,[1] Clerio Azevedo, MD,[1] Caterina Silva, MD,[1] Bernhard Gerber, MD,[1] Sandeep Gupta, PhD,[2] David A. Bluemke, MD, PhD,[2] Thomas Foo, PhD,[2] Joao A. C Lima, MD,[1] Katherine C. Wu, MD.[1] [1]*Cardiology, Johns Hopkins University, Baltimore, MD, USA,* [2]*Radiology, Johns Hopkins University, Baltimore, MD, USA.*

Introduction: Left ventricular (LV) systolic dysfunction is a poor prognostic marker following acute myocardial infarction. The presence of chronic dysfunction post-infarct is likely to be related to the extent of myocardial necrosis. Because contrast-enhanced MRI (ceMRI) accurately quantifies infarct size and the extent of non-viable myocardium, its use in the acute phase peri-infarct can potentially identify those patients who will have chronically reduced ejection fractions (EF).

Purpose: We sought to evaluate the role of acute IS by ceMRI as a marker of chronically reduced LV systolic function.

Methods: 45 patients underwent ceMRI 3.3 ± 2.7 days after first reperfused MI and 7 months later. IS extent was measured after a 0.2 mmol/kg bolus injection of Gadodiamide on delayed enhancement images using an inversion recovery fast gradient echo pulse sequence. Infarct size (IS) was measured using custom software (CINE Tool, GE). IS mass (expressed as percentage of total LV mass) was correlated with EF obtained by Simpson's method on SSFP MR images. Patients were divided into two groups according to the extent of IS in the acute phase (Group I $\leq$ 20%-14 pts; Group II $\geq$ 20%-31 pts). Linear regression, unpaired t-tests and Fisher's exact test were used to compare the extent of interactions between EF and IS.

Results: EF at 7 months correlated significantly with acute IS ($r = 0.59$; $p < 0.0001$). EF after 7 months was significantly higher ($p = 0.0004$) in group I (55 ± 8%) compared to group II (44 ± 9%). If acute IS was equal to or greater than 20% after an acute MI, the relative risk of having an EF below 40% 7 months later was 5.4.

Conclusions: Infarct size equal to or greater than 20% of the total LV mass as assessed by ceMRI in the acute phase of a first myocardial infarction is highly associated with a significant risk of LV dysfunction after 7 months.

	EF < 40%	**EF > 40%**	Totals
DE $\geq$ 20%	12	19	31
DE < 20%	1	13	14
Totals	13	32	45

458. Magnetic Resonance Angiography and Gadolinium-Enhanced Magnetic Resonance Imaging Offer a Noninvasive "One Stop" Assessment in Patients with Kawasaki Disease

Sophie Mavrogeni,[1] Giorgos Papadopoulos,[2] Marouso Douskou,[3] Savas Kaklis,[2] Alexios Giakoumelos,[3] George Varlamis,[4] John Seimenis,[5] Polixeni Nikolaidou,[2] Chryssa Bakoula,[2] Evangelos Karanasios,[2] Dennis V. Cokkinos.[1] [1]*Onassis Cardiac Surgery Center, Athens, Greece,* [2]*Aghia Sophia Childrens' Hospital, Athens, Greece,* [3]*Bioiatriki MRI Unit, Athens, Greece,* [4]*AHEPA Hospital, Thessaloniki, Greece,* [5]*Philips Hellas Medical Systems, Athens, Greece.*

Introduction: Coronary artery abnormalities in Kawasaki disease (KD) develop in about 15–25% of young patients, mostly in the form of aneurysms. Although the incidence of pediatric disease is low (2–3%), the mortality rate due to myocardial infarction is 22%. Magnetic resonance angiography (MRA) can reliably identify coronary aneurysms in affected patients. Gadolinium-enhanced MRI (Gd-enMRI) is the gold standard for scar detection due to myocardial infarction.

Purpose: The purpose of this study was: 1) to measure the dimensions of coronary artery aneurysms using magnetic resonance coronary angiography (MRA) and 2) to correlate the dimensions of coronary artery aneurysms measured by MRA with the presence of myocardial infarction measured by Gd-enMRI in a pediatric population.

Methods: Ten patients, aged 1–12 yrs., were studied. The maximal diameter and length of the aneurysm was recorded.

Coronary MRA was performed using a 1.5 T Philips Intera CV MR scanner with two ECG-triggered pulse sequences. The first was a three-dimensional segmented k-space gradient-echo sequence (TE = 2.1 ms, TR = 7.5 ms, flip angle = 30°, eff. slice thickness = 1.5 mm) employing a T2-weighted preparation prepulse and a frequency selective fat-saturation prepulse. Data acquisition was performed in mid-diastole. All scans were carried out with the patient free breathing using a 2D real time navigator beam. Gd-enMRI images were acquired 15 minutes after the IV injection of 0.2 mmol/kg Gd-DTPA using an inversion recovery gradient echo pulse sequence.

Results: In 6 patients discrete aneurysms (AN) of the coronary arteries were identified, while difuse coronary ectasia (EC) alone was present in the remaining 4 patients. Aneurysm diameter ranged from 2 to 9 mm (5.7 ± 2.8), aneurysm length ranged from 4.4 to 16 mm (10.1 ± 5.0), and ectasia length ranged from 2.5 to 4.6 mm (3.8 ± 0.6). Transmural apical scar, due to myocardial infarction, was detected by Gd-enMRI only in one case, while small patchy necrosis was identified in another case. No correlation between aneurysm diameter or ectasia length and myocardial infarction was found.

Conclusions: In conclusion, MRA and Gd-enMRI is a reliable diagnostic tool in Kawasaki disease able to perform noninvasive coronary artery evaluation and infarct size detection in a single study. MRA and Gd-enMRI may prove of great value for the serial follow-up of these patients.

459. Discrepancies in Estimating the Transmural Extent of Myocardial Infarction on Delayed Enhancement Cardiac Magnetic Resonance Imaging

Li-Yueh Hsu, ScD, Peter Kellman, PhD, W. Patricia Ingkanisorn, MD, Anthony H. Aletras, PhD, Andrew E. Arai, MD. *National Institutes of Health, Bethesda, MD, USA.*

Introduction: Recent publications suggest dobutamine CMR more accurately predicts recovery of function after coronary artery revascularization than delayed enhancement imaging (Wellnhofer et al., 2004) but the field has not defined standards in quantifying the extent of myocardial infarction (MI).

Purpose: We studied the degree to which visual assessment of the transmural extent of infarction, a commonly used clinical method, and manual traces of MI agreed with a quantitative computerized method previously validated by triphenyltetrazolium (TTC).

Methods: In 20 patients with known MI, inversion recovery delayed enhancement imaging was performed ∼ 20 minutes after 0.2 mmol/kg gadolinium administration. Transmural extent of infarction was graded visually by consensus of 3 cardiologists. Infarct size was reported using the clinical grading scale for transmural extent of infarction (grade 0 = 0%, grade 1 = 1–25%, grade 2 = 26–50%, grade 3 = 51–75%, and grade 4 = 76–100%). Infarct size was measured by manual planimetry and with a computer program that was previously validated against TTC in 11 dogs (Hsu et al., 2004).

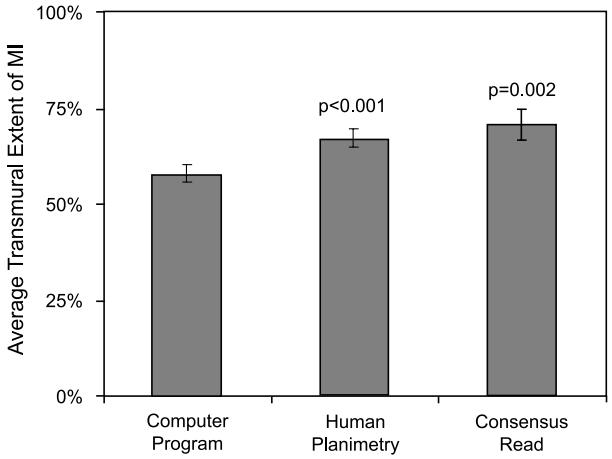

Figure 1.

Results: Both the consensus clinical reading and the manual planimetry significantly overestimated MI size compared with the computer program ($p = 0.002$ and $p < 0.001$ respectively) (Figure 1). Infarct size averaged 16% of the left ventricle (LV) and manual planimetry overestimated the number of infarcted pixels by 4% of the LV (equivalent to 24% of the MI area). The transmural extent of infarction determined by manual planimetry agreed with the computer program in 60% of infarcted segments but overestimated MI by one or more grades in 35% of infarcted segments (Figure 2). The errors in manual planimetry of transmural extent of infarction were 2.6 times larger than the errors in circumferential extent of infarction.

Conclusions: Despite accurate representation of MI by gadolinium, clinically relevant overestimation of the infarction can occur in visual interpretation and in manual planimetry, particularly with respect to the transmural extent of MI. Objective methodologies can improve the accuracy of determining the extent of MI.

N=161	Human 1-25%	Human 26-50%	Human 51-75%	Human >75%
Computer 1-25%	**45**	18	5	0
Computer 26-50%	4	**27**	21	3
Computer 51-75%	0	2	**12**	10
Computer 75-100%	0	0	2	**12**

Figure 2.

REFERENCES

Hsu, L., et al. (2004). *7th SCMR Scientific Sessions, Spain*.
Wellnhofer, E., et al. (2004). *Circulation* 109:2172–2174.

460. MR Perfusion Imaging in Conjunction with a Blood-Pool Contrast Agent Clearly Delineates Infarcted Myocardium

Jian Wang, MD,[1] Bo Xiang, DDS,[1] Hongyu Liu, MD, PhD,[2] Gang Li, MD, PhD,[2] Roxanne Deslauriers, PhD,[1] Ganghong Tian, MD, PhD.[1] [1]*Biosystems, Institute for Biodiagnostics, NRC, Winnipeg, MB, Canada,* [2]*Cardiac Surgery, Harbin Medical University, Harbin, China.*

Introduction: Myocardial infarction is associated with decrease in regional blood flow, which can be readily assessed with MR perfusion imaging. As such, we believe that infarct myocardium can be detected with MR perfusion imaging.

Purpose: The present study was designed to determine whether T_2*-weighted MR imaging in combination with P792 (a gadolinium-based blood-pool contrast agent) helps assess myocardial infarction.

Materials and Methods: Myocardial infarction was induced in 5 pig hearts with a 90-minute occlusion of the left anterior descending coronary artery (LAD) followed by 30-minute reperfusion. The hearts were then removed from animals and perfused in a Langendorff apparatus. Sixty milliliters of P792 (1.9 mM) was injected as a bolus into the aortic perfusion line. Its first pass through the heart was followed using T_2*-weighted imaging. Subsequently contrast-induced T_1 changes of the myocardium were measured for 30 minutes using a TurboFLASH inversion-recovery sequence with 9 different inversion delays. At the end of experiment, 10×10^6 colored microspheres (15 ± 1.9 μm diameter) were injected into the perfusion line. The hearts were then cut into 5-mm thick slices and stained with 2% triphenyltetrazolium chloride (TTC).

Results: T_1 relaxation times of normal myocardium (1115 ± 275 ms) measured at the 30th minute after contrast injection were not significantly different from those of infarct rim (1092 ± 304 ms). Infarct core had a significantly longer T_1 value (1641 ± 242 ms) relative to normal myocardium and infarct rim. As a result, infarct rim could not be differentiated from normal myocardium on P792-enhanced T_1 maps. As expected, the wash-in slope of P792 in the infarct region (6.9 ± 0.9 arbitrary unit) was significantly less than that of normal region (22.0 ± 13.7 a.u.). P792-induced maximum changes in T_2* signal intensity (T_2*-max) during its first pass was significantly smaller in infarct region (49.3 ± 14.0 a.u.) than in normal region (79.0 ± 2.6 a.u.). Thus, infarct myocardium (including both rim and core) was clearly demarcated as a hypo-enhanced region on the maps of the wash-in slope and T_2*-max (Figure 1). Size of infarct myocardium measured on the maps of wash-in slope ($27.7\% \pm 13.8\%$ of the entire heart) and T_2*-max ($27.8\% \pm 14.1\%$) was comparable to that determined on TTC stained section ($27.6\% \pm 13.9\%$) (Table 1). Regional blood flow in infarct rim and infarct core was found to be significantly lower than that in normal myocardium.

Table 1. Infarct size (% entire heart) measured with three different maps and TTC-staining

Size (%)	T_2*-max map	T_2* slope map	T_1 map	TTC-staining
A	7.501	7.804	5.699	7.699
B	19.77	19.80	12.76	19.56
C	34.49	33.56	27.94	33.78
D	34.61	34.77	29.35	34.62
E	42.89	42.60	17.55	42.84

Discussion and Conclusions: Our results indicate that permeability of capillaries to P792 was not significantly higher in infarct region than in normal region during acute myocardial infarction. As such, infarct myocardium could not be differentiated from normal myocardium with P792-enhanced T_1 imaging. On the other hand, because of significant decrease in its blood flow, infarct myocardium was clearly demarcated on the maps of P792 wash-in slope and T_2*-max. We therefore concluded that T_2* imaging in combination with P792 allows reliable assessment of myocardial infarction.

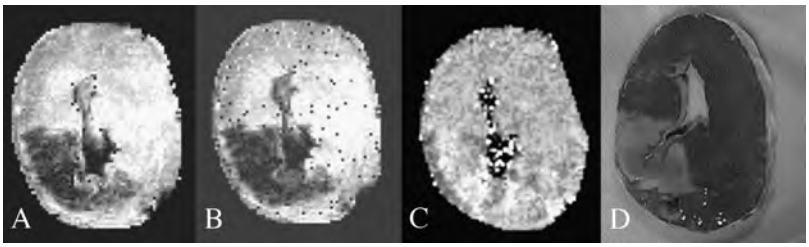

Figure 1. Intraindividual comparison of infarct size determined by T_2* max map (A), T_2* wash-in slope map (B), P792-enhanced T_1 map (C) and TTC-stained section.

461. Transmural Extension of Myocardial Necrosis: Delayed Constrast-Enhanced MRI and Tissue Doppler Imaging Correlations Following Reperfused ST-Elevation Myocardial Infarction

Alessandro Battagliese, MD,[1] Chiara Bucciarelli-Ducci, MD,[1] Maria Bianchi, MD,[1] Leonardo De Luca, MD,[1] Jacopo Carbone, MD,[2] Paola Proietti, MD,[1] Marco Francone, MD,[2] Roberto Passariello, MD,[2] Francesco Fedele, MD.[1] [1]*Cardiovascular and Respiratory Sciences, University of Rome "La Sapienza", Rome, Italy,* [2]*Radiology, University of Rome "La Sapienza", Rome, Italy.*

Background: Accurate identification of regional myocardial dysfunction is pivotal to the identification and management of patients with ischemic heart disease. Contrast-enhanced MRI (ce-MRI) identifies the transmural extent of myocardial necrosis. Tissue Doppler imaging (TDI) quantitatively assess regional myocardial function by measuring systolic strain, an index reflecting the extent of myocardial fiber shortening. Previous studies have compared this parameter with regional velocity gradients obtained by 3-dimentional tagged MRI. Limited data are available on the correlation of the infarct extent by ce-MRI and the corresponding regional systolic function by TDI in patients with acute myocardial infarction.

Methods: Cine and contrast-enhanced MRI (ce-MRI) studies were performed in 9 patients within 10 days of successful percutaneuosly reperfused ST-elevation myocardial infarction. All examinations were conducted on 1.5-T system (Vision, Siemens). A bolus of Gd-DTPA (0.2 mmol/kg) was injected and a multi-slice, breath-hold, segmented inversion-recovery turbo FLASH pulse sequences images were acquired at 15–20 minutes as multiple short-axis views encompassing the entire ventricle from base to apex. Inversion time (TI = 250–350 ms) was progressively optimized to null normal myocardium. Regional myocardial function was performed in the corresponding delayed-hyperenhanced regions, by measuring peak longitudinal systolic myocardial strain by TDI (Vivid 7, GE). The 16-segments model was applied to correlate the areas of delayed hyperenhancement with the corresponding systolic strain values. Delayed hyperenhancement was calculated as percentage of wall thickness.

Results: Seven (78%) of the 9 patients showed hyperenhancement on delayed contrast-enhanced images. Mean ejection fraction in the population was 49 ± 9.3%. Thirty-two segments with delayed hyperenhancement were studied by TDI and mean systolic strain was − 14 ± 6.9%. The extent of delayed hyperenhancement ranged from 45% to 95% of wall thickness. We observed an inverse correlation between systolic strain and the extent of delayed hyperenhancement ($r = -0.73$; $p < 0.05$), as illustrated in Figure 1.

Conclusion: Abnormal values of systolic strain were observed in myocardial segments with delayed hyperenhancement. The inverse correlation between the transmurality of myocardial necrosis and systolic strain suggests the contractile impairment that occur after an acute myocardial

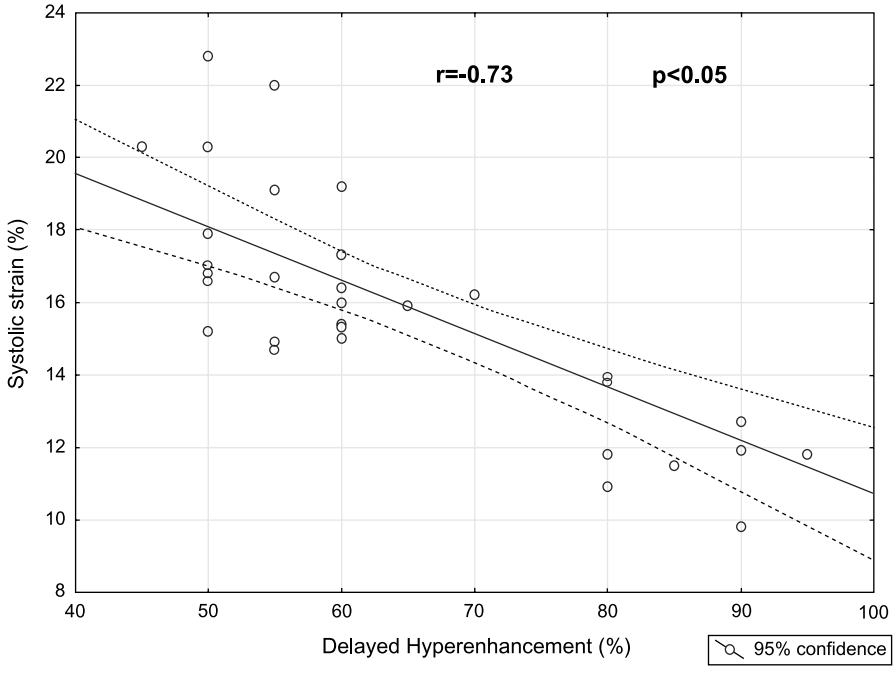

Figure 1.

infarction. We postulate that systolic strain may represent an important predictive index of the extension of myocardial transmural necrosis in patients with successful percutaneuosly reperfused ST-elevation myocardial infarction.

462. The Impact of Total Infarct Volume and Degree of Myocardial Wall Thickness Involvement on Global Left Ventricular Function

Gina R. Shirah, BS,[1] Andrew H. Nelson,[1] Katherine R. Schneider,[1] Mary Zasadil, MD,[2] Timothy F. Christian, MD.[2]
[1]*University of Wisconsin, Madison, WI, USA,* [2]*Medicine, University of Wisconsin, Madison, WI, USA.*

Introduction: Contrast enhanced viability imaging with CMRI has allowed the ability to measure both infarct volume and the percent thickness of the myocardial wall affected. Prior techniques have measured infarct volume and linearly related these measures to global LVEF, but they have been unable to explore the interplay between total infarct volume and infarct transmurality.

Purpose: The aim of this study is to determine 1) whether total infarct volume is significantly linearly associated with LVEF and 2) whether the degree of endocardial penetration provides an equivalent or incremental association with global LV function.

Methods: Patients with prior myocardial infarction (n = 11) were studied. Patients were excluded if there was

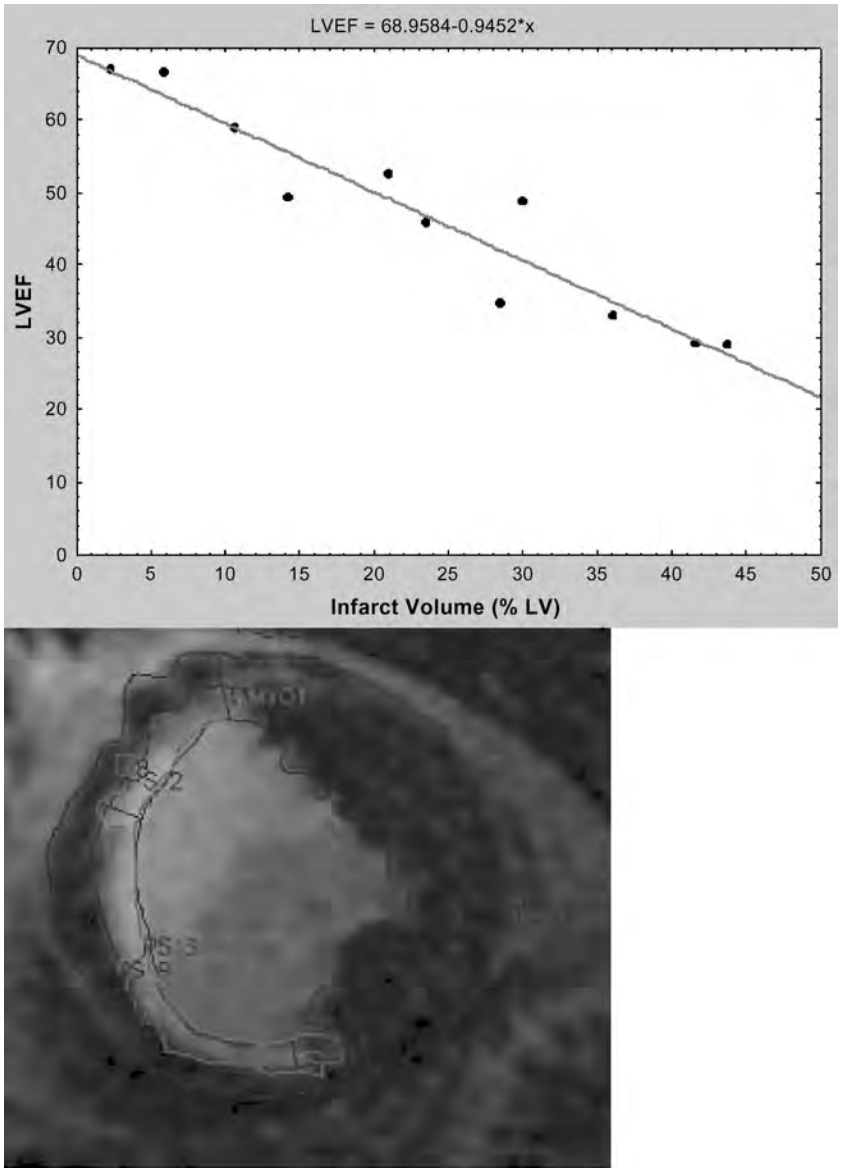

Figure 1.

Table 1.

Grade	0	1	2	3	4
# Segments	329	15	25	30	111

known concurrent nonischemic cardiomyopathy. Patients underwent cardiac MRI examination using one of two 1.5 T magnets (GE Signa, operating with v11.0 software). LV function was determined from ECG gated cine steady-state free precession imaging sequences (20 phases/R–R interval) in the LV short-axis plane (8 mm thick slices). LV volumes were measured offline using a digital planimetry program (Cine, GE Medical systems). LVEF was calculated from the end-systolic and end-diastolic volumes. For patients with recent infarction (< 6 weeks from the CMR exam, $n = 2$) the volumes were measured from a repeat CMR exam 90 days later. Infarct imaging was performed 10 minutes following an IV injection of 0.2 mmol/Kg gadolinium-DTPA. Delayed hyperenhancement imaging was performed of the entire LV in 8 mm short-axis slices using an inversion recovery sequence. Infarct volume was planimetered using "Cine" and expressed as a percentage of the total myocardial volume. Each short-axis slice was sectored into 6 segments and divided into an endocardial and epicardial zone at the 50% thickness mark (see Figure 1). Each segment was graded for wall thickness of hyperenhancement from endocardium to epicardium as 0 = no infarct, 1 < 25%, 2 = 25–50%, 3 = 50–75% and 4 > 75% thickness. An index for the degree of transmurality was calculated for each patient: transmural degree index (TMDI) = segment thickness score/total segments per patient. The deepest penetration of the infarct was also recorded for each patient as was the total number (extent) of segments with any hyperenhancement.

Results: Mean infarct volume was 23 ± 13%LV, range 2.2–43.7%LV. Mean LVEF for the group was 44.8 ± 14.4%. In six patients, at least a portion of the infarct was transmural (grade 4). The number of segments for each thickness grade is shown in Table 1. There was a strong correlation between total infarct volume and LVEF ($r = 0.95$, $p < 0.000$, $R^2 = 0.90$ see Figure 1). The correlation between TMDI and LVEF was also significant but less close: $r = 0.64$, $p < 0.001$. By multiple linear regression analysis, infarct volume remained significantly associated with LVEF when TMDI was added to the model. The latter was not independently associated with LVEF. Neither segment extent or severity was able to add independent information to infarct volume.

*Conclusions:*Total infarct volume is closely linearly associated with LVEF. The transmural extent of hyperenhancement does not appear to add significantly to this relationship. This linear association may allow for the prediction of global LVEF based on infarct volume early in the post-MI period when stunning is more likely to be present but larger studies are required.

463. A New Pulse Sequence of Combined Delayed Enhancement and SENC Function for Imaging Myocardial Viability in a Single Breath Hold

El-Sayed H. Ibrahim, MSc, MSE,[1] Li Pan, MSE,[2] Wesley D. Gilson, PhD,[3] Dara L. Kraitchman, PhD, VMD,[3] Matthias Stuber, PhD,[3] Nael F. Osman, PhD.[3] [1]*Department of Electrical & Computer Eng., Johns Hopkins University, Baltimore, MD, USA,* [2]*Department of Biomedical Eng., Johns Hopkins University, Baltimore, MD, USA,* [3]*Department of Radiology, Johns Hopkins University, Baltimore, MD, USA.*

Introduction: In recent years, there has been great progress in determining myocardial viability using MRI. Regional viability within the affected area or the dysfunctional region is a good predictor of myocardium recovery (Kim et al, 2003). Inversion recovery (IR) MRI is commonly used to acquire contrast enhanced T1-weighted image to mark irreversibly injured regions (Kim et al, 2003). A new technique is presented to provide more information by simultaneously acquiring a combined delayed enhancement and functional images using strain encoding (SENC) MRI (Osman et al, 2001).

Purpose: In the proposed technique, the SENC method is modified to acquire both viability and contractility images of the myocardial tissue at end-systole in a single short breath hold. Therefore, infarcted myocardium and mechanically dysfunctional regions are imaged simultaneously with the same spatial resolution.

Methods: In SENC, the tagging planes are placed parallel to the imaging plane. Upon contraction or stretching of the tissue, tags frequency increases or decreases, respectively, and these changes can be detected by appropriately tuning (modulating) the phase encoding in the tagging direction during imaging. Two images with two tunings, which we refer to as Low Tuning (LT) and High Tuning (HT), are sufficient to get function images of the myocardium (Osman et al, 2001). To get a contrast enhanced image, we propose to acquire a third SENC image with no modulation (No Tuning, NT). When imaging after contrast injection (e.g., delayed contrast), a contrast enhanced T1-weighted image is acquired with NT.

The imaging sequence acquires the three images in a single breath-hold (Figure 1). The 1–1 SPAMM pulse, which creates the tags, is triggered by the QRS complex of the ECG. After a delay until end-systole, three excitation pulses are generated for acquisition with three different tunings. This sequence is repeated until complete acquisition of k-space is achieved. It should be noted that the HT, LT, and NT signal intensities show different patterns of change with time due to relaxation.

A dog with a reperfused myocardial infarction was scanned on a 1.5 T scanner (Philips Gyroscan Intera) using a spiral pulse sequence. The experiment parameters are: Gadolinium (Gd) dose = 0.20 mmol/kg, breath hold duration = 6 seconds, trigger delay = 200 ms, TR = 23 ms, SENC Low Tune = 0.3 mm^{-1}, and SENC High Tune = 0.38 mm^{-1}.

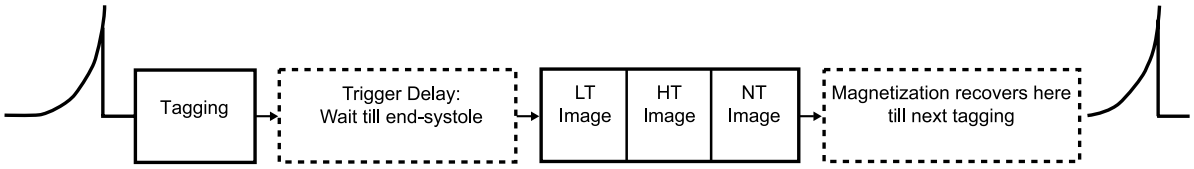

Figure 1. The pulse sequence used.

Results: Figure 2 shows a conventional IR delayed contrast image in (a). NT and HT images are shown in (b) and (c), respectively, while the strain image, calculated from LT and HT (2), is shown in (d). Notice in the HT that the remote region is bright, indicating contraction.

Conclusions: The NT image acquired using the proposed technique shows excellent agreement with the contrast enhanced image acquired using the conventional IR method. Moreover, the information about contractility from the LT and HT images helps better identify regions of the myocardium that may not hyperenhance in the contrast enhancement image, but still do not contract (e.g., stunned or hibernating myocardium). Another advantage of SENC images is that they have good blood/myocardium contrast. So, the 15 minute delay period prior to viability imaging, which is normally needed after Gd injection to get a high image contrast, is not needed in the SENC case.

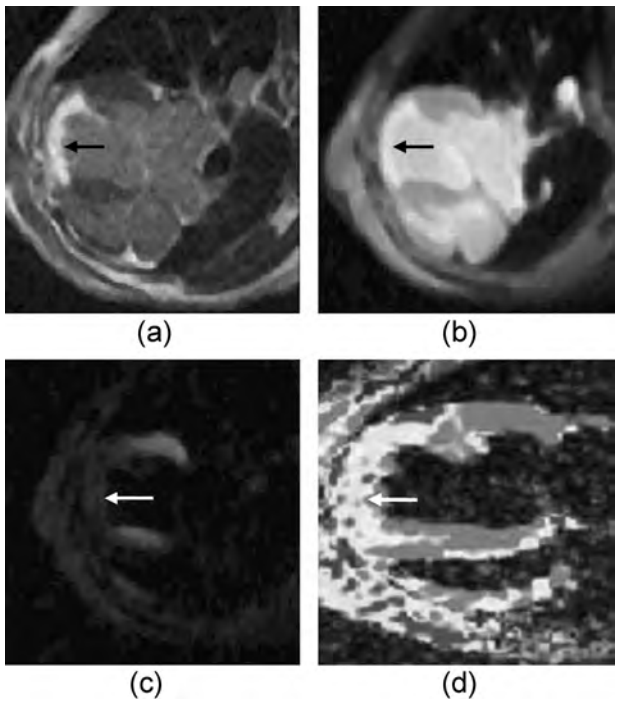

Figure 2. (a) Viability image acquired using inversion recovery method. (b) No tuning (NT) image shows the contrast enhanced information. (c) High tuning (HT) image shows the non-contracting regions. (d) Function image, computed from LT and HT, shows strain (red and blue represent max and min strain, respectively.). The arrows point to the infarct.

ACKNOWLEDGMENTS

This work was supported by grants from the Donald W. Reynolds Foundation, NHLBI R01-HL072704, R01-HL 073223, and K02-HL04193 (DLK).

REFERENCES

Kim, R. J., et al. (2003). How we perform delayed enhancement imaging. *J. Cardiol. Magn. Reson.* 505–514.

Osman, N. F., et al. (2001). Imaging longitudinal cardiac strain on short-axis images using strain-encoded MRI. *Magn. Reson. Med.* 324–334.

464. Phenotyping of Asymptomatic Adults with Hypertrophic Cardiomyopathy By Cardiac Magnetic Resonance Strain Analysis

Matt Riordan, Jina Chung, Marvin Ashford, Shelton Caruthers, Samuel Wickline. *Biomedical Engineering, Washington University in St. Louis, St. Louis, MO, USA.*

Introduction: Left ventricular (LV) hypertrophic cardiomyopathy (HCM) is a heterogeneous multigenic disorder marked by myocardial hypertrophy, myofiber disarray, and myocardial scarring. HCM has been associated with decreased global circumferential strain (CS) and maximum torsion (MT). However, the effect of the presence of intramyocardial scar tissue versus the disease process itself on these indexes is unknown. We propose that more informed clinical phenotyping of disease expression in individual patients will be critical to predict untoward outcomes such as sudden cardiac death.

Purpose: To determine LV global and regional differences in peak CS and MT in HCM patients as compared to healthy controls and determine the effect of the extent and distribution of scarring in HCM patients on peak CS and MT.

Methods:

Subjects: Six adult HCM patients without evidence of heart failure were recruited from an outpatient clinic. Six healthy adults were age-matched controls. The HCM and control groups manifested no differences in age, heart rate, or systolic pressure.

Imaging Protocol: Tagged CMR short-axis images were acquired at apical, mid-ventricular, and basal levels with a 1.5 T scanner. MT and CS were measured in the septal,

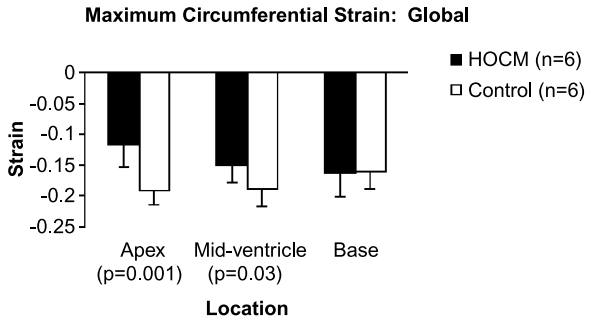

Figure 1.

anterior, lateral, and inferior walls. MT was computed by normalizing twist by apex to mitral valve plane distance.

Data Processing: Spline curves were fit to the tagging grid and the vertices of the grid were triangulated. As a result, the in-plane strains and torsion of each triangular element could be computed at each of 25 phases imaged during the cardiac cycle.

Scar Quantification: The extent and distribution of scarring in the HCM patients was estimated in Gd-hyperenhanced short-axis images. Late hyperenhancement-based imaging was used to quantify scarring by counting pixels above a given intensity threshold. The intensity threshold was established for each scar as the pixel value two standard deviations below the mean intensity of the manually selected hyperenhanced region (Lund et al., 2004).

Results: Peak CS was reduced in HCM subjects at apical ($P = 0.001$) and mid-ventricular ($P = 0.03$) levels (Fig. 1). The controls exhibited greater peak CS in each circumferential region, but only the inferior region ($p < 0.002$) and global average ($p < 0.03$) were significant (supporting previous findings (Ennis et al., 2003), (Palmon et al., 1994)). Fig. 2 illustrates reduced torsion anteriorly in HCM patients, which appears offset by increased torsion inferiorly (both $p < 0.05$). Surprisingly, the average CS *increased* in HCM patients with increasing scar volume as a percent of LV volume ($R^2 = 0.88$). The septal ($R^2 = 0.69$) and anterior ($R^2 = 0.94$) regions also exhibited increased CS with scarring. MT was greater in the HCM patients inferiorly ($p < 0.04$) but less anteriorly ($P = 02$) vs. controls. Overall MT *increased* with increasing scar volume as a percent of LV volume ($R^2 = 0.53$), with the inferior region especially significant ($R^2 = 1.00$).

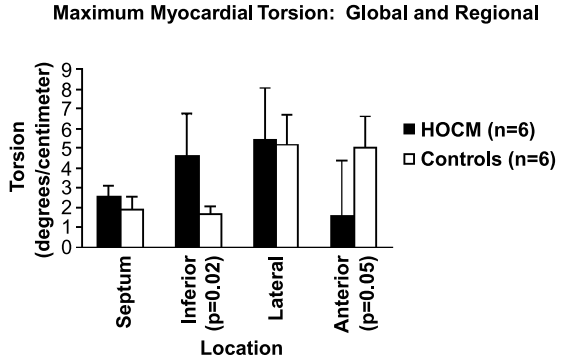

Figure 2.

Conclusions: Quantification of regional and global cardiac dysfunction in HCM with CMR tagging reveals unique patterns of phenotypic expression in silent disease states. Notably, increased LV scarring in HCM patients is associated with a concomitant and paradoxical *increase* in both CS and MT, which is only partly explained by decreasing LV volume. Accordingly, scar tissue extent may not explain the observations of overall decreased mechanical indexes of regional LV function in HCM. We propose that longitudinal assessment of strain and torsion may provide a means to characterize disease progression and to follow therapies designed to preserve cardiac function.

REFERENCES

Ennis, D. B., et al. (2003). Assessment of regional systolic and diastolic dysfunction in familial hypertrophic cardiomyopathy using MR tagging. *Magn. Reson. Med.* 50:638–642.

Lund, G. K., et al. (2004). Acute myocardial infarction: evaluation with first-pass enhancement and delayed enhancement MR imaging compared with ^{201}T1 SPECT imaging. *Radiology* 232:49–57.

Palmon, L. C., et al. (1994). Intramural myocardial shortening in hypertensive left ventricular hypertrophy with normal pump function. *Circulation* 89:122–131.

465. Transmural Distribution of Myocardial Infarction with Delayed Contrast Hyperenhancement: Its Perfusional and Functional Correlates

Alessandro Pingitore, Assuero Giorgetti, MD, Daniele De Marchi, RT, Annette Kusch, RT, Mirko Passera, BSc, Paolo Marzullo, MD, Massimo Lombardi, MD. *Clinical Physiology Institute, CNR, Pisa, Italy.*

Background: magnetic resonance (MR) delayed contrast hyperenhancement is a direct sign of myocardial infarction (MI). This peculiarity combined with the high spatial resolution of MR allows the imaging of the transmural distribution of MI. Aim of the study: to assess the relationship between the transmural extent of hyperenhancement (THE) and the traditional indirect signs of myocardial necrosis, diastolic wall thickness (DWT), systolic thickening (SWT), wall motion and perfusion defect.

Methods: 29 patients (63 ± 6 years) with previous Q-wave MI underwent contrast MR and post i.v. nitrate gated single photon emission computed tomography (G-SPECT) using 99 mTc-tetrofosmin.

Results: 493 myocardial segments were analyzed. The correlations between percent THE, and DWT and SWT, in the same segment were R = 0.45, (p = 0.001) and R = 0.54, (p = 0.001) respectively. Percent segmental THE was 1.8 ± 5.9 in the normokinetic, 15.7 ± 17.3 in the hypokinetic, 42.3 ± 24 in the akinetic and 93.5 ± 7 in the dyskinetic segments. A strong negative correlation was found between THE and regional percent radiotracer uptake (R = − 0.75, $p < 0.001$). In segments classified as necrotic at G-SPECT according to the post-nitrate 99 mTc-Tetrofosmin % uptake < 60%, the mean percent THE was only 46.1 ± 25.4.

Conclusion: as expected, segments with HE had on the average lower DWT, lower SWT, impaired motion and perfusion defect, as compared to segments without HE. However, the relationship between THE and all the other variables appears much more complex and largely unpredictable. The complexity might be related to the coexistence in the same myocardial segment and in different combinations of necrotic, ischemic, hibernated, stunned and normal contracting myocardium.

466. Low Dose Dobutamine Stress Magnetic Resonance Imaging with Myocardial Strain Analysis Accurately Predicts Myocardial Recoverability After Coronary Artery Bypass Grafting

D. Dean Potter, MD,[1] Philip A. Araoz, MD,[2] Kiaran P. McGee, PhD,[2] Thoralf M. Sundt, III, MD.[1] [1]*Surgery, Mayo Clinic, Rochester, MN, USA,* [2]*Radiology, Mayo Clinic, Rochester, MN, USA.*

Introduction: Patients with decreased left ventricular function may benefit from surgical revascularization. Predicting recovery of stunned or hibernating myocardium optimizes surgical risk to benefit in this subset of patients with coronary artery disease. Tissue tagged magnetic resonance (MR) imaging with myocardial strain analysis allows for quantitation of ventricular function. Quantitating changes in ventricular function during dobutamine stress testing may improve prediction of myocardial recovery after coronary artery bypass grafting (CAB).

Purpose: To determine whether tissue tagged MR imaging with myocardial strain analysis accurately predicts recovery of hibernating myocardium after CAB.

Methods: Twenty (20) patients were consented for preoperative and postoperative dobutamine stress MR imaging. Thirteen (13) patients completed the protocol with infusion of 5 mcg/kg/min, and 10 mcg/kg/min of dobutamine. 2-dimensional myocardial strain analysis was performed on a single mid-ventricular short axis image that was divided into 6 regions for each patient (n = 78). Minimum principal, circumferential, and radial strain values were calculated for each region at each stress level. Regional changes in strain after CAB were correlated with changes in preoperative strain values with dobutamine stress at 5 and 10 mcg by Chi-square tables. Receiver operator characteristic curves were created to determine the accuracy of low dose dobutamine stress testing with quantitative myocardial strain for the prediction of postoperative myocardial recoverability.

Results: There were no complications associated with dobutamine stress. Minimum principal, circumferential, and radial strain values at 5 and 10 mcg of dobutamine differed significantly from baseline ($p < 0.05$). Receiver operator characteristic curves found minimum principal strain to be 75% accurate for prediction of recoverability at both stress levels. Circumferential strain was 72% and 70% accurate for 5 and 10 mcg, respectively, while radial strain was 77% and 64% for 5 and 10 mcg, respectively.

Conclusions: Low dose dobutamine tissue tagged MR with strain analysis accurately predicted myocardial recoverability after CAB. This modality quantitatively assessed these differences. Further study is required to determine which strain parameter is most accurate for predicting myocardial recoverability after surgical revascularization.

467. Right Ventricle Shape and Contraction Patterns and Relationship to MRI Findings

Jan Fritz,[1] Meiyappan Solaiyappan,[2] Harikrishna Tandri,[3] Chandra Bomma,[3] João A.C. Lima,[3] Claus D. Claussen,[1] David A. Bluemke.[2] [1]*Department of Diagnostic Radiology, Eberhard-Karls-University, Tuebingen, Germany,* [2]*Russell H. Morgan Department of Radiology and Radiological Science, Johns Hopkins University School of Medicine, Baltimore, MD, USA,* [3]*Division of Cardiology, Johns Hopkins University School of Medicine, Baltimore, MD, USA.*

Introduction: Transaxial images of the right ventricle are commonly acquired using CT and MRI but vary in their appearance. This presents a clinical challenge in discerning the shape differences related to actual morphological conditions of the heart from the differences that might be due to the double oblique orientation of the heart with respect to conventional imaging axes.

Purpose: The purpose of this study was to analyze and to describe the shape and contraction pattern of the normal RV as visualized by MR imaging in transaxial plane versus the long axis plane which takes in to account the orientation of the heart.

Methods: 30 normal volunteers were imaged using cine MRI in axial, short and long axis planes. The shape of the right ventricle was classified by two observers. Quantitative measurement of base-to-apex distance and the angle subtended between the planes of horizontal long axis and axial view were calculated and compared to qualitative assessment of right ventricular shape. Multiplanar reformation was used to directly visualize changes in right ventricular shape between different views. Multiplanar reformation demonstrated the identified major RV shapes as part of a continuum

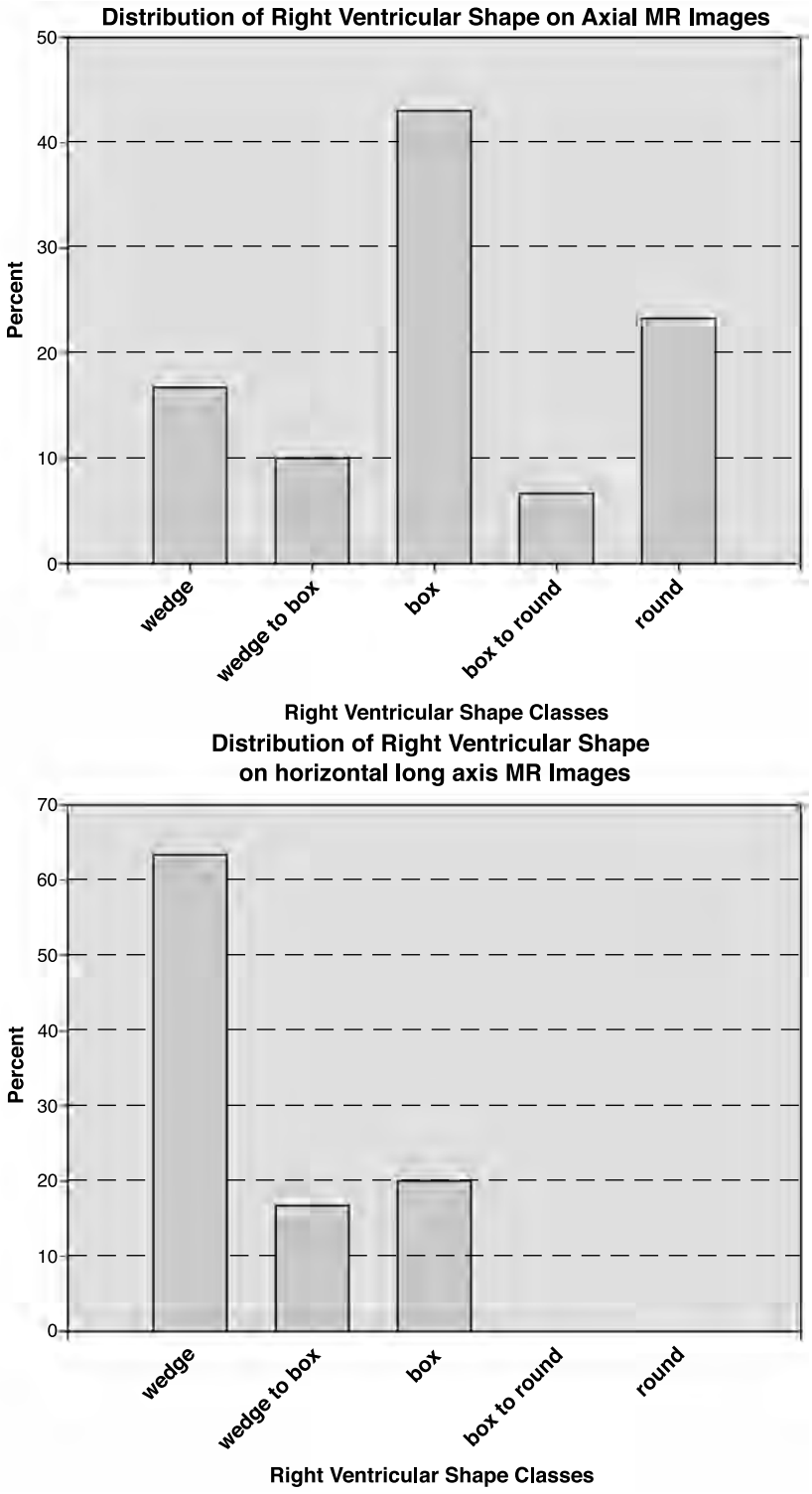

extending from wedge over box to round RV shape and dependence to the angle subtended between HLA and axial views. Changes in shape and appearance of focal outpouching of the RV free wall were due to foreshortened RV and increased portions of the right ventricular outflow tract that were visualized on axial compared to HLA views. The One-Sample Kolmogorov-Smirnov test was used to test the assumption of normality. A bivariate correlation was used to determine the extent and direction of association between base-to-apex-distance ratio and subtended angle between HLA and axial views. P values less than 0.05 were defined as statistically significant.

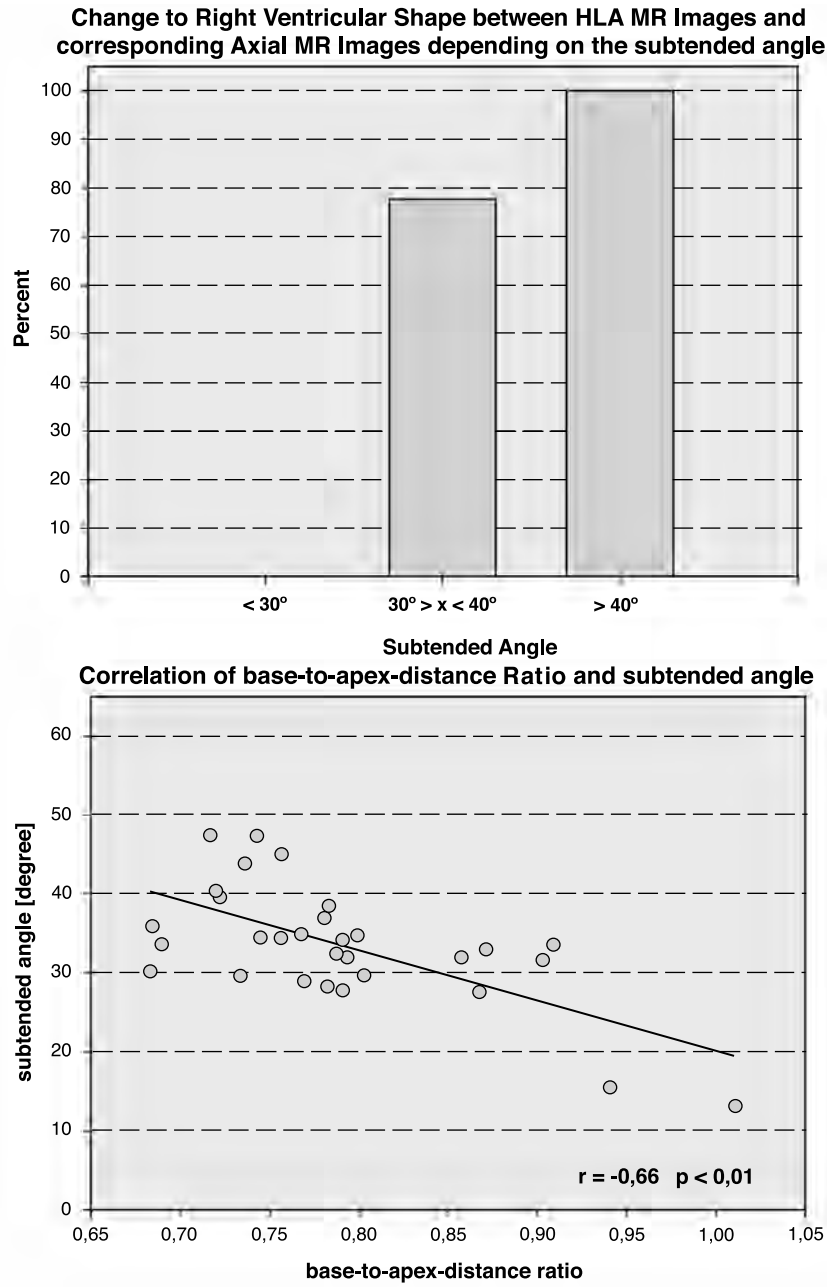

Results: Three major right ventricular shapes (wedge, box, round) were identified. On axial MR images, box shape was seen in 13/30 cases (43.3%) followed by round in 7/30 (23.3%) and wedge in 5/30 cases (16.7%). On the horizontal long axis view, wedge shape was seen in 19/30 cases (63.3%) followed by box in 6/30 cases (20.0%). Focal outpouching of the right ventricular free wall during systole was more frequently on axial (17/30 cases, 56.7%) than on horizontal long axis images (3/30 cases, 10%). The subtended plane angle and base-to-apex distance showed statistically significant dependence ($r = -0{,}66$, $p < 0.01$) indicative of the elongated right ventricle appearing foreshortened in the axial view.

Conclusions: Interpretation of normal right ventricular function is substantially different on axial compared to horizontal long axis views. Horizontal long axis views can add valuable information in order to avoid misdiagnosis of structural and functional right ventricular variations as abnormalities by axial MRI only.

468. MRI Evaluation of Ventricular Septal Motion in Patients With Constrictive Pericarditis and Restrictive Cardiomyopathy

Karen G. Ordovas, Gautham P. Reddy, MD, MPH, Matthew J. Sharp, MS, Oliver M. Weber, PHD, Charles B. Higgins, MD. *Radiology, UCSF, San Francisco, CA, USA.*

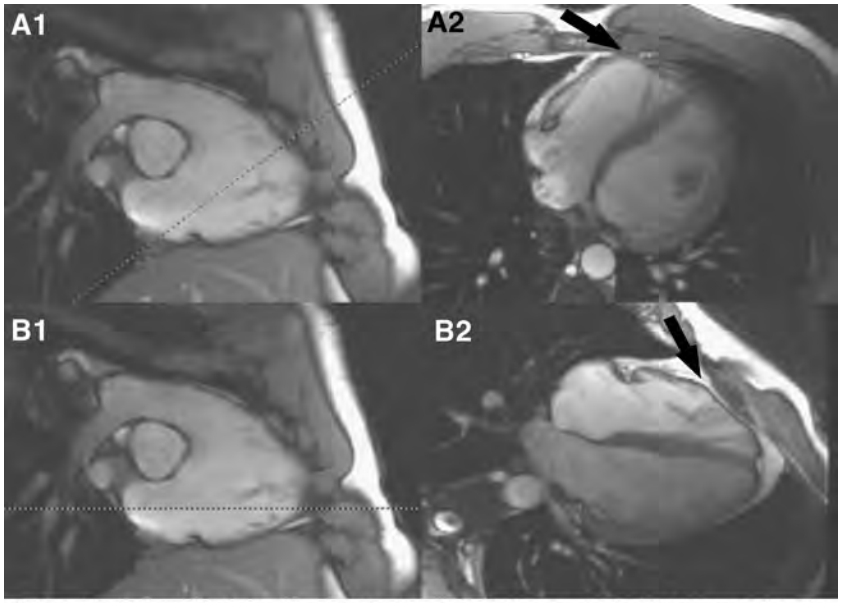

Right ventricular vertical long axis MR images (A1, B1) (segmented k-space steady state free precession pulse sequence) with corresponding axial (A2) and horizontal long axis images (B2) in the same volunteer. The image set shows that the right ventricular anterior free wall on axial views (A2) has an anterior bulge (arrow) that is much more prominent than on corresponding horizontal long axis view (B2).

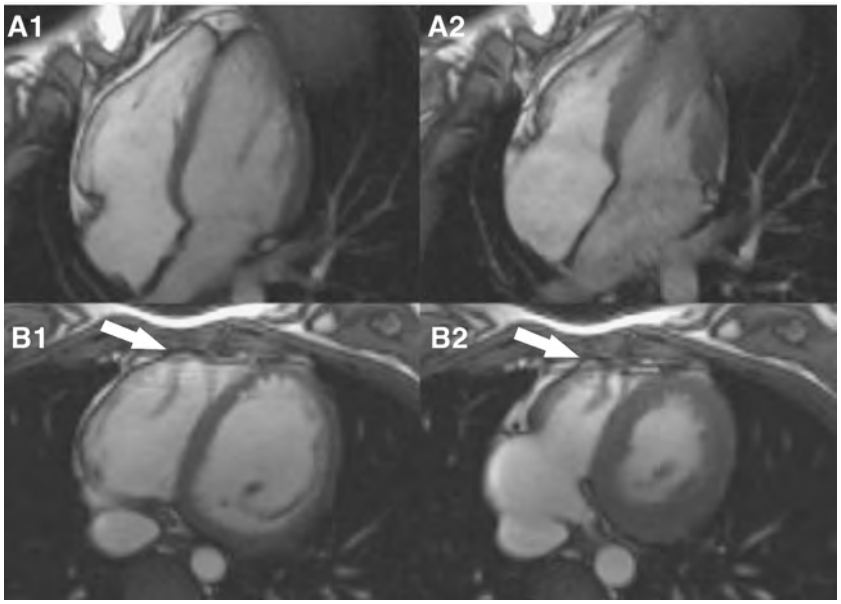

End diastolic and end systolic horizontal long axis (A1, A2) and axial (B1,B2) cine MR images (segmented k-space steady state free precession pulse sequence) of a volunteer with a subtended angle of 43° between planes of HLA view and axial view. MR images demonstrate a normal contraction pattern of the right ventricular free wall on horizontal long axis view (A1, A2) and an variant contraction pattern of axial images (B1, B2) with apparent bulging (arrows) of the apical third of the right ventricular free wall.

Introduction: Differentiation between constrictive pericarditis (CP) and restrictive cardiomyopathy (RCM) can be problematic but crucial, since CP can be alleviated by surgical pericardiectomy while RCM is usually not curable (Hancock, 2001). CMR has become the method of choice for non-invasive differentiation of these conditions, based on pericardial thickness (Sechtem et al., 1986). Abnormal ventricular septal motion (septal bounce) is known to be suggestive of CP on two-dimensional echocardiography (Nishimura, 2001). An abnormal right ventricular diastolic shape and septal motion have been reported using cine MR in patients with CP in comparison to normal subjects (Giorgi et al., 2003). However, it is not clear that this diastolic abnormality distinguishes between CP and RCM. The purpose of this study was to assess sensitivity, specificity and accuracy of septal bounce by MRI for the diagnosis of CP.

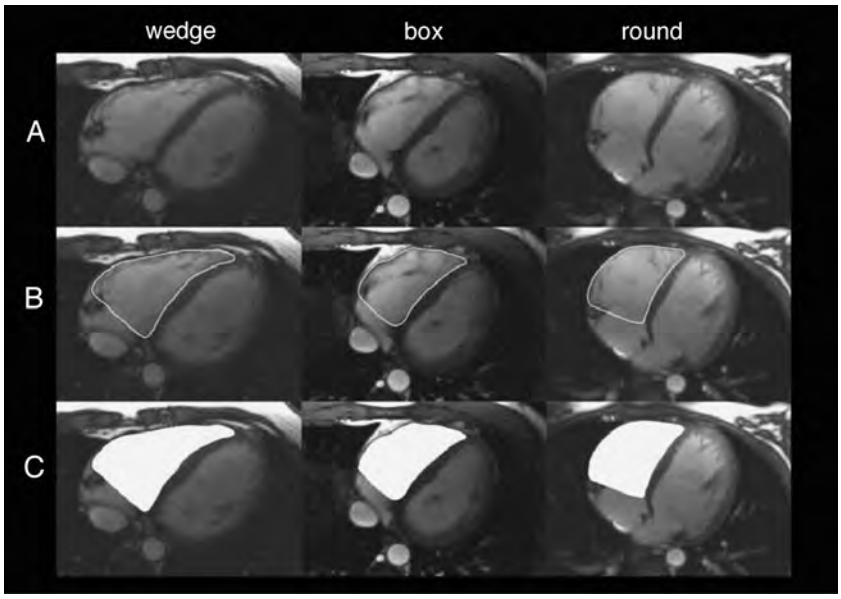

End diastolic axial MR images (segmented k-space steady state free precession pulse sequence) of three different patients demonstrating three major right ventricular shapes: wedge shaped right ventricles (left column), box shaped right ventricles (middle column) and round shaped right ventricles (right column). Each row demonstrates a) the original image, b) the contour trace of the right ventricle and c) the solid area of the right ventricle.

Patients and Methods: MRI studies of 12 patients with CP and 14 patients with RCM with known constrictive/restrictive heart physiology were reviewed retrospectively. MRI was performed with at least spin-echo and gradient-recalled echo (GRE) cine sequences on one of two 1.5 T scanners. Two experienced observers evaluated the images for pericardial thickening (defined as > 4 mm) and abnormal ventricular septal motion towards left ventricle during early diastole. The diagnosis of CP was based on surgery (8 patients) or the presence of pericardial thickening on CMR and constrictive physiology on catheterization (4 patients). The diagnosis of RCM was based on histology (6 patients) or constrictive physiology on catheterization with normal pericardial thickness on CMR and improvement of clinical status with medical therapy (8 patients).

Results: Abnormal diastolic septal motion was visualized in 10 of 12 (83%) patients with CP and in 2 of 14 patients (14%) with RCM. For the diagnosis of CP, sensitivity of abnormal early diastolic septal motion was 83%, specificity was 86%, positive predictive value was 83%, negative predictive value was 86%, and accuracy was 85%.

Conclusion: Combining morphological and functional CMR sequences, it is possible to demonstrate with only one noninvasive examination pericardial thickening and the presence of ventricular interdependence (abnormal diastolic septal motion), both of which independently have high accuracy for the diagnosis of CP.

REFERENCES

Giorgi, B., Mollet, N. R. A., Dysmarkowski, S., Rademakers, F. E., Bogaert, J. (2003). Clinically suspected constrictive pericarditis: MRI of ventricular septal motion and configuration in patients and healthy subjects. *Radiology* 228:417–424.

Hancock, E. W. (2001). Differential diagnosis of restrictive cardiomyopathy and constrictive pericarditis. *Heart* 86:343–349.

Nishimura, R. A. (2001). Constrictive pericarditis in the modern era: a diagnostic dilemma. *Heart* 86:619–623.

Sechtem, U., Tscholakoff, D., Higgins, C. B. (1986). MRI of the abnormal pericardium. *AJR* 147:245–252.

469. Presence and Pattern of Scar on Delayed-Enhanced MRI Differentiates Ischemic from Non-Ischemic Cardiomyopathy

Manesh R. Patel, MD, John F. Heitner, MD, Igor Klem, MD, Peter J. Cawley, MD, Jonathan W. Weinsaft, MD, Burkhard Seivers, MD, Anna Lisa Crowley, MD, Michelle Parker, MSc, Michael Elliott, MD, Robert Judd, PhD, Raymond J. Kim, MD. *Cardiology, Duke University, Durham, NC, USA.*

Background: Small pilot studies have suggested the presence of scar identified as hyperenhanced (HE) regions on delayed-enhanced MRI (de-MRI) correlates with coronary artery disease (CAD) in patients with cardiomyopathy. We hypothesized that both the presence and pattern of HE on de-MRI will differentiate ischemic from non-ischemic cardiomyopathy in a broad population.

Methods and Results: 234 consecutive patients with cardiomyopathy (EF $\leq$ 30%) referred for de-MRI from June 2002 to January 2004 were evaluated. 172 patients without congenital heart disease or prior bypass surgery underwent ECG, cardiac catheterization, and de-MRI. All studies were blindly read to patient identity and results of other

Table 1. Assessment of ce-MRI for CAD in patients with heart failure

ce-MRI criteria	CAD on CATH 112	No CAD on CATH 60	Sensitivity	Specificity	Diagnostic accuracy
Any HE Present	105	24	94%	60%	82%
Any HE Absent	7	36			
HE-CAD Pattern–Present	103	4	92%	93%	92%
HE-CAD Pattern–NOT Present	9	56			

modalities. De-MRI studies were scored for the presence and pattern of HE. A non-CAD pattern was defined as isolated mid-myocardial or epicardial HE, or global HE. Cardiac catheterization identified CAD (any coronary stenosis > 50%) in 112(65%) patients, and 60 (35%) without significant CAD. The mean age was 60 years and the mean EF was 20%(± 5.9%). Patients with CAD were more likely to have HE on de-MRI (94% vs. 40%, $p < 0.0001$) than patients without CAD, (Table 1). Of the 24 patients without CAD with HE, 20(88%) of these were identified as having a non-CAD pattern (mid-myocardial in 8, RV insertion in 5, and global in 7). Utilizing the pattern of HE significantly improved the specificity ($p < 0.0001$) and accuracy of de-MRI for CAD, see Table 1.

Conclusion: The presence of scar (HE) on de-MRI in patients with heart failure is sensitive for ischemic cardiomyopathy. Utilizing the pattern of myocardial scarring helps differentiate ischemic from non-ischemic cardiomyopathy.

470. Comparison of Right Ventricular Function Measurements By a Visual Estimate, a Geometric Method, and a Short Axis Summation Method

Daniel P. Drake, MD, Steven Lloyd, MD, PhD, Himanshu Gupta, MD. *Cardiovascular Disease, University of Alabama at Birmingham, Birmingham, AL, USA.*

Background: Accurate and reproducible serial measurements of right ventricular volumes and function are important in certain disease processes. The "gold standard" of determining ventricular volume is Simpson's method, which involves summation of multiple parallel slices through the ventricle. However, it is time consuming since it requires manually drawing contours on multiple short axis slices. A visual estimate is sometimes used as a quick method for determining RV function. We sought to determine the accuracy and reproducibility of the visual estimate, using a short axis summation method as the benchmark, and compare it to another shorthand approach- a geometric model- that requires only one area and length measurement on two orthogonal planes to determine RV volumes.

Methods: Cine cMRI (20 phases/cycle) images of 29 patients with a wide range of RV function (RVEF 32–70.3%) were retrospectively analyzed by three independent methods. The MR studies were performed using a 1.5 T magnet with either SSFP ($n = 22$) or FSPGR ($n = 7$) sequences (slice thickness 8–10 mm/gap 0–5 mm). First, a short axis summation (SAS) method was applied to multiple slices through the RV at end-diastole and end-systole using an automated software package with user defined contours. Papillary muscles and the moderator band were included in the volumes. Secondly, two experienced observers made a visual estimate (within 5%) of RVEF from short axis and 4-chamber views. Third, an estimation

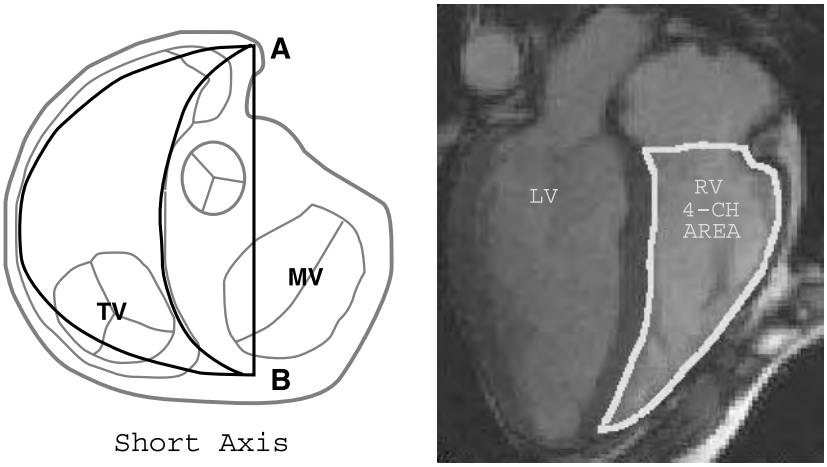

Figure 1.

Table 1. RVEF: comparison of three methods

	SAS vs. Geometric	SAS vs. Visual estimate
Bias	−2.57	−5.47
% Difference	4.8%	10.2%
Limits of Agreement	−14.1 to 9.0	−24.1 to 13.1
Correlation coefficient (r)	0.87	0.77
p-value	0.00001	0.00001
Spearman's correlation	0.80	0.61
p-value	0.0000001	0.0005

of RV volumes and RVEF was made using area and length measurements from 2 orthogonal planes based on a geometric model (difference of ellipsoids). The formula used was: Volume = 2/3 × (Area (RV4ch) * short axis Length AB) - see Figure 1.

A Bland-Altman analysis was applied to the data to test the agreement between the methods and the reproducibility of the visual estimate. Pearson's correlation and paired sample t-test were also calculated. RVEF values were further categorized into normal (≥ 55%), mild (45–54.9%), moderate (35–44.9%), and severe (25–34.9%) dysfunction and analyzed using Spearman's rank correlation.

Results:

RVEF. Mean RVEF ± SD was **53** ± 10%, **51** ± 12%, and **48**±15% for the SAS method, the geometric method, and the visual estimate respectively. Table 1 demonstrates that when the visual estimate and the geometric model are compared with the SAS method, there is a larger bias and wider limits of agreement for the visual estimate; the geometric method shows better correlation (both linear & Spearman's) and a line closer to unity (Fig. 2a and b). Analysis of the bias plot (Fig. 3b) of the visual estimate reveals a strong trend towards underestimation with lower RVEF.

Reproducibility of the visual estimate. Table 2 shows wide limits of agreement for interobserver and intraobserver variability of the visual estimates.

Accuracy of volume estimation by the geometric method. Table 3 shows the agreement between the SAS method and the Geometric model for estimating RV ventricular volumes. Wider limits of agreement are seen for RVEDV. Analysis of the bias plots (Fig. 4a and b) suggests that the disagreement is greater at higher ventricular volumes.

Conclusions: Using a short axis summation method as the benchmark for determining RVEF, a geometric model showed closer agreement than a visual estimate and therefore may be more appropriate for following RVEF in serial studies. In this analysis, visual estimates tend to underestimate the true RVEF in cases of poor RV function.

471. CMR Evaluation in Patients with High-Grade Ventricular Arrhitmias

Agostino Meduri,[1] Luigi Natale, MD,[1] Massimiliano Missere, MD,[1] Riccardo Fenici, MD,[2] Donatella Brisibda, MD,[2] Lorenzo Bonomo, MD.[1] [1]*Radiology, Università Cattolica, Roma, Italy,* [2]*Biomagnetism Unit, Università Cattolica, Roma, Italy.*

Introduction: MRI is a valid technique to assess the morphologic and functional alterations in patients with non ischemic ventricular arrhythmias.

Purpose: To test the hypothesis that MRI can identify in arrhythmic patients myocardial damage reflected by wall thickness or signal changes, focal or global kinetic abnormalities, or chamber dilatation.

Methods: We examined 43 patients with ventricular arrhythmias of non ischemic nature. Premature ventricular complexes had left bundle block morphology (LBBB) in 29 cases, in 7 a right bundle branch block contour (RBBB) In 7 patients arrhythmias had polymorphic patterns (PV). Echocardiography or physical examination was negative in 78.4% of patients.

Studies were performed with a 1.5 MR scanner. Cine sequences (Fastcard or FIESTA), axial short echo and short axis T2 weighted black blood FSE images and post-contrast (FSE or delayed enhancement) images were obtained.

Results: High prevalence (87%) of MRI morphological and kinetic myocardial abnormalities was found in patients with primary ventricular arrhythmias. LV abnormalities were found in 53.5% and RV abnormalities in 67.4% of patients. Biventricular anomalies were found in 49% of cases. Right ventricular dilatation was present in 85% and 48.3% of patients with PV and LBBB type arrhytmias while only in 12.5% of patients with RBBB morphology. Left ventricular (LV) dilatation was found in 25, 24.1 and 28,6% of PV, LBBB and RBBB patients respectively.

Right and left ventricular kinetic abnormalities were found in 50% and 25% of PV, in 36.7% and 10.3% of LBBB patients.

Seven patients underwent myocardial biopsy. One patient positive for ARVD had 1 major and 2 minor MR McKenna criteria. Of the 5 patients biopsy-positive for myocarditis 2 showed LV T2 hyperintensity and hyperenhancement, 1 RV wall T1 hyperintensity and sistodiastolic bulging. One patient with 3 minor McKenna criteria was biopsy negative for ARVD.

Conclusions: In patients with primary ventricular arrhythmias MR documented high prevalence (87%) of morphological, signal and kinetic abnormalities and was able to identify myocardial damage signs in an high percentage of patients with negative echocardiogram (Table 1).

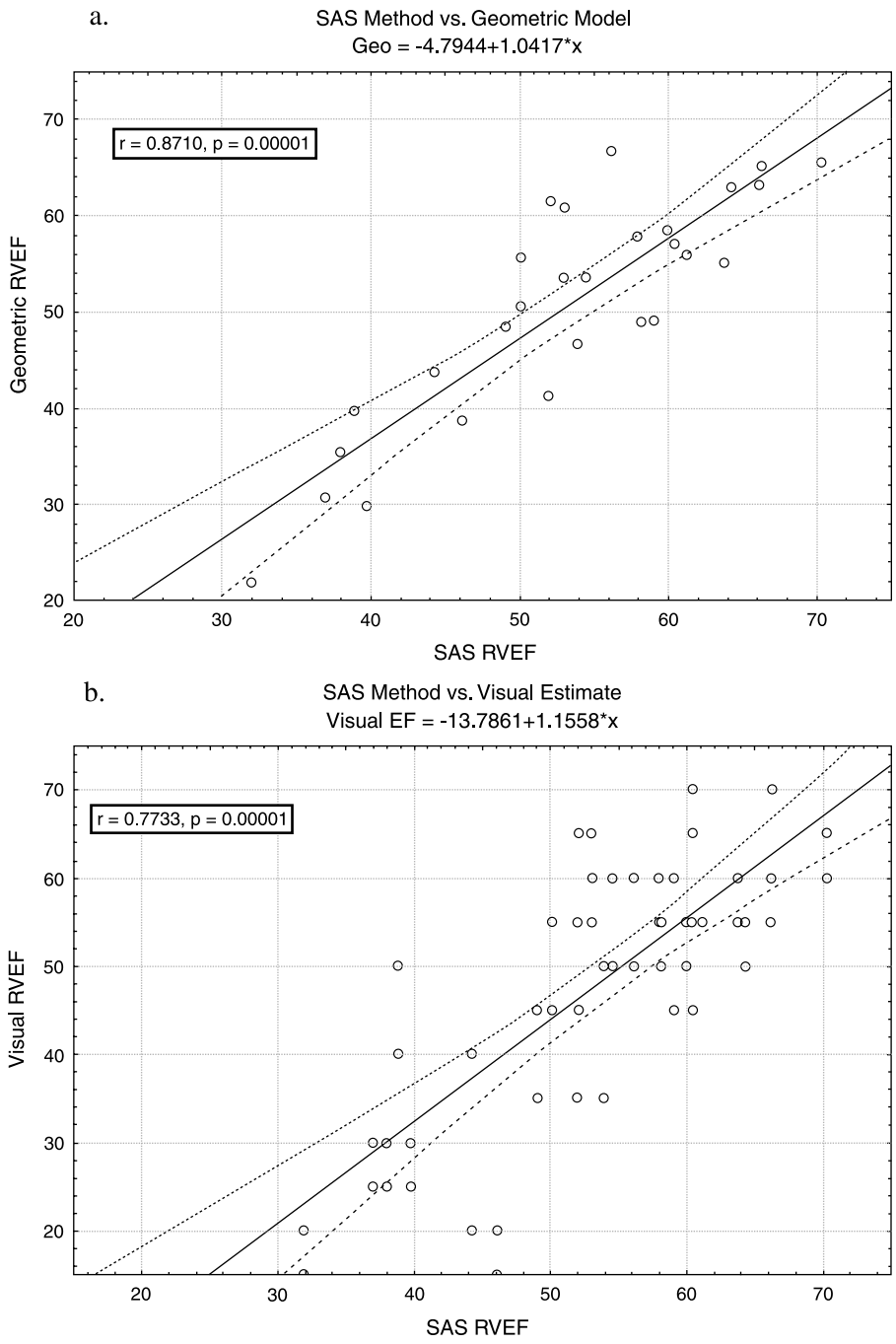

Figure 2.

472. Pacing Model of Heart Failure Produces Heterogeneous Changes in MRI Measured Myocardial Strain Parameters

D. Donald Potter, Jr., MD,[1] Philip A. Araoz, MD,[2] Leong L. Ng, MD,[3] David G. Kruger, PhD,[2] Jess L. Thompson, MD,[1] Chad E. Hamner, MD,[1] Joeseph A. Rysavy,[1] Thoralf M. Sundt, III, MD.[1] [1]*Cardiothoracic Surgery, Mayo Clinic, Rochester, MN, USA,* [2]*Radiology, Mayo Clinic, Rochester, MN, USA,* [3]*Department of Medicine and Therapeutics, University of Leicester, Leicester, UK.*

Introduction: The pacing model of heart failure is widely used to model dilated cardiomyopathy. It is traditionally assumed to produce homogenous changes.

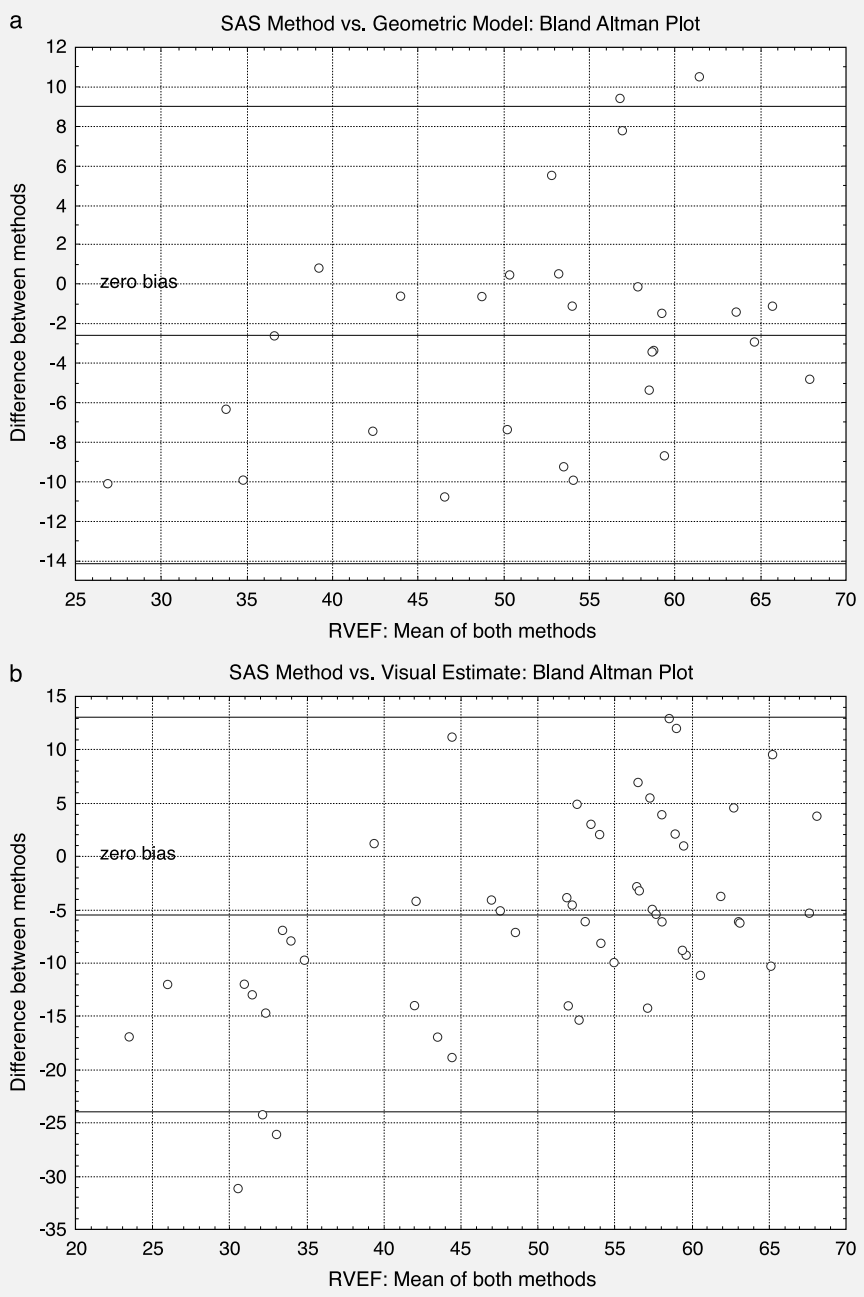

Figure 3.

Table 2. Interobserver and intraobserver variability of visual estimates of RVEF

Interobserver (n = 29)	
Bias	−1.4%
Limits of Agreement	−21.2 to 18.4%
SDD	9.9
Intraobserver (n = 15)	
Bias	2.7%
Limits of agreement	−9.1 to 14.5%
SDD	5.9

Table 3. RV volumes (in ml): comparison of SAS and geometric method

	RVEDV	RVESV
Mean ± SD (SAS)	143.42 ± 46.7	67.34 ± 29.8
Mean ± SD (Geometric)	141.95 ± 51.0	71.26 ± 34.2
Bias	−1.48	3.91
% Difference	1.0%	5.8%
Limits of agreement	−55.0 to 52.1	−25.5 to 33.3
Correlation coefficient (r)	0.85	0.90
p-value	0.000000004	0.00001

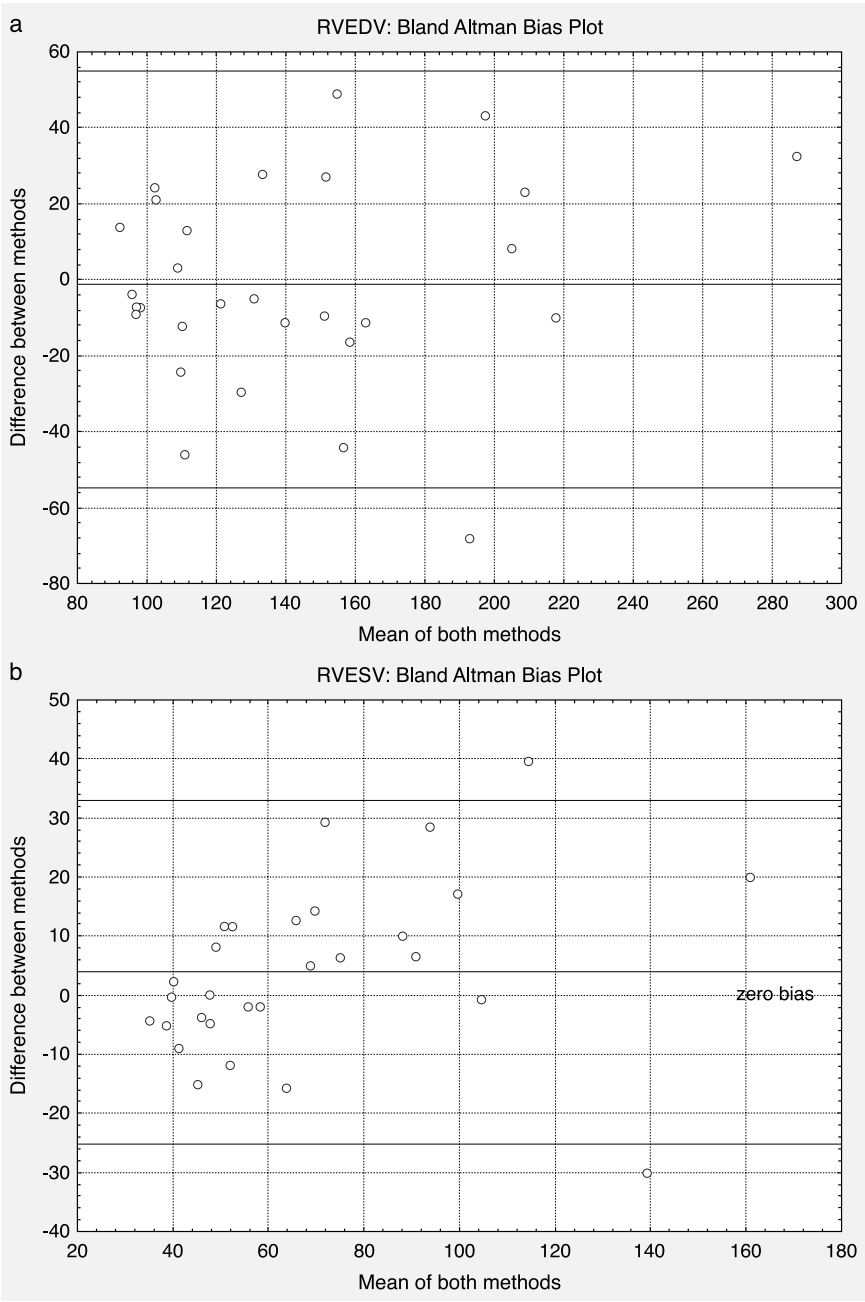

Figure 4.

Purpose: To measure regional changes in LV strain as measured with MRI.

Methods: 9 mongrel dogs underwent baseline MRI with tagging. All 9 dogs had heart failure induced by rapid pacing over a 4 week period using a pacemaker implanted in the RV apex. The dogs then underwent post-heart failure MRI with tagging. Three myocardial strain parameters - minimal principal (MPS), circumferential (CS), and radial (RS) - were separately measured for the anterior, lateral, inferior, and septal walls. Baseline and post-heart failure LV volumes were also measured.

Results: Strain levels were heterogeneous with significant changes from baseline in the septal and inferior walls for most measurements, but not in the anterior and lateral walls. For MPS, strain levels significantly decreased in the inferior ($p = 0.004$) and septal walls ($p = 0.004$) but not in the anterior ($p = 0.164$) or lateral ($p = 0.570$) walls. For CS, strain levels significantly decreased in the inferior ($p = 0.004$) and septal ($p = 0.004$) walls but not in the anterior ($p = 0.820$) or lateral ($p = 0.570$) walls. For RS, strain level decreased in the anterior ($p = 0.008$) and septal walls ($p = 0.004$) but not in the inferior ($p = 0.164$) or lateral ($p = 0.129$) walls. Comparison within the post-heart failure measurements showed that strain measurements between the 4 walls were significantly different from each other: (MPS

Table 1. Percentage of positive examinations in ventricular arrhytmic patients

	Echo	RM	RM: Dilatation	RM: Kineticanomalies	RM: Signal anomalies
LBBB	2.3	42.9	42.9	20	14.3
RBBB	23.3	82.8	36.7	34.6	34.5
VP	4.7	100	85.7	57.1	28.6

$p = 0.0036$; CS $p = 0.0003$; RS $p = 0.050$). Global LV volume measurements showed that ejection fraction decreased significantly from baseline to post-heart failure ($p = 0.004$) and LV end-diastolic volume increased significantly ($p = 0.020$).

Conclusion: The pacing model of heart failure produces heterogeneous changes in heterogeneous changes in regional wall motion as measured with strain. The greatest changes are in the walls closest to the pacemaker implantation site: the inferior and septal walls.

473. Cardiovascular Magnetic Resonance Assessment of Cardiac Sarcoidosis: The Localization of Cardiac Involvement and Its Relation with Plasma Brain Natriuretic Peptide

Azusa Ichinose,[1] Minako Oikawa,[2] Hiroki Otani,[2] Kei Takase,[1] Haruo Saito,[1] Tsuyoshi Shinozaki,[2] Yutaka Kagaya,[2] Kunio Shirato,[2] Tadashi Ishibashi,[1] Shoki Takahashi.[1]
[1]*Radiology, Tohoku University Graduate School of Medicine, Sendai, Japan,* [2]*Cardiovascular Medicine, Tohoku University Graduate School of Medicine, Sendai, Japan.*

Introduction: Cardiac involvement of sarcoidosis is a major prognostic factor in patients with sarcoidosis. Therefore, the accurate depiction of myocardial scarring due to cardiac sarcoidosis is needed. Furthermore, it is unknown whether the extent of myocardial scarring is related with neurohumoral activation in patients with cardiac sarcoidosis.

Purpose: We examined whether cardiovascular magnetic resonance (CMR) is useful to know the presence and extent of myocardial scarring in patients with sarcoidosis. We also examined whether the extent of myocardial scarring measured by CMR is related with plasma level of brain natriuretic peptide (BNP).

Methods: CMR was performed in 8 patients with histologically proven sarcoidosis and highly suspected cardiac involvement. Using a 17-segment model of the left ventricle (LV), the extent of delayed enhancement (DE) (0 = none, 1 = 1 to 25%, 2 = 26 to 50%, 3 = 51 to 75%, 4 = 76 to 100% enhancement) and the severity of regional wall motion (0 = normal, 1 = mild hypokinesis, 2 = severe hypokinesis, 3 = akinesis, 4 = dyskinesis) were visually assessed on a 4-point scale.

Results: All patients exhibited regional wall thinning, regional wall motion abnormalities (Figure 1, arrow) and myocardial DE (Figure 2, arrows). The average LV end-diastolic volume was 156 ± 30 ml and LV ejection fraction was 37 ± 9%. The average DE score was 24 ± 13 point. The average wall motion score was significantly worse in the basal slice compared with the midventricular and apical slices (1.8 ± 1.2, 0.9 ± 0.9 and 0.5 ± 0.9 point/slice, basal, midventricular and apical slices, respectively; $p < 0.0001$). The average DE score was significantly increased in the basal slice compared with the midventricular and apical slices (2.0 ± 1.4, 1.3 ± 1.3 and 0.9 ± 1.3 point/slice, respectively; $p < 0.0001$). The average DE scores of the septal, anterior, lateral and inferior walls were not significantly different (1.5 ± 1.4, 1.4 ± 1.4, 1.6 ± 1.4, and 1.5 ± 1.4 points/each wall, respectively; p = NS). The DE was significantly more

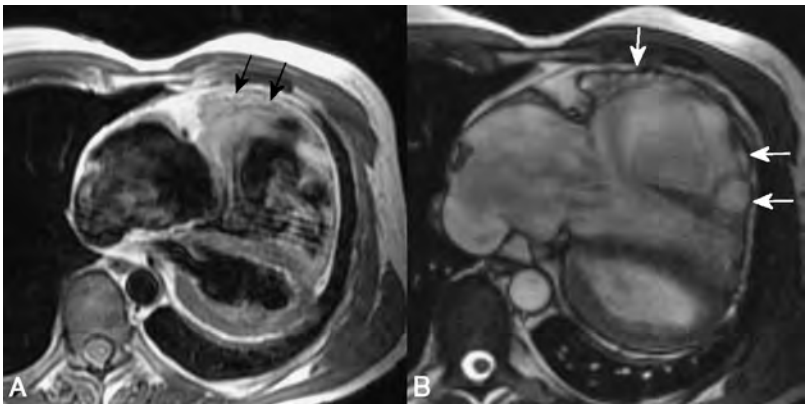

Figure 1. Patient with ARVD. The right ventricle (RV) is abnormally enlarged A: Axial Black Blood FSE areas of fatty infiltration of the RV free wall are evident (arrows). B: Axial FIESTA: Diskinesia with multiple systo-diastolic bulgings of the RV free wall (arrows).

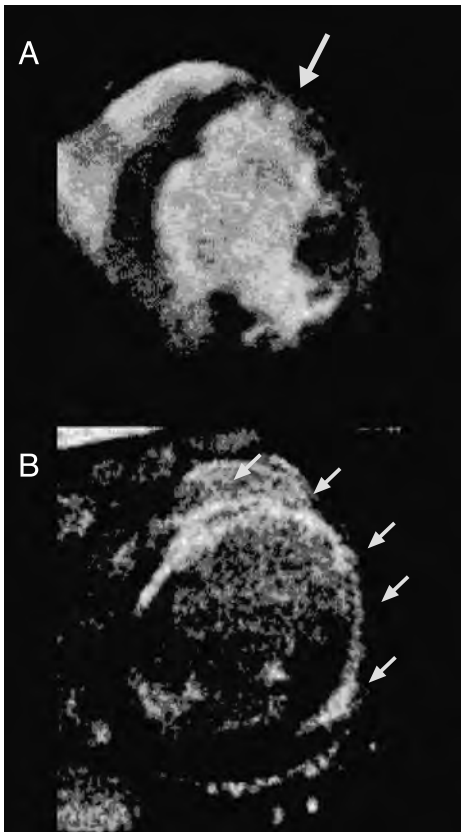

Figure 1.

frequent in the subepicardial and midmyocardial segments compared with the subendocardial segments (14.9 ± 7.1, 13.5 ± 7.6 and 10.5 ± 6.3 segments/patient, respectively; $p < 0.01$). The DE scores were significantly correlated with the plasma level of BNP ($r = 0.91, p < 0.01$). The LV ejection fraction and the LV end-diastolic volume index were not significantly correlated with plasma level of BNP.

Conclusion: In patients with sarcoidosis and highly suspected cardiac involvement, wall motion abnormalities and myocardial scarring were well detected by CMR. Myocardial scarring was significantly frequent in the basal myocardium and in the subepicardial layer of the LV myocardium. The extent of myocardial scarring correlated with the plasma level of BNP.

474. Left Ventricular Mass by CMR and Different ECG Criteria for Left Ventricular Hypertrophy in Healthy Individuals

Minna Carlsson, Henrik Engblom, MD, Håkan Arheden, MD, PhD. *Clinical Physiology, Lund University Hospital, Lund, Sweden.*

Background: There is a considerable variability in the 12-lead electrocardiogram (ECG) among individuals without cardiac disease. Demographic variables such as age, sex, height, weight, and physical fitness are shown to influence variability in QRS duration and voltage amplitudes, especially the latter. Thus, heterogeneity within study populations with respect to these determinants partly explains the limited accuracy of ECG in estimating LVM from QRS complex properties and, consequently, to diagnose left ventricular hypertrophy (LVH).

Purpose: Our aim was to investigate the relationship between LVM and QRS duration in healthy subjects and in this group test the hypothesis that there is a strong relationship between LVM and QRS duration in relation to different ECG criteria for LVH, which include voltage amplitude criteria.

Methods: Seventy-one healthy volunteers (36 males, age range 21–82 years) were included in the study. Inclusion criteria were 1) no signs of global or local decrease in left ventricular function or signs of left or right ventricular hypertrophy on CMR 2) normal 12-lead ECG (no signs of bundle branch block, fascicular block, or ischemic heart disease; frontal QRS axis between $-30°$ and $+90°$) 3) normal blood pressure (SB$p \leq 140$ mmHg and DB$p \leq 90$ mmHg). Subjects were excluded if they had history or clinical signs of cardiovascular disease, systemic or metabolic disease or treatment with medication. A turbo FLASH MR sequence was used to acquire short-axis images covering

Table 1. Relation between LVM and different ECG criteria for LVH

ECG criteria	Voltage alone, R (p)	Voltage-duration product, R (p)	Duration alone, R (p)	Definition of ECG criteria
Sokolow-Lyon	0.25 (0.033)	0.42 (< 0.001)		S-wave amplitude in V1 + R-wave amplitude in V5 or V6
Gubner-Ungerleider	0.27 (0.021)	0.38 (0.001)		R-wave amplitude in I + S-wave amplitude in III
RV5	0.36 (0.002)	0.47 (< 0.001)		R-wave amplitude in V5
Cornell	0.47 (< 0.001)	0.55 (< 0.001)		R-wave amplitude in aVL + S-wave amplitude in V3
12-lead sum	0.49 (< 0.001)	0.59 (< 0.001)		Sum of Q-, R- and S-wave amplitudes in all 12 leads
QRS duration			0.59 (< 0.001)	

the left ventricle. LVM was determined by planimetry. Commonly used ECG criteria for LVH were calculated (Table 1). QRS duration and voltage amplitudes were all measured by computer.

Results: All ECG criteria tested showed a statistically significant relationship with LVM. The ECG criteria most strongly correlated with LVM were QRS duration and the 12-lead sum product ($r = 0.59$, $p < 0.001$ for both). The weakest correlation was found for the Sokolow-Lyon criterion ($r = 0.25$, $p = 0.033$). Correlations between LVM and the different ECG criteria all improved by adding the QRS duration to each of the simple voltage criteria (Table 1). The variability of LVM measurement was 0.5 ± 4 g between readers (R^2 0.98, ICC 0.98).

Conclusions: In healthy subjects QRS duration alone is more strongly correlated to LVM than most ECG criteria used to diagnose LVH.

475. The Benefit of Aortic Valve Replacement for Severe Aortic Stenosis is Thwarted by Coexistent Coronary Artery Disease; A Magnetic Resonance Imaging Study

Robert W.W. Biederman, MD,[1] Mark Doyle, PhD,[1] Vikas K. Rathi, MD,[1] Tarun Tewatia, MD,[1] June Yamrozik,[1] Ronald B. Williams,[1] Diane A. Vido,[1] Valerie Bress,[1] Sunil Mankad, MD,[1] James A. Magovern, MD,[1] Nathanial Reichek, MD.[2]
[1]*Allegheny General Hospital, Pittsburgh, PA, USA,* [2]*St. Francis Hospital, Rosalyn, NY, USA.*

Background: In patients with aortic stenosis (AS), the mechanism of improvement following aortic valve replacement (AVR) is not fully understood. Further, the influence of CAD following AVR on the LV has not been evaluated.

Hypothesis: We hypothesize that CAD + (lesions > 50%) will mitigate the otherwise advantageous effects of reverse remodeling in AS pts post AVR.

Methods: Severe AS pts (29), [60–90 yr, 10 F] underwent MRI pre-AVR and 7 ± 2 mo post AVR (24 pts survived and/or returned). LV mass Index (LVMI), volume (LVMI/vol) and EF were measured, along with 1D base to apex transmural circumferential intramyocardial strain (%S).

Results: EF was not different between groups at baseline, remaining unchanged post-AVR (61 ± 19 vs 64 ± 9%, p = NS). However, LVMI (g/m^2) and LVMI/vol (g/m^2/ml) decreased post AVR (93 ± 22 vs 77 ± 17 g/m^2; 0.73 ± 0.31 vs 0.63 ± 016, $p < 0.001$ and < 0.05, respectively). On subset analysis, the fall in LVMI and LVMI/vol was confined to CAD − pts ($p < 0.05$). Pre-AVR, %S was similar for CAD − and CAD + pts, (19 ± 10 vs 20 ± 10%). Pre-Post AVR %S rose in the CAD − pts (19 ± 10 vs 22 ± 9%, $p < 0.001$) and fell in CAD + pts (20 ± 10 to 16 ± 11%, $p < 0.0001$). A transmural gradient in %S was present post AVR in both CAD − and CAD + pts (beneficial only in CAD −) $p < 0.005$, for both (see graph).

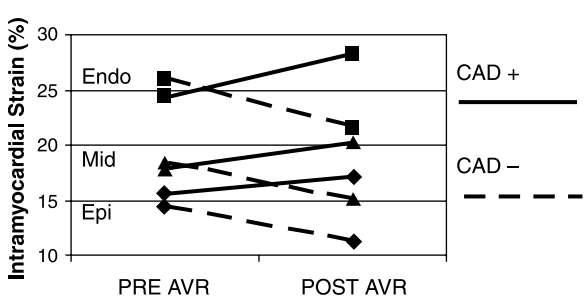

Conclusion: In AS pts following AVR, reverse remodeling parallels improvement in LV intramyocardial strain. This MRI analysis demonstrates that AVR benefit is confined to those without CAD, while those with CAD remodel in a deleterious manner at the myocardial level.

476. Elevated Leptin Levels are Associated with Left Ventricular Hypertrophy in Obese Adults

Monique R. Robinson,[1] Michaela Scheuermann-Freestone,[1] C Paul Leeson,[1] Kieran Clarke,[2] Stefan Neubauer.[1] [1]*Cardiovascular medicine, University of Oxford Centre for Clinical Magnetic Resonance Research, Oxfordshire, UK,* [2]*University of Oxford, University Laboratory of Physiology, Oxfordshire, UK.*

Introduction: Investigation of cardiac pathology in obesity is commonly complicated by insulin resistance (IR) and hypertension, making it difficult to determine the independent effect of obesity on the heart. Experimental work has suggested that leptin and inflammation may act independently to cause left ventricular hypertrophy (LVH) in obesity.

Purpose: We aimed to investigate whether increased leptin and CRP levels are associated with LVH in subjects with uncomplicated obesity.

Methods: LV function of 45 normotensive obese subjects with a body mass index (BMI) $\geq$ 30 kg/m^2 was compared to that of 26 age- and sex-matched controls. Using a 1.5 Tesla MR system, a short axis stack of contiguous images was acquired and LV end-diastolic volume (EDV), LV end-systolic volume (ESV), left ventricular ejection fraction (LVEF), stroke volume (SV) and left ventricular mass (LVM) (normalised for height) were measured or calculated. Fasting leptin, C-reactive protein (CRP), glucose, and insulin were measured and relative insulin resistance (IR) was assessed by HOMA.

Results: Insulin sensitivity was normal in the obese subjects, but leptin was significantly higher (35.1 ± 3.0 vs.9.2 ± 0.7 ng/ml, $p < 0.001$) as was CRP (7.8 ± 0.5 vs.3.7 ± 0.4 mg/L, $p < 0.001$). There were no significant differences in systolic function. EDV was significantly lower in the obese (115 ± 4 vs.127 ± 6 ml, $p < 0.05$), but did not correlate with anthropometric measures or leptin. LVM was significantly higher in the obese (87 ± 3 vs.70.5 ± 4 g/m, $p < 0.001$). LVM indexed for height was log transformed for

better approximation to a normal distribution (LnLVM). LnLVM correlated with BMI ($r = 0.7$, $p < 0.001$) and leptin ($r = 0.5$, $p < 0.03$). LnLVM did not correlate with CRP, insulin, glucose or HOMA.

Conclusions: Uncomplicated obesity is closely associated with LVH. Further, leptin demonstrates a strong association with LVH. Lowering leptin levels in obesity may improve cardiovascular health and may have a beneficial effect by reducing LVM.

477. MRI Features of Cardiac Manifestations of Fabry Disease

Lora A. Medoro, MBBS,[1] Richard E. Slaughter, MBBS FRACR,[1] Wendy E. Strugnell, BSc,[1] Christopher Denaro, MBBS FRACP.[2] [1]*Cardiovascular MRI Research Centre, Prince Charles Hospital, Brisbane, Australia,* [2]*Department of Cardiology, Royal Brisbane Hospital, Brisbane, Australia.*

Introduction: Fabry disease is a rare X-linked lysosomal storage disorder. These patients have a deficiency in alpha-galactosidase with progressive intracellular accumulation of glycosphingolipid. Cardiac involvement is frequent and some reports suggest that it may be an under-recognised cause of left ventricular hypertrophy (Sachdev et al., 2002). Recombinant enzyme therapy is available for treatment of this condition with some promising results (Spinelli et al., 2004). There has been little published data with respect to MR imaging of the cardiac manifestations in Fabry disease.

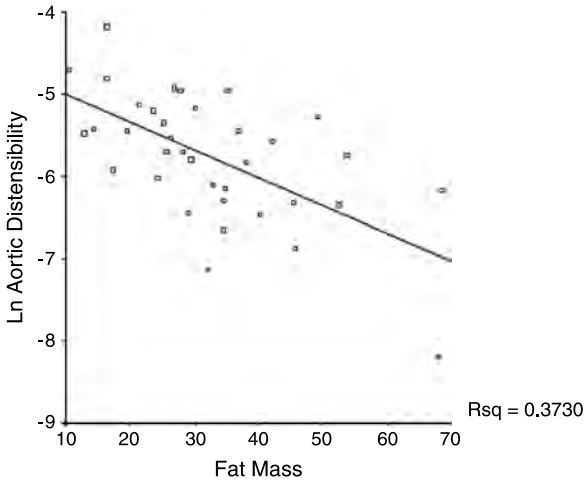

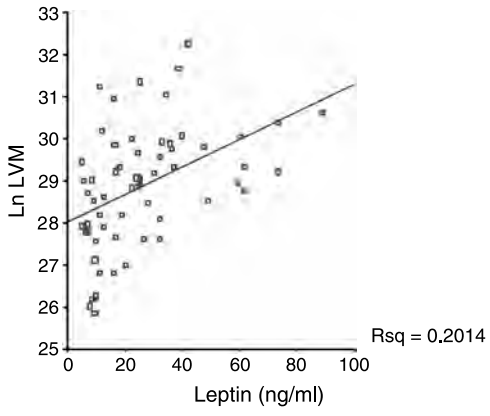

Purpose: To assess the MRI features of cardiac manifestations of Fabry disease and any features that may aid in the diagnosis of the severity of cardiac involvement.

Methods: 7 patients (5 male, 2 female) referred for MRI assessment between April and June of 2004 were reviewed. Mean age was 37 years (males 31.6 years, females 51.5 years). MR imaging was performed on a GE Medical Systems 1.5 Tesla Signa Twinspeed system with a 4-element cardiac phased array coil. Steady state free precession (SSFP) cine MR imaging series were acquired to provide functional assessment of the ventricles. Double and Triple Inversion Recovery sequences were performed in the vertical long axis, horizontal long axis and short axis orientations. Delayed enhancement imaging was performed in the same imaging planes and acquired 8–15 minutes after administration of 0.2 mmol/kg of gadolinium-DTPA, using an inversion time of 200–250 ms. Indices including left ventricular end diastolic volume (LVEDV), stroke volume, ejection fraction, wall thickness (LVWT) and end diastolic mass (LVEDM) were derived on a GE Medical Systems Advantage Windows workstation using Medis Mass Analysis software.

Results: All patients had normal left ventricular systolic function with ejection fractions and LVED volumes within normal limits. LVED mass was at the upper limits of normal or increased in most cases with an average of 83 g/m^2. Females 62 g/m^2 (normal range 36–67 g/m^2), males 91 g/m^2 (normal range 46–83 g/m^2). Left ventricular wall thickness was increased or at the upper limits of normal in 6 of the 7 patients with an average of 1.3 cm (females 1 cm, males 1.46 cm). Two patients demonstrated hyperenhancement of the myocardium on the delayed enhancement images. The pattern was not typical of ischaemia, being midwall with subendocardial sparing. The changes involved the antero-apical region in one patient and apical half of the anterolateral wall in the other. These two patients had the most markedly increased LVED mass (averaged at 119.5 62 g/m^2) and greatest LVWT at 1.8 cm.

Conclusions: The most common cardiac manifestations of Fabry disease such as left ventricular hypertrophy and increased wall thickness and mass have been well described in the literature, usually based on clinical and echocardiography findings. Hyperenhancement on MR delayed enhancement imaging has been described in one published series (Moon et al., 2003). Hyperenhancement was reported in over 50% of 24 patients, predominantly in a basal inferolateral distribution. Our study has demonstrated hyperenhancement in only 2 cases (28%) and in a different distribution. This may be due to earlier presentation or to less severe manifestation of the disease. Follow-up is required to help assess the nature of this enhancement (fibrosis versus inflammatory), its natural

evolution and its potential prognostic implications. Cardiac MRI provides a complementary non-invasive role in the primary assessment and follow-up of these patients in evaluating LV function, in particular left ventricular mass and wall thickness. MR delayed enhancement imaging of the myocardium may help in predicting the severity of the cardiac involvement and the potential clinical implications.

REFERENCES

Moon, J., et al. (2003). *Eur. Heart J.* 24:2151–2155.
Sachdev, B., et al. (2002). *Circulation* 105:1407–1411.
Spinelli, L., et al. (2004). *Clin. Genet.* 66(2):158–165.

478. Relationship of Volumetrically-Determined Left Ventricular Mass and Performance to Anthropomorphic Characteristics and Obesity: Implications for Indexation

Michael L. Chuang, MD, Carol J. Salton, BA, Kraig V. Kissinger, BS, RT(R), (MR), Warren J. Manning, MD. *Division of Cardiovascular Medicine, Beth Israel Deaconess Medical Center, Boston, MA, USA.*

Introduction: Obesity is associated with increased left ventricular (LV) mass as measured by echocardiography, but the functional performance and ''appropriateness'' of the hypertrophy as adiposity increases is not well characterized.

Purpose: We sought to determine the relationships between height (HT), weight (WT, i.e. total body mass), fat-free body mass (FFM) and calculated body surface area (BSA) versus LV mass determined using volumetric cardiovascular magnetic resonance (CMR) imaging. We also sought to determine whether LV functional performance is reduced in obesity. Ejection fraction (EF) measures LV endocardial-surface or ''chamber'' performance, while myocardial contraction fraction (MCF = stroke volume divided by myocardial volume) is a volumetric measure of myocardial function analogous to the unidimensional midwall fractional shortening measure.

Methods: 112 normotensive adults (systolic blood pressure < 140 mmHg, 66 women, 46 men, aged 57 ± 9 years) free of cardiovascular disease underwent CMR study on a 1.5-Tesla system (Philips) using a contiguous multi-slice TFE-EPI cine sequence (TR = RR-interval, TE = 9 ms, FA = 30°, voxel size 1.25 × 2.0 × 10.0 mm^3). LV volumes and mass were determined using a summation of disks method. Subjects with body mass index (BMI) > 27.0 kg/m^2 were classified as ''obese'' while those with BMI < 27.0 kg/m^2 were ''non-obese.'' Gender-specific adipose mass (AM) was calculated from subject reported HT and WT (Kvist et al., 1988) and used to determine FFM. Pearson correlation was used to assess relationships between LV mass and HT, WT, FFM, and BSA. Student's t test was used to test the null hypothesis of no relationship between parameters of interest; $p < 0.05$ was considered significant. We also compared EF and MCF between obese and non-obese subjects.

Results: Non-obese subjects comprised 46 women and 27 men, leaving 20 obese women and 19 obese men. Overall LV mass was 109 ± 19 g for women and 151 ± 23 g for men. For both sexes, LV mass significantly correlated with WT (women: r = 0.48, $p < 0.001$; men:r = 0.24, $p < 0.02$) and with FFM (women: r = 0.42, $p < 0.01$; men: r = 0.34, $p < 0.001$). LV mass significantly correlated with height in men (r = 0.37, $p < 0.001$) but not in women (r = 0.26, p = NS). There was significant correlation between LV mass and calculated body surface area (BSA) for both sexes (women: r = 0.51, men: r = 0.32, $p < 0.001$ both). There was no difference between obese and non-obese subjects with respect to EF, $p > 0.05$ for the entire group and for each gender. Similarly, MCF did not differ based on obesity ($p > 0.05$) for either men or women. LV mass indexed to WT was uniformly greater in non-obese vs obese subjects (women: 1.72 ± 0.29 vs 1.37 ± 0.24, $p < 0.001$; men: 2.06 ± 0.32 vs 1.66 ± 0.23, $p < 0.001$), but indexation to FFM varied by sex (women: non-obese = 2.57 ± 0.46 < obese = 2.79 ± 0.30, $p = 0.049$; men: non-obese = 2.53 ± 0.35 > obese = 2.31 ± 0.33, $p = 0.041$).

Conclusions: LV mass is significantly correlated with total body mass (WT), FFM and BSA. LV mass correlated with HT in men but not women. Thus indexation of volumetric LV mass to WT, FFM or BSA are reasonable, but indexation to HT may not be appropriate. Indexation to WT yields greater relative LV mass in non-obese versus obese subjects of both sexes, whereas indexation to FFM has a gender-differential effect, in which obese women have greater relative LV mass as compared with their non-obese counterparts. Finally, in this patient group we found no difference in LV chamber function (EF) or myocardial function (MCF) between obese and non-obese subjects. The implications of these findings with respect to the ''cardiomyopathy of obesity'' merit further investigation.

REFERENCE

Kvist, H., et al. (1988). *Am. J. Clin. Nutr.* 48:1351.

479. ECG Criteria of Left Ventricular Hypertrophy Detect Patients with Significantly Elevated Left Ventricular Mass Index

Khaled Alfakih, MD, Kevin Walters, PhD, Gavin Bainbridge, BSc, John Ridgway, PhD, Alistair Hall, PhD, Mohan Sivananthan, MD. *Cardiac MRI, Leeds General Infirmary, Leeds, UK.*

Purpose: The ECG is widely used to detect left ventricular hypertrophy (LVH) based on several previously validated criteria. We sought to assess the severity of LVH for individuals with positive ECG criteria for LVH by defining their mean LVM index using cardiac MRI.

Methods: LVM studies were performed on 288 hypertensives and 60 normal volunteers on a 1.5-Tesla MRI system. A stack of 10–14 short axis slices were acquired, during breath hold, using a segmented K-space turbo gradient echo pulse sequence (TR = 8.8 ms, TE = 5.2 ms, flip angle = 35°). The endocardial and epicardial contours of the LV were traced at end diastole. LVM = 1.05 × (epicardial volume- endocardial volume). A standard 12-lead ECG was recorded at 25 mm/s. Four ECG LVH criteria were evaluated; Sokolow-Lyon voltage, Sokolow-Lyon product, Cornell voltage and Cornell product. Means and S.D were calculated for the LVM and indexed to body surface area (BSA). Hypertensives were defined as having an elevated LVM index if they were 2 S.D above the mean for the normal volunteers. Hypertensives were defined as either ECG LVH positive or negative based on the four different ECG LVH criteria. We compared the mean LVM index for the ECG positive patients against the LVM index of the normal volunteers, for each ECG criteria, for men and women separately.

Results: The mean LVM index for male volunteers was 77.8 ± 9.1 g/m^2, n = 30 and for the female volunteers was 61.5 ± 7.5 g/m^2, n = 30. 40% of the hypertensive males (mean LVM index = 93.4 ± 18.3 g/m^2, n = 168) and 37% of the hypertensive females (mean LVM index = 73.6 ± 13.2 g/m^2, n = 120) had elevated LVM index. The mean LVM index values for subjects with LVH based on the four different ECG Criteria were calculated (Table 1). Comparing the mean LVM index values for subjects who were ECG LVH positive to the normal volunteers shows that, in men, the Cornell and Cornell product criteria detect subjects with LVM index four S.D above normal while, in women, Sokolow-Lyon, Sokolow-Lyon product and Cornell product criteria detect subjects with LVM index three S.D above normal (Figure 1).

Conclusion: The ECG criteria of LVH detect a group of hypertensive patients with a substantially elevated LVM index. This is clinically relevant as the cardiovascular risk is higher in patients with high LVM index (Schillaci et al., 2000). This also implies that ECG criteria do not detect patients with lesser degrees of elevated LVM who are likely to be ECG LVH negative but who still have an increased cardiovascular risk (Schillaci et al., 2000). These patients should be identified using echocardiography or cardiac MRI.

Table 1. LVM index values for normals, hypertensives and hypertensives who were ECG LVH positive on ECG criteria for men and women

	LVM index (g/m^2) men	LVM index (g/m^2) women
Normals	77.8	61.5
Hypertensives	93.4	73.6
Sokolow-Lyon	106.6	83.4
Sokolow-Lyon Product	103.9	84.7
Cornell	115.5	80.7
Cornell Product	116.0	84.6

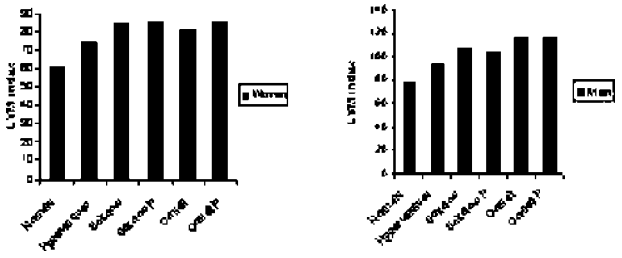

Figure 1. Bar Charts demonstrating the higher LVM index in hypertensive subjects who are ECG LVH positive compared with normals and the overall hypertensive cohort.

REFERENCE

Schillaci, G., Verdecchia, P., Porcellati, C., et al. (2000). Continuous relation between left ventricular mass and cardiovascular risk in essential hypertension. *Hypertension* 35:580–586.

480. Delayed Myocardial Enhancement in Hypertrophic Cardiomyopathy (HCMP) on MRI: Correlation with LV Motion Analysis by MR Tagging

Young Jin Kim, MD,[1] Jae Seoung Seo, MD,[1] Ji Eun Nam,[1] Byoung Wook Choi, MD,[1] Kyu Ok Choe, MD,[1] Jong Won Ha.[2] [1]*Diagnostic Radiology, Yonsei University College of Medicine, Severance Hospital, Seoul, Republic of Korea,* [2]*Department of Cardiology, Yonsei University College of Medicine, Severance Hospital, Seoul, Republic of Korea.*

Purpose: Delayed myocardial enhancement (DE) in the hypertrophic areas of HCMP that likely represent fibrosis has been recently reported. The purpose of our study was to evaluate the relationship of DE to regional left ventricular function using myocardial tagging method.

Methods: Cine imaging, gadolinium enhancement imaging with inversion recovery fast gradient echo sequence and myocardial tagging (CSPAMM) MRI were performed in 13 patients with HCMP. We analyzed 33 slices of the 13 patients, dividing each slice into 6 segments (total 198 segments). Location (6 segments), degree (mild or high), and pattern of DE were evaluated. End diastolic wall thickness (EDWT) and systolic wall thickening (SWT = end systolic WT-EDWT/EDWT) were measured in each segment on cine MRI. For the evaluation of regional LV function, circumferential strain

(Ecc; circumferential shortening) was calculated by analyzing CSPAMM images with HARP software.

Results: DE occurred in 11(84.6%) of the 13 patients and in 103 (52%) of the 198 segments, with a high frequency of localization in septum and regions where the right ventricle was attached. Circumferential strain (Ecc) was significantly low at the enhanced segments, compared with non-enhanced segments (-13.5 ± 0.60 vs -19.5 ± 0.38, $p < 0.0001$). In each segment, Ecc of the group with DE was significantly lower than that of the group without DE ($p < 0.05$). EDWT was thicker and SWT was less degree in enhanced segments than in non-enhanced segments (EDWT: 17.9 ± 0.59 mm vs 14.4 ± 0.46 mm, $p < 0.0001$, SWT: 0.42 ± 0.03 vs 0.50 ± 0.03, $p = 0.0472$). The degree of DE and Ecc shows an inverse correlation. The pattern of DE (ill-defined patchy, focal nodular, or circumferential) is not correlated with Ecc.

Conclusions: Delayed myocardial enhancement with various patterns and degrees is commonly found in the patients with HCMP. DE characteristically occurs in hypertrophied areas and the junctions of the septum and RV wall, and correlates inversely with regional LV function by myocardial tagging analysis.

481. Hypertrophic and Apical Cardiomyopathy: Myocardial Scarring by Gadolinium Cardiovascular Magnetic Resonance is an Independent Risk Factor for Sudden Death

Sophie Mavrogeni,[1] Panagiotis Iakovis,[1] George Athanasopoulos,[1] Athanasios Manginas,[1] Gregory Pavlidis,[1] Gregory Giamouzis,[1] Alexandros Anifantakis,[1] Marouse Douskou,[2] Alexios Giakoumelos,[2] John Seimenis,[3] Dennis V. Cokkinos.[1] [1]*Onassis Cardiac Surgery Center, Athens, Greece,* [2]*Bioiatriki MRI Unit, Athens, Greece,* [3]*Philips Hellas Medical Systems, Athens, Greece.*

Introduction: Myocardial scarring (SC) has been found in patients (pts) with hypertrophic cardiomyopathy (HCM) who are highly symptomatic or die suddenly.

Purpose: We assessed by cardiovascular magnetic resonance (CMR) the extent of SC in pts with HCM and apical cardiomyopathy (ApCM) and its correlation with incidence of risk factors for sudden death.

Methods: In a prospective study 15 HCM and 10 ApCM pts were selected for the presence of high (n = 10) or low (n = 15) risk for sudden death. Cine and gadolinium-CMR was performed. Gadolinium hyper-enhancement was assumed to represent SC. The extent of SC was compared with left ventricular morphology and function.

Results: SC was present in both HCM and ApCM pts. In HCM it was present only in hypertrophied areas (> 10 mm). It was patchy in 15 low risk HCM and extremely diffuse in the rest 10 high risk HCM. The extent of hyper-enhancement was greater in high risk HCM pts compared to those in low risk (32% vs. 10%, $p < 0.01$). The extent of SC correlated positively with diastolic wall thickness ($r = 0.41$, $p < 0.001$) and negatively with systolic wall thickening ($r = -0.31$, $p < 0.001$). In ApCM patchy SC was detected mainly in the apical area, but the extent of SC was significantly lower compared to high risk HCM (8% vs.29%, $p < 0.01$). No difference in the extent of SC was found between ApCM and low risk HCM.

Conclusions: Myocardial scarring is common in both HCM and ApCM, but ApCM presents a more benign form of the disease. It correlates positively with regional hypertrophy and has a diffuse and extensive pattern in high risk HCM. The extent of SC measured by gadolinium CMR is an independent predictive factor for sudden cardiac death and can be of great help in risk stratification of these patients.

482. Paradoxical *Increase* in Ventricular Torsion in Type I Diabetic Patients Under Tight Glycemic Control

Jina Chung, MD, Paul Abraszewski, MD, Xin Yu, ScD, Wei Liu, ScD, Shiow Jiuan Lin, MS, Marvin Ashford, MD, Andrew Krainik, MD, Shelton D. Caruthers, PhD, Janet B. McGill, MD, Samuel A. Wickline, MD. *Cardiology, Washington University School of Medicine, Saint Louis, MO, USA.*

Introduction: Fundamental mechanisms responsible for the putative "diabetic cardiomyopathy" have not been rigorously characterized, nor have earliest manifestations of cardiac dysfunction been reported in asymptomatic diabetic patients under tight glycemic management. Potentially subtle defects in ventricular twist and torsion, which are fundamental features of physiological cardiac contraction and relaxation, are quantifiable with cardiac magnetic resonance (CMR) tagging.

Purpose: We hypothesized that torsion measurements would identify subclinical contractile abnormalities in type I diabetic patients (DM) with normal left ventricular (LV) ejection fraction and mass. Because we observed higher resting heart rates (HR) in DM than in controls, we also sought to characterize the HR influence on torsion in healthy volunteers undergoing chronotropic stimulation.

Methods: Thirteen DM (42.2 ± 6.8 years old, 7 male) and six healthy controls (39.3 ± 6.6 years old, 4 male) underwent CMR studies with a 1.5 T scanner. Cine functional images were acquired with vector ECG-triggered steady-state gradient echo sequence. Two tagged short-axis images were acquired at base and apex using CSPAMM and the following parameters: TR, RR interval/25 phases; TE, 5–6 ms; FOV, 35 cm × 35 cm; Matrix size 115 × 256; Tag Resolution, 8 mm; Slice Thickness, 7 mm. Tagging analysis methods were previously described (Liu et al., in press). Briefly, myofiber twist was measured in four walls. Torsion was computed by normalizing twist by distance between basal and apical images.

To quantify the influence of chronotropic stimulation on torsion, nine healthy volunteers (32.8 ± 10.1 years old, 9 men) underwent CMR tagging. Short-axis apical images were acquired first at rest, then after atropine injection (0.7 ± 0.2 mg). The goal HR post-atropine was 30% above baseline HR to achieve the average resting HR of the DM. Twist was normalized by distance between mitral valve plane and apical images to obtain torsion.

The two sample t-test of unequal variance was used to compare results between DM and controls.

Torsions at baseline and post-atropine were compared using the paired Student's t-test.

Results: The duration of diabetes in DM was 21.8 ± 9.7 years. In all cases, insulin pumps were used for aggressive glycemic control (HbA_{1C} of 7.3 ± 1.3%). LV ejection fraction (55.1 ± 7.0 vs. 56.1 ± 3.1, %; $p = 0.69$) and LV mass/BSA (52.6 ± 15.2 vs. 60.4 ± 13.0, g/m2; $p = 0.31$) were normal and equivalent in DM and controls. However, significant *increases* in resting HR (77.2 ± 11.7 vs. 59.8 ± 1.9, bpm; $p = 0.009$) and global ventricular torsion (3.7 ± 0.9 vs. 2.7 ± 0.5, degree/cm; $p = 0.004$) were observed between DM and controls (see Fig. 1 and 2).

In the study to examine chronotropic influence on torsion, the mean HR was 66.7 ± 9.7 bpm at baseline, 88.0 ± 10.5 bpm post-atropine ($p < 0.001$). However, torsion was not significantly changed ($p = 0.19$), even at these HR augmentations exceeding the difference between DM and controls.

Conclusions: We observed a paradoxical increase in torsion in DM with tight glycemic control. The mechanism was shown to be unrelated to chronotropic influences of HR known as the "Treppe" effect. The *augmented* torsion in DM may represent a compensatory adaptation during systole whose cause is yet to be defined. Regardless, these early responses (increased torsion) differ considerably from the typical late maladaptive features (decreased torsion) manifesting in most cardiomyopathies. Accordingly, we propose that *increased* torsion may represent a sensitive and early predictive marker of the propensity to cardiac dysfunction in asymptomatic type I diabetic patients.

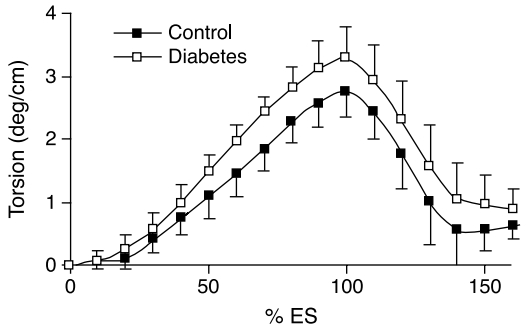

Figure 1. Torsion during cardiac cycle in % systolic duration (ES).

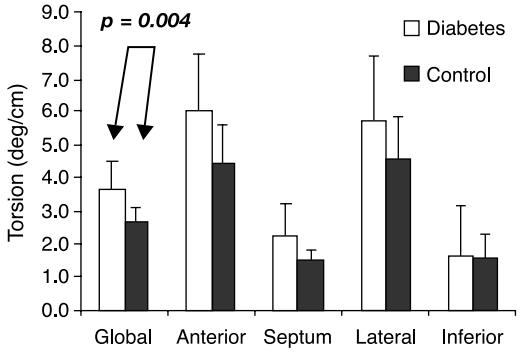

Figure 2. Global and segmental torsion.

REFERENCE

Liu, W., et al. HARP MRI tagging for direct quantification of lagrangian strains in rat hearts after myocardial infarction. *Magn. Reson. Med.* In press.

483. Cardiovascular Magnetic Resonance Imaging: The Gold Standard for Diagnosis of Left Ventricular Non-Compaction?

Steffen E. Petersen, MD,[1] Joseph B. Selvanayagam, MBBS, FRACP,[1] Frank Wiesmann, MD,[1] Matthew D. Robson, PhD,[2] Jane M. Francis, DCRR, DNM,[1] Robert H. Anderson, MD, FRCPath,[3] Hugh Watkins, MD, PhD, FRCP,[1] Stefan Neubauer, MD, FRCP.[1] [1]*Cardiovascular Medicine, John Radcliffe Hospital, Oxford, UK,* [2]*Ocmr, John Radcliffe Hospital, Oxford, UK,* [3]*Cardiac Unit, Institute of Child Health, University College London, London, UK.*

Introduction: Left ventricular non-compaction (LVNC) is characterized by a non-compacted myocardial layer in the left ventricle. Cardiovascular magnetic resonance (CMR) images this layer with unprecedented quality, particularly in the ventricular apex, where echocardiography has inherent difficulties.

Purpose: We aimed to test the diagnostic accuracy of CMR in distinguishing pathological LVNC from lesser degrees of trabecular layering seen in healthy volunteers, and in those with cardiomyopathies and concentric LV hypertrophy, potential differential diagnoses. We hypothesized that pathological trabeculation could be distinguished by determining the ratio of diameters of non-compacted to compacted myocardium (NC/C ratio) and that RV involvement would be common in LVNC.

Methods: We analyzed MR cine images using the 17 segment model in 45 healthy volunteers, 25 athletes, 39 patients with hypertrophic and 14 with dilated cardiomyopathy, 17 with hypertensive heart disease, and 30 with aortic stenosis, as well as images from 7 patients previously

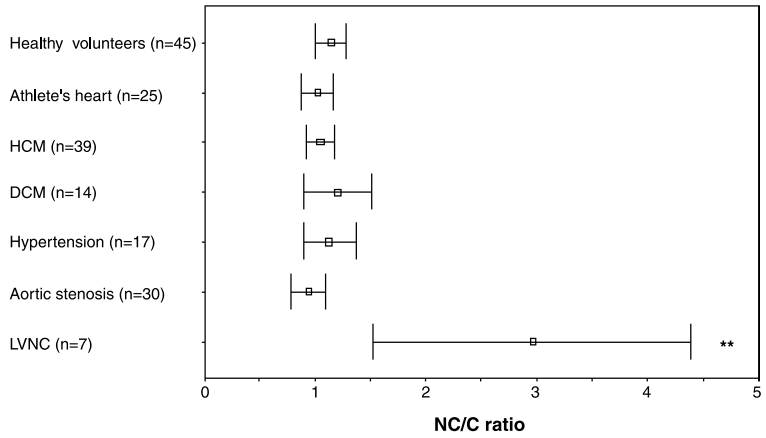

Figure 1.

diagnosed with LVNC in whom the diagnosis was supported by additional features.

Results: Areas of non-compaction were common, and occurred more frequently in all groups studied in apical and lateral, rather than in basal or septal, segments. A NC/C ratio of greater than 2.3 in diastole distinguished pathological non-compaction (Figure 1), with values for sensitivity, specificity, positive, and negative predictions of 86%, 99%, 75% and 99%, respectively. All patients with LVNC also showed RV non-compaction.

Conclusions: LVNC is diagnosed accurately with CMR using the ratio of non-compacted to compacted myocardium, and right ventricular non-compaction is typically present. This technique should be valuable in clinical practice for diagnosis and assessment of suspected LVNC.

484. Aortic Valve Area Calculation Using the Continuity Equation and Cine Planimetry: A Comparison with Echocardiography

Paula Tejedor, MD, Preeti Kansal, MD, Edwin Wu, MD, Kameswari Maganti, MD, Chiara Bucciarelli-Ducci, MD, Daniel C. Lee, MD, James C. Carr, MD, Thomas A. Holly, MD, Robert O. Bonow, MD. *Northwestern University, Chicago, IL, USA.*

Introduction: Unlike echocardiography (echo), the determination of aortic valve area (AVA) by cardiac MRI (CMR) has not yet been standardized or widely adopted. The continuity equation using velocity measurements and planimetry of the aortic valve orifice are two proposed methods to measure the AVA. However, optimal imaging parameters and methods of calculation have not been established. Additionally, data are limited comparing these CMR techniques with each other and to echocardiography.

Purpose: Using a phase-contrast, flow quantification sequence (PC-CMR), we obtained AVA measurements by continuity equation principles and direct planimetry of the aortic valve orifice. Additionally, we compared both CMR techniques to the standard methods used in transthoracic echocardiography.

Methods: We studied the AVA in 17 asymptomatic and symptomatic subjects referred for valvular assessment using a standard transthoracic echo and CMR protocol. CMR velocity-mapped images were obtained using a breath-hold, phase-contrast, cine flow sequence at a slice perpendicular to the aortic valve leaflet tips (Ao) at maximal opening in systole and in the left ventricular outflow tract (LVOT) below the valve annulus. Lowest possible velocity-encoding (VENC) values were chosen without causing velocity aliasing artifacts. Typical imaging parameters were: frames = 30, VENC = 300–700 cm/s, FOV = 260–360 mm, matrix size = 192, and breath-hold = 20–30 secs. Regions of interest (ROI) were traced along the margins of the elevated systolic velocity frames (increased signal intensity) at the aortic valve leaflets and the LVOT. Peak velocities corresponded to the maximal signal intensity within each ROI. Velocity time integrals (VTI) were measured by integrating the area under the peak velocity-time curve. The LVOT area was measured by planimetry of regions of maximal signal intensity in the phase-contrast flow images. Using these values, the AVA was determined using the continuity equation (LVOT area * LVOT-VTI/Ao-VTI) for both CMR and echo. Planimetry of the AVA by CMR was also measured in the same slice position used for the continuity equation measurements. The maximal signal intensity on the magnitude PC-CMR images was directly planimetered.

Results: The peak velocities for CMR (3.2 ± 0.6 m/s, range 2.1 to 4.4 m/s) correlated well with echo (3.7 ± 0.7 m/s, range 2.4 to 4.5 m/s; r = 0.7). However, the peak velocities by echo were greater by 0.5 ± 0.5 cm/s ($p = 0.002$). The mean AVA by CMR continuity equation (1.3 ± 0.6 cm^2) and planimetry (1.2 ± 0.5 cm^2) were not significantly different than that by echo continuity equation (1.1 ± 0.5 cm^2; $p = 0.08$ and $p = 0.07$ respectively). In addition, there was

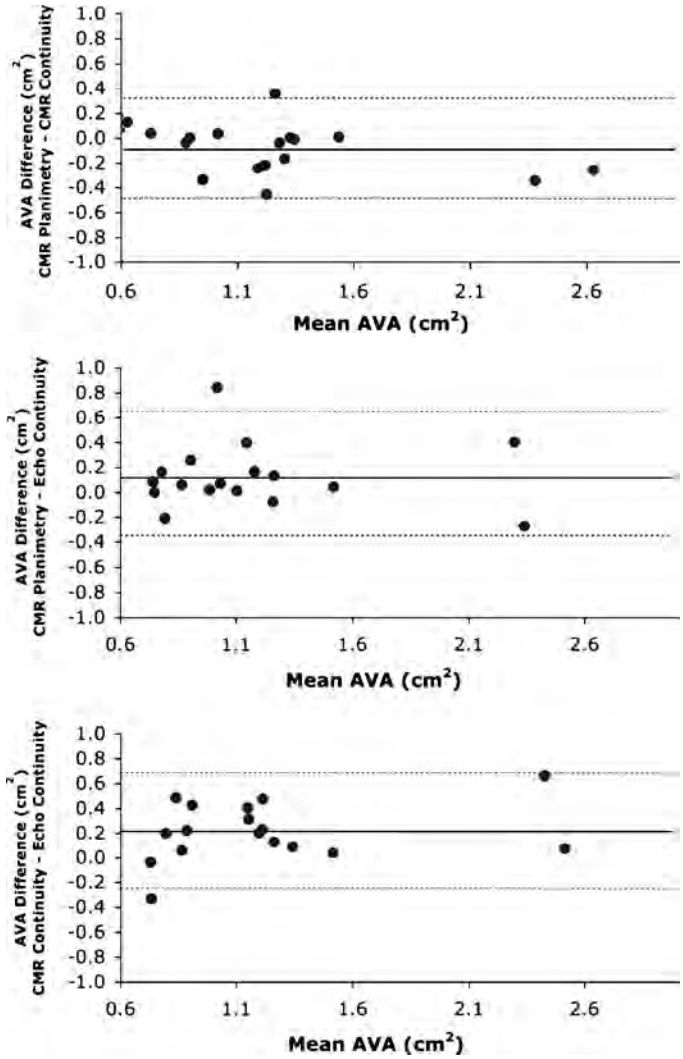

excellent correlation between the three different methods (CMR planimetry to CMR continuity, r = 0.94; CMR planimetry to echo continuity, r = 0.93; CMR continuity to echo continuity, r = 0.92). Bland-Altman analysis showed bias and limits of agreement (2 standard deviations) between CMR planimetry and CMR continuity of −0.09 (−0.50, 0.31) cm^2, between CMR planimetry and echo continuity of 0.12 (−0.39, 0.63) cm^2, and between CMR continuity and echo continuity of 0.21 (− 0.26, 0.68) cm^2.

Conclusion: AVA is easily determined by PC-CMR using planimetry and continuity methods. CMR planimetry valve areas correlate strongly with little bias compared to CMR continuity equation measurements. Although CMR AVA by both methods appear slightly larger, they also correlate strongly with AVA calculations obtained by echo. Differences between the continuity equation calculation by CMR and echo could be attributed to the smaller CMR velocity measurements and measurements of the LVOT areas. Therefore, CMR planimetry can readily and accurately determine the severity of aortic stenosis, although CMR-based continuity equation measurements are also applicable.

485. Complete Post-Operative (Ross Operation) Results Compared in Follow-Up Using Echocardiography and Magnetic Resonance Imaging

Brigitte Bathgate, MD,[1] Gabriele Saemann-Ischenko, MD,[1] Corina Cozub-Poetica, MD,[2] Rainer Ott, MD,[1] Ralf Banach-Planchamp, MD,[3] Hans-J. Schwarzmaier, Prof. MD,[4] Heinz-G. Klues, Prof. MD,[1] Volkhart Fiedler, Prof, MD,[2] Ibrahim Farah, MD,[5] Hans Greve, Prof, MD,[5] Hans Greve, Prof, MD.[5] [1]*Cardiology, Klinikum Krefeld, Krefeld, Germany,* [2]*Radiology, Klinikum Krefeld, Krefeld, Germany,* [3]*Cardiovascular MRI, Klinikum Krefeld, Krefeld, Germany,* [4]*Medical Technology, Klinikum Krefeld, Krefeld, Germany,* [5]*Heart Surgery, Klinikum Krefeld, Krefeld, Germany.*

Introduction: Ross operation is a method of aortic valve replacement involving autograft transplantation of the pulmonary valve, annulus and trunk into the aortic position. This is combined with reimplantation of the coronary ostia into the neo-aorta and reconstruction of the right ventricular outflow tract with a homograft conduit. For post-operative examination, TTE remains the de facto "gold standard." Even well-known limitations in the current assessment exist. Up to now, only particular segments of echocardiographic examinations were compared with MRI results.

Purpose: The aim of this study was to compare the efficacy of the method MRI and TTE, in order to evaluate comprehensive post-operative results in Ross patients.

Methods: Seventeen subjects- 14 male and 3 female (ages 31−57)- with a mean follow-up time of 30 months-underwent MRI and transthoracic echocardiography on the same day. The TTE (GE system 5) consisted of two dimensional, M-mode, colour flow measurement and doppler flow mode echocardiography. The MRI (1,5 Tesla Siemens Sonata scanner) protocol included cine true fisp bh images in short-axis slices and 2,3,4 CV for functional and volumetric analysis. Furthermore, this sequence was used for images of the right and left ventricular outflow tract; segments for the pulmonary autograft diameter (annulus, sinus region, sino-tubular junction and the distal part of the autograft); segments of the homograft diameter (annulus, distal part of the homograft) and areas of both valves. Flash 2 d through plane images (TR 61 ms; TE 3.1 ms) were used for the calculation of flow. True fisp 3 D bh native images (TR 180 ms; TE 1.29) were used to show the departure of the coronary arteries from the neo-aorta.

Results: All patients were examinable by echocardiography. However in 32 percent of those examined, the 2 D-mode images of the RVAT, homograft and pulmonary artery were suboptimal, due to obesity and/or anatomic limitations. By MRI, two patients (11 percent) could not enter the machine because of excess weight or anxiety problems. The pressure gradient across autograft and pulmonary homograft was found to be physiologic in all cases, except for one of mild pulmonary stenosis. A positive correlation

of $p = 0.157$ and $p = 0.035$, respectively, was recorded for tests of regurgitation of the autograft and homograft valves. One Patient was documented with a moderate regurgitation. Others showed minimal to mild levels or none at all. The valves showed good leaflet separation in both tests. But the valve areas measured with MRI were generally greater than those with TTE. There was a weak correlation between resulting values derived from these two tests, when valve area of homografts were considered (echocardiography limitation of exactitude in this area). Ejection fraction readings of the left ventricle showed a significance of 1.0 in the Wilcoxon Test. The comparison of the autograft (sinus region, sino-tubular junction), and homograft (homograft annulus) diameters showed a strong correlation of 0.779 and 0.823, followed by 0.774, respectively, by both methods. Only the diameters at the position of the autograft annulus and distal homograft anastomosis were poorly correlated (0.29, 0.34) using both techniques. Even in the absence of the navigator technique of MRI, the coronary ostia were clearly visible. In no cases were stenoses evident.

Conclusion: MRI is a valid tool in the follow-up examination of "Ross patients." In comparison to echocardiography, postive correlations were recorded for most parameters. Valve areas and some diameters of grafts were larger in MRI than in TTE. Some diameters could not be imaged reliably with echocardiography but could with MRI. Coronary ostia could only be demonstrated by MRI.

486. An Assessment of Early Cardiomyopathy in Autosomal Dominant Emery-Dreifuss Muscular Dystrophy

Gillian C. Smith, MSc,[1] Sanjay K. Prasad, MD,[1] Maria Kinali, MD,[2] Sharmeen Masood, PhD,[3] Guang-Zhong Yang, PhD,[4] Francesco Muntoni, MD,[2] Petros Nihoyannopoulos, MD,[5] Dudley J. Pennell, MD.[1] [1]*CMR Unit, Royal Brompton Hospital, London, UK,* [2]*Dubowitz Neuromuscular Unit, Hammersmith Hospital, London, UK,* [3]*Royal Society/Wolfson Medical Image Computing Laboratory, Imperial College, London, UK,* [4]*Imperial College, London, UK,* [5]*Department of Cardiology, Hammersmith Hospital, London, UK.*

Introduction: Emery-Dreifuss (EDMD) muscular dystrophy is an important condition comprising a phenotypically and genotypically heterogeneous familial disorder, initially characterised as an X-linked disease caused by mutations in the gene encoding the nuclear protein emerin. Recently the gene for the autosomal dominant form of Emery-Dreifuss muscular dystrophy (EDMD2) has been identified which encodes the lamins A and C. Whereas skeletal muscle symptoms are often mild, cardiac involvement may be profound and usually manifests by the second or third decade. These abnormalities range from ventricular arrhythmias and conduction defects to cardiomyopathy. Early detection of cardiac abnormalities is important therefore to select the best therapeutic strategy.

Aim: In this study, we attempted to identify a CMR marker of early myocardial dysfunction in unselected patients with EDMD2.

Methods: We studied eight consecutive genotyped patients with EDMD2 without pacemakers (age range 7–42, 6 males) and compared them to eight age-matched controls. All subjects underwent cardiovascular magnetic resonance (CMR) to assess function, intrinsic myocardial tissue contrast using T1 and T2 weighted spin echo (TSE) and extrinsic contrast (Gadolinium-DTPA late enhancement imaging). Harmonic phase imaging (HARP) was also performed to give an index of principal strain. Patients and control groups also underwent a comprehensive echocardiographic-Doppler examination. This included measurement of mitral annular velocities using pulsed tissue Doppler. Myocardial Velocity Gradients (MVG) were derived from colour m-mode images from the parasternal long axis view.

Results: Strain patterns derived from HARP sequences, demonstrated a significant impairment in anterior wall contractility compared with the normal subjects, $0.73 \pm 0.55\%$ vs $0.25 \pm 0.28\%$ ($p = 0.03$). There was no significant difference in corrected left atrial volumes, 41 ± 25 ml/m^2 vs 38 ± 6 ml/m^2 for the control group ($p = 0.69$). Left ventricular mass index was 60 ± 18 g/m^2 vs 61 ± 14 g/m^2 ($p = 1$). Left ventricular volumes were similar at 73 ± 15 ml/m^2 for the study group and 72 ± 7 ml/m^2 for the controls ($p = 0.86$) and there was no difference between ejections fractions at 0.72 ± 5 and 0.72 ± 4 ($p = 0.78$) respectively. Neither right ventricular corrected volumes showed a significant difference at 62 ± 18 ml/m^2 vs 69 ± 10 ml/m^2 ($p = 0.36$) or right ventricular ejection fraction, 58 ± 11 vs 63 ± 8 ($p = 0.32$). Finally right atrial volumes showed no significant difference at 60 ± 28 ml/m^2 vs 55 ± 13 ml/m^2 ($p = 0.68$). No patient showed late gadolinium enhancement to suggest myocardial fibrosis. Of the echo derived parameters the early diastolic MVG was lower in patients than in controls, 4 ± 1.2 s^{-1} vs. 7.1 ± 2.7 s^{-1} ($p = 0.02$). while systolic MVG were similar between groups 3.4 ± 1.14 s^{-1} vs 3.5 ± 1.07 s^{-1} ($p = 0.88$).

Conclusion: These results suggest that patients with EDMD2 exhibit abnormal left ventricular function prior to developing any cardiac symptoms. The absence of late enhancement following administration of gadolinium-DTPA suggests that there may be an intrinsic intracellular abnormality which may be evident at an early stage of the disease rather than fibrosis. HARP tagging and myocardial velocity gradients from TDI differentiated between asymptomatic EDMD2 patients and controls and thus provide sensitive methods of assessing myocardial dysfunction prior to the development of cardiovascular symptoms.

487. Influence of the Cardiac Cycle on Measures of Pulmonary Vein Size

Thomas H. Hauser, Susan B. Yeon, Seth McClennen, Kraig V. Kissinger, Mark E. Josephson, Neil M. Rofsky, Warren J. Manning. *Cardiovascular Division, Beth Israel Deaconess Medical Center, Boston, MA, USA.*

Introduction: Understanding pulmonary vein (PV) anatomy is important for investigating the pathophysiology of atrial fibrillation (AF) and the consequences of PV ablation, such as post-procedure PV stenosis. Current magnetic resonance angiography (MRA) and computed tomography angiography methods for imaging the PV are not ECG gated and do not account for potential changes in PV anatomy during the cardiac cycle. We hypothesized that significant changes occur during the cardiac cycle and that measures from non-ECG gated techniques reflect mean data during the cardiac cycle.

Methods: A consecutive series of patients with a history of AF referred for evaluation of PV anatomy were imaged with conventional non-ECG gated contrast-enhanced (CE) MRA and gated cine-SSFP MR. PV diameter, perimeter and cross-sectional area (CSA) were measured using both MR methods. Cardiac cycle data were normalized to a heart rate of 60/min.

Results: A total of 14 subjects were included in the study cohort. There were 10 men and 4 women with a mean age of a 51 ± 12. A total of 48 PV were evaluated. All subjects were in sinus rhythm at the time of MR imaging. The difference between the maximal and minimal size was 16 ± 9% for diameter, 15 ± 8% for perimeter, and 27 ± 13% for CSA. Maximal PV size occurred in early ventricular diastole (101 ± 112 ms after ventricular end-systole). Minimal PV size occurred in early ventricular systole (212 ± 90 ms before ventricular end-systole). All CE-MRA measures of PV anatomy were significantly greater than the ECG gated minimal PV size ($p < 0.001$ for all) and similar to the maximal PV size ($p \geq 0.2$ for all, Table 1). Six subjects (20 PV) underwent repeat imaging 32 ± 7 days after PV ablation. There was no significant change in the maximal-minimal difference for any measure of PV anatomy after ablation ($p > 0.05$ for all).

Conclusion: All measures of PV anatomy vary significantly within the cardiac cycle. This variation persists after PV ablation. Anatomic measurements from non-ECG gated CE-MRA are similar to the maximal size during the cardiac cycle. Variations in PV anatomy over the cardiac cycle should be considered when comparing measures of PV size obtained using gated and non-gated imaging modalities.

Table 1. Maximal and minimal pulmonary vein size compared to measures from contrast enhanced MRA

	Diameter (mm)	Perimeter (mm)	CSA (mm^2)
Maximal PV Measure	18 ± 4	53 ± 11	216 ± 95
Minimal PV Measure	15 ± 4	45 ± 10	155 ± 67
CE-MRA PV Measure	19 ± 5	52 ± 11	200 ± 82

488. Cardiovascular 3D MRI Assessment of Diastolic Dysfunction; A Comparison with Echocardiography

Vikas K. Rathi, MD, Mark Doyle, PhD, June Yamrozik, Ronald B. Williams, Craig Truman, Diane A. Vido, Valerie Bress, Ketheswaram Caruppannan, MD, Robert W. W. Biederman, MD. *Allegheny General Hospital, Pittsburgh, PA, USA.*

Introduction: Cardiac MRI's (CMR) spatial resolution, 3D nature and precision provide superiority over echocardiography (TTE) for systolic function. However, no assessment of diastolic function (DF) over a range of lusitropy has been performed by CMR. Limitations of DF by TTE are manifest, yet it remains the *de facto* "gold standard."

Hypothesis: We hypothesize that CMR DF data is comparable to TTE but without its acquisition limitations.

Methods: 31 subjects, age: 26–84 (male 21, female 10), including 10 controls, underwent optimized CMR (TR = 19 ± 3 ms) phase velocity mapping (PVM) (GE 1.5 TCV/i, Milwaukee, WI). DF was diverse: 11 impaired relaxation, 3 restrictive, 2 pseudonormalized, 3 EA fusions and 12 normal. Sampling: 3D mitral (MV) plane, 3D right upper pulmonary vein (PV), 2 hr post CMR a blinded PW Doppler TTE was performed (Philips 5500, Andover, MA).

Results: All MV and PV were imaged by CMR (31/31,100%), while TTE imaged all MV (31/31,100%) but only 19/31 PV (61%). No difference in acquisition + offline processing time existed. Morphologically, CMR 100% correctly identified inflow abnormalities as assessed by TTE. MV E and A velocities by CMR were somewhat lower than TTE but well correlated ($r = 0.81$, $p < 0.05$, Fig. 1). The E:A ratio and deceleration time (DT) were not statistically different between CMR and TTE and had excellent agreement by Bland-Altman analysis: Bias − 0.29, and − 10.3 for E/A and DT, Fig. 2.

Conclusions: CMR PVM can derive accurate diastolic indices. Morphologically, there is homology between CMR and TTE despite heterogeneous pathology with near exact inflow velocities. Given the advantages CMR provides for systole, diastolic applications appear equally possible.

489. Influence of Scar Extent as Detected By Contrast Enhanced Magnetic Resonance Imaging on Left Ventricular Parameters in Patients with Hypertrophic Cardiomyopathy

Giancarlo Casolo,[1] Rosanna Manta, MD,[1] Jacopo Del Meglio, MD,[1] Jacopo Olivotto, MD,[1] Franco Cecchi, MD,[1]

Luigi Rega, MD.[2] [1]*Clinica Medica e Cardiologia, Florence, Italy,* [2]*Department of Radiology, Florence, Italy.*

Introduction: Some patients with Hypertrophyc Cardiomyopathy (HCOM) show in-vivo evidence for intramyocardial scarring when imaged by Contrast Enhanced (CE) Cardiovascular Magnetic Resonance (CMR). Regions of scar appear as hyperenhanced areas of variable size and shape in these subjects. Some data indicate that the presence of scarring may have independent prognostic value.

Purpose: We investigated the presence and amount of scarring by CE-CMR in a population of HCOM patients participating to a specialised ambulatory program. Also we studied the relationship between the pattern and extent of hyperenhancement and several different parameters including left ventricular volume, regional and global function, and mass.

Methods: 28 patients with HCOM (23 males and 6 females; age 46 ± 18 yrs) were studied. All of them had a left ventricular septal thickness > 15 mm. CMR was performed by using a 1.5 Tesla imager (Philips, Intera; The Netherlands) and a 5 element cardiac surface coil. A 3D breath-hold IR-TFE sequence was used 15 minutes after the I.V. injection of 0.2 mM/Kg of Gd-DTPA. The inversion time was adjusted to null the signal of the myocardium, usually between 225 and 275 msec. The left ventricle was studied from the base to the apex within a breath-hold.

Functional parameters were measured in each patient by using repeated breath-hold Cine-Balanced FFE series and the SENSE technology to cover the whole left ventricle. Quantitative measurements were performed on a dedicated consolle (Viewforum, Philips; The Netherlands).

STUDY POPULATION

Age (Yrs)	46 ± 18
Sex	23 M, 6 F
ECHO Maron Class	I 27%
	II 10%
	III 59%
NYHA Class	I 59%
	II 34%
	III 7%
LVEF	
> 65%	72%
< 65%	27%
LV obstruction	27%

Results: Areas of hyperenhancement on delayed images (SCAR) were detected in all the subjects. We found 3 main patterns of SCAR: 1) Infarct-like, well detectable, with a variable position with respect to the endocardium, 2) Salt-and-pepper, with small scattered foci of hyperenhancement, and 3) Junctional, with nodular foci located in the interventricular septum where the right ventricle connects to the left. SCAR volume was significantly related to left ventricular mass ($r^2 = 0.55$; $p < 0.0001$) while SCAR% was related directly to end-systolic volume ($r^2 = 0.6$; $p < 0.0001$) and inversely to ejection fraction ($r^2 = -0.39$; $p < 0.003$). Segmental wall thickness was weakly but significanlty related to wall thickening ($r^2 = 0.21$; $p < 0.0001$). The segmental volume of SCAR was also related to wall thickness ($r^2 = 0.089$; $p < 0.001$), while % SCAR of each segment was inversely related to wall thickening ($r^2 = 0.09$; $p < 0.001$).

RESULTS OF CE-CMR

LVEF	69 ± 12%	36–82%
Stroke volume	78 ± 26 ml	37–107 ml
End diastolic volume	113 ± 33 ml	50–211 ml
End systolic volume	35 ± 18 ml	13–75 ml
Left ventricular mass	212 ± 122 g	81–609 g
Maximum septal thickness	23 ± 6 mm	15–30 mm
Volume of hyperenhancement	37 ± 32 mm^3	2–150 mm^3
Volume of hyperenhancement % over LVmass	18–14%	2–70%

Conclusions: Intramyocardial scar is common in HCOM patients as higlighted in-vivo by CE-CMR. The extent of fibrosis is significantly and directly related to the amount of left ventricular mass. Also, scar affects left ventricular volume and function in HCOM patients as it appears to be related to left ventricular dimensions, ejection fraction, and regional segmental parameters. The detection and measurement of SCAR in HCOM has clinical relevance as relates to both left ventricular dimensions and function. Further studies are needed to establish the prognostic value of SCAR and of its different patterns.

490. Detection of Myocardial Infarction in Symptomatic Patients Without Coronary Artery Disease Undergoing Electrophysiological Testing

Rishi Kaushal,[1] David Fieno, MD,[2] Michael Radin, MD,[3] Jagat Narula, MD,[4] Alan Kadish, MD,[5] Kalyanam Shivkumar, MD, PhD,[1] Jeffrey Goldberger, MD,[5] David Bello, MD.[4] [1]*David Geffen School of Medicine at UCLA, Los Angeles, CA, USA,* [2]*Medicine, Cedars-Sinai Medical Center, Los Angeles, CA, USA,* [3]*Pacific Coast Imaging, Irvine, CA, USA,* [4]*Medicine, University of California at Irvine, Irvine, CA, USA,* [5]*Medicine, Northwestern University, Chicago, IL, USA.*

Introduction: Cardiac Magnetic Resonance Imaging (CMRI) can identify myocardial infarction (MI). Detection of unrecognized MI has significant clinical implications. MI is the most common substrate for reentrant ventricular arrhythmias. In patients with coronary artery disease (CAD), infarct size determined by CMRI is a better identifier of patients who have ventricular tachycardia than ejection fraction (EF). In the absence of CAD, MI is rare.

Purpose: We sought to use cardiac MRI in patients without CAD, but with symptoms and/or documented arrhythmias who were undergoing electrophysiological testing.

Methods: Planimetry of contrast images obtained from CMRI was used to measure infarct mass and surface area by two readers blinded to electrophysiological study (EPS) results.

Results: 23 patients without CAD (mean age: 45 ± 16 years, 48% male, mean EF 49 ± 13%) underwent EPS for evaluation of palpitations (34% of patients), syncope (25%), and/or documented ventricular arrhythmias (34%). 5 patients had hypertrophic obstructive cardiomyopathy (HOCM) and 8 had dilated cardiomyopathy (DCM). During EPS, 15 patients (65%) had no inducible ventricular arrhythmias, 2 patients (8%) had inducible monomorphic ventricular tachycardia (VT), and 6 patients (26%) had inducible polymorphic VT or ventricular fibrillation (PVT/VF). CMRI identified MI in 11 patients (48%) with a mean infarct size as percentage of left ventricular mass of 11 ± 10. MI was visualized in 4/5 patients with HOCM (mostly septal infarcts), 5/8 patients with DCM, and in 2 patients with normal EF.

Conclusions: In patients without CAD undergoing electrophysiological testing for symptoms and/or documented ventricular arrhythmias, the prevalence of myocardial infarction is higher than in the general population. Cardiac MRI should be considered in patients presenting with unexplained spontaneous or inducible ventricular arrhythmias.

491. Long-Term Follow-Up of Patients with Acute Myocarditis: Comparison of Different MRI Techniques

Anja Zagrosek, MD, Hassan Abdel-Aty, MD, Ralf Wassmuth, MD, Philipp Boyé, MD, Andreas Kumar, MD, Daniel Messroghli, MD, Petra Bock, MD, Jeanette Schulz-Menger, MD, Matthias G Friedrich, MD, Rainer Dietz, MD. *Franz-Volhard-Klinik, Charité Campus Buch, Kardiologie, Universitätsmedizin Berlin (HELIOS Klinikum), Berlin, Germany.*

Introduction: Different MRI techniques have been used to study and to diagnose myocardial inflammation in patients with acute myocarditis. The prognostic value of the various techniques has not been compared to each other.

Purpose: To assess the prognostic performance of two different contrast-enhanced MRI techniques currently in use for the diagnosis of acute myocarditis.

Methods: 15 patients (12 male, mean age ± SD 38 ± 12 years) with a history of acute myocarditis as defined by typical clinical symptoms, history, ECG changes, rise of myocardial enzymes, and absence of coronary artery disease on X-ray angiography, underwent contrast-enhanced MRI in the acute stage (5.6 ± 4.2 days after onset of symptoms) and 23.5 ± 10 months later. The imaging protocol included "early" relative enhancement (RE; axial spin-echo sequence comparing myocardial and skeletal uptake of contrast agent) and delayed enhancement (DE) imaging (inversion recovery-prepared gradient-echo sequence). The results of RE imaging were compared to those of a control group of 23 healthy subjects (13 males, 29.3 ± 10 years). Left-ventricular (LV) function was assessed from biplane cine steady-state free precession images.

Results: Relative enhancement was increased in all patients in the acute phase (6.0 ± 4.9 vs. 3.7 ± 2.3 in healthy subjects, $p < 0.001$), but had normalized in 11 cases (73%) on follow-up (mean 4.4 ± 2.1). 5 patients (66%) showed irregularities on DE imaging in the acute phase, which were still present in all of the patients on follow-up. The LV ejection fraction increased from 58.9 ± 8.9% to 65.2 ± 7.6% ($p < 0.01$), and none of the patients reported any clinical symptoms at follow-up. Neither the presence of RE or DE findings, nor the size of RE in the acute phase were predictive for LV function on follow-up.

Conclusions: While RE showed greater sensitivity to detect myocardial inflammation in the acute stage of myocarditis, neither RE nor DE imaging predicted long-term recovery of LV function in our group of patients. However, RE can be used to monitor the decay of the disease. This is not possible with DE imaging, which remains positive even in the chronic phase. Larger studies are required to assess outcome in specific sub-groups of patients.

492. Left Ventricular Outflow Tract Planimetry by Cardiovascular Magnetic Resonance Detects Latent Obstruction in Patients with Hypertrophic Cardiomyopathy

Jeanette Schulz-Menger, Hassan Abdel-Aty, Rainer Dietz, Matthias G. Friedrich. *Cardiology, Franz-Volhard-Klinik, Charité Campus Buch, Berlin, Germany.*

Background: Measurement of the left ventricular outflow tract (LVOT) using cardiovascular magnetic resonance (CMR) in hypertrophic cardiomyopathy (HCM) is feasible and has been shown to correlate with the clinical severity of the disease. Data relating this measurement to the more clinically utilized

Doppler-derived pressure gradient (PG) applying echocardiography (Echo) are lacking. Whether rest LVOT measurement can differentiate between the obstructive and non-obstructive forms of the disease remains illusive. We sought to correlate CMR-LVOT measurement to Echo-PG and to investigate the utility of CMR-LVOT to identify the different types of HCM (obstructive, latent and non-obstructive).

Methods: We studied 37 HCM patients (22 males, 56 ± 15 years) and 14 healthy subjects (7 males, 28 ± 10 years) using CMR and Echo. CMR and Echo were performed on state of the art machines. Minimal systolic LVOT area was quantified by applying steady state free precession sequence (TR 3.8 ms, TE 1.6 ms, number of phases = 20) after full coverage of the LVOT area (4–7 slices, slice thickness = 4 mm, no gap). PG was quantified at rest and after Valsalva maneuver. The median inter-study duration between CMR and echocardiography was 2 days. Patients were divided into 3 groups based on their PG: 1) non-obstructive HCM (PG < 30 at rest and after provocation, n = 11) 2) Latent obstructive HCM (PG < 30 at rest and > 30 after provocation, n = 10),) and 3) Obstructive HCM (PG > 30 at rest, n = 16).

Results: LVOT measurements in HCM patients showed a significant inverse correlation with the Doppler-derived PG both at rest (Spearman correlation coefficient = − 0.64, $p < 0.0001$) and after provocation (− 0.71, $p < 0.0001$). Compared to volunteers with a mean LVOT area of 4.8 ± 0.8 cm^2, the area was significantly smaller in patients with non-obstructive HCM (3.5 ± 1.1 cm^2, $p < 0.002$), latent obstructive (2.2 ± 1.5 cm^2, $p < 0.002$) and obstructive HCM (1.6 ± 0.6 cm^2, $p < 0.0001$) respectively. Patients with non-obstructive HCM had significantly larger LVOT than latent (3.5 ± 1.1 cm^2 vs. 2.2 ± 1.5 cm^2, $p < 0.013$) or obstructive HCM (3.5 ± 1.1 cm^2 vs. 1.6 ± 0.6 cm^2, $p < 0.0001$) respectively. When the latent obstructive and obstructive forms were considered together as obstructive HCM, significant differences in LVOT still existed between the obstructive and non-obstructive forms of the disease (1.8 cm^2± 1.0 vs. 3.5 ± 1.1 cm^2, $p < 0.0001$). No significant difference was found between the LVOT in latent and obstructive HCM (2.2 ± 1.5 cm^2 vs. 1.6 ± 0.6 cm^2, $p = 0.478$).

Conclusion: CMR-derived LVOT area measurements correlate with pressure gradient as assessed by Echo. Measuring the LVOT area by CMR has the potential to differentiate between obstructive and non-obstructive HCM and to identify patients with latent LVOT obstruction without the need for provocation.

493. Assessment of Ventricular Coupling with Real-Time MRI, and Its Value to Differentiate Patients with Constrictive Pericarditis from Restrictive Cardiomyopathy. Preliminary Results

Marco Francone,[1] Maria Kalantzi,[1] Frank E. Rademakers,[2] Marie-Christine Herregods,[2] Ilse Crevits,[1] Steven Dymarkowski,[1] Jan Bogaert.[1] [1]*Radiology, Gasthuisberg University Hospital, Leuven, Belgium,* [2]*Cardiology, Gasthuisberg University Hospital, Leuven, Belgium.*

Purpose: Since pericardial thickness is not unfrequently normal (< 2 mm) in patients with surgically-proven constrictive pericarditis (CP), this morphologic parameter may not be reliable to diagnose CP. Assessment of the functional impact of CP on ventricular filling with real-time MRI may be more reliable to differentiate CP from restrictive cardiomyopathy (RCM).

Method and Materials: In 15 CP, 10 RCM patients and 15 normal subjects, real-time MRI using a SSFP sequence in the midventricular cardiac short-axis (temporal resolution: 60 ms) was performed during continuous breathing with deep in- and expiration. The influence of respiration on ventricular septal position and total septal excursion normalized to total biventricular diameter was evaluated.

Results: Inspiratory flattening/inversion was found in CP: 15; normals: 1; RCM: 0. Flattening/inversion during early ventricular filling was always most prominent during onset of inspiration. Total respiratory septal excursion was significantly large in CP (18.7 ± 1.2%) than in normals: (7.1 ± 2.4%) $p < 0.0001$ and RCM (5.8 ± 2.1%) $p < 0.0001$. A cut-off value of 11.9% (mean ± 2SD) is useful to discriminate CP patients from normal subjects and RCM patients, even in the presence of a normal pericardial thickness on MRI (present in 33% of CP in this series).

Conclusions: Pathologic ventricular coupling, ie, abnormal ventricular septal flattening or inversion during onset of inspiration and increased total respiratory septal excursion, is a reliable criterium to differentiate CP from RCM patients.

494. Improved Image Quality for Edema Detection in Acute Myocarditis Using T2-Weighted Sequences

Corina Cozub-Poetica, MD,[1] B. Bathgate, MD,[2] R. Ott, MD,[2] R. Banach-Planchamp,[3] H. J. Schwarzmaier, Prof. MD,[4] V. Fiedler, Prof. MD,[1] H.-G. Klues, Prof. MD.[2] [1]*Department of Radiology, Klinikum Krefeld, Krefeld, Germany,* [2]*Department of Cardiology, Klinikum Krefeld, Krefeld, Germany,* [3]*Department of Cardiovascular MRI, Klinikum Krefeld, Krefeld, Germany,* [4]*Department of Medical Technology, Klinikum Krefeld, Krefeld, Germany.*

Introduction: MR-imaging can detect myocardial changes due to acute myocarditis. However, the strong T2-weighted TIRM sequence currently used for this purpose is often inflicted with substantial artifacts hindering the precise differentiation between the inflammation related edema and the unaffected myocardial tissue. Therefore, new imaging concepts are desired.

Purpose: Comparison of different fluid-sensitive T2-weighted sequences for the visualization of localization and extent of the myocardial edema in patients clinically diagnosed (ECG, troponin, ultrasound) with acute myocarditis.

Methods: Twenty-six patients (22 male, 4 female, no coronary heart disease) with clinically documented myocarditis were included into this study. They underwent MR-imaging using three different T2-weighted sequences (TIRM (TR/TE: 2RR*/60 ms), HASTE fs (multislice, TR/TE: 2RR*/72 ms), and HASTE-IRM (multislice, TR/TE: 500/25–39 ms, 2 RR: 1400–2000 ms). In addition, all patients were also investigated for a late enhancement and received a CINE imaging. The images were analyzed visually (2 independent readers). The respective images were assigned to three different categories: good (+ +), acceptable (+), and not suited for clinical diagnostics (−). Twelve of these patients exhibited a myocardial edema.

Results: All sequences allowed the detection of the myocardial edema if present. Good image quality (+ +) were documented for TIRM in 14, for HASTE fs in 23 and for HASTE-IRM in 13 patients. An acceptable visualization (+) was found for TIRM in 8, for HASTE fs in 2, and for HASTE-IRM in 9 patients. The remaining images (TIRM: 4, HASTE fs: 1, HASTE-IRM: 4) were regarded as unsuited for clinical diagnostics (−).

Conclusions: In the present study, T2-weighted images based on the HASTE fs technique provided the best image quality. The diagnostic quality of these images was superior to the material obtained from the TIRM sequences usually employed for edema diagnostics in the framework of acute myocarditis.

495. Does Subclinical Hypothyroidism Affect Cardiac Pump Performance? Evidence from a Magnetic Resonance Imaging Study

Alessandro Pingitore, MD, PhD, Barbara Sacttini, MSc, Vincenzo Positano, MSc, Brunella Favilli, MSc, Daniele De Marchi, RT, Stefano Turchi, BSc, Andrea Ripoli, PhD, Giorgio Iervasi, MD, Massimo Lombardi, MD. *Clinical Physiology Institute, CNR, Pisa, Italy.*

Objectives: To assess the effects of subclinical hypothyroidism (SHT) on the cardiac volumes and function.

Background: The cardiovascular system is one of the principal targets of thyroid hormone. Subclinical hypothyroidism (SHT) is a common disorder that may represent "early" thyroid failure.

Methods: Thyroid profile was evaluated in 30 SHT females and in 20 matched controls (N). Left ventricular end-diastolic (ED), end-systolic (ES) volume (V), stroke volume (SV), cardiac index (CI) and systemic vascular resistance (SVR) were calculated by cardiac magnetic resonance (CMR). Regional greatest systolic lengthening (E1) and shortening (E2) were calculated by tagging CMR.

Results: EDV was lower in SHT than in N (64.3 ± 8.7 vs 81.4 ± 11.3 ml/m2, $p \leq 0.001$) as well as SV (38.9 ± 7.5 vs 52.5 ± 6.1 ml/m2, $p < 0.001$) and CI (2.6 ± 0.5 vs 3.7 ± 0.4 l/(min•m2), $p < 0.001$). SVR was higher in SHT (12.5 ± 2.5 vs 8.6 ± 1.1 mmHg•min/(l•m2), $p = 0.003$). E1 was higher in N than in SHT at basal ($p = 0.007$), equatorial ($p = 0.05$), and apical ($p = 0.008$) levels, and E2 at equatorial ($p = 0.001$) and apical ($p = 0.001$) levels. All parameters normalised after replacement therapy. A negative correlation between TSH and EDV ($p < 0.001$), SV ($p < 0.001$), CI ($p < 0.001$), and E1 at the apical level ($p < 0.001$), and a positive correlation between TSH and SVR ($p < 0.001$) and E2 at the apical level ($p < 0.001$) were found.

Conclusions: SHT significantly decreased cardiac preload while increased after-load with consequent reduction in stroke volume and cardiac output. Replacement therapy fully normalized the hemodynamic alterations.

496. Coronary Sinus Flow Measurement at 3T

Karin Markenroth,[1] Catarina Holmqvist,[2] Marcus Carlsson,[3] Peter Cain,[3] Håkan Arheden,[3] Freddy Ståhlberg.[4] [1]*MR-department, Lund University Hospital, Lund, Sweden,* [2]*Department of Radiology, Lund University Hospital, Lund, Sweden,* [3]*Department of Clinical Physiology, Lund University Hospital, Lund, Sweden,* [4]*Department of Radiophysics, Lund University Hospital, Lund, Sweden.*

Introduction: Velocity mapping of blood flow in the coronary sinus (CS) remains challenging due to large vessel motion and distortion over the RR-cycle (Hofman et al., 1998). Quantitative flow (QF) measurements in this vessel require simultaneous high temporal and spatial resolution, in addition to accurate phase mapping. This can be achieved in small, moving vessels as demonstrated in phantom (Arheden et al., 2001) and experimental studies (Lund et al., 2000). Velocity mapping at 3 T has been demonstrated and the concept of parallel imaging has been evaluated in phase contrast imaging (Thunberg et al., 2003).

Purpose: The aim of this study was to obtain QF measurements in the coronary sinus by combining high field strength, SENSE and segmented k-space velocity mapping, as well as calculating global myocardial perfusion.

Methods: Phase images were acquired in vitro and in vivo on a Philips Gyroscan Intera 3.0 T, using a retrospective VCG-triggered segmented fast GRE velocity-mapping sequence (TE/TR/α = 3.5/5.3/10°, resolution 1.44 × 1.55 × 8.00 mm^3, v_{enc} 40–50 cm/s). A six-channel phased-array cardiac coil was used for SENSE parallel imaging (R = 2). Integration of the flow curve over the RR-interval gave the CS flow (ml/min) (CSQF). Several consecutive measurements were performed on four healthy volunteers, testing repeatability. The left ventricular mass (LVM) was also determined. Two independent observers analyzed the data. No additional phase corrections were made.

Results: In a flow phantom, flow values measured manually and with MR showed high correlation (0.99). In vivo, the pattern of flow showed a similar and bi-phasic pattern in all

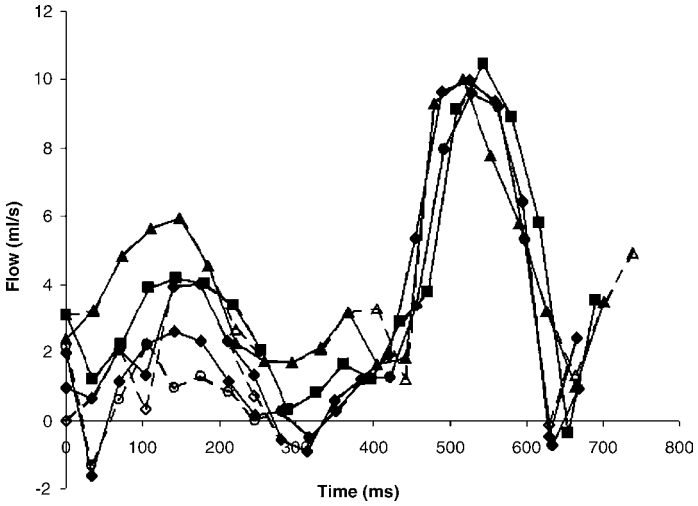

Figure 1. Four consecutive measurements of CS flow in one volunteer. Evaluation of first observer (solid lines) and second observer (dashed lines).

volunteers. Measured average perfusion (CSQF/LVM ml/(g min)) was in the range 0.7–1.1 ml/(g min), and in agreement with values found in the literature (Kawada et al., 1999).

Conclusions: Velocity mapping at 3 T holds promise for accurate QF results in the CS using a segmented k-space strategy combined with SENSE parallel imaging (Fig. 1).

REFERENCES

Arheden, H., et al. (2001). *J. Magn. Reson. Imaging* 18:722–728.
Hofman, M. B., Wickline, S. A., Lorenz, C. H. (1998). *J. Magn. Reson. Imaging* 8:568–576.
Kawada, N., et al. (1999). *Radiol* 211:129–135.
Lund, G., et al. (2000). *Radiol* 217:487–493.
Thunberg, P., Karlsson, M., Wigström, L. (2003). *Proc 11th ISMRM Abstract*. 1677.

497. Brachial Arterial Reactivity in Thalassemia Major with Significant Cardiac Iron Loading

Mark A. Westwood,[1] Mark A. Tanner, MBBS,[1] Morten Sorensen, MD,[1] Renzo Galanello, MD,[2] Dudley J. Pennell, MD.[1] [1]*CMR Unit, Royal Brompton Hospital, London, UK,* [2]*Thalassemia Department, Ospedale Microcitemico, Cagliari, Italy.*

Introduction: In Thalassaemia Major (TM), repeated transfusions are needed to treat anaemia and this leads to inexorable iron accumulation in the tissues. Cardiomyopathy and cardiac failure remain the commonest cause of death in TM in developed countries and myocardial iron deposition is believed to be the cause. However, the iron deposition occurs not only in the myocardium, but also in the vasculature. Iron deposition in the vasculature leads to endothelial dysfunction and could contribute to the development of cardiac complications in TM.

Endotheial function is accurately and reproducibly assessed by CMR via changes in cross sectional area of the brachial artery. CMR T2* has been established as an accurate method for the detection of myocardial iron deposition. Brachial arterial reactivity has been shown to correlate with myocardial iron deposition in a small, highly selected cohort of males, only some of which had significant myocardial iron deposition. We therefore sought to determine if the same relationship existed with a larger less selected cohort, but in all of whom there was significant myocardial iron deposition.

Methods: 74 patients with TM (29 male, 45 female) with a mean age of 29 ± 6 years (males), 31 ± 5 years (females) were studied. Myocardial T2* was measured at the same time to assess myocardial iron loading, and only patients with a myocardial T2* between 8 and 20 msec were chosen (which indicated mild to moderate iron loading). Flow mediated

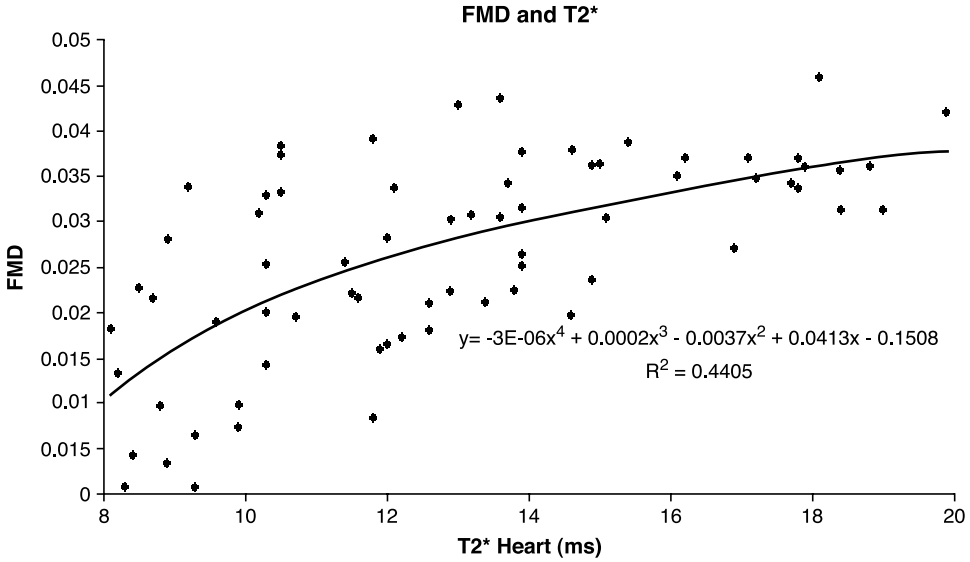

Figure 1.

(FMD) and nitrate dependent (GTN) changes in brachial artery in brachial artery cross sectional area were measured by cardiovascular magnetic resonance (CMR) for accurate assessment of endothelium dependent and independent reactivity respectively.

Results: FMD in the TM cohort was significantly correlated with myocardial T2* ($r = 0.66$, $p < 0.0001$, see Figure 1). There was no significant correlation for endothelin independent brachial arterial reactivity ($r = -0.129$, $p = 0.276$).

Conclusions: Endothelium dependent arterial reactivity is significantly correlated to myocardial iron loading, even despite potentially confounding variables such as sex (which may exert influences by hormonal differences) or significant comorbidity (such as diabetes). This suggests that in TM, iron deposition in the endothelium is a prime determinant of endothelium dependent arterial reactivity, that targeting of this may prove an important factor in response to potential iron chelating therapies.

498. Use of Inversion Recovery Contrast-Enhanced MRI (IR-CE-MRI) in the Evaluation of Patients with Clinically Suspected Pericarditis

Marco Francone, Andrew Taylor, Maria Kalantzi, Steven Dymarkowski, Jan Bogaert. *Radiology, Gasthuisberg University Hospital, Leuven, Belgium.*

Purpose: Diagnosis of pericarditis with current imaging techniques is not always straightforward. As pericarditis is an inflammatory process, IR-CE-MRI (similar to late enhancement myocardial MRI) may be of value for detecting pericardial inflammation.

Method and Materials: An MRI study that included late enhancement acquisitions after contrast-administration (0.2 mmol/kg bodyweight Gd-DTPA) was performed in 31 patients with clinical suspicion of pericardial disease (PD group), 22 patients with a recent history (< 3 weeks) of acute MI (AMI group), and 12 patients with no clinical evidence of pericardial disease (CON group). Images were analyzed for the presence of pericardial effusion, pericardial thickening and pericardial enhancement.

Results: Enhancement of the pericardial layers was found in 11/31 (moderate: 4, strong: 7) patients in the PD group, which was not related to the concomitant presence of pericardial fluid. Enhancement was helpful for demonstrating acute inflammation of the pericardial layers, differentiating inflammatory from fibrosing forms of chronic pericarditis, and defining the different components of pericardial thickening (e.g. pericardial layers vs pericardial effusion). Although in the AMI group minimal pericardial effusion was found in 12 patients, in only 4 was pericardial enhancement detected (moderate: 2, slight: 2). The two patients with moderate pericardial enhancement had clinical evidence of post-infarction pericarditis. In all 12 patients in the CON group, no pericardial thickening or enhancement was demonstrated.

Conclusions: The present study results suggest a more versatile use for IR-CE-MRI, enabling visualisation of pericardial inflammation in patients with clinical suspicion of pericardial disease and detection of post-infarction pericarditis in patients with recent acute MI.

499. Correction for Systematic Overestimation of Left Ventricular Volume by the Teichholz Formula

Carol J. Salton, BA,[1] Michael L. Chuang, MD,[1] Kraig V. Kissinger, BS, RT(R), (MR),[1] Christopher J. O'Donnell, MD, MPH,[2] Daniel Levy, MD,[2] Warren J. Manning, MD.[1]
[1]*Cardiology, Beth Israel Deaconess Medical Center, Boston, MA, USA,* [2]*The NHLBI's Framingham Heart Study, Framingham, MA, USA.*

Introduction: The Teichholz formula is clinically used to estimate left ventricular (LV) end-diastolic volume (EDV) from a single linear measurement of LV diameter. Reliance on the geometric model of LV shape implicit in the Teichholz formula may lead to errors in true EDV.Purpose: We sought to determine the accuracy of this formula against volumetric measurements by cardiovascular magnetic resonance (CMR) imaging, and if indicated to derive a correction formula to allow more accurate measurement of LV EDV based on the Teichholz method.

Methods: 292 adults (150 F, 142 M) from the Framingham Heart Offspring Study, who were free of cardiovascular disease by history and physical exam, underwent contiguous multislice breathhold cine CMR. Imaging parameters included TR = RR interval, TE = 9 ms, FA = 30 degrees, voxel size = $1.25 \times 2.0 \times 10.0$ mm^3. Volumetric ("true") EDV (volEDV) was determined by using the summation of disks (modified Simpson's rule) method. The end-diastolic diameter (D) was measured from an LV short axis slice just basal to the papillary muscle tips. Teichholz EDV (TEDV) was computed using the formula $TEDV = 7D^3/(2.4 + D)$. We compared raw TEDV and volEDV values using a scatter plot, which suggested a linear relationship between TEDV and volEDV. Thus we randomly divided the FHS data set into "Training" and "Test" sets and a linear least squares estimation (LLSE) method was applied to the Training set to derive regression coefficients for a linear correction equation of the form $y = mx + b$. The correction equation was then applied to the Test set to assess the validity of the equation. Data are summarized as mean ± SD. Differences were assessed using Student's t test, and $p < 0.05$ was considered significant.

Results: CMR studies were completed in all 292 subjects. VolEDV = 98.0 ± 23.0 ml was significantly overestimated by TEDV = 151.6 ± 29.2 ml, $p < 0.001$. Limits of agreement between volEDV and TEDV were mean

bias ± 2SD = 53.6 ± 40.2 ml. The correction equation derived using LLSE on the Training set was volEDV = 0.58*TEDV + 8.6. Applying this formula to the Test set yielded a set of corrected Teichholz EDVs (corrTEDV) where corrTEDV = 96.1 ± 16.8 ml (p = NS vs volEDV, limits of agreement − 2.0 ± 31.8 ml). Since the Teichholz formula makes an implicit assumption about ventricular shape (sphericity) and we have previously demonstrated greater sphericity in women than men, we also derived gender-specific correction equations, but correction was not markedly improved (gender specific correction: mean ± SD = 97.2 ± 19.4 ml, p = NS vs volEDV, limits of agreement − 0.8 ± 28.6 ml).

Conclusion: The clinically used (uncorrected) Teichholz formula significantly overestimates EDV as compared with volumetric measures of EDV by CMR. We derived a linear equation to correct for the systematic overestimation of volEDV by the Teichholz formula: corrTEDV = $4.06*D^3/(D + 2.4) + 8.6$. The corrected Teichholz formula yields EDVs that are not significantly different from true EDV. Gender-specific regression formulas did not substantially improve accuracy of corrected TEDV. Although volumetric determination of EDV is preferred, in situations where volumetric imaging is not available or impractical, use of the regression-corrected Teichholz formula is likely to yield more accurate estimates of true EDV.

500. Measurement of Right Ventricle Mass for the Evaluation of Pulmonary Hypertension

Shigeo Okuda, MD,[1] Akihiro Tanimoto, MD,[1] Toru Satou, MD,[2] Minoru Yamada,[1] Hiroshi Shinmoto, MD,[1] Sachio Kuribayashi, MD.[1] [1]*Diagnostic Radiology, Keio University School of Medicine, Tokyo, Japan,* [2]*Cardiology, Keio University School of Medicine, Tokyo, Japan.*

Introduction: Assessment of the right ventricle (RV) function is important for the evaluation of pulmonary hypertension. Cardiac ultrasound cannot provide accurate RV mass due to complicated shape of RV. Cardiac MR (CMR) is expected as non-invasive method for RV mass measurement. However, RV is commonly studied with the left ventricle (LV) short axis, and there was little discussion for establishing the optimal plane for RV measurement.

Purpose: 1) To establish the optimal scan plane for RV measurement and 2) to compare the right ventricle volume between normal subjects and pulmonary hypertension patients.

Methods: The subjects were 6 healthy volunteers (mean 35 y/o, range 32–38) for discussing the optimal plane for RV. The scan was performed on SIGNA Twinspeed 1.5 T (GE) with a cardiac phased array coil. ECG-gated 2D FIESRA was utilized for the image acquisition with following parameters: TR/TE = 3.6/1.6 msec, Flip angle = 55, BW = 125 KHz, FOV = 30 cm and the matrices were 224 × 224. Slice thickness was 10 mm without gap. The sequential slices were planned for covering the entire RV. Twenty phases for one cardiac cycle were acquired in 12 sec with a breathhold. We compared three different planes for measuring RV mass as following; 1) RV short axis that is commonly used for LV mass measurement, 2) Four chamber view and 3) RV long axis. RV long axis view was defined as sequential planes covering entire RV parallel to a line connecting between the upper ridge of the mitral valve and the apex on coronal images. Two observers traced the cavity of the right ventricle manually on the commercial available software (Mass Analysis on AdvantageWorkstation, GE) without knowing other's result. The volume of RV at endosystolic (ES) and endodiastolic (ED) phases were automatically calculated. Two observers independently measured each case twice with interval of more than 2 weeks. The results obtained in the first and second observations were compared to reveal

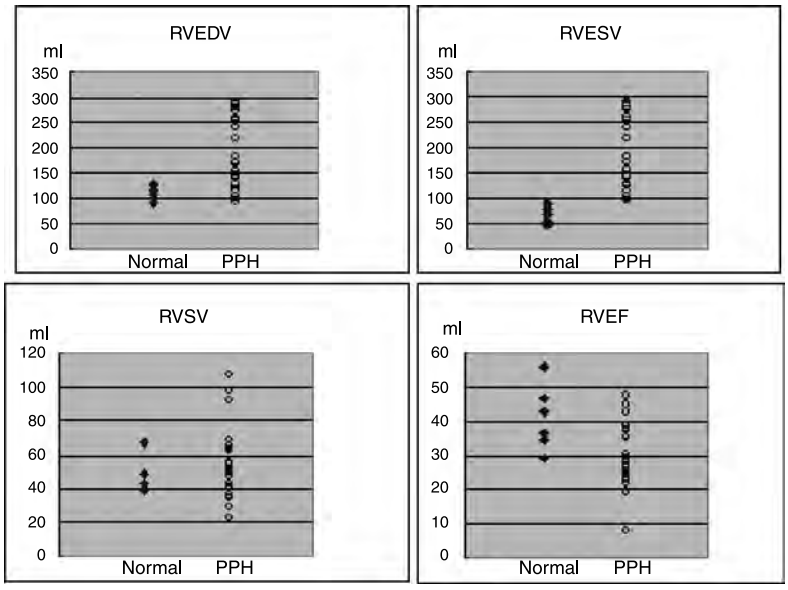

intraobserver variability. Interobserver variability was evaluated with Bland-Altman bias plots. The measurements of RV volume of 20 patients were performed on RV long axis. RVEDV, RVESV, RV systolic volume (SV) and RV ejection fraction (EF) were calculated. The results of patients were statically compared with normal volunteers using Mann–Whitney U-test.

Results: The interobserver difference of the results obtained on the RV long view was calculated as 1.2, −9 to 11.4 and 4.6 for bias, limits of agreement and standard deviation of the difference (SDD), respectively. Bias, limits of agreement and SSD were − 3.6, − 17.6 to 10.3, 7.1 (−0.5, − 0.5 to 14.3, 7.5) on the volume measurements based on LV short axis view (four chamber view). RV long axis measurement provided less variable results rather than other planes. RVEDV and RDESV of the patients were in the range between 94.9 and 288.1 ml; 53.4 and 263.1 ml, respectively. The difference between normal subjects and the patients was statically observed in RVEDV and RVESV ($p < 0.01$).

Conclusions: RV long axis view was better for measuring RV mass than RV short axis. The difference between normal subjects and the patients was statically observed in RVEDV and RVESV.

501. Tricuspid Annular Plane Systolic Excursion (TAPSE) Measurement Predicts Right Ventricular Ejection Fraction: MRI Validation in 173 Patients with Normal or Diseased Right Ventricle

Xavier Lyon, MD,[1] Arshid Azarine, MD,[2] Alban Redheuil, MD,[2] Elie Mousseaux, MD, PhD.[2] [1]*Service of Cardiology, University Hospital, Lausanne, Switzerland,* [2]*Department of Radiology, European Hospital, Paris, France.*

Introduction: Measurement of right ventricular (RV) ejection fraction (EF) is difficult due to the complex geometry of the chamber. EF can be accurately determined by MRI on short axis slices, but this method is cumbersome as it requires multiple breatholds to cover the entire ventricle then off line analysis. Measurement of the tricuspid annular plane systolic excursion (TAPSE) is readily available on the 4 chambers view and was demonstrated to reflect RV EF in echocardiographic studies on selected populations.

Purpose: The aim of this study was to validate by MRI the correlation of TAPSE and RV FE in normal subjects and in patients with a large range of myocardial pathology.

Methods: MRI was performed in 173 patients with a normal heart (NML, n = 46), arrhythmogenic RV dysplasia (ARVD, n = 25), RV outflow tract tachycardia (RVOTT, n = 27), idiopathic dilated cardiomyopathy (IDCM, n = 36) or ischemic cardiopathy (ISCH, n = 39). RV EF was derived from the measurement of volumes by applying the Simpson rule on short axis slices covering the entire RV. TAPSE was defined as the maximal excursion of the lateral aspect of the tricuspid annulus on the 4 chamber view during cardiac cycle. TAPSE was correlated to EF in each group and a cut off value identifying patients with EF > 40% was tested.

Results: TAPSE was significantly correlated with RV EF for the entire population (n = 173, R square 0.44, $p < 0.0001$) as well as in patients with a normal heart and in each group of pathology. Considering all patients, TAPSE > 15 mm was predictive of a RV EF > 40% with a 79% specificity, 77% sensitivity and 93% positive predictive value.

Conclusions: TAPSE is a very simple measurement that is correlated to RV EF in normal subjects and in patients suffering from various pathology susceptible to involve the RV. This parameter can rapidly and adequately indicate which patient has a preserved RV function.

	n	RV EF (%) mean ± SD (range)	TAPSE (mm) mean ± SD (range)	R square
All patients	173	44 ± 11 (13–65)	17 ± 51 (4–29)	0.44
NML	46	49 ± 6 (40–64)	18 ± 3 (11–29)	0.06
ARVD	25	35 ± 13 (16–65)	13 ± 5 (4–23)	0.59
RVOTT	27	47 ± 9 (32–65)	17 ± 5 (9–27)	0.36
IDCM	36	45 ± 10 (23–64)	17 ± 4 (10–22)	0.24
ISCH	39	43 ± 11 (13–65)	16 ± 6 (4–29)	0.44

502. Long Term Follow-Up on 17 Patients of Apical Hypertrophic Cardiomyopathy with Magnetic Resonance Imaging and ECG Changes

Hajime Yokota, Akiko Maehara, Yoshinao Yazaki, Yoshiro Kamoi, Takanobu Yamamoto, Yo Fujimoto, Tetsuya Seko, Haruo Mitani, Sugao Ishiwata, Shinichirou Nishiyama, Shigemoto Nakanishi, Shin-ichi Momomura, Tetsu Yamaguchi. *Cardiovascular Center, Toranomon Hospital, Tokyo, Japan.*

Introduction: Apical hypertrophic cardiomyopathy (Apical HCM) is a variant of non-obstructive hypertrophic cardiomyopathy with high prevalence in East Asia. Although this type of HCM has been considered to be benign, a part of them have shown poor prognosis during the long term follow up period.

Purpose: To evaluate myocardial damage visualized by late enhancement and wall motion abnormality using cardiovascular magnetic resonance (CMR) imaging and its relation with ECG changes or clinical problems in apical HCM.

Methods: Seventeen cases (15 males and 2 females) diagnosed as apical HCM by morphological changes (apical wall hypertrophy alone, so called spade shape) on echocardiography and characteristic ECG (giant negative T wave) were evaluated retrospectively. CMR was performed using 1.5 T Siemens Symphony scanner. Gd-DTPA hyperenhancement in the myocardium was determined 15 minutes after a bolus dose of 0.1 mmol/kg using IR-FLASH. True FISP cine images were obtained for volumetric analysis.

Results: The mean age at the initial diagnosis was 51 years old and the mean follow-up period was 9.8 years. The mean cardiac mass index (= cardiac mass/body surface area) and ejection fraction of left ventricular was within normal limits (90 ± 25 g/m^2, 62 ± 14%). Thirteen patients had late enhancement of apical wall and 9 of them had abnormal apical wall motion. These patients with late enhancement had tendency of longer follow-up period (mean follow-up 15.2 years), and in 8 patients associated with normalization or decrease of T wave inversion during follow up. There were no patients for history of congestive heart failure need for admission. There were 2 patients with abnormal apical wall motion and atrial fibrillation. Both suffered cerebral infarctions. Three patients with abnormal apical wall motion and late enhancement suffered ventricular tachycardia and one of them died.

Conclusions: In patients with long history of apical HCM, late enhancement and wall motion abnormality of apical wall is common. Normalization of T wave inversion of ECG may relevant with abnormal apical wall motion and myocardial damage detected by CMR. Late enhancement and wall motion abnormality of apical wall may be the predictors for clinical poor prognosis.

503. Main Pulmonary Artery Morphological Alterations in Patients with Idiopathic Pulmonary Hypertension. A Study with Phase-Contrast Magnetic Resonance Imaging

Santo Dellegrottaglie, Javier Sanz, MD, Martin Goyenechea, MD, Roxana Sulica, MD, Valentin Fuster, MD, PhD, Sanjay Rajagopalan, MD, Michael Poon, MD. *Z. and M.A. Wiener Cardiovascular Institute, Mount Sinai School of Medicine, New York, NY, USA.*

Introduction: Idiopathic pulmonary hypertension (IPH) is a progressive disorder with raised pulmonary artery pressures and typical pathological changes affecting small muscular pulmonary arteries. The relationship of main pulmonary artery (PA) morphological paramters and pulmonary hemodynamics in patients with IPH is not completely understood.

Purpose: To measure PA morphological parameters by phase-contrast magnetic resonance imaging (PC-MRI) and to evaluate their correlation with the pulmonary hemodynamics in patients with IPH.

Methods: In 12 patients (2 men; mean age 39.3 ± 11.9 years) with diagnosis of IPH (by US NIH Registry criteria) and in 12 control subjects (1 man; mean age 47.1 ± 15.9 years, p = n.s. vs. IPH), PC-MRI and right heart catheterization (RHC) were performed (mean interval 1.6 ± 3.7 days). PC-MRI measurements were obtained from images perpendicular to the PA and to the ascending aorta (Ao). A retrospectively ECG-gated, breath-hold, velocity-encoded sequence in a 1.5 T system was used. From PC-MRI, normalized minimal, maximal and mean areas (cm^2/m^2), were measured for PA and Ao, using a post-processing workstation. By RHC the following parameters were measured: pulmonary systolic, diastolic and mean pressures (mmHg), systolic and end-diastolic right ventricular pressure (mmHg), right atrial pressure (mmHg), capillary-wedge pressure (mmHg), and vascular pulmonary resistance (Wood units). Ao mean pressure was measured non-invasively. A surrogate index for PA and Ao arterial distensibility (Dist) was calculated by the formula: [(maximal area − minimal area)/maximal area] × 100.

Results: Table 1 shows the PA and Ao values for minimal and maximal areas measured by PC-MRA. Comparing IPH patients and controls, no significant differences in Ao mean area (3.23 ± 1.01 vs. 3.82 ± 1.05 cm^2/m^2, p = n.s.) and Ao Dist (21 ± 8% vs. 24 ± 9%, p = n.s.) were observed. On the contrary, the PA mean area values obtained in IPH patients were significantly higher compared to controls (7.04 ± 2.72 vs. 3.59 ± 1.14 cm^2/m^2, p = 0.001). In subjects with IPH compared to controls significantly lower values for PA Dist (22 ± 9% vs. 46 ± 16%, $p < 0.0001$) were obtained. Interestingly, no significant correlation was found between PA mean area or PA Dist and any RHC parameters.

Table 1.

	PA minimal area (cm^2/m^2)	PA maximal area (cm^2/m^2)	Ao minimal area (cm^2/m^2)	Ao maximal area (cm^2/m^2)
PPH Patients	6.3 ± 2.4	7.7 ± 2.8	2.8 ± 1.0	3.5 ± 1.0
Control patients	2.9 ± 0.9	4.2 ± 1.2	3.3 ± 1.1	4.4 ± 1.3
P value	0.001	0.002	n.s.	n.s.

Conclusion: PA dimensions and PA Dist are significantly affected in IPH patients. These alterations do not seem to be directly correlated to the abnormal PA hemodynamics, suggesting that other factors are probably involved.

504. Does Extent of Mitral Regurgitation Regress After Aortic Valve Replacement for Severe Aortic Stenosis? A Cardiac Magnetic Resonance Imaging Study of LV Structure, Function and Mitral Apparatus Geometry

Ketheswaram Caruppannan, MD, Mark Doyle, PhD, Diane A. Vido, Ronald B. Williams, June Yamrozik, Vikas K. Rathi, MD, Valerie Bress, James A. Magovern, MD, Robert W. W. Biederman, MD. *Allegheny General Hospital, Pittsburgh, PA, USA.*

Background: Mitral regurgitation (MR) frequently accompanies severe aortic stenosis. In patients undergoing aortic valve replacement (AVR) for AS, there is often considerable ambiguity when faced with a double valve replacement.

Hypothesis: We hypothesize that extent and grade of MR decreases following AVR and is detectable by cardiac MRI (CMR) due to its high resolution of LV structure, function and mitral valve apparatus.

Methods: Thirteen patients with severe compensated AS underwent CMR 3 ± 2 days prior and 10 ± 3 mo post AVR. Extent and grade of MR was semi-quantitatively determined by CMR (GE 1.5 CV/i) using optimized FIESTA cine. 2D mitral valve geometry (tenting angle, tenting area and annular dimension) and LV geometry (sphericity) were measured and compared using non-parametric testing as was LVmass Index (LVMI) and LVMI/volume pre and post AVR. Patients with > 2 + aortic regurgitation and/or structural mitral pathology were excluded.

Results: The pre AVR range and grade of MR was trace through severe: (< 1 to > 4 +). The mean grade was moderate: (2 +). Post AVR, the mean grade of MR decreased in 11/13 (85%) to trace − 1 +, was unchanged in one and increased in another to 1 + (who had the least beneficial LV remodeling post AVR). LV mass and volume index improved post AVR as expected (93 ± 23 vs. 76 ± 15 g/m^2 and 42 ± 33 vs. 24 ± 7, $p < 0.05$ for both and were highly correlated with MR improvement (r = 0.51 and 0.60) as was stroke volume (r = − 0.57). EF increased (55 ± 19 vs. 66 ± 16%, $p < 0.05$ but was not correlated with MR reduction post AVR. LV sphericity improved ($p < 0.05$). Improvement in MR correlated with 2D tenting area (r = 0.39), annular dimension (r = 0.44) and LV major (r = 0.71) and minor (r = 0.57) axis while only tenting angle significantly changed post AVR ($p < 0.05$). Importantly, there was no correlation with pre or post aortic transvalvular gradient or extent of co-existent CAD. No patient required a double valve as determined in the operating room independent of this analysis.

Conclusion: Aortic valve replacement achieved regression in mitral regurgitation in severe AS patients that was detectable by CMR. Favorable changes were attributable to LV and mitral valvular geometry, mass, and EF but not to reduction in transvalvar gradient or degree of CAD. LV and/or annular reverse remodeling portends less MR post AVR. As considerable morbidity and mortality exists for simultaneous AVR and MVR, CMR suggests that AVR without MVR may be indicated in such patients.

505. 3D Diastolic Function Assessment of the Right Ventricle; Interrogation by Cardiovascular MRI

Vikas K. Rathi, MD, Mark Doyle, PhD, June Yamrozik, Ronald B. Williams, Valerie Bress, Geetha Rayarao, Robert W. W. Biederman, MD. *Allegheny General Hospital, Pittsburgh, PA, USA.*

Introduction: Complex flow and velocity characterizations of the mitral valve (MV) for LV diastolic function (DF) has been extensively studied. However, right ventricular (RV) DF has been sparsely examined and it is unknown if RV diastolic indices mirror LV DF. We have previously shown that cardiac MRI (CMR) MV inflow acquisition is highly comparable to echocardiography for DF.

Hypothesis: We hypothesize that 3D CMR not only can interrogate RV DF but also determine if physiologic comparisons exist between key clinical metrics of LV and RV DF.

Methods: 14 subjects (4 normal: male: 8; female: 6; mean age 55 yr: range 22–79 yr) underwent 3D assessment of MV and tricuspid valve (TV) on a commericial 1.5 T GE CV/i scanner (Milwaukee, WI). RV and LV inflow were interrogated by phase velocity mapping in the X, Y and Z coordinate for E_{vel}, A_{vel} velocities and deceleration time (DT) according to ASE criteria.

Results: All (14/14) MV and TV flow velocity data were successfully acquired and analyzed in a mean time < 15 min. The mean MV E_{vel} and A_{vel} were higher than the TV: 71.2 ± 20.5 and 49.8 ± 22.1 vs. 46.79 ± 13.45 and 32.2 ± 10.4 cm/s, respectively, $p = 0.0003$. However, there was no difference in E:A ratio, p = NS. Importantly, 12/14 patients (86%, $p < 0.05$) had identical morphological patterns between RV and LV DF (7 impaired relaxation, 1 restrictive, 4 normal). The remaining 2 pts had discordant TV and MV flows (one had restrictive MV with a pseudonormal TV flow-ischemic cardiomyopathy; and the other had normal MV and restrictive TV flow-pt referred for constriction). The DT for TV were consistently higher compared to MV (233 ± 65 vs. 171 ± 35 ms, $p < 0.005$).

Conclusion: The right and left ventricular diastolic function can be readily, efficiently and accurately assessed by CMR. Clinically important, TV flow data morphologically corresponds with that of MV patterns. The lower velocities,

longer DT and shorter diastasis likely represents insights into RV lusitropic physiology. Where discordance exists, likely there is ipsilateral abnormal RV DF. Near simultaneous evaluation by CMR of RV and LV diastolic function provides insight into the physiology of both ventricles and their interdependence.

506. Quantification of Aortic Valve Stenosis—Comparison of Different MR Sequences and Transesophageal Echocardiography

Thomas Schlosser, MD,[1] Peter Hunold, MD,[1] Markus Jochims, MD,[2] Kai-Uwe Waltering, MD,[1] Oliver Bruder, MD,[2] Joerg Barkhausen, MD.[1] [1]*Radiology, University Hospital Essen, Essen, Germany,* [2]*Cardiology, Elisabeth Hospital Essen, Essen, Germany.*

Introduction: The severity of aortic valve stenosis can be assessed using different non-invasive techniques such as transthoracic and transesophageal echocardiography as well as invasive pressure measurements during cardiac catheterisation. Recently, it has been demonstrated that cardiac magnetic resonance imaging allows quantification of the aortic valve area (John et al., 2003). However, using gradient echo sequences contrast as well as temporal and spatial resolution are limited.

Purpose: The aim of this study was to assess aortic valve areas in aortic stenosis using two different MR sequences [steady state free precession (SSFP) and gradient-echo fast low-angle shot (FLASH)] in comparison to transesophageal echocardiography (TEE).

Methods: 31 patients with known aortic stenosis were examined with MR and echocardiography. MR imaging was performed on a 1.5 T MR scanner (Magnetom Sonata, Siemens, Erlangen, Germany) using a cine SSFP sequence (TR = 2.9 ms, TE = 1.3 ms, FA = 65°, slice thickness = 5 mm, temporal resolution = 19 ms, spatial resolution = 1.3 mm × 1.3 mm) and a cine FLASH sequence (TR = 8 ms, TE = 3.3 ms, FA = 20°, slice thickness = 5 mm, temporal resolution = 33 ms, spatial resolution = 1.9 mm × 1.3 mm). The imaging plane for planimetry was perpendicular to the aortic root. Planimetry was performed in cross-sectional images in systole by a radiologist blinded to the results of the TEE. The results of the MR measurements were compared with planimetry performed based on the TEE data.

Results: MR planimetry could be performed in all patients. The valve leaflets could be delineated more clearly on SSFP images, particularly in severely calcified valves (Fig. 1). Mean aortic valve area measured by TEE was 0.97 mm^2, 1.00 mm^2 for SSFP and 1.25 mm^2 based on FLASH images. Good correlation was found between aortic valve areas measured by TEE and based on SSPF images. The mean difference between the valve areas assessed based on SSFP and TEE images was 0.15 ± 0.13 cm^2 (FLASH vs. TEE: 0.29 ± 0.17 cm^2). Bland-Altman plots demonstrate that measurements using FLASH images overestimate the aortic valve area compared to TEE (Fig. 2).

Conclusions: MR planimetry of aortic valve areas is feasible using SSFP and FLASH sequences. Measurements of the aortic valve area based on SSPF images correlate better with TEE compared to FLASH images. The higher spatial and temporal resolution as well as the improved image contrast must be considered as major advantages of the SSFP images.

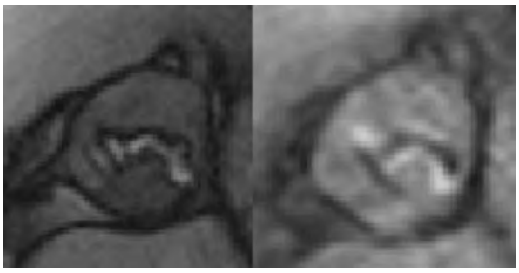

Figure 1. Cross-sectional images of the aortic valve acquired by SSFP (left) and FLASH sequence (right).

REFERENCE

John, A. S., Dill, T., Brandt, R. R., Rau, M., Ricken, W., Bachmann, G., Hamm, C. W. (2003). Magnetic resonance to assess the aortic valve area in aortic stenosis: how does it compare to current diagnostic standards? *J. Am. Coll. Cardiol.* 42:519–526.

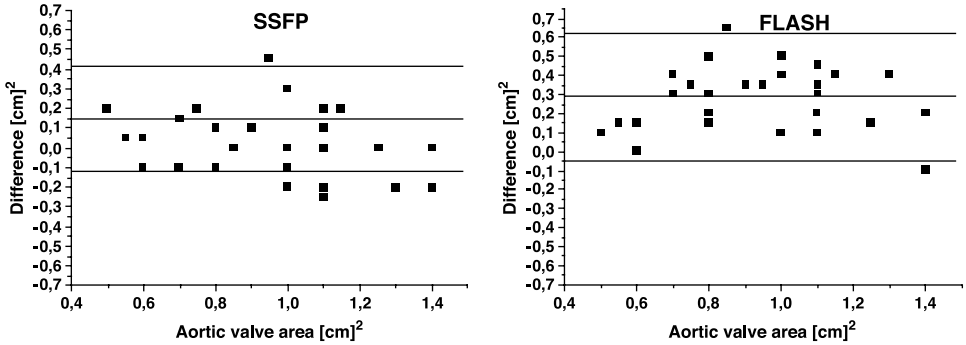

Figure 2. Bland-Altman plots of SSFP and FLASH-derived aortic valve area compared to TEE.

507. Late MR Contrast Enhancement in Arrhythmogenic Right Ventricular Cardiomyopathy (ARVC)

David Maintz, MD,[1] Murat Ozgun, MD,[1] Kai Uwe Juergens, MD,[1] Matthias Grude, MD,[2] Thomas Wichter, MD,[2] Roman Fischbach, MD,[1] Walter Heindel, MD.[1] [1]*Department of Diagnostic Radiology, University of Muenster, Muenster, Germany,* [2]*Department of Cardiology, University of Muenster, Muenster, Germany.*

Introduction: Late contrast enhancement in Magnetic Resonance Tomography (MRT) is used as a diagnostic marker in various myocardial pathologies such as myocardial infarction, scar, edema or inflammation.

Purpose: To evaluate LE in patients with ARVC.

Methods: 8 patients with ARVC, as diagnosed using the criteria of the task force of the working group of cardiomyopathies of the European Society of Cardiology, were included in the study. The MR protocol (Philips Intera 1.5 T) included steady state free precession CINE sequences and T1-weighted turbo spin echo (TSE) sequences in the short axis of the heart and in the transverse plane, a fat-suppressed T1-w TSE sequence in the transverse plane and inversion recovery sequenzen in the short axis and four chamber view 15 minutes after i.v. applikation of 0.2 ml/kg body weight of Magnevist (Late Enhancement). MR studies were analyzed by two blinded readers in consensus.

Results: 4/8 patients (50%) showed late contrast enhancement within the right ventricular (RV) myocardium. One patient showed additional enhancement in the left ventricular (LV) myocardium, indicating LV involvement of the disease. Other MR findings were: dyskinesia of RV: 8/8 patients, dilatation of RV: 6/8, thinning and/or aneurysmatic transformation of RV: 5/8, abnormal thickening or structural changes of RV: 5/8, fatty transformation of RV 2/8 (Fig. 1).

Conclusions: Late myocardial enhancement can be observed in a significant portion of patients with ARVC. The late enhancement technique may emerge as a part of the diagnostic workup of ARVC in the future.

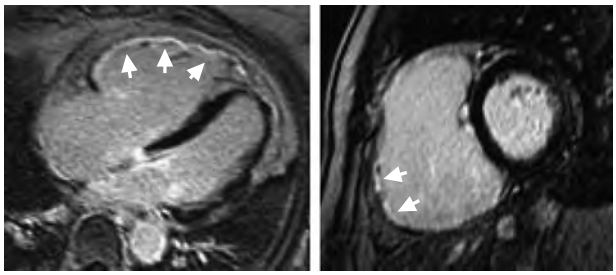

Figure 1. Patient with severe ARVC. Late enhancement images in 4-chamber view (left) and short axis view (right) demonstrate marked contrast uptake of right ventricular myocardium.

508. Characteristics of Myocardial Enhancement in Nonischemic Dilated Cardiomyopathy with Contrast-Enhanced MRI

Young Jin Kim, MD, Byoung Wook Choi, MD, Jae Seoung Seo, MD, Ji Eun Nam, MD, Kyu Ok Choe, MD. *Diagnostic Radiology, Yonsei University College of Medicine, Severance Hospital, Seoul, Republic of Korea.*

Purpose: Recently, the pattern of myocardial enhancement in nonsichemic dilated cardiomyopathy (DCMP) with MRI has been reported to be differentiated from that of ischemic cardiomyopathy. However, we do not know which part is normal myocardium to null the signal if diffuse and mild myocardial enhancement is present. We studied the characteristics of enhancement in DCMP by contrast-enhanced MRI with a fixed inversion time.

Methods: Thirty nine patients (male 26, female 13, mean age 59 ± 12 yrs) with DCMP and normal coronary artery proven by conventional coronary angiography underwent contrast-enhanced MRI. MRI parameters were TR = 5.4 ms, TE = 1.6 ms, FA = 15, two cardiac cycles per acquisition, and 1 NSA. Inversion time was fixed at 280 ms to apply the same nulling effect on normal myocardial enhancement 10 minutes after contrast administration of Gd-DPTA at 0.2 mmol/kg. Thirty patients with myocardial infarction underwent MRI with the same protocol. The signal intensity of skeletal muscles on the chest wall (SIsm) was used as reference signal intensity (SI). The ratio of SI of remote myocardium (SIrm) from hyperenhanced infarction to SIsm was compared with the ratio of SI of abnormally enhanced myocardium (SIem) to SIsm and the ratio of SI of non-enhanced myocardium (SInem) to SIsm in DCMP patients.

Results: Visual assessement of the myocardium in patients with DCMP resulted in no enhancement in 13 (33%) patients, and enhancement in 26 (67%), while all patients with infarction showed hyperenhancement on the infarcted region. Enhancement in DCMP was mild to moderate in 18 (46%), strong in 4 (10%) and both in 4 (10%). The SIem/SIsm in DCMP was 4.02 ± 2.46 in average, while the SIrm/SIsm in infarction showed 0.79 ± 0.91 which was nearly same as SInem/SIsm of 0.79 ± 0.67 in DCMP without enhancement. The SIem/SIsm of mild to moderate enhancement in DCMP was 3.68 ± 1.78 and that of hyperenhancement was 5.55 ± 3.38. In 26 patients with myocardial enhancement, enhancement was frequent on basal (42.3%) and septal (42.3%) area. Diffuse transmural enhancement (46.2%) was more frequent than middle layer enhancement (34.6%). Ejection fraction and end-diastolic volume of the left ventricle showed no significant correlation with the presence, degree, and pattern of abnormal myocardial enhancement in DCMP.

Conclusions: The mild to moderate degree of diffuse transmural or middle layer enhancement especially on the basal septum is a frequent and characteristic enhancement pattern of myocardium in DCMP patients.

509. Delayed Enhanced MRI Detects Myocardial Fibrosis in Patients with Peripartum Cardiomyopathy

Robson Macedo Filho, MD, FÃ¡bio Berezowsky Rocha, MD, Ricardo Loureiro, MD, Maria Elisa Carneiro Carvalho, MD, Luiz Francisco Ã! vila, MD, JosÃ© R. Parga, MD, WalquÃria S. Ã!vila, MD, Carlos E. Rochitte, MD. *Cardiology, Heart Institute-InCor-University of São Paulo Medical School, São Paulo, Brazil.*

Background: Peripartum cardiomyopathy (PC) is a rare form of cardiomyopathy with unknown etiology and difficult diagnosis, requiring the exclusion of other causes. The presence of myocardial fibrosis (MF) in endomyocardial biopsy studies has shown variable results. Cardiac delayed enhanced MRI (DE) has exquisite accuracy for MF detection in several clinical settings.

Objectives: To test whether DE can detect MF in patients with typical diagnosis of PC.

Methods: We evaluated ten patients with clinical diagnosis of PC. All pts underwent MRI examination in a 1.5 T SIGNA CV/i GE scanner using a gradient echo with an inversion-recovery pre-pulse after injection of 0.2 mmol/kg of gadolinium-DTPA for detection of MF (DE) with the following parameters: TR 7.1 ms, TE 3.1 ms, TI 150–250 ms, FA 20, BW 31.25 kHz, Matrix 256 × 192, NEX 2, RR 1. A steady state gradient echo (FIESTA-GEMS) was used for LV function evaluation. Time interval between delivery and MRI study was less than six months for all patients. Left ventricular ejection fraction (LVEF), end diastolic (EDV) and end systolic (ESV) were measured by Simpson's rule. MF was quantified by planimetry and expressed as percent of LV mass.

Results: DE detected MF in 4 patients (25%). Mean MF was 5.3 ± 1.2% of LV mass. Several patterns of DE were observed: subendocardial, subepicardial, midwall and transmural. Midwall DE pattern resamble those seen on idiopathic cardiomyopathy (Fig. 1). Only 2 patients had LVEF greater than 40% and mean LFEV was 40.8 ± 2.8%. Mean EDV was 140.5 ± 13.3 ml and ESV was 82.3 ± 7.7 ml.

Conclusions: Delayed enhanced MRI can detect and quantify myocardial fibrosis in patients with peripartum cardiomyopathy.

Myocardial fibrosis is variably present in peripartum cardiomyopathy. Whether the presence of myocardial fibrosis has a relationship with prognosis or left ventricular function recovery will require further studies. Therefore, delayed enhanced MRI can be a useful tool for further investigation on this cardiomyopathy.

510. The Visual Assessment of Mitral Regurgitation by Cine-Magnetic Resonance Imaging Compared to Echocardiography and Cardiac Catheterization

John F. Heitner, Anna Lisa Crowley, MD, Jonathan W. Weinsaft, MD, Igor Klem, MD, Raymond J. Kim, MD, James G. Jollis, MD. *Duke Univeristy, Durham, NC, USA.*

Introduction: Valvular regurgitation causes a loss of signal on cine magnetic resonance imaging (cine-MRI). This loss of signal is proportional to the severity of regurgitation due to the increase turbulence. The ability to assess mitral regurgitation by cardiac catheterization and trans thoracic echocardiography (TTE) has already been validated in prior studies.

Purpose: To compare the visual assessment of mitral regurgitation by cine-MRI, using True-FISP pulse sequence, to TTE and cardiac catheterization.

Methods: We evaluated 67 patients who underwent both a TTE and cine-MRI within 2 weeks. Forty-nine patients underwent left ventriculography by cardiac catheterization within 1 week of the MRI and TTE. True-FISP pulse sequence is currently the gold standard in MRI cine imaging and was therefore chosen as the pulse sequence, in order to assess routine clinical practice, as opposed to assessing velocity encoded flow mapping and gradient recall echo. Mitral regurgitation was visually assessed by blinded readers for all 3 imaging modalities and given a score of none, mild, moderate, or severe. The characteristics that were used to assess the severity of mitral regurgitation by cine-MRI included: jet length, jet width, jet area, jet eccentricity, and the jetÃ¢â‚¬â„¢s color intensity. Standard assessments were

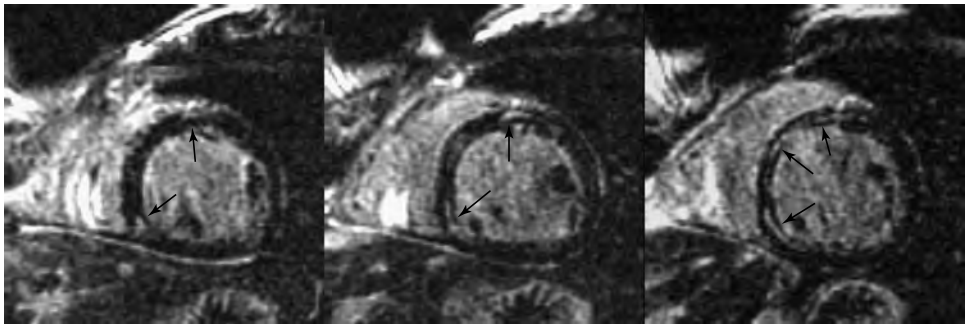

Figure 1.

used to measure the severity of mitral regurgitation in both TTE and cardiac catheterization.

Results: There was modest agreement between mitral regurgitation assessed by cine-MRI and cardiac catheterization (Weighted Kappa = 0.27, ASE = 0.07), as well as, cine-MRI and TTE (Weighted Kappa = 0.42, ASE = 0.08). There was also modest agreement between TTE and cardiac catheterization (Weighted Kappa = 0.38, ASE = 0.09). Cine-MRI appeared to identify more regurgitation than cardiac catheterization or TTE for a substantial portion of patients considered mild or moderate by these other techniques (Tables 1–3).

Conclusions: This study supports the use of cine-MRI (True-FISP) to visually assess the severity of mitral regurgitation. Cine-MRI may be more sensitive in detecting mitral regurgitation than TTE or cardiac catheterization. Prognostic studies are needed to determine if this increase sensitivity is an overestimation or a more accurate assessment of mitral regurgitation.

Table 1. Mitral regurgitation severity by cine-MRI vs. TTE

		TTE			
		None	Mild	Moderate	Severe
MRI	None	1	4	1	0
	Mild	5	18	0	0
	Moderate	0	14	5	2
	Severe	1	3	4	9

Table 2. Mitral regurgitation severity by cine-MRI vs. cardiac catheterization

		Cardiac catheterization			
		None	Mild	Moderate	Severe
MRI	None	4	1	0	0
	Mild	9	7	0	0
	Moderate	4	7	1	2
	Severe	2	4	5	3

Table 3. Mitral regurgitation severity by TTE vs. cardiac catheterization

		Cardiac catheterization			
		None	Mild	Moderate	Severe
TTE	None	2	3	0	0
	Mild	13	12	0	1
	Moderate	1	3	1	1
	Severe	0	1	3	4

511. Comparison of Cardiac MRI to Transthoracic Echocardiography in the Evaluation of Ventricular Dysfunction in Adolescents with Duchenne Muscular Dystrophy

William Gottliebson, MD,[1] Larry Markham, MD,[1] Eric Crotty, MD,[2] Robert Fleck, MD,[2] Janaka Wansapura, PhD,[2] Brenda Wong, MD,[3] Linda Cripe, MD.[1] [1]*Cardiology, Cincinnati Childrens Hospital and Medical Center, Cincinnati, OH, USA,* [2]*Radiology, Cincinnati Childrens Hospital and Medical Center, Cincinnati, OH, USA,* [3]*Neurology, Cincinnati Childrens Hospital and Medical Center, Cincinnati, OH, USA.*

Introduction: Progressive dilated cardiomyopathy is a nearly ubiquitous finding in adolescents and young adults with Duchenne Muscular Dystrophy (DMD). The primary means used in the past to assess ventricular function in DMD patients has been transthoracic echocardiography (TTE). However, TTE indexes of left ventricular (LV) function in this population can be inaccurate due to poor acoustic windows and wall motion abnormalities, and right ventricular (RV) function cannot be reliably quantitated. Cardiac magnetic resonance (CMR), which is not limited by geometry or body habitus, and can reliably quantitate RV volume and systolic function, may provide an alternative, superior imaging modality for the cardiac evaluation of DMD patients.

Purpose: This pilot study sought to compare the results of CMR to TTE in the evaluation of ventricular function in DMD patients.

Methods: 12 male subjects (mean age 17.3 years) were included. Standard TTE and CMR studies were performed within 3 weeks of one another on all patients. Standard TTE 2D and M-mode tracings were obtained (parasternal long axis at the mitral leaflet tips) on GE Vivid V® or Siemens Sequoia® Ultrasound systems, then measured and analyzed off-line (Camtronics *Vericis*®) for LV global function. Oblique short axis cine TrueFISP SSFP stack CMR image sequences were obtained after localizer images on a Siemens 3 Tesla *Trio* magnet with a cardiac coil and analyzed off-line via Siemens Argus® software, for biventricular chamber volumes, global, and regional function.

Results: All patients tolerated both modalities of study without incident, requiring no sedation. Global LV dysfunction was diagnosed by TTE in 7 and in 9 by CMR. 12 had RV global dysfunction by CMR, a result not identified by TTE. In addition, 8 patients had regional biventricular dysfunction by CMR, another result not reported on TTE. Further details are provided in Table 1.

Conclusion: CMR is an effective modality in the evaluation of cardiac function in DMD patients. Since CMR is not limited by body habitus and allows accurate and reproducible assessment of both left and right global and regional ventricular function in this population, it may be superior to TTE in this population. We speculate that identification of early RV global and regional systolic

Table 1. TTE and CMR results, DMD patients

	TTE	CMR
Technical quality		
Good	33%	100%
Poor	67%	0%
Global function mean ± std dev (range)		
LV SF %	26.2 ± 13.1 (15–36)	
LV EF %		46.5 ± 5.2 (23–62)
RV EF %		40.4 ± 3.7 (33–47)
Age	17.3 ± 3.7 (11.7–23.7)	

dysfunction will lead to earlier initiation of heart failure treatment in this population, which in turn may decrease the morbidity and mortality of DMD.

512. Noninvasive Prediction of Exercise-Induced Pulmonary Hypertension with Resting Cardiac Magnetic Resonance Imaging

Javier Sanz, MD, Santo Dellegrottaglie, MD, Martin Goyenechea, MD, Roxana Sulica, MD, Concepcion Learra, MD, Hipolito Gutierrez, MD, Sanjay Rajagopalan, MD, Michael Poon, MD. *Cardiology, Mount Sinai School of Medicine, New York, NY, USA.*

Introduction: Exercise-induced pulmonary hypertension (EIPH) is defined by normal mean pulmonary pressure (MPAP) at rest (< 25 mmHg) but abnormally increased with exercise (> 30 mmHg). Diagnosis requires exercise performance during invasive right heart catheterization (RHC), the gold standard, or during Doppler echocardiography evaluation.

Purpose: To identify, with cardiac magnetic resonance imaging (CMRI), abnormal features in resting right ventricular function or pulmonary artery flow that can be used as useful predictors of EIPH.

Methods: The study population included 27 subjects (24 females, age = 54.3 ± 15.7 years) with normal rest MPAP, evaluated with rest CMRI (1.5 Tesla) and rest-exercise RHC for suspected pulmonary hypertension. For the right ventricle, the following parameters were measured with trueFISP: end-diastolic volume, end-systolic volume, ejection fraction. The pulmonary average velocity (PAV, cm/sec) was obtained from retrospectively gated, breath-hold, phase-contrast imaging of the main pulmonary artery (velocity encoding = 100 cm/sec). RHC-derived parameters were MPAP (mmHg) and pulmonary vascular resistance (PVR, Wood units).

Results: RHC detected EIPH in 9 (33.3%) subjects. There were no significant differences in right ventricular volumes or ejection fraction in patients with or without EIPH. The PAV at rest was significantly lower in subjects with EIPH (12.4 ± 4.4 vs. 16.7 ± 4.2 cm/sec; $p = 0.02$). There were negative moderate correlations between the PAV and the exercise MPAP ($r = -0.51$; $p = 0.008$) and PVR ($r = -0.52$; $p = 0.007$). Receiver-operator curve analysis using a best cutoff value of PAV = 12.9 cm/sec (area under the curve = 0.76, $p = 0.008$) revealed a sensitivity of 66.7% and specificity of 94.4% for the prediction of EIPH.

Conclusions: The PAV measured at rest with phase-contrast is lower in individuals with EIPH than in normal subjects. This CMRI feature may be useful to identify with high specificity the subset of patients with EIPH.

513. Left Atrial Volume Assessment by Cardiac Magnetic Resonance

W. Patricia Ingkanisorn, MD, Andrew E. Arai, MD. *NHLBI, Laboratory of Cardiac Energetics, National Institutes of Health, Bethesda, MD, USA.*

Background: Left atrial volume has prognostic value after myocardial infarction and varies with left ventricular filling pressure in patients with hypertrophic cardiomyopathy. Standard 2D echocardiography uses a single linear measurement to detect left atrial enlargement. We hypothesized that simple measurements from only the 2-chamber and 4-chamber cine cardiac magnetic resonance (CMR) exam could accurately estimate left atrial volume and would be superior to linear dimensions for detecting left atrial enlargement.

Methods: CMR was performed on 18 patients (mean patient age was 45 ± 14 years). Cine CMR using steady-state free precession was performed in the standard 3-chamber, 2-chamber, and 4-chamber views. The left atrium was imaged volumetrically with a stack of images parallel to the 4-chamber prescription (slice thickness of 8 mm and a separation of 0). All imaging was performed on a GE 1.5 T, CV/i scanner. A linear measurement of the left atrial dimension in the 3-chamber view was performed as one assessment of left atrial size. The simple estimate of left atrial volume was based on planimetry of the left atrium in the 2-chamber and 4-chamber views and calculated using the modified equation of V (Volume) = 0.85 × (Area1 × Area2)/L (Length of the left atrium). Left atrial volume from planimetry of the images with volumetric coverage was used as the gold standard. All measurements were performed at end systole.

Results: Based on published cutoffs for left atrial volume normalized to body surface area (32 ml/m^2), 10 of the 18 patients had left atrial enlargement. Left atrial volume ranged from 28 ml to 130 ml spanning normal through moderate left atrial enlargement. As hypothesized, the calculated left atrial volume correlated with the reference left atrial volume ($r = 0.83$) better than linear dimensions ($r = 0.72$ in the 3-chamber view and 0.44 in the 4-chamber view). In Bland–Altman analysis, the limits of agreement were 14 ml (2 standard deviations). Furthermore, estimated left atrial volume correctly categorized 83% of patients as having normal or enlarged left atria. Only three patients with left

atrial enlargement were missed by the estimated left atrial volume and all had borderline enlargement. However, linear left atrial dimension on the 3-chamber view $\geq$ 40 mm only detected 3 of 10 patients with left atrial enlargement.

Conclusion: Simple linear measurements of left atrial size underestimate left atrial enlargement. The modified formula for calculating left atrial volume using only the 2-chamber and 4-chamber views provides an accurate assessment of left atrial volume, comparable to that obtained by performing time and labor intensive fully volumetric measurements. The limits of agreement for estimating left atrial volume were about 3 times better than a recent validation of 3D echocardiographic measurements.

514. Increase of Left Ventricular Mass as an Adaptative Mechanism to Volume Preload. An MRI Assessment in Normal and Naive Hypertensive Patients

Anna Maria Sironi, Amalia Gastaldelli, Daniele De Marchi, Brunella Favilli, Vera Scampuddu, Antonio L'Abbate, Massimo Lombardi. *MRI Lab, Institute of Clinical Physiology CNR-CREAS, Pisa, Italy.*

Introduction: Cine magnetic resonance imaging (MRI) has been shown to provide highly accurate and reproducible measures of ventricular mass and volume. However, left ventricular (LV) mass shows highly intersubject variability even in the normal population. The relationship between LV pre-load and LV-mass has not been well established.

Purpose: To investigate, using cine dynamic cardiac magnetic resonance imaging (MRI), the impact of LV-volumes on the changes in LV-mass and the role of increased blood pressure.

Methods: Forty male subjects. (age 25–61 y; BMI 22–37 kg/m^2) of which 14 newly diagnosed with essential hypertension (HT; PAS 154 ± 3 mmHg, PAD 92 ± 2 mmHg) and 26 with normal blood pressure (NT; PAS 123 ± 2 mmHg, PAD 70 ± 2 mmHg) underwent cardiac MRI (1.5 T, CVi, GEMS, Milwaukee, USA). Left and right ventricular (RV) volumes and function were assessed using a FIESTA sequence to obtain parallel short axis of the ventricles; 3D reconstruction was obtained in post-processing.

Results: All subjects had normal cardiac function and the measured parameters were within the normal ranges previously established. However, LV-mass, normalized by surface area, was higher in the HT group than in controls (69 ± 2 vs. 78 ± 4 g/m^2 in NT vs. HT $p < 0.05$). On the other side, LV and RV end-systolic (ESV) and end-diastolic (EDV) volumes were similar among the two groups: LV-EDV was 73 ± 2 vs. 67 ± 3 ml/m^2; LV-ESV was 26 ± 1 vs. 22 ± 3 ml/m^2; RV-EDV was 75 ± 3 vs. 71 ± 2 ml/m^2; RV-ESV was 29 ± 2 vs. 26 ± 1 ml/m^2 in NT vs. HT, all p = ns. Ejection fractions of both ventricles were similar (LV-EF 64 ± 1 vs. 67 ± 3%; RV-EF 61 ± 1 vs. 63 ± 2% in NT vs. HT, all p = ns). In the NT group LV-mass, was independently related to both LV-EDV (partial r = 0.47 $p < 0.03$) and systolic blood pressure (partial r = 0.61 $p < 0.003$) but not to LV-ESV even after accounting for age and BMI. The same relationship holds when the entire population was analyzed: LV-mass was independently related to LV-EDV (partial r = 0.47 $p < 0.004$) and systolic blood pressure partial (r = 0.52 $p < 0.002$) but not to LV-ESV after accounting for age and BMI.

Conclusions: In subjects with cardiac parameters within the normal ranges, left end-diastolic volume appears one of the most critical mechanism in increasing left ventricular mass independently of age and BMI. The augmented LV mass seems to be a compensatory physiological response to consistent pre-load increase.

515. Determination of Normal Gender-Specific Left Atrial Dimensions by Cardiovascular Magnetic Resonance Imaging

Burkhard Sievers, MD, Simon Kirchberg, Ulrich Franken, MD, Asli Bakan, Marvin Addo, Binu John-Puthenveettil, Hans-Joachim Trappe, MD. *Cardiology and Angiology, University of Bochum, Herne, Germany.*

Background: Cardiovascular magnetic resonance imaging (CMR) is becoming increasingly available in clinical practice. Therefore, there is a need to establish normal values for left atrial dimensions as determined by this method, to allow accurate assessment of cardiac dimensions and to provide standardization for follow up studies. For clinical purpose measurements of the left atrial end diastolic diameter (LAEDD) are most appropriate to assess left atrial size.

We aimed to establish normal values for LAEDD using CMR and a fast gradient-echo sequence with steady-state free precession (SSFP).

Methods: A total of 111 healthy subjects (52 women and 59 men, mean age 51.5 ± 14.5 years) were examined by CMR. Images were acquired using SSFP in the horizontal (HLA) and vertical (VLA) long axis planes, and the left ventricular outflow tract plane (LVOT) to measure the LAEDD, Fig. 1.

Results: Age between men and women was not different (p = 0.7050). CMR yielded the following normal ranges for LAEDD: HLA 4.5 ± 0.4 cm for men and 4.2 ± 0.5 for women, VLA 4.5 ± 0.5 cm for men and 4.2 ± 0.4 for women, and LVOT 2.8 ± 0.3 cm for men and 2.8 ± 0.4 for women. LAEDD were significantly larger in HLA and VLA than in LVOT ($p \leq 0.0001$). There was no significant difference in the measurements between HLA and VLA (p = 0.4617). Significantly gender-related differences for LAEDD were found in HLA (p = 0.0087) and VLA (p = 0.0015), but not in LVOT (p = 0.5281). LAEDD were not found to be age-related ($p \geq 0.0994$).

Conclusions: LAEDD differ significantly according to the image plane used. Differences are gender-specific. It can

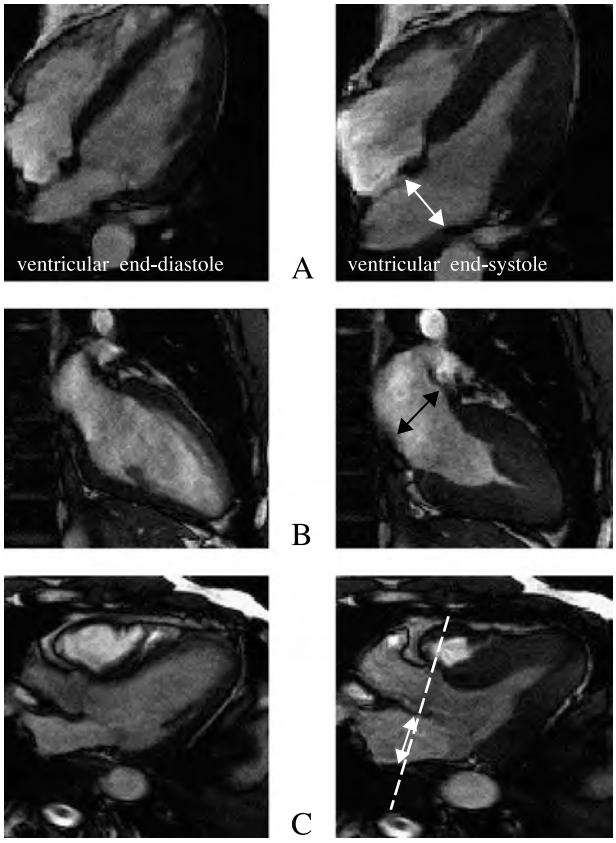

Figure 1.

be concluded that these normal ranges can be used for CMR measurements using SSFP and prospective triggering in the evaluation of left atrial diameters to identify patients with enlarged atria, and for follow-up studies to evaluate the efficacy of treatment.

516. Detection and Quantification of Pulmonary Hypertension Using Phase Contrast and Cine Cardiac Magnetic Resonance Imaging

Javier Sanz, MD, Santo Dellegrottaglie, MD, Roxana Sulica, MD, Martin Goyenechea, MD, Sanjay Rajagopalan, MD, Rafael Salguero, MD, Paola Kuschnir, MD, Teresa Rius, MD, Valentin Fuster, MD, PhD, Michael Poon, MD. *Cardiology, Mount Sinai School of Medicine, New York, NY, USA.*

Background: Right heart catheterization (RHC) is the *gold standard* for diagnosing pulmonary hypertension (PH). Although echocardiography is the most used non-invasive imaging technique, cardiac magnetic resonance imaging (CMRI) offers theoretical advantages for the evaluation of patients with PH. However, quantification of pulmonary pressures is currently not possible with CMRI.

Purpose: To develop a model for pulmonary pressure quantification using phase-contrast (PC) and cine CMRI.

Table 1.

n = 30	CMRI function			PC-CMRI		
RHC	RVEDV	RVESV	RVEF	Maximal area	PPV	PAV
MPAP	0.45	0.59	− 0.83	0.70	− 0.49	− 0.73
SPAP	0.46	0.62	− 0.87	0.74	− 0.43	− 0.79

Methods: Thirty patients with known or suspected chronic PH were evaluated with CMRI (1.5 Tesla) and RHC in the same day. Patients with shunts, venous PH and/or exercise-induced PH were excluded. Right ventricular end-diastolic and end-systolic volumes (RVEDV and RVESV; ml) and ejection fraction (RVEF; %) were measured in cine images (trueFISP). Pulmonary average velocity (PAV, cm/sec), cardiac output (CO; ml/min) and main pulmonary artery areas (minimal, maximal, mean; cm^2) were obtained using retrospectively gated, breath-hold, PC imaging (velocity encoding = 100 cm/sec) orthogonal to the main pulmonary artery. CMRI was compared with invasive determinations of mean and systolic PA pressures (MPAP and SPAP; mmHg).

Results: RHC confirmed PH in 22 patients. Correlation coefficients between PC and cine CMRI measurements and RHC-derived parameters are shown in Table 1. From the function images, RVEF was the single most useful parameter. From the PC images, PAV and maximal main pulmonary area showed the highest correlation with pulmonary pressures. Receiver-operator curve analysis identified RVEF < 51% and PAV < 13.4 cm/sec as optimal cutoffs for detection of PH (rest MPAP > 25 mmHg) with respective sensitivities/specificities of 86%/100% and 95%/100%. Using regression analysis, the following CMRI-derived equations for pulmonary pressures prediction were obtained: $MPAP = 62.17\ e^{-0.0066X}$ ($r^2 = 0.82$) and $PSAP = 106.83\ e^{-0.007X}$ ($r^2 = 0.85$) where X = PAV × RVEF/CO. The real and CMRI-estimated MPAP were 35.4 ± 14.4 and 34.5 ± 11.8 mmHg respectively (p = NS); mean bias = − 0.9 mmHg (12.88/− 14.68; 95% CI). The real and CMRI-estimated SPAP were 58.5.4 ± 24.3 and 57.5 ± 20.6 mmHg respectively (p = NS); mean bias = − 1 mmHg (18.5/− 20.5; 95% CI).

Conclusions: These preliminary results demonstrate the feasibility of noninvasive pulmonary pressure quantification using CMRI. This approach may be clinically useful in subjects with chronic PH.

517. Gender Differences in Normal Left Ventricular Structure and Function

Sunil T. Mathew, MD, Rebecca Donovan, William Schapiro, BS, RT, Nora Ngai, PhD, Nathaniel Reichek, MD. *Research, St. Francis Hospital, Roslyn, NY, USA.*

Introduction: Gender effects in left ventricular (LV) size, mass, geometry and function may be obscured by subclinical disease, systolic hypertension and obesity. Therefore, we performed cardiac MRI in carefully screened, normotensive, nonobese healthy subjects.

Methods: We imaged normal men and women ages 20–90 years (n = 156, mean = 51, 82 F), with body mass index < 28, no known cardiovascular disease and normal echocardiograms. Normal blood pressure (BP) was defined as < 140/90 mm Hg without hypertension or treatment history at all ages. Using a 1.5 T Siemens Sonata scanner, breath-hold short and long axis TrueFISP cines for LV volumes, mass, ejection fraction (EF), length and mean short axis area were obtained and indexed to body surface area using MASS (Medis).

Results: Women had lower systolic BP, end-diastolic and end-systolic volume indices, LV mass and mass/volume ratio than men overall. In women, EF was also higher and LV shape more elliptical. At age > 60, systolic BP became similar(men: 124 ± 11 mmHg, women: 124 ± 10 mmHg). LV volumes fell with constant mass in both men and women, resulting in higher mass/volume ratios. Gender differences in volumes, mass, EF and LV shape were unchanged.

	Males (n = 74) Age = 51 ± 15 y	Females (n = 82) Age = 51 ± 15 y	*p-value*
Systolic blood pressure (mm Hg)	121 ± 11	116 ± 12	< 0.02
EF (%)	57 ± 5	62 ± 5	< 0.0001
End-diastolic volume index (ml/m^2)	73 ± 14	66 ± 12	0.0017
End-systolic volume index (ml/m^2)	31 ± 7	25 ± 7	< 0.0001
LV mass index (g/m^2)	69 ± 10	55 ± 9	< 0.0001
LV end-diastolic mass/volume index	0.973 ± 0.197	0.858 ± 0.194	0.0003
LV length index (cm/m^2)	5.12 ± 0.43	5.60 ± 0.55	< 0.0001
LV area index (cm^2/m^2)	14.1 ± 2.5	11.8 ± 2.0	< 0.0001

Conclusions: Normal women have higher EF, more elliptical LV shape, lower indexed LV volumes, mass and mass/volume ratios than men, with lower systolic BP. After age 60, systolic BP rises, particularly in women, and chamber volumes fall similarly, with constant LV mass. However, gender differences in absolute volume and mass indices, EF and LV shape persist.

518. Adaptive *k-t* Blast/*k-t* Sense for Accelerating Cardiac Perfusion MRI

Alexei Samsonov,[1] Edward DiBella,[2] Peter Kellman,[3] Eugene Kholmovski,[2] Chris Johnson.[1] [1]*Scientific Computing and Imaging Institute, University of Utah, Salt Lake City, UT, USA,* [2]*Utah Center for Advanced Imaging Research, University of Utah, Salt Lake City, UT, USA,* [3]*Laboratory of Cardiac Energetics, National Insititutes of Health, Bethesda, MD, USA.*

Introduction: Recently proposed *k-t* BLAST/*k-t* SENSE techniques (Tsao et al., 2003) have proven very efficient for monitoring periodic changes, for instance, heart wall motion in cine cardiac MRI. The periodicity permits acquiring training data prior to actual scan to learn spatiotemporal correlations for optimized reconstruction of reduced data. However, using *k-t* BLAST/*k-t* SENSE in situations when the dynamic changes are arbitrary is problematic.

We present adaptive *k-t* BLAST/*k-t* SENSE that features self-calibration and self-training, which allow application of the methods to imaging a wide range of dynamic processes. The adaptation is achieved by using Variable Density (VD) sampling and TSENSE calibration (Kellman et al., 2001). The new method was tested on first-pass contrast enhanced myocardial perfusion data.

Methods and Results: The proposed approach relies on the observation that coil sensitivities and training data could be well approximated by low-resolution estimates. The VD *k*-space trajectory (Fig. 1) used in the method has a lower reduction factor in the *k*-space center ($R_C = 2$). The low-resolution data are supplied to TSENSE to provide training data and time varying sensitivities for *k-t* BLAST/*k-t* SENSE reconstruction. The *k*-space edges are undersampled with a much higher factor (4). Total acquisition speedup depends on a fraction of central *k*-space area n_{cntr} used for calibration. The reconstruction procedure is shown in Fig. 2.

The cardiac perfusion data were obtained on a 1.5 T Siemens Sonata MR system using saturation recovery TrueFISP (TR = 2.3 ms, TI = 90 ms, flip angle = 50°, 4 slices, 40 frames) and 8-element surface coil array (Nova Medical, Inc.). The VD sampling ($R_C = 2$, $R_O = 4$, $n_{cntr} = 0.15$) was simulated from data acquired with $R = 2$. *k-t* BLAST/*k-t* SENSE equations were solved iteratively by a conjugate gradient algorithm.

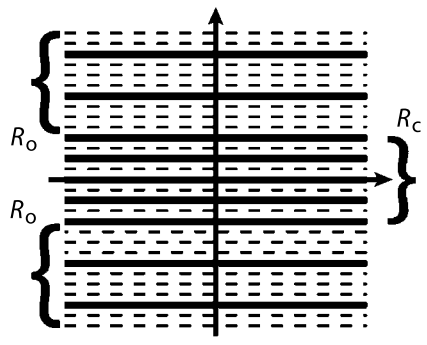

Figure 1. Variable density *k*-space sampling. The pattern is shifted in time with a period equal to local reduction factor (i.e., R_C for the central area, and R_O for the *k*-space edges).

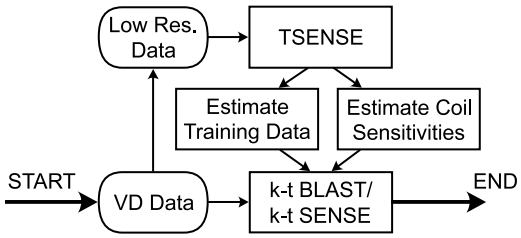

Figure 2. Adaptive *k-t* BLAST/*k-t* SENSE.

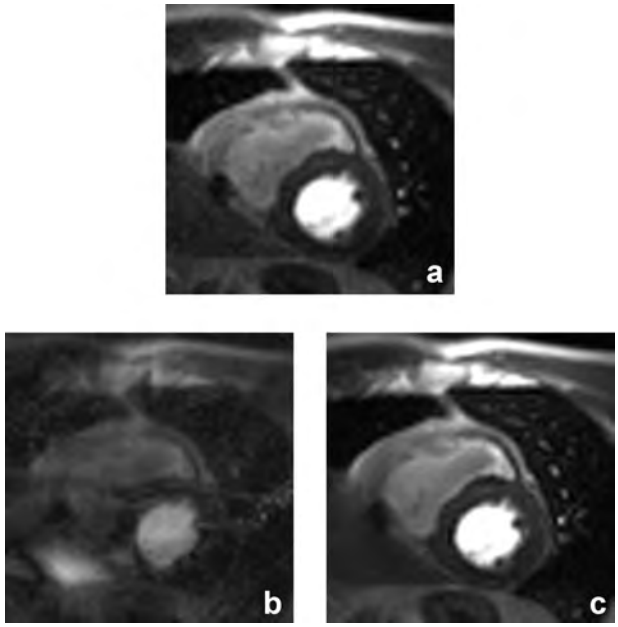

Figure 3. Magnified part of a slice from (a) TSENSE ($R = 2$) reconstruction, (b) direct inversion of VD data, and (c) adaptive *k-t* SENSE reconstruction ($R = 3.53$).

Figure 3 shows results of reconstruction of the data and comparison to the reference TSENSE reconstruction.

Discussion: We developed an adaptive *k-t* BLAST/*k-t* SENSE method that may be used for imaging aperiodic dynamic changes, without prior acquisition of training and reference data. The flexibility comes at an expense of acquisition speedup, which is somewhat lower for the adaptive method ($R = 3.53$ compared to $R = 4$ for non-adaptive method in the example).

The method was tested on cardiac perfusion data. Further studies are needed to investigate practical aspects of the method including optimal VD sampling and reconstruction artifacts, and to compare it to the related approaches (Boubertakh et al., 2004).

ACKNOWLEDGMENTS

NIH NCRR award P41RR12553-05 and NIH grant 1R01EB000177.

REFERENCES

Boubertakh, R., et al. (2004). *ISMRM*:343.
Kellman, P., et al. (2001). *MRM* 45:846–852.
Tsao, J., et al. (2003). *MRM* 50:1031–1042.

519. Semi-Automatic Segmentation of Tagged Myocardial Short-Axis Images

Andrea Rutz,[1] Salome Ryf,[1] Juerg Schwitter,[2] Marcus Alex Spiegel,[1] Sebastian Kozerke,[1] Peter Boesiger.[1] [1]*Institute for Biomedical Engineering, University and ETH, Zurich, Switzerland,* [2]*Division of Cardiology, University Hospital, Zurich, Switzerland.*

Introduction: Myocardial tagging combined with harmonic phase analysis (HARP) (Osman et al., 1999) has proven to be an accurate and fast method for the quantification of myocardial deformation. As a prerequisite for the calculation of functional indices, the myocardial tissue should be delineated reproducibly and desirably automatically. A method has been described previously (Schwitter et al., 2002) to accurately identify endo- and epicardial borders on short-axis CSPAMM (Fischer et al., 1993) images. It could be shown that by applying this method, the endo- and epicardial contours of the CSPAMM-images correspond well to the contours drawn on anatomical images. In this work, this reproducible but manual approach is further developed. Endo- and epicardial contours are detected automatically on threshold-images, allowing analyses of tagged short-axis images with minimal observer-interaction.

Methods: A magnitude image of the underlying anatomical structure in a tagged image is obtained by filtering out one peak in k-space and applying the inverse Fourier transform. The myocardium is identified with a few markers set by an observer. A spline is fitted through these markers and signal intensity along this contour is determined. The application of an adaptive threshold in a rotating sector along the spline yields the threshold-image for the detection of the myocardial borders. Starting from 72 landmark points equally distributed on the spline, the edges of the threshold-image are detected in both radial directions (Fig. 1a). Depending on the radial distance to the center of the spline, outliers are discarded and reallocated on a spline through the remaining points (Fig. 1b). The same procedure is independently applied for 4 separate sectors in order to smooth out papillary muscles and other irregularities in the threshold-image (Fig. 1c). Further smoothing of the epi-and endocardial contours is achieved by reallocating all points onto a spline through 12 equally distributed points which are radially defined by averaging the radii of all points in the respective sector (Fig. 1d).

CSPAMM images of 5 patients with hypertension and mild ventricular hypertrophy were acquired at three cardiac levels with a 1.5 T Philips scanner using a single breath hold EPI sequence (EPI-factor:9, FOV:300–330 mm, matrix:128 × 27, ramped flip angles:8–25°, 17 cardiac

phases). Endo- and epicardial contours were identified at the end of the cardiac cycle both manually on the threshold-images and automatically by applying the described algorithm. To compare the obtained contours, all points were resampled and the root mean square difference of the contours in radial direction was calculated. From the epi- and endocardial borders a midwall contour was calculated and tracked throughout the cardiac cycle using HARP incorporating peak-combination (Ryf et al., 2004). Circumferential shorting was compared for the tracked midwall contours.

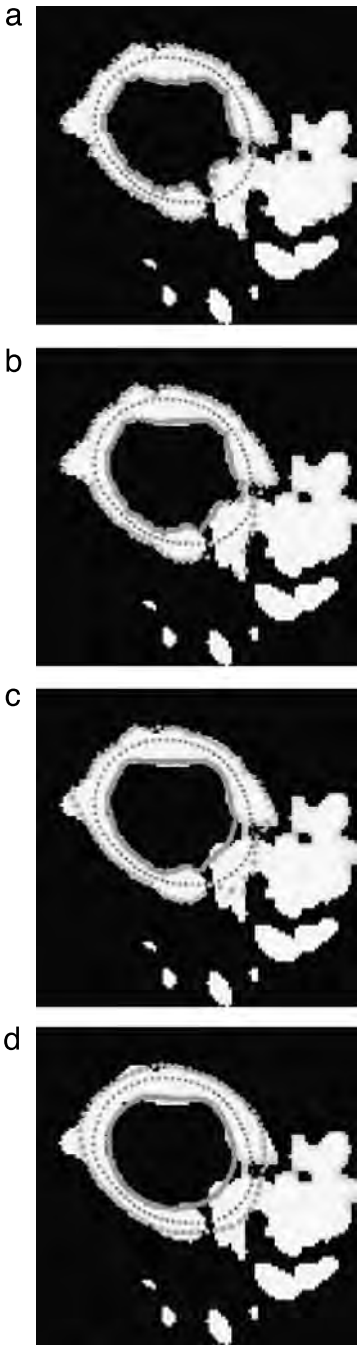

Figure 1.

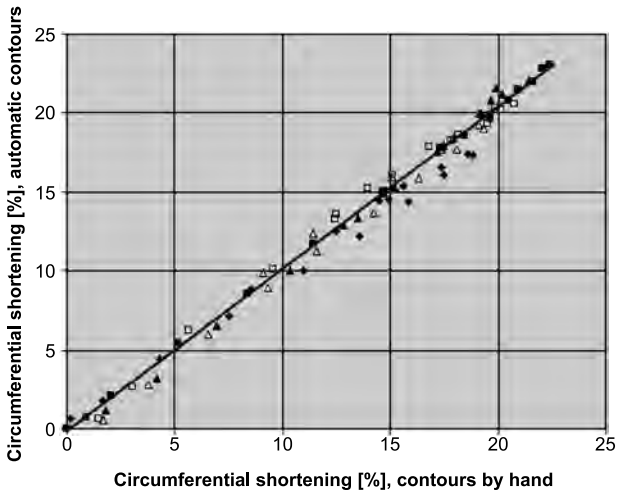

Figure 2. Each set of symbols corresponds to the contour of one patient tracked over 17 cardiac phases. For two independent observers, the root mean square difference in radial direction was 0.84 ± 0.31 mm for the endocardial and 0.73 ± 0.38 mm for the epicardial contours.

For the inter-observer reproducibility, the algorithm was applied independently by an experienced and an unexperienced observer. The root mean square value for the differences of the obtained contours was calculated.

Results: In one case the algorithm was unreliable for the epicardial border which had to be corrected manually. In all other cases the root mean square difference between the manually and automatically identified contours was 0.90 ± 0.27 mm for the endo- and 1.26 ± 0.61 mm for the epicardial contours. No significant differences were obtained for the circumferential shortening of the midline throughout the cardiac cycle (Fig. 2, regression: $y = 1.03 \times - 0.28$, $R^2 = 0.99$).

Conclusions: Applying the described method, endo- and epicardial contours can be calculated semi-automatically i.e. with minimal user interaction. The method is robust and allows for a faster and user independent analysis of tagged myocardial short-axis images.

REFERENCES

Fischer, S. E., et al. (1993). *MRM* 30:191–200.
Osman, N., et al. (1999). *MRM* 42:1048–1060.
Ryf, S., et al. (2004). *Proc. SCMR* 451.
Schwitter, J., et al. (2002). *Proc. ISMRM* 1676.

520. Spatial Resolution and Blood-to-Myocardium Contrast Effects in Perfusion Studies

Edward DiBella. *University of Utah, Salt Lake City, UT, USA.*

Introduction: How critical is the acquisition spatial resolution for myocardial perfusion imaging with dynamic contrast MRI?

Figure 1.

Partial volume effects are increased with lower resolution, and artifacts such as the endocardial dark rim artifact are expected with lower resolution. The impact of resolution and the blood-to-myocardium contrast (or edge strength) on perfusion images and kinetic flow estimates is studied here.

Methods: A high resolution dynamic contrast MRI dataset was acquired of a canine with an LAD occlusion. A turboFLASH saturation recovery sequence (TI = 100 ms, TR/TE = 2.2/1 ms, fli*p* = 10, 8 element coil, GRAPPA R = 2, 1.7 × 2 mm pixels, 0.05 mmol/kg) was performed on a 3 T Siemens Trio. Endocardial and epicardial contours were drawn on a selected slice and the left ventricle myocardium divided into 16 subendocardial and 16 subepicardial regions. Each region was replaced with its fit to a two compartment model and the rest of the image was left as it was originally to create a simulation with known parameters. These ''true images'' were Fourier transformed to give dynamic 144 × 192 simulated k-space data.

Lower resolution acquisitions were simulated by truncating k-space in the phase encode direction. The reconstructions were repeated with 100%, 50%, and 25% of the phase encodes (truncation centered around the origin of k-space and zero-padded to give the same reconstructed pixel size). In the resulting images, the myocardium was divided into 8 transmural regions that were each fit to a two compartment model to give K^{trans}. The fits were also done pixelwise.

This truncating and subsequent analysis was repeated after multiplying the blood pool of the simulation by a factor of 4, to increase the edge strength.

Results: At the lower edge strength, the dark rim artifact was minimal to non-existent for all of the differently truncated datasets. The truncated datasets gave average K^{trans} errors of absolute percent difference of 1% at half truncation, and 5% at one-quarter of the phase encodes for the 8 region case. Figure 2 shows the comparison with pixelwise fits.

At the higher edge strength, the dark rim artifact was clearly evident for truncation of 50% and 25% (Fig. 1: Left-One time frame from lower edge strength simulation, using 25% of the full k-space columns. Right-Same image but using higher edge strength simulation shows marked dark rim artifact due to ringing of the sharp edge.) The dark rim artifact is consistent with blurring in the horizontal direction. However, the dip this truncation artifact caused in the time

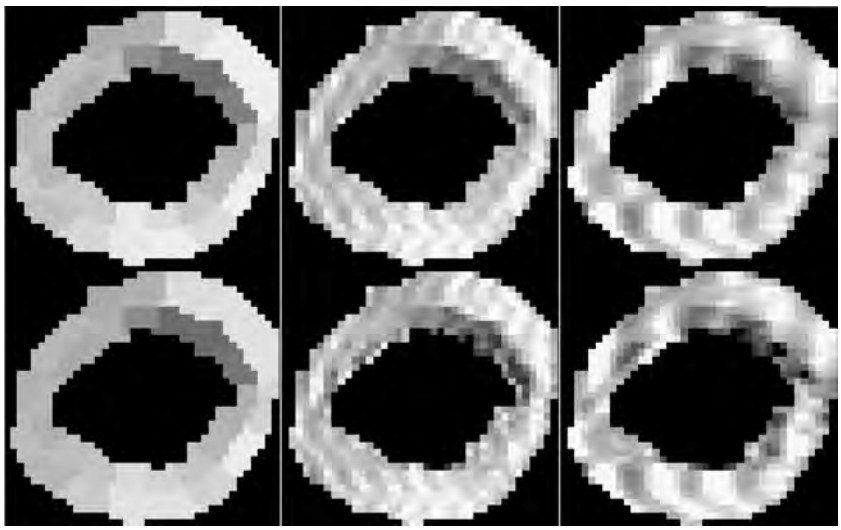

Figure 2.

curves was "ignored" by the fitting routine since it was not consistent with the mathematical model used. Thus the parameter estimates were affected very little. The 8 region case with higher edge strength had errors of 3% and 7% for 50% and 25% of the data, respectively. The pixelwise K^{trans} parameter estimates are displayed in Fig. 2. From left to right: no truncation, 50% truncation, and truncating to 25% of the phase encodes. Top: lower edge strength, bottom: higher edge strength. Compare to Fig. 1 and note the absence of effect of the dark rim artifact. The wavy vertical lines are due to ringing from the bright edge next to the surface coils.

Conclusion: This study sheds light on the nature of the dark rim artifact and its interdependence on edge strength and spatial resolution. This illustrates that studies with poor resolution may not suffer from dark rim artifact, depending on the edge strength of the blood/myocardium interface. This follows from Gibbs theory, but has not been made evident previously.

The degrading effect of spatial resolution on kinetic parameter estimates was shown to effect the parameter estimates rather modestly in this simulation.

521. Real-Time Imaging of Regional Myocardial Function Using Fast-SENC

Li Pan, MSE,[1] Matthias Stuber, PhD,[2] Dara L. Kraitchman, VMD, PhD,[2] Nael F. Osman, PhD.[2] [1]*Department of Biomedical Engineering, Johns Hopkins School of Medicine, Baltimore, MD, USA,* [2]*Department of Radiology, Johns Hopkins School of Medicine, Baltimore, MD, USA.*

Introduction: Strain Encoded (SENC) (Osman et al., 2001) MRI has been introduced as a technique that can *directly* image regional contractility of the heart without a need for time-consuming post-processing. In this study, an accelerated SENC imaging sequence, with scan time as short as a single heartbeat, was implemented. It included three features: 1) spiral imaging for rapid acquisition, 2) localized excitation for reduced FOV without foldover artifacts, and 3) interleaved low-and high-tuning frequencies (required for SENC imaging) in a single acquisition.

Purpose: To quantitatively image regional function of the heart with a scan time as short as a single heartbeat using accelerated SENC imaging.

Methods:Localized Excitation: To shorten the scan time, a reduced FOV enables the size of the sampled matrix in the *k*-space to be reduced. Similar to a technique proposed by Fischer et al., 1994, a *2D localized SENC* was developed (Fig. 1). The signal from the surrounding untagged region is suppressed in the acquired images, and a smaller FOV image without foldover artifacts can be acquired.

Interleaved Tuning: The pulse sequence was modified so that the low-and high-tuning images required for SENC imaging were acquired in an interleaved fashion throughout the cardiac cycle. Thus, the imaging time was reduced in half.

Spiral Imaging: A spiral readout is used to shorten acquisition intervals. Considering that most of the information of SENC images is localized in the center of *k*-space, spiral imaging with a densely sampled center of *k*-space is particularly well-suited.

Fast-SENC Acquisition: By the combination of localized excitation, interleaved tuning and spiral imaging, images can be acquired in as fast as one cardiac cycle (*fast-SENC*).

Normal Human Subject: MR imaging was performed on a Philips 1.5 Tesla MR whole body system. Images were acquired in a four chamber view using conventional SENC (two breath-holds, 12 heartbeats each, with TR = 22.4 ms) and fast-SENC (one heartbeat, with TR = 37.2 ms). From the two image series, the circumferential strains at six points, located in the basal-, mid-, and apico-septum and basal-, mid-,

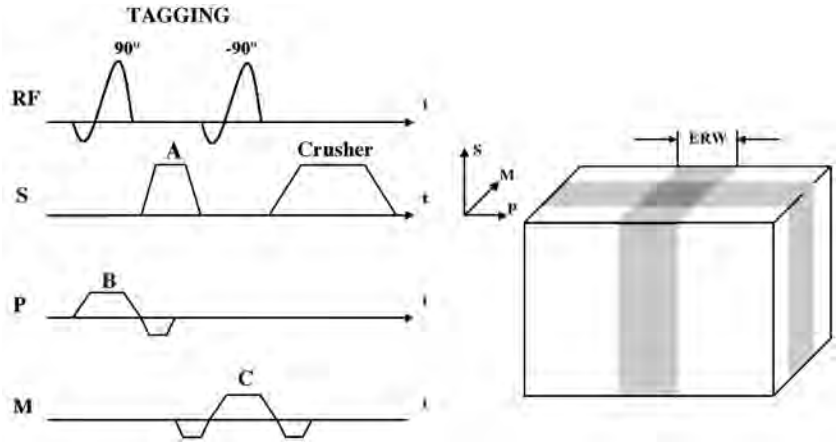

Figure 1. 2D localized SENC pulse sequence. By modifying the two 90-degree tagging RF pulses from non-selective to slice-selective (changing the shape of the RF pulse and adding an extra slice selection gradient, shown as B and C, at both the frequency-encoding and the phase-encoding direction), the tagged region is restricted to a cuboid orthogonal to the slice selection direction. (ERW = Excited Region Width, S = slice selection, *p* = phase encoding, and M = measurement).

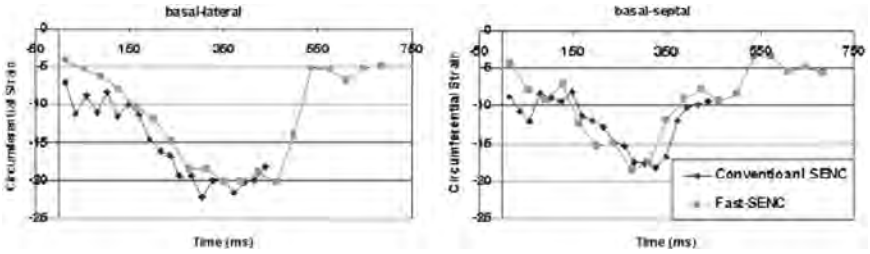

Figure 2. Strain measurements from two randomly selected points, located at two regions of the left ventricle on the four-chamber view of the normal human subject study. Strain values were measured by fast-SENC and conventional SENC, respectively.

and apico-lateral region of the left ventricle, were computed for comparison.

Animal Study: The fast-SENC pulse sequence was tested in a dog with a 9-week reperfused myocardial infarction in the anterioseptal part of the left ventricle. A fast-SENC image sequence was acquired in one heartbeat with TR = 37.2 ms. After an intravenous contrast injection of 0.2 mmol.kg^{-1} Gd-DTPA, a high resolution image was acquired using conventional SENC in two breath-holds (48 heartbeats each) with TR = 22.6 ms. Fifteen minutes after contrast injection, a delayed enhancement image (inversion time = 175 ms) was obtained to determine the infarct location.

Results: The strain measurements of conventional SENC and fast-SENC methods throughout the cardiac cycle were very similar (Fig. 2). The two acquisition methods (fast-SENC data was linearly interpolated to obtain the same temporal resolution as conventional SENC) also showed high agreement ($r^2 = 0.81$, $y = 0.96 \times + 0.65$). Figure 3 shows the SENC images at end-systole corresponding to the delayed enhancement image. Both the SENC and fast-SENC images clearly show the dysfunctional area, indicated by the arrows, which very closely matches the infarcted area in the delayed enhancement image. Furthermore, the high-tuning fast-SENC image clearly reveals the infarcted, dysfunctional area, which disappears from the image due to akinesia.

Conclusions: The fast-SENC pulse sequence enables the acquisition of strain encoded images in a single heartbeat, does not require major post-processing or segmentation, and therefore has the potential to image the onset of arrhythmia, and ischemia during dobutamine stress tests.

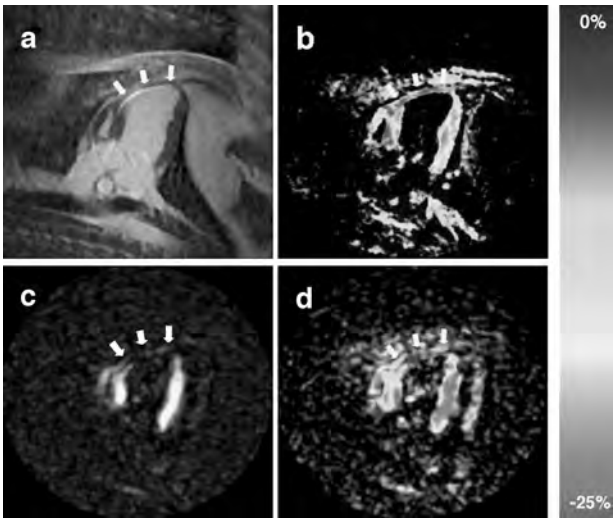

Figure 3. Comparison of SENC functional images with the delayed enhancement image. All images were acquired at end-systole. a. Delayed enhancement image 15 minutes after gadolinium injection (TI = 175 ms, t = 185 ms) with non viable infarcted myocardium hyper-enhanced (arrows). b. Conventional SENC functional image (t = 219 ms) showing dysfunction (arrows) in infarcted myocardium. c. Fast-SENC high-tuning image (t = 239 ms) showing no contraction in infarcted myocardium (arrows). d. Fast-SENC functional image (t = 239 ms) showing lack of contraction in infarcted tissue (arrows).

ACKNOWLEDGMENTS

This research was supported by RO1HL072704.

REFERENCES

Fischer, S. E., et al. (1994). *Magn. Reson. Med.* 31:401–413.
Osman, N. F., et al. (2001). *Magn. Reson. Med.* 46:324–334.

522. DENSE with SENSE

Anthony H. Aletras, PhD, W. Patricia Ingkanisorn, MD, Andrew E. Arai, MD. *Laboratory of Cradiac Energetics, National Institutes of Health, Bethesda, MD, USA.*

Introduction: Cardiac motion imaging with displacement encoding with stimulated echoes (DENSE) has been used for mapping regional contractile function (Aletras et al., 1999; Kim et al., 2004). Tag-like artifacts can arise from unwanted spectral peaks within the k-space pass-band when small gradient encoding moments are used for reduced intravoxel dephasing (Aletras et al., 2004). Artifact suppression by RF phase cycling prolongs the breath-hold time (Aletras et al., 2004; Epstein et al., 2003). DENSE with sensitivity encoding (SENSE) is presented to accelerate the acquisition for patient scanning.

Purpose: To implement sensitivity encoding (SENSE) with DENSE in order to accelerate the acquisition for patient breath-hold scanning.

Methods: Short axis 2D DENSE images at 1.5 T were acquired from a patient with an eight element phased array and the following parameters: voxel size 2.9 × 2.9 × 8 mm, TE 5 ms, TR 1 heartbeat, ETL 24, bandwidth ± 62.5 kHz, encoding strength 4 mm/π, orthogonal phase cycling. X, Y and Reference (X−Y−R) images were acquired within one breath-hold. SENSE acceleration (R = 2) reduced scan time from 26 to 14 heartbeats. Circumferential shortening (CS) and radial thickening (RT) were computed. Strain noise was measured by acquiring three reference scans along each direction in a normal volunteer (Aletras et al., 2001).

Results: CS and RT maps of a patient show that the hypokinetic area in the infarcted inferior wall (A) and the normal myocardium are mapped similarly with SENSE acceleration (B, C) as well as without (D, E). Strain noise for the 3 different scans is shown in the Table 1.

Table 1. Strain noise table

	R/R/R	X/X/X	Y/Y/Y
CS R = 2	− 0.46 ± 3.79	− 0.37 ± 4.28	− 0.31 ± 4.28
CS R = 1	+ 0.31 ± 3.34	+ 0.14 ± 4.42	− 0.94 ± 4.92
RT R = 2	− 0.88 ± 4.45	− 0.49 ± 5.10	+ 0.49 ± 4.96
RT R = 1	+ 1.59 ± 3.88	+ 1.42 ± 4.91	+ 1.22 ± 4.81

Conclusions: SENSE accelerated DENSE reduces the breath-hold time for patient scanning. Thus, X−Y−R images can be acquired in the same breath-hold to avoid registration errors. This is the first application of SENSE to a phase-based motion mapping method such as DENSE.

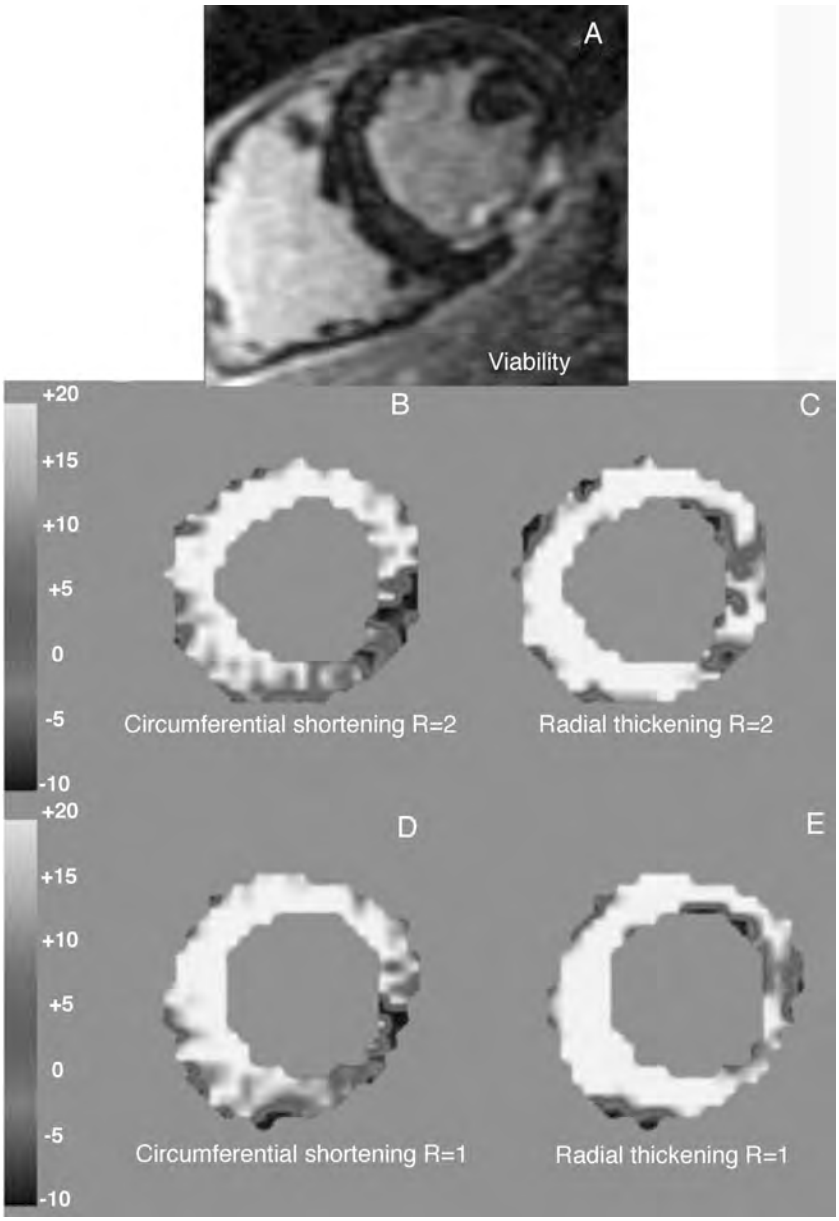

REFERENCES

Aletras, A. H., et al. (1999). *J. Magn. Reson.* 137(1):247–252.
Aletras, A. H., et al. (2001). *Magn. Reson. Med.* 46(3):523–534.
Aletras, A. H., et al. (2004). *J. Magn. Reson.* 169(2):246–249.
Epstein, F. H., et al. (2003). *Proc. Int. Soc. Magn. Reson. Med.* 11:1566.
Kim, D., et al. (2004). *Radiology* 230(3):862–871.

523. A Multi Half-Echo Projection Reconstruction MR Technique for Myocardial Viability

Orhan Unal, PhD,[1] Ethan K. Brodsky, MS,[2] Walter F. Block, PhD,[2] Tim F. Christian, MD,[3] Thomas M. Grist, MD.[4]
[1]*Medical Physics, University of Wisconsin, Madison, WI, USA,* [2]*Biomedical Engineering, University of Wisconsin, Madison, WI, USA,* [3]*Department of Cardiaology, University of Wisconsin, Madison, WI, USA,* [4]*Department of Radiology, University of Wisconsin, Madison, WI, USA.*

Introduction: Myocardial viability assessment is important to predict which patients might benefit from revascularization. T1-weighted post-contrast delayed-enhancement MR imaging is a promising technique that can be used in distinguishing infarcted from normal myocardium since infarcted myocardium regions exhibit higher signal than normal myocardium. Typically, the inversion time (TI) is set to null normal myocardium signal to increase the contrast between normal and infarcted myocardium. However, the TI to null normal myocardium signal varies from patient to patient and also depends on the contrast dosage. A fast and robust technique that allows retrospective selection of TI to null normal myocardium would be advantageous.

Purpose: The purpose of this work is to develop an MR imaging technique with improved data acquisition efficieny. The sampling efficiency is doubled by acquiring data during dephaser, readout, and rephaser gradients as well as ramps during each TR. This gain in the data acquisition efficiency can be utilized either to shorten scan time or improve SNR and CNR. In addition, sampling the center of k-space multiple times during each TR should lead to reduced fat sensitivity.

Methods: A 2D multi half-echo (SPGR/SSFP), cardiac-gated, angularly undersampled PR-based, segmented inversion-recovery MR technique for post-contrast myocardial viability imaging with improved data acquisition efficiency that allows retrospective selection of inversion time (TI) to null normal myocardium effectively by taking advantage of the intrinsic oversampling of the center of the k-space in projection reconstruction (PR) acquisition and a sliding-window reconstruction technique with a temporally varying aperture with radial distance was developed.

The four half-echo pulse sequence and k-space trajectory are shown in Fig. 1a and 1b, respectively. All experiments were performed on a 1.5 T cardiac scanner (GE Medical Systems, Milwaukee, WI). Projections were acquired in an interleaved fashion with typical scan parameters of TR/TE/Flip = 3.9 ms/1.4 ms/20–50°, 32–64 projections, 4–8 projections per interleave, 16 interleaves, FOV = 350 mm × 350 mm, slice thickness = 5 mm, and RBW = ± 125 kHz. Scan time varied between 8–12 heart beats. During each heart beat, 3–5 distinct sets of interleaved projections were repeatedly acquired. When an ECG trigger was detected, projection angle was incremented and new unique sets of interleaved projections were acquired. A sliding-window reconstruction scheme with a temporal aperture varying with radial distance (or Tornado filter) was utilized to combine data from several time frames (3–5) in k-space to form images.

Results: When data from multiple frames are combined, streak artifacts were less visible and SNR was higher as expected.

Short scan times achieved with this improved technique should make breathholding more tolerable. These advantages and our preliminary results suggest that a PR-based segmented inversion-recovery technique may be a viable alternative for the myocardial delayed-enhancement viability imaging.

Conclusions: Our initial results suggest that the 2D multi half-echo cardiac-gated PR-based inversion-recovery technique allows retrospective selection of inversion time (TI) for nulling normal myocardial signal. The method provides an attractive alternative for the imaging of the viability of myocardium as well as wall motion abnormalities.

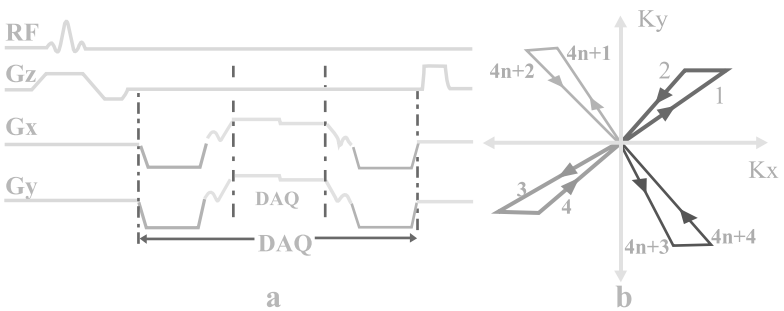

Figure 1.

524. Optimized Fat Suppression Sequence for Cardiac Imaging Using Stimulated Echo Mode (STEAM)

Ahmed S. Fahmy,[1] Nael F. Osman, Ph.D.[2] [1]*Electrical and Computer Engineering, Johns Hopkins University, Baltimore, MD, USA,* [2]*Department of Radiology, Johns Hopkins University, Baltimore, MD, USA.*

Introduction: Imaging using stimulated echo mode (STEAM) sequences has many applications in imaging tissue NMR parameters as well as tissue deformation especially the heart. An important requirement for imaging the myocardium deformation is high temporal resolution without sacrificing the image quality or the scan time. Nevertheless, avoiding chemical shift artifact by means of fat suppression usually encounters reduction of the temporal resolution and increase in the scan time and specific absorption ratio (SAR) level.

Purpose: Developing a fat suppression technique for STEAM sequences without sacrificing the scan temporal resolution, scan time or increasing the SAR level.

Methods: Conventionally, fat suppression is usually achieved by repeating a fat-suppressing sequence at each excitation pulse, e.g. STIR, SPIR, spectral-spatial excitation techniques [Fig. 1(a)]. In this work, fat suppression is achieved by applying a single pre-saturation fat-selective RF pulse that precedes the modulation pulses of the STEAM sequence [Fig. 1(b)]. As a result, only the tissue water content will produce stimulated echo while the tissue fat content will generate only T1 echo. Because only the stimulated echoes are acquired and used to reconstruct the images, no fat signal appears on the resulting images.

To test the method, human subject experiments were performed, where a healthy volunteer was examined using fast STEAM sequence (Frahm et al., 1991). Fat suppression using spectral-spatial selective pulses (1-3-3-1) method, with suppression repeated every imaging excitation, and our proposed method. The general imaging parameters were as

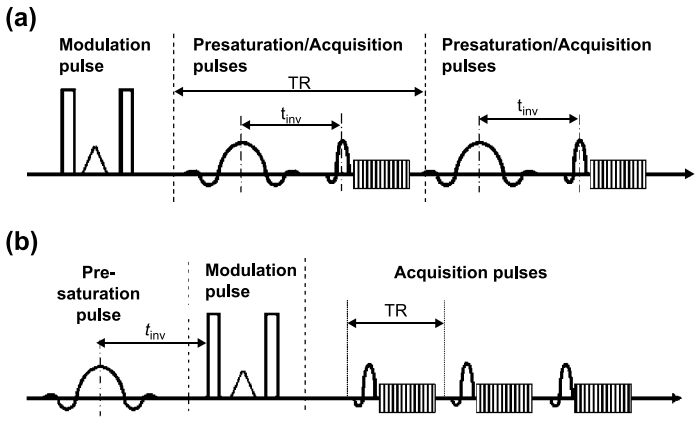

Figure 1. Pulse sequence for fat suppression in STEAM sequences (a) optimized, and (b) conventional.

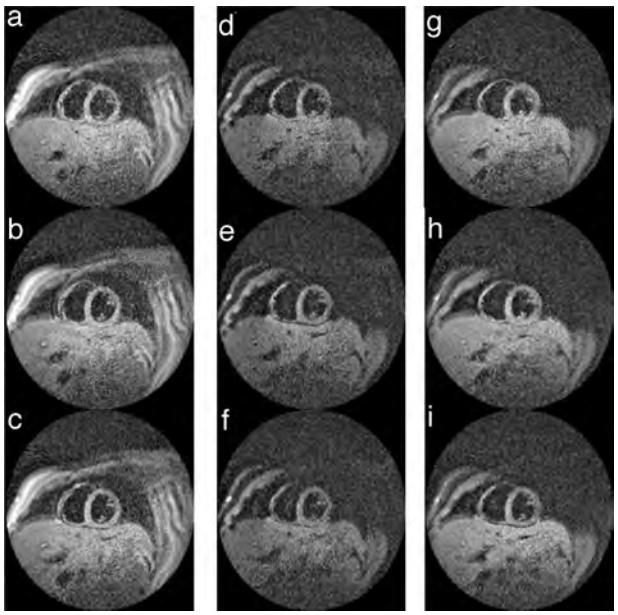

Figure 2. Three time frames acquired using fast STEAM sequence. Images from left to right are acquired without fat suppression, with spectral-spatial selective technique and with the proposed fat suppression technique.

following: spiral acquisition of 12 interleaves, FOV = 350 mm, number of cardiac phases = 19, slice thickness = 10 mm, and flip angle = 40°. The TR/TE times were equal to 22.5/4.9 ms for images obtain using spectral-spatial selective fat suppression technique and 15.1/1.1 ms for images obtained using the proposed method. The total area of the modulation gradient for the STEAM sequence was 3.92 G.ms/cm.

Results: The first three time frames of short axis images of the volunteer's heart are shown in rows in Fig. 2. Images in Fig. 2(a)–(c) were acquired without using any fat suppression technique (27, 42, 57 ms after the ECG trigger). Images in Fig. 2(d)–(f) and 2(g)–(i) were acquired using spectral-spatial selective fat suppression technique and the proposed method respectively. Due to the difference in the scan temporal resolution when using spectral selective fat suppression, the times of images 2(d)–(f) were 36, 58, and 81 ms after the ECG trigger.

Discussion: As shown in Fig. 2(a)–(c), the fat surrounding the heart causes blurring of the myocardium, which affects the image quality. Using spectral-spatial selective RF pulses improves the image quality as shown in Fig. 2(d)–(f) and removes the artifacts, but at the cost of reducing the temporal resolution of the scan (TR = 22.5, max possible number of cardiac phases = 28). Our proposed pre-saturation fat-selective RF pulse immediately preceding the modulation part of the STEAM sequence proved effective in suppressing the fat signal as shown in Fig. 2(g)–(i). Because the proposed method does not repeatedly apply pre-saturation pulses at every acquisition, the SAR level is maintained at nearly the

same level of the pulse sequence when applied without fat suppression. The proposed technique is also applicable to STEAM-like sequences, such as complementary spatial modulation of magnetization (CSPAMM), strain encoded (SENC) MRI, harmonic phase (HARP) MRI and displacement encoding (DENSE).

Conclusion: A method is proposed to suppress the fat signal in STEAM imaging sequences without increasing the SAR level or the total scan time, nor degrading the temporal resolution.

ACKNOWLEDGMENTS

This research was supported by a grant from the National Heart, Lung, and Blood Institute (RO1 HL072704).

REFERENCES

Frahm, J., et al. (1991). *Magn. Reson. Med.* 34:80–91.

525. Marked Reduction in Acquisition Times for Velocity Quantification Using iPAT

Preeti Kansal, MD,[1] Qiang Zhang, PhD,[2] Orlando P. Simonetti, PhD,[2] Chiara Bucciarelli-Ducci, MD,[1] Paula Tejedor, MD,[1] Thomas A. Holly, MD,[1] James C. Carr, MD,[1] Edwin Wu, MD.[1] [1]*Northwestern University, Chicago, IL, USA,* [2]*Siemens Medical Solutions, Inc, Chicago, IL, USA.*

Introduction: Phase contrast cine MR imaging (PC-MR) can be reliably used for blood flow quantification to assess valvular heart lesions. However, clinical studies are limited by either long patient breath hold times or insufficient temporal resolution. Parallel imaging techniques such as iPAT (GRAPPA) allow the acquisition of flow quantification data with decreased acquisition time by reducing the number of acquired phase-encoding lines.

Purpose: The purpose of our study was to compare the reproducibility of peak and mean blood flow velocities using PC-MR with and without GRAPPA.

Methods: Blood flow measurements across the mitral and aortic valves and the left ventricular outflow tract were made in 7 research volunteers using a Siemens 1.5 T Sonata or Avanto scanner. 3 subjects were referred for evaluation of known valvular disease, 3 for adenosine stress MR and 1 for viability assessment. Regions of interest (ROI) were measured in a total of 119 individual frames and analysis was performed using a Siemens Argus flow package. Images were obtained during sequential breath-holds with and without GRAPPA. Typical imaging parameters were: matrix size = 192, FOV = 340 mm, TR = 50 msec, 4 segments and 1 average. GRAPPA images were obtained with 20 reference lines and a reduction factor (R) of 2. Phantom studies at a flow rate of 2 L/min were also obtained using similar imaging parameters with and without GRAPPA (R = 2).

Results: Peak and mean velocities ranged from 21 cm/sec to 444 cm/sec and from 12 cm/sec to 306 cm/sec, respectively. In the research volunteers, peak flow measurements with GRAPPA correlated strongly to the values obtained without GRAPPA (Pearson's correlation coefficient, $r = 0.999$; $p < 0.01$). Mean velocities showed a similar relationship (correlation coefficient, $r = 0.998$, $p < 0.01$). Breath hold times were reduced by 42%, from an average of 23.9 ± 2.3 secs to 14.1 ± 1.4 secs. In the flow phantom, the average velocities at a flow rate of 2.0 L/min, with and without GRAPPA (R = 2) were 50.9 cm/sec and 51.9 cm/sec (percent difference: 1.9%).

Conclusions: PC-MR for flow quantification using GRAPPA can be reliably used in the measurement of peak and mean blood flow velocities. Our results confirm that using GRAPPA parallel imaging, peak and mean valvular velocities are highly reproducible and offer a more than 40% reduction in breath hold times. This substantial decrease in acquisition time makes a comprehensive evaluation of patients with significant cardiac disease more feasible.

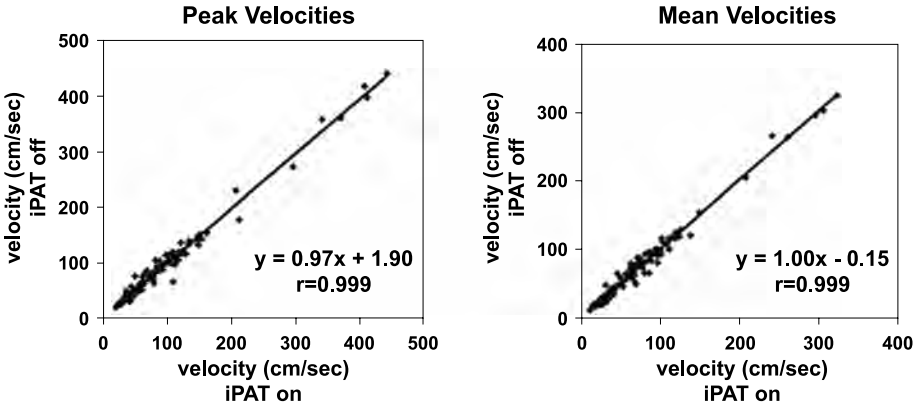

526. Myocardial T2 Estimation for Measurements of Iron Loading in the Heart

Taigang He, PhD, Peter D. Gatehouse, PhD, Mark Tanner, MD, Mark Westwood, MD, Jill Smith, Tim Cannell, Dudley J. Pennell, MD, David N. Firmin, PhD. *CMR Unit, Royal Brompton Hospital, London, UK.*

Introduction: Recent studies have shown cardiovascular magnetic resonance (CMR) can provide a non-invasive procedure for assessing the iron content of the myocardium, which is useful for early diagnosis and treatment (Anderson et al., 2001; Mavrogeni et al., 1998; Westwood et al., 2003). Previously, a T2* technique has been developed and clinically validated for this (Anderson et al., 2001; Westwood et al., 2003). Conventional T2 measurement techniques have also been attempted but have not found widespread use because of lack of sensitivity, motion artifacts and poor signal-to-noise ratios (SNR) (Westwood et al., 2003). The aim of this study was accordingly 1) to improve T2 measurement methods for better quantification of myocardial iron concentration, 2) to compare the results with a clinically validated T2* technique. For this purpose, a breath-hold multiecho FSE sequence (BH-FSE) was developed. This sequence permits acquisition of multiecho images in one breath-hold, but with a relatively low spatial resolution. A navigator controlled multiecho spin-echo sequence (NAV-SE) was also developed, which allows the acquisition of higher resolution images during free breathing. Phantom studies and scans in thalassaemia patients are reported.

Purpose: To develop CMR sequences for myocardial T2 measurement in thalassaemia major and to compare the measurements with those of T2* in the same patients.

Methods: A 1.5 T scanner (Siemens Sonata) with 4-channel body array coil and gradient performance up to 40 mT/m and 200 T/m/s was used. Scans were synchronized to diastole and mid short axis images were acquired. Blood suppression was accomplished with a nonselective 180° inversion pulse followed immediately by an adiabatic slice-selective 180° inversion pulse (Mavrogeni et al., 1998). Non-selective refocusing train was adopted to suppress motion artifacts and to minimize stimulated echoes, and large balanced gradients were used before and after all refocusing pulses in both slice selection and phase encoding directions to suppress image artefacts.

The parameters common to both sequences were: 10 mm slice thickness, field of view (FOV) 40 cm and TR defined by the heart rate or fixed at 2000 ms (phantom). Parameters for the BH-FSE sequence were: 12 successive acquisitions, 128*64 matrix, turbo factor 3, shortest TE = 4.8 ms, and echo spacing 14.4 ms. For the NAV-SE sequence, parameters were 16 successive acquisitions, 256*256 matrix, shortest TE 6 ms, and echo spacing also 6 ms. Navigator echoes were positioned through the diaphragm to track respiratory motion.The phantom was made of 6 tubes filled with dilutions of gadolinium (T2 20–100 ms). The methods were tested and then compared with measured T2* (Anderson et al., 2001) in nine thalassemia patients. The measured signal intensity (mean of ROI) for different echo times was fitted by using a nonlinear regression to determine both T2 and T2*.

Table 1. T2 Values (ms) of phantoms obtained with different sequences

No.	1	2	3	4	5	6
MSE	22.7	34.4	39.2	58.8	76.3	91.7
BH-FSE	24.3	36.5	42	63.3	81.3	91.7
NAV-SE	23.9	36.2	41.3	63.3	78.1	97.7

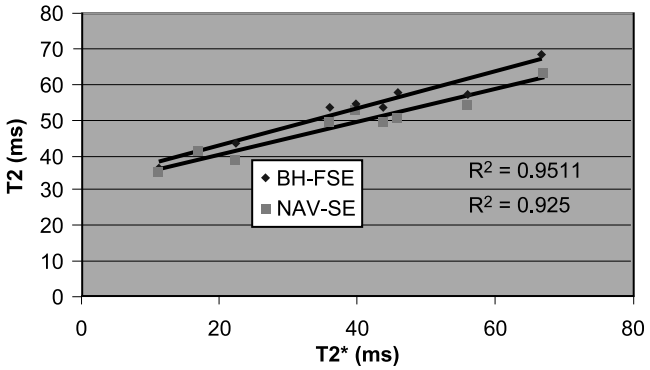

Figure 1.

Results: On the phantom, multiple standard SE (MSE) measurements were taken as the gold standard. Only minor differences in T2 were shown between BH-FSE, NAV-SE, and the MSE sequences (Table 1). T2* and T2 were linearly related (Fig. 1). Artefacts on the T2 images were limited despite a breath-hold duration of about 20 s.

Discussion and conclusion: This work demonstrates that accurate T2 measurements in phantoms can be obtained with the new sequences, and that good results were also obtained from myocardium with limited problems from artefacts.

The myocardial T2 correlated linearly with T2* in patients, but T2 might less sensitive to change than T2*. However T2 is unaffected by susceptibility artefact, and it may be a useful parameter in combination with T2* for determining different forms of storage iron.

ACKNOWLEDGMENTS

This work is part of the project "MR OF HEART IRON: T2*/T2 CALIBRATION AND APPLICATION," supported by NIH Grant R01 DK66084-01.

REFERENCES

Anderson, L. J., et al. (2001). *Eur. Heart J.* 22:2171–2179.
Mavrogeni, S. I., et al. (1998). *Int. J. Card. Imaging* 14:117–122.
Westwood, M., et al. (2003). *J. Magn. Reson. Imaging* 18:33–39.

527. Is a Free Software an Alternative for the Analysis of Ejection Fraction in Cardiac Magnetic Resonance?

Fabio Berezowsky Rocha, MD, Flavio Luiz Rua Ribeiro, MD, Marcelo Sá Vieira de Brito, MD, Fátima Cristina Pedroti, MD, Luiz Francisco Rodrigues de Àvila, MD, PhD, Carlos Eduardo Rochitte, MD, PhD, José Rodrigues Parga, MD, PhD. *Cardiovascular Magnetic Resonance Laboratory, Heart Institute-InCor-University of São Paulo Medical School, São Paulo, Brazil.*

Introduction: Ejection Fraction (EF) is the most used parameter in the clinical assessment of cardiac function. The scientific literature has shown evaluation of EF by many methods (ex: echocardiography, nuclear medicine and Cardiac Magnetic Resonance) in the variety of clinical settings. Cardiac Magnetic Resonance (CMR) is considered nowadays the gold standard method in the cardiac function evaluation with proven reliable measures of left ventricle (LV) volumes and EF, avoiding mathematical models. EF analysis is performed by commercial specifics softwares, which usually run in dedicated workstation using DICOM protocol. Automatic or manually measurements for each cardiac phase are traced to obtain the volumes and EF values. Recently some freeware softwares are available for this objective. The EF is variable composed by product of final left ventricular diastolic volume (FLVDV) minus the final left ventricular systolic volume (FLVSV) divided by the FLVDV that could be obtained by such freeware programs, after tracing each LV contours.

Purpose: To compare a free planimetric software (ImageJ), as an inexpensive option to a commercial already validated specific software (MASS® ANALYSIS PLUS 4.0.1-MEDIS, LEIDEN) for EF measurements.

Methods: We studied consecutively one hundred patients referred for ventricular function evaluation in the MR laboratory between January to July 2004. Studies were performed in a Signa LX/CVi 1.5 T (GE HEALTH CARE, Milwaukee, Wisconsin). A Steady State Free Precession Fast Gradient Echo (FIESTA®) sequence was used with following parameters: FOV 34–40; TR/TE 3.4/1.3; Slice thickness 8 mm; Gap 2 mm; Matrix 160 × 160; View Per Segment 12–18; Nex 1; Cardiac Phases 20. The analysis was performed by two observers, utilizing the MASS® ANALYSIS PLUS in the workstation and the ImageJ software in a personal computer. The images were transfer to an offline workstation (MASS® ANALYSIS PLUS) and to personal computer (ImageJ) for each slice at end systole and end diastole contour tracing. All data were collected and the statistical analysis was done in the StatView software. The data was evaluated using Paired T-test, comparative linear regression and Bland-Altmann.

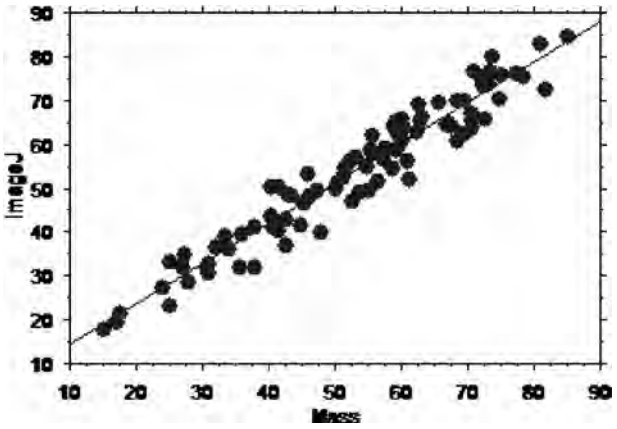

Linear regression plot result.

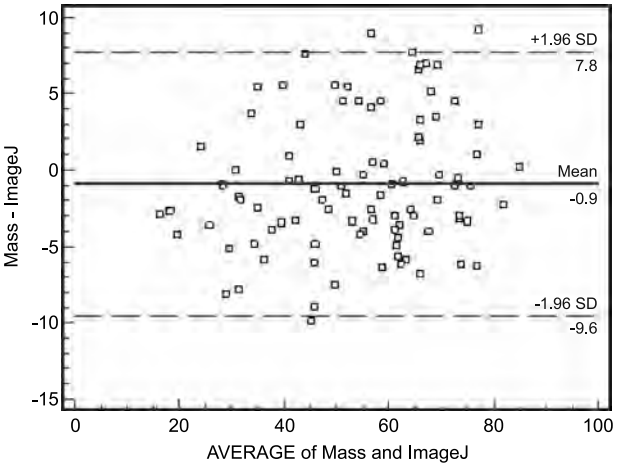

Bland-Altmann result.

Results: Descriptive results of EF are shown in the Table 1.

Values for EF between two methods has not shown statistical differences ($p = 0{,}518$), excellent correlation (r = 0,964) and very high agreement. Graphics 1 and 2.

Conclusions: Our study showed strong agreement of EF between ImageJ and MASS® ANALYSIS PLUS. This result may indicate that ImageJ is a reliable and inexpensive option for EF measurement.

Table 1.

	EF Mean	Std. Dev	Std. Error	No. Patients	Minimum EF	Maximum EF
MASS (%)	53,60	16,51	1,70	100	14,93	84,93
ImageJ (%)	54,49	15,66	1,61	100	17,8	84,72

528. B1-Insensitive Preconditioning Pulse for the Quantitative Analysis of First-Pass Perfusion MRI

Daniel Kim,[1] Alexandru Cernicanu,[2] Leon Axel.[1] [1]*New York University, New York, NY, USA,* [2]*University of Pennsylvania, Philadelphia, PA, USA.*

Introduction: First-pass myocardial perfusion MRI is potentially a quantitative method for assessing the severity of coronary artery disease (Wilke et al., 1995). Perfusion or blood flow can be estimated, in principle, by converting the T1-weighted signal-time curves to contrast agent concentration-time curves. T1-weighting is achieved by saturating the magnetization with a preconditioning pulse (typically, 90° or 180°) prior to imaging. Inaccurate and/or imprecise saturation will introduce uncertainties in T1 measurements.

Purpose: The purposes of this study were: 1) to demonstrate that B1 inhomogeneity at 1.5 T can be a significant problem for the quantitative analysis of perfusion MRI using single-shot, echo-planar imaging (EPI), and 2) to perform accurate saturation of magnetization using B1-insensitive rotation (BIR) pulse.

Methods: A single-shot EPI sequence (Mansfield, 1977) was implemented to image B1 inhomogeneity in the heart. The EPI protocol was designed to reduce artifacts due to T_2^* decay, motion, and field inhomogeneity and to image without any evolution of magnetization after saturation. Three preconditioning pulses were implemented: non-selective single 90° (90_x), non-selective composite 90° ($90_x–180_y–90_y$) (Levitt et al., 1979), and non-selective BIR-4 90° (Staewen et al., 1990), which is also insensitive to resonance offsets. The pulse durations for single 90°, composite 90°, and BIR-4 90° were 1 ms, 3 ms, and 4.1 ms, respectively, and the gradient spoiling duration was 3 ms. Proton density-weighted (PDW) images were also acquired to correct for the receive coil inhomogeneity. The pulse sequence was implemented on a 1.5 T scanner (Avanto, Siemens). Four healthy human subjects were imaged at 3 short-axis (apical, mid-ventricular, basal) and 2 long-axis (2-chamber, 4-chamber) views of the heart. A spherical phantom (T_1 = 2.7 s) was also imaged at 2 locations per each of 3 orthogonal planes (coronal, sagital, and transverse). Imaging parameters included: field of view = 400 × 200 mm^2, acquisition matrix = 64 × 32, in-plane resolution = 6.25 × 6.25 mm^2, slice thickness = 8 mm, scan duration = 19 ms, imaging flip angle = 90°, and bandwidth = 2790 Hz/pixel. Electrocardigram gating and breath holding, though not required, were performed for image registration purpose. In a separate experiment, non-selective single and composite pulses were tuned by repeating the acquisition with nominal flip angles ranging from 80–100° (2° steps). The effects of B1 inhomogeneity were computed as percent residual magnetization after saturation. Specifically, saturation images were normalized by the PDW image and multiplied by 100%. The mean and standard deviation of percent residual magnetization were computed from segmented regions of interest (left ventricle and phantom). Statistical comparison was performed using ANOVA.

Figure 1. Representative short-axis images acquired using non-selective single (top) and composite (bottom) pulses tuned to nominal saturation flip angles ranging from 82–98° (8° steps).

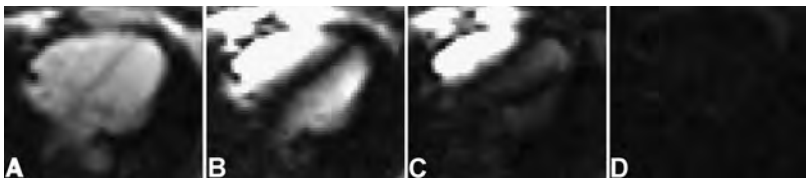

Figure 2. Representative 4-chamber images comparing different saturation schemes: A) PDW, B) single 90°, C) composite 90°, and D) BIR-4 90° [(B–D) same intensity].

Table 1. Mean and standard deviation of percent residual magnetization after saturation

	Single 90°	Composite 90°	BIR-4 90°
Phantom	6.91 ± 5.07	1.96 ± 2.39	0.50 ± 0.36
Left Ventricle	10.58 ± 7.70	4.90 ± 5.13	1.05 ± 0.81

Results: In Fig. 1, representative short-axis images acquired using non-selective single and composite pulses tuned to nominal flip angles ranging from 82–98° (8° step) are shown. Our findings suggest that non-selective single and composite pulses may not be suited for saturating the entire heart. Figure 2 shows representative 4-chamber images comparing the saturation schemes. Table 1 summarizes the statistical findings from phantom and in vivo experiments. Mean values of percent residual magnetization produced by BIR-4, composite, and single pulses were significantly different ($p < 0.001$).

Conclusions: We have demonstrated that B1 inhomogeneity at 1.5 T can be a significant problem for the quantitative analysis of perfusion MRI. Among three preconditioning pulses tested, only the BIR-4 pulse consistently performed accurate and precise saturation of magnetization. Single-shot EPI with non-selective hard pulse is potentially a robust sequence for producing B1 maps in vivo.

REFERENCES

Levitt, M. H., et al. (1979). *J. Magn. Reson.* 33:473–476.
Mansfield, P. (1977). *J. Phys., C* 10:L55–L58.
Staewen, R. S., et al. (1990). *Invest. Radiol.* 25:559–567.
Wilke, N., et al. (1995). *JMRI* 5:227–237.

529. Registration of Cardiac DHE-MRI with X-Ray Angiography for Visualization of Infarcted Myocardium

Luis F. Gutierrez, BE,[1] Ranil DeSilva, MD,[2] Amish Raval, MD,[2] Robert J. Lederman, MD,[2] Elliot R. McVeigh, PhD,[3] Cengizhan Ozturk, MD, PhD.[2] [1]*Laboratory of Cardiac Energetics, Johns Hopkins Univeristy and DHHS-NIH-NHLBI, Bethesda, MD, USA,* [2]*Cardiovascular Branch, DHHS-NIH-NHLBI, Bethesda, MD, USA,* [3]*Laboratory of Cardiac Energetics, DHHS-NIH-NHLBI, Bethesda, MD, USA.*

Introduction: MRI and X-Ray Angiography (XA) are complementary modalities, with XA offering high spatial and temporal resolution and MRI providing soft tissue contrast mechanisms and arbitrary scan planes. Location and extent of infarcted myocardium cannot be visualized on XA but can be defined exceptionally by Delayed Hyper-Enhancement (DHE) MRI. We use dual-modality fiducial markers to register MR and XA images, then display infarct contours from DHE-MRI on the XA images.

Methods: Our imaging suite consists of a Siemens Sonata 1.5 T scanner and an Axiom Artis cardiac XA system connected by a Miyabi sliding table (Siemens, Erlangen, Germany). The fiducial markers are glass spheres (14 mm diameter) filled with a solution of 5 mM Gd-DTPA in standard iodine contrast agent.Phantom studies were used to characterize registration errors. A coronary vessel phantom was placed within a hollow ellipsoidal MR calibration phantom (minor axis, 35 cm; major axis, 40 cm) which had eight markers arranged on its surface. 3D MRI was performed before XA. XA images were acquired at seven C-arm settings. Distortion present in both sets of images (gradient distortion in MRI, and geometric distortion due to the interaction of the electrons in the image intensifier with the earth's magnetic field in XA) were corrected, and XA projection parameters were previously calibrated using a custom phantom. In both image sets, marker locations were manually segmented.

Using the calibrated projection and distortion correction parameters, the 3D MR marker locations were projected onto the XA scene and 2D errors were calculated as the pixel differences between the reprojected MR markers and the manually segmented marker positions in the XA images. The best 3D rigid-body transformation of the MR points was found using an iterative least squares minimization of the 2D errors.

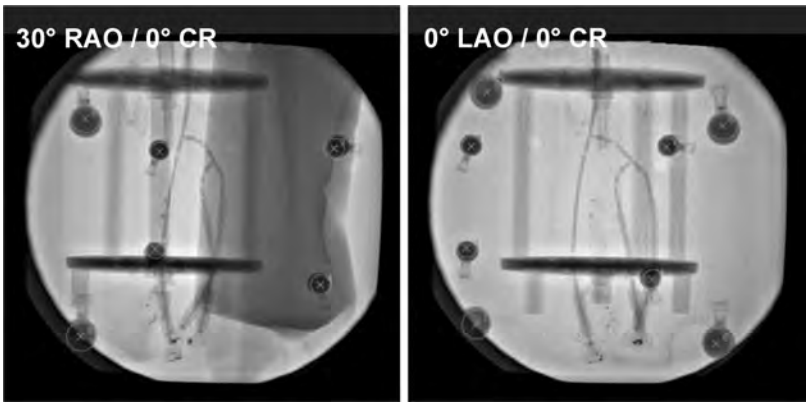

Figure 1.

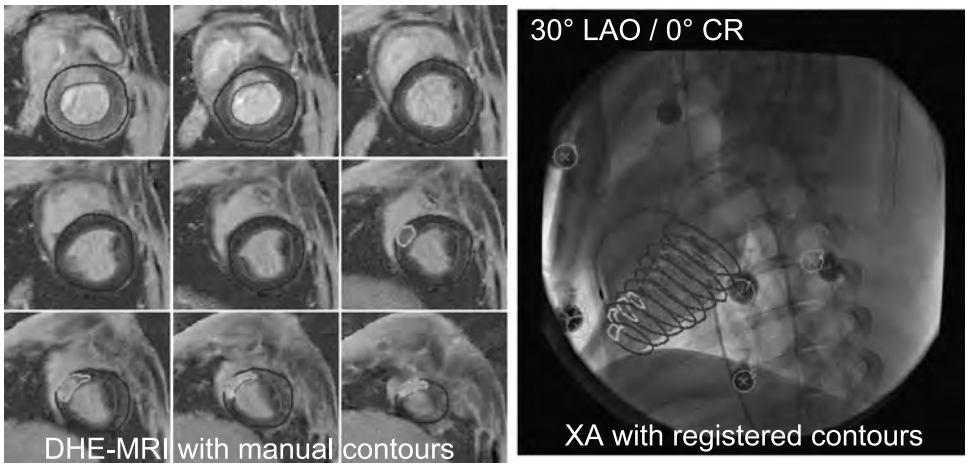

Figure 2.

This procedure was also applied for an in vivo case. Markers were placed on the chest of a pig with anteroseptal myocardial infarct. Infarct imaging was performed by DHE-MRI 15 min after intravenous injection of 0.2 mM/kg Gd-DTPA. Phase-sensitive inversion recovery was used with the following parameters: inversion-time, 300 msec; FOV, 300 mm; matrix, 256 × 208; slice-thickness, 8 mm. The infarct and LV epi-and endo-cardial borders were manually segmented using Siemens' Argus software. After registration using the fiducials, LV contours were reprojected onto the XA using the same rigid-body transformation parameters that were calculated for the markers.

Results and Discussion: Figure 1 shows XA images from the phantom study with the manually-segmented (+) and registered markers (× and circle).The 2D RMS (Max) error of the fiducials following registration was 3.34 (5.36) pixels.

Figure 2 (left) shows the DHE images with the infarct and LV epi- and endo-cardial contours. Figure 2 (right) is an XA image from the same experiment with the manually-segmented (+) and registered markers (× and circle), and the registered and reprojected LV contours. The results show an increase in registration error in comparison to phantom studies. We hypothesize that this is due to the MR imaging experiment being performed with a surface coil array, strapped tightly onto the chest wall of the animal, causing it to adopt a conformation different to that during the XA procedures. However, despite the marker error, the registration produces satisfactory initial results for the LV contours.

Conclusions: We developed a registration system using fiducial markers for combining MRI and XA data, which allows the delineation of infarcts on XA images. Our phantom tests show excellent registration results. Our preliminary in vivo experiment showed an increase in registration error, and further experiments to compensate for this error are underway. This technique may be applied for enabling trans-catheter targeted delivery of therapies to infarct borders.

530. Artifact-Free Whole-Heart Black-Blood MRI in a Single Breath-Hold Using Inner Volume SSFSE on Cardiac Patients

Belinda S. Y. Li, PhD,[1] Wei Li, MD,[2] Linda Pierchala, BS,[2] Robert R. Edelman, MD.[2] [1]*Applied Science Laboratory Central, GE Healthcare, Evanston, IL, USA,* [2]*Department of Radiology, Evanston Hospital and Northwestern University Feinberg School of Medicine, Evanston, IL, USA.*

Introduction: Conventional method of acquiring black-blood (BB) cardiac MRI, double inversion (DIR) segmented FSE, acquires 1–2 slices per breath-hold, resulting in prolonged exam and patient discomfort for whole-heart imaging. The segmented k-space scheme makes this method prone to respiratory motion artifacts, especially since cardiac patients often have difficulty holding their breaths. The use of half-Fourier single-shot FSE (SSFSE) substantially shortens scan time, allowing acquisition of all slices in a single breath-hold. To reduce image blurring due to the use of long echo train lengths (ETL), inner volume (IV) technique (Feinberg et al., 1985; Li et al., 2003) was applied to DIR-SSFSE; IV also allows for improved spatial resolution by the use of smaller FOV without suffering from aliasing artifacts.

Purpose: To evaluate the feasibility of using IV-DIR-SSFSE for multi-slice BB imaging in cardiac patients, and compare it with conventional segmented DIR-FSE.

Methods: Eleven patients (7 M, 5 F, 22–84 yr, avg. 58 yr) with various known cardiovascular diseases underwent this IRB-approved study; all gave informed consent. Studies were performed on a 1.5 T TwinSpeed MR scanner (GE Healthcare, Waukesha WI, USA), using either an 8-element body, or a 4-element torso, phased-array coil. Whole-heart short axis BB imaging was performed with both IV-DIR-SSFSE (whole-heart in single breath-hold) and DIR-FSE (1 slice per breath-hold). FOV ranged from 36–42 cm for FSE scans and only 22–26 cm for IV scans, since aliasing is not a concern

Table 1. Average SNR and CNR, and p-value from the paired t-test

	Avg. SNR (m)	Avg. SNR (bl)	Avg. CNR (m/bl)
DIR-FSE	34.81 ± 13.94	7.56 ± 5.44	27.25 ± 10.12
IV-DIR-SSFSE	32.33 ± 10.37	4.21 ± 1.17	28.12 ± 10.80
p-value from paired t-test	> 0.05	> 0.05 (= 0.075)	> 0.05

for IV images. The matrix size for the IV scans is kept smaller (192 × 128, vs. 256 × 192 for FSE) to reduce blurring, but with the much smaller FOV used, the in-plane spatial resolution for the IV scans was still higher than that for the FSE scans- average = 1.6 × 2.1 mm^2 for FSE vs. 1.2 × 1.9 mm^2 for IV. Slice thickness was 10 mm for FSE, and 8–10 mm (avg. 8.8 mm) for IV. Images were acquired at end-diastole, with an interval of 2 heartbeats between slices. A receiver bandwidth of ± 62.5 kHz was used for all scans, while ETL = 24 for FSE. With half-Fourier, the effective TE for IV was shorter than that for FSE (mean TE = 29 ms vs. 41 ms, for IV vs. FSE). Scan time per slice ranged from 9.3–13.3 sec (avg. 11.2) for FSE vs. only 1.4–2.1 sec (avg. 1.7) for IV. The short IV scan time made it possible to repeat the IV scan in 2- and 4-chamber views for some patients.Many of the FSE images contained respiratory motion artifacts. For each patient, one FSE short-axis slice, containing the least artifacts, was chosen for quantitative analysis, together with a matching slice from the IV series. Signal-to-noise ratios (SNR) and contrast-to-noise ratios (CNR) were measured: SNR(x) = SI(x)/SD(bk), where SI is signal intensity, x is either myocardium (m) or blood (bl), SD is standard deviation, and bk is background noise; CNR(m/bl) = [SI(m)–SI(bl)]/SD(bk). Paired t-test was then performed.

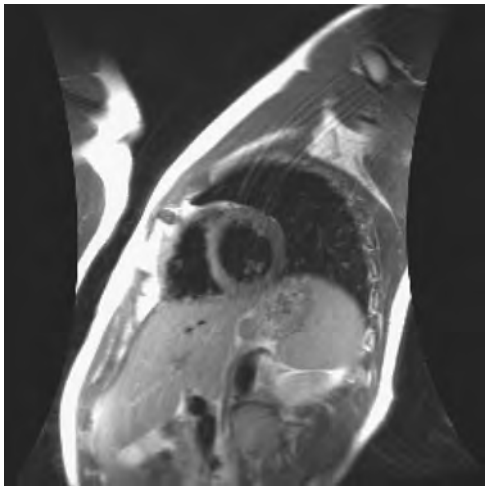

Figure 1.

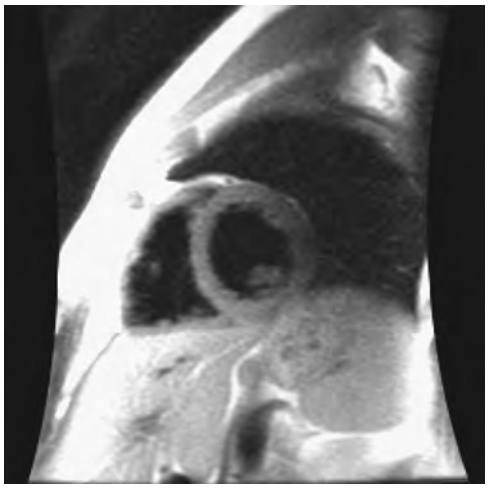

Figure 2.

Results: Table 1 shows average SNR and CNR results. No significant difference could be found, for any of the values, between the 2 methods. Figure 1 shows a FSE image, with respiratory motion artifact, obtained in 9.8 sec, 1.6 × 2.1 mm^2, 10 mm thick, while Fig. 2 shows a matching IV image from the same subject, without any such artifact, obtained in 1.5 sec, 1.4 × 2.0 mm^2, 8 mm thick.

Conclusions: Our initial experience shows that IV-DIR-SSFSE is a feasible method for acquiring whole-heart BB cardiac images, with significantly reduced scan time, number of breath-holds, and motion artifacts, as well as improved spatial resolution, as compared with standard FSE approach. However, some blurring is evident with the IV-SSFSE images- this can be further reduced by applying parallel imaging technique, a work-in-progress in our group.

REFERENCES

Feinberg, D. A., et al. (1985). *Radiology* 156:743–747.
Li, B. S.Y., et al. (2003). *RSNA*. Poster 463CA-P.

531. Accurate Assessment of the Arterial Input Function Using MRI with Radial Sampling

Eugene G. Kholmovski, PhD,[1] Edward V. DiBella, PhD,[1] Alexei A. Samsonov, PhD.[2] [1]*UCAIR, Department of Radiology, University of Utah, Salt Lake City, UT, USA,* [2]*Scientific Computing and Imaging Institute, University of Utah, Salt Lake City, UT, USA.*

Introduction: The accuracy of quantitative analysis of myocardium perfusion derived from dynamic contrast

enhanced T1-weighted MRI critically depends on the knowledge of the arterial input function (AIF). The AIF is typically estimated from the mean signal intensity of a ROI placed in the left ventricular cavity. In many practical cases, such an AIF can be unreliable due to saturation effects caused by high concentration of contrast agent (CA) and/or long saturation recovery time of the applied pulse sequence.

Purpose: To test the applicability of T1-weighted sequence with radial k-space acquisition for accurate assessment of AIF.

Method: In T1-weighted imaging with saturation recovery, effective saturation recovery time (eSRT) is defined by the time delay between the saturation pulse and the time when the central part of k-space is acquired. In a myocardial perfusion study, the choice of eSRT is a compromise between the accuracy in AIF estimate and the SNR of tissue enhancement curves. With shortening eSRT, the accuracy of the AIF estimate improves but myocardium signal decreases and vice versa. A T1-weighted pulse sequence with Cartesian sampling has only one eSRT. However, when radial sampling is used, each projection passes through the center of k-space making it possible to reconstruct a set of images with various eSRT by using different subsets of k-space projections. Images reconstructed from subsets with short eSRTs can be used to accurately estimate AIF because saturation effects are significantly suppressed for the images.To test the proposed concept of AIF assessment, MRI studies were performed on a 3 T scanner (Trio, Siemens Medical Solutions, Erlangen, Germany) using a T1-weighted turbo-FLASH sequence with saturation recovery magnetization preparation (TR/TE = 1.58/0.86 ms, time interval between saturation and the first excitation pulse: TI = 24 ms, flip angle = 12°, 96 projections with 128 readout points, FOV = 380 mm, 8 mm slicethickness). A CA bolus of 0.15 mmol/kg of Gd-DPTA was used. The data sampling was implemented in such a way that each subset of 24 time-adjacent projections covers 180°. A set of images with various eSRT were reconstructed from the corresponding subsets of 24 projections. To significantly suppress streaking artifacts, the high frequency components of all available projections were included in each image reconstruction.

Results: Figure 1 shows AIF estimates found from the images reconstructed using a complete set and four subsets of available projections. Saturation effects are obvious in the AIFs corresponding to long eSRTs (the peaks of the AIFs with eSRT > 70 ms are practically the same). The true AIF is equivalent to the function describing change in CA concentration in the blood during the bolus passage. Typically, this function cannot be reliably recovered from MR images with one eSRT. In the case of radial sampling, images with different eSRT can be reconstructed making CA concentration calculation applicable. Figure 2 demonstrates the AIF converted to CA concentration using the AIFs shown in Fig. 1 and the analytical expression describing both magnetization evolution for turbo-FLASH sequence with saturation recovery preparation and effects of the image reconstruction scheme employed.

Conclusion: The AIF can be accurately assessed using T1-weighted sequences with radial sampling. Higher doses of CA may be applicable for quantitative myocardium perfusion measurements when sequences with radial sampling are used for imaging.

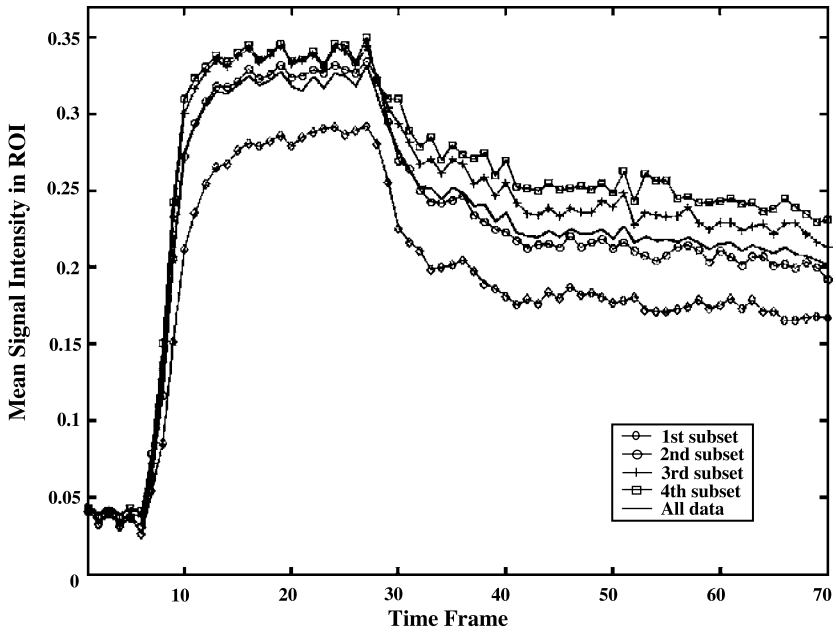

Figure 1. AIFs calculated from the images reconstructed from a complete set and four subsets of available projection data. eSRT for the images: 1st subset—43 ms, 2nd—81 ms, 3rd—119 ms, 4th—157 ms, complete set—100 ms.

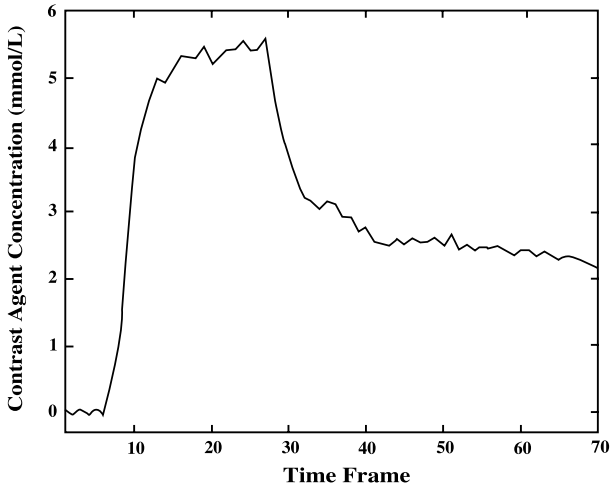

Figure 2. AIF converted to CA concentration.

ACKNOWLEDGMENTS

We would like to thank Dr. G. Laub and Dr. A. Zhang for supplying the radial sequence. This study was supported in part by NIH 1R01EB000177.

532. High Spatial and Temporal Resolution Cardiac Tagging Under Free-Breathing Conditions

Vinay M. Pai,[1] Leon Axel, PhD, MD,[1] Dan Kim, PhD,[1] Peter Kellman, PhD.[2] [1]*Radiology, New York University School of Medicine, New York, NY, USA,* [2]*Laboratory of Cardiac Energetics, National Heart, Lung and Blood Institute, Bethesda, MD, USA.*

Introduction: We present an approach combining multi-echo SSFP, PAGE, and joint cardiac and respiratory gating to acquire high temporal and spatial resolution myocardial tagging data under free-breathing conditions. We also introduce a dual tagging approach in order to have high tag contrast in both early systolic and diastolic phases.

Purpose: The development of high temporal and spatial resolution tagging imaging methods may permit the evaluation of regional activation and relaxation patterns in early systolic and diastolic phases.

Methods: A multi-echo steady-state free precession (MESSFP) pulse sequence with a phased array approach to ghost elimination (PAGE) (Herzka et al., 2002; Kellman and McVeigh, 2001) was modified to include combined cardiac and respiratory gating to permit the acquisition of high temporal and spatial resolution data under free-breathing conditions.

In order to evaluate the motion in early phases of systole and diastole, this study also included a dual-tagging approach. It has been previously shown (Herzka et al., 2003) that increasing the readout flip angles for SSFP sequences reduces the tag persistence in the diastolic phases of the cardiac cycle, and that a lower flip angle reduces the blood-myocardium contrast. In order to permit tag tracking in diastole, and maintain blood-myocardium contrast, we have adopted the approach of using high flip angles (typically 75°) for the MESSFP readout, in conjunction with applying the tagging pulse after the R-wave (early systole) and in early diastole, as shown in Fig. 1. Dummy scans are played out between the systolic and diastolic acquisition, in order to maintain steady-state and to further reduce tag persistence from the previous acquisition. A cine (manufacturer supplied) sequence was used to determine the approximate temporal location of end systole, before running the dual tagging sequence.

The sequence was implemented on a 1.5 T clinical scanner (Siemens Medical Solutions), and evaluated on human volunteers and patients. Typical scan parameters were: echo train length = 3, TR = 7 ms, TE = 3.57 ms, FOV = 320 × 320 mm^2, resolution = 384 × 234 pixel, slice thickness = 8 mm, flip angle = 40° (single tagging)—75° (dual tagging), respiratory acceptance window = 15% of end-expiration, receiver bandwidth = 868 Hz/pixel, 5-7-9-7-5 SPAMM pulse; tag spacing = 6 mm, phased array elements = 6 (4 anterior and 2 posterior). Dual tagging was used to acquire 20 cardiac phases for each half of the cardiac cycle (7 ms temporal resolution), with the second tagging pulse played 270–320 ms after the R-wave. Single tagging (i.e. tagging applied only at end-diastole) was used to acquire 60–100 cardiac phases.

Results: Tagged cine images with spatial resolution of 0.8 × 1.4 mm^2 (frequency-encoding direction X phase-encoding direction), and temporal resolution of 7 ms were acquired. Typical acquisition times ranged between 4 and 6 minutes per slice (average gating acceptance efficiency: 30%). Figure 2 shows representative images from the single tagging experiment. Figure 3a–b shows representative images from the first and second halves of the dual-tagging experiment, respectively.

Conclusion: High spatial and temporal resolution myocardial tagging may enable clinical studies quantifying distinct patterns of contraction and expansion, observed in normal, infarcted and reperfused myocardium. In this abstract, we present an approach combining multi-echo SSFP,

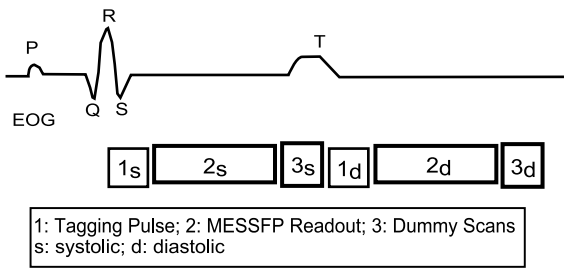

Figure 1. Dual tagging during a cardiac cycle.

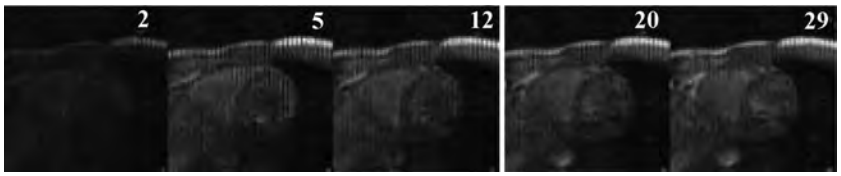

Figure 2. High resolution tagged cardiac data set obtained using single tagging pulse (selected phases displayed). Temporal resolution: 7 ms, Spatial resolution: 0.8 mm × 1.4 mm.

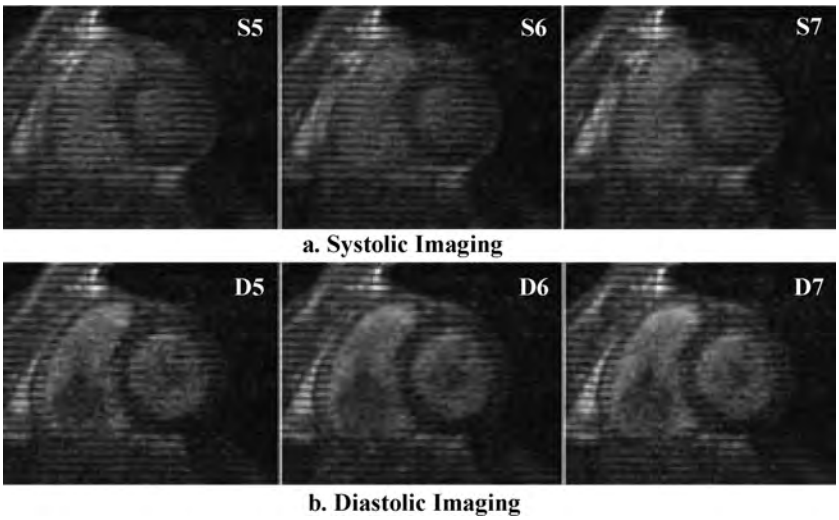

Figure 3. Systolic (a) and diastolic (b) phases (5–7) acquired using the dual tagging approach (selected phases shown). Temporal resolution: 7 ms, Spatial resolution: 0.8 × 1.4 mm.

PAGE, and joint cardiac and respiratory gating to acquire high temporal and spatial resolution myocardial tagging data. A dual tagging may be an alternative approach to maintain high tag contrast throughout the cardiac cycle, allowing tagged imaging of early contraction and rapid filling phases during the cardiac cycle.

REFERENCES

Herzka, D. A., et al. (2002). *MRM* 47(4):655–664.
Herzka, D. A., Guttman, M. A., McVeigh, E. R. (2003). *MRM* 49:329–340.
Kellman, P., McVeigh, E. (2001). *MRM* 46(2):335–343.

533. Real-Time Cardiac Imaging Using Balanced SSFP with Ultra-Short Variable-Density Spiral Readouts

Brian A. Hargreaves, PhD,[1] Juan M. Santos, MS,[1] Dwight G. Nishimura, PhD,[1] John M. Pauly, PhD,[1] Bob S. Hu, MD.[2]
[1]*Electrical Engineering, Stanford University, Stanford, CA, USA,* [2]*Cardiovascular Medicine, Palo Alto Medical Foundation, Palo Alto, CA, USA.*

Introduction: Real-time cardiac MR imaging is being used or investigated for evaluation of ventricular and valve function, catheter tracking, and scan localization. SSFP imaging has become the standard sequence for the evaluation of cardiac anatomy and function. However, current SSFP imaging techniques are too slow for real-time applications, or compromise spatial resolution. In this work, we investigate the use of variable-density spiral readouts with balanced SSFP imaging to provide a high temporal and spatial resolution real-time cardiac imaging sequence.

Purpose: We show the feasibility of variable-density spiral imaging to improve the spatial and/or temporal resolution of real-time balanced SSFP imaging, which provides excellent contrast between blood and myocardium.

Methods: Spiral balanced SSFP imaging has previously been explored for cardiac imaging (Meyer et al., 2001; Nayak et al., 0000 in press). We extend this work by designing ultrashort-duration (2.8 ms) variable-density spiral readout gradient waveforms to improve the temporal or spatial resolution. Figure 1 shows the pulse sequence and spiral k-space trajectory. The spiral rewinder gradients are moment-nulled, and incorporate the slice "dephasing" gradient (Hargreaves et al., 2004). The spiral waveforms (18 interleaves) last 2.8 ms and achieve 1.6 mm in-plane resolution over a field of view that decreases linearly from 24 cm to 12 cm with k-space radius. Other scan parameters include TR = 5.4 ms, flip angle of 60 degrees, slice thickness of 7 mm, resulting in 10 true frames per second. We imaged

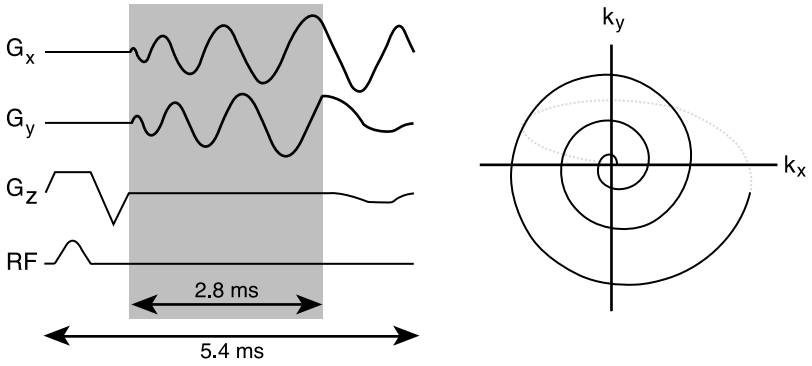

Figure 1. Variable-density spiral balanced-SSFP imaging sequence (left) and in-plane k-space readout trajectory (right). In-plane gradient areas and first-moments are zero over a sequence repetition to preserve the steady state.

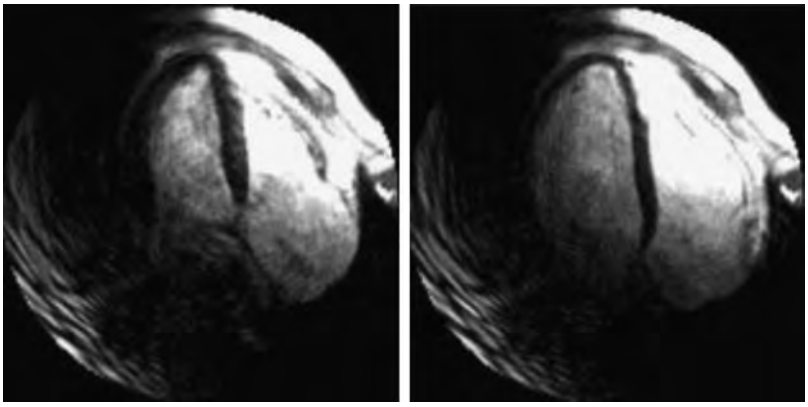

Figure 2. Long axis views in systole (left) and diastole (right) using real-time variable-density spiral balanced SSFP imaging.

long-axis and short-axis views of several normal volunteers using a 5-inch surface coil and a GE Signa LX scanner with 40 mT/m, 150 mT/m/ms gradients.

Results and Discussion: Figures 2 and 3 show successive frames from short-axis and long-axis cardiac views. Excellent contrast is seen between blood and myocardium in all cases. Some motion artifact is seen in frames acquired during systole, likely due to the 100 ms temporal window. However the frames during diastole are extremely clear, as evidenced by the clear depiction of the RCA in the short-axis view.

Like other radial imaging schemes, spiral balanced SSFP benefits from sampling the k-space center on each acquisition. The coverage requires approximately one eighth as many excitations as a full-coverage Cartesian scan.

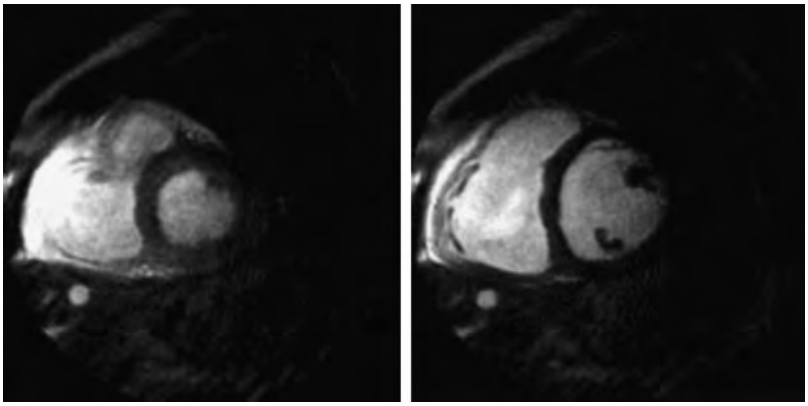

Figure 3. Short axis views in systole from a real-time sequence with 10 true frames per second. The RCA is clearly visible in the image on the right, showing the benefits of high spatial resolution.

Finally, the acquisition duty-cycle (Fig. 1, gray region) is over 50%, so that loss of SNR efficiency due to preparatory gradients is minimal compared with other balanced SSFP sequences.

Conclusions: Using a combination of ultra-short variable-density spiral readouts and balanced SSFP, we are able to achieve temporal resolution that is comparable to results obtained using parallel-imaging-accelerated Cartesian scanning (Guttman et al., 2003), but with significantly improved spatial resolution (half the pixel size). The combination of variable-density spiral imaging with parallel imaging could further increase frame rates.

REFERENCES

Guttman, et al. (2003). *Magn. Reson. Med.* 50(2):315–321.
Hargreaves, et al. (2004). *Magn. Reson. Med.* 51(1):81–92.
Meyer, et al. (2001). *Proceedings of the 9th ISMRM*. 442.
Nayak, et al. Real-time interactive spiral balanced SSFP cardiac imaging. In: *Magnetic Resonance in Medicine*. in press.

534. Simpson's Rule Underestimates Volume Compared with Reconstructing the Right Ventricle in its Entirety

William Kerwin, PhD,[1] Florence Sheehan,[2] Shuping Ge, MD,[3] Wes Vick, MD.[3] [1]*Radiology, University of Washington, Seattle, WA, USA,* [2]*Medicine, University of Washington, Seattle, WA, USA,* [3]*Medicine, Baylor College of Medicine, Houston, TX, USA.*

Introduction: Simpson's rule applied to short axis images is the standard method for measuring ventricular volume from magnetic resonance images. However, use of this approach to measure right ventricular volume may not be ideal because of difficulty in identifying right ventricular endocardial borders in basal images.

Purpose: We compared right ventricular volume measured by Simpsons's rule vs. the volume of 3-dimensional reconstructions generated from tracing both long axis and short axis images. Two imaging prescriptions were also compared.

Methods: We acquired both short and long axis images of 2 normal subjects and 7 patients with tetralogy of Fallot, using a CINE gradient echo sequence on a 1.5 T MRI scanner. Imaging was performed at 3 sites: Seattle (N = 2), Iowa City (N = 4), and Houston (N = 3). The right ventricular endocardial borders were traced at end diastole and end systole and used to measure volume based on two methods: first, using 3-dimensional reconstruction of the right ventricle by the piecewise smooth subdivision surface method and second, using Simpson's rule from short axis borders between the apex and tricuspid annulus. In imaging protocol #1 the long axis images were parallel. In imaging protocol #2 the long axis images were rotated about the left ventricular long axis at 20 degree intervals with additional right ventricular inflow/outflow track views perpendicular to the short axis images and parallel to a line connecting the right ventricular inflow and outflow tracks.

Results: Simpson's rule underestimated right ventricular volume by 35 ± 29 ml (261 ± 162 vs. 227 ± 136 ml, $p < 0.001$). The percent error was similar at end diastole and end systole (11 ± 6 vs. $13 \pm 5\%$, respectively, p = NS), and in normal and abnormal subjects. Review of border tracings in 3D revealed that part of the right ventricular outflow track lies basal to the tricuspid annulus. The error arose because Simpson's rule was only applied to short axis views in which the right ventricle was clearly identified as filling the entire contour. There were short axis views basal to the tricuspid valve but they contained right atrium as well as right ventricle, a distinction not possible without a 3D viewer and prior definition of the tricuspid valve from the long axis views. For example, Fig. 1 shows borders traced from long and short axis views of a patient's right ventricle; the pulmonary valve points are black and the tricuspid annulus points are white. The asterisk indicates the right ventricular border traced from a basal short axis view in which part of the plane lies within the right atrium. Imaging protocol #2 visualized the valves better than imaging protocol #1, and avoided oblique views of right ventricular myocardium.

Conclusions: Right ventricular volume is more accurately measured from 3-dimensional reconstruction than from Simpson's rule. Acquisition of long axis images is needed to identify right ventricular contours at the level of, and basal to, the tricuspid annulus. The preferred protocol for the right ventricle combines short axis images, long axis views

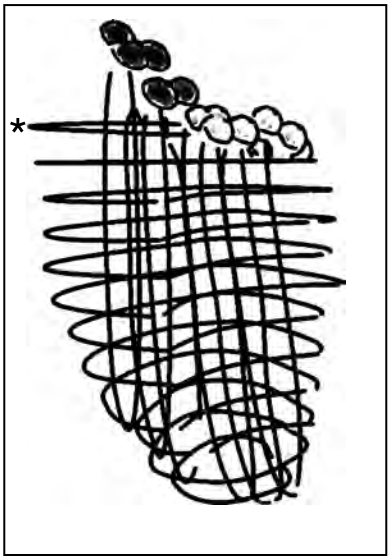

Figure 1.

prescribed by rotation about the left ventricular long axis, and right ventricular inflow/outflow track views.

535. Cine Delayed Enhancement Imaging of the Heart

Randolph M. Setser, DSc,[1] Yiu Cho Chung, PhD,[2] Jae K. Kim, MD, PhD,[1] Kevin Chen, MD,[1] Arthur E. Stillman, MD, PhD,[1] Ralf Loeffler, PhD,[3] Joan A. Weaver, RT(MR),[1] Orlando P. Simonetti, PhD,[2] Richard D. White, MD.[1] [1]*Radiology, The Cleveland Clinic Foundation, Cleveland, OH, USA,* [2]*Siemens Medical Solutions, Chicago, IL, USA,* [3]*Siemens Medical Solutions, Erlangen, Germany.*

Introduction: Magnetic resonance imaging (MRI) is unique in its ability to accurately characterize both regional left ventricular (LV) wall motion as well as the extent of myocardial scar during a single examination. However, using existing techniques these data must be acquired separately, requiring multiple image acquisitions. Furthermore, interpretation can be hampered by the need to mentally integrate the wall motion and viability information from separate, potentially misregistered image series.

Purpose: To introduce a novel cine delayed enhancement pulse sequence, which permits simultaneous visualization of wall motion and myocardial scar extent in a single acquisition.

Methods: The cine delayed enhancement technique is based on inversion recovery, single-shot, balanced steady state free procession (TrueFISP) imaging. As shown in Fig. 1 below (top portion), each image frame of the cine series is acquired during a separate RR-interval using a constant inversion time (TI). However, the trigger delay (TDEL) for the inversion prepulse is varied between images, resulting in a cine series of images covering the cardiac cycle. Images are acquired every other heart beat. The sequence has been implemented on a 1.5 T scanner (Siemens Sonata, Erlangen, Germany) using the following typical acquisition parameters: α 50°, TR 322 ms, TE 1.1 ms, BW 1090 Hz/mm, FOV 380 mm, RFOV 75%, acquisition matrix 192 × 115 (frequency, phase). By default, 15 image frames are acquired in each cine, with a variable frame rate to cover the cardiac cycle. Each cine series is acquired during a single breath-hold, approximately 10–15 minutes after intravenous injection of 40 ml of 0.5 mmol/ml

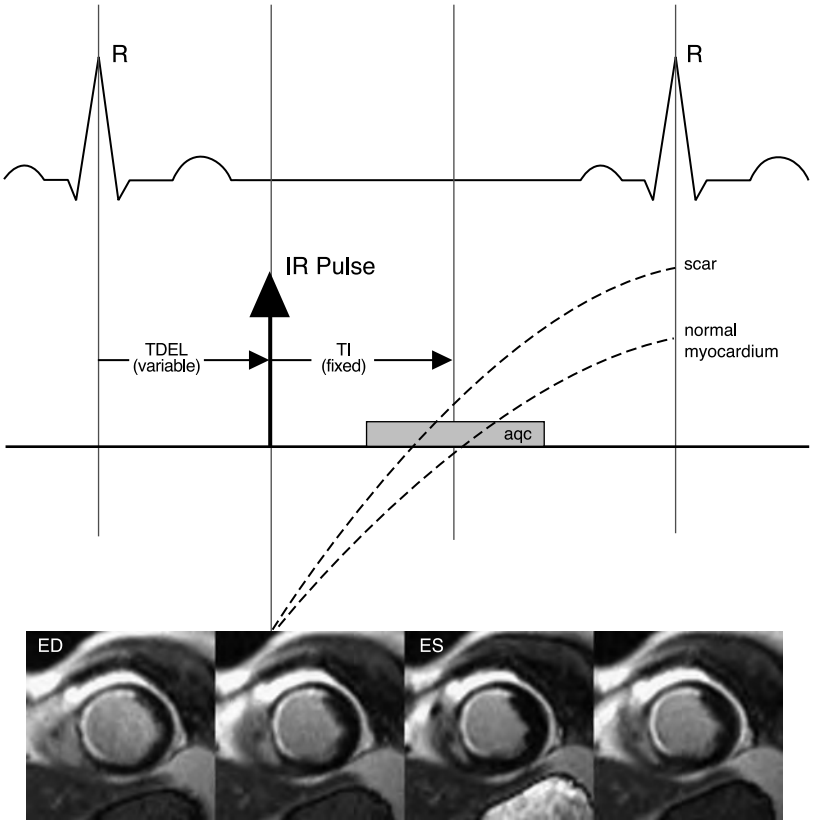

Figure 1.

gadopentetate dimeglumine (Magnevist, Berlex Imaging, Wayne NJ).

Results: To date, cine delayed enhancement images have been acquired in 16 patients undergoing clinical assessment of myocardial viability, using an IRB approved protocol with waiver of individual consent. End-diastolic and end-systolic images from a patient with chronic ischemic heart disease are shown below. Overall, breath-holds varied from 18–25 seconds, depending on heart rate; temporal resolution averaged 61 ± 9 msec. No scar was visible in 4 of 16 patients (25%), a finding verified by standard delayed enhancement imaging. Contrast was consistent throughout each cine; the average ratio of non-viable to viable signal intensity was 7 ± 2, the average ratio of non-viable to blood pool signal intenstity was 4 ± 1.

Conclusions: Cine delayed enhancement imaging is a promising technique for simultaneous visualization of wall motion and myocardial scar extent.

536. Phase-Sensitive SSFP Imaging with Fat Suppression May Reduce Scanning Time in MRI Evaluation of Arrhythmogenic Right Ventricular Dysplasia: A Pilot Study

William Gottliebson, MD,[1] Janaka Wansapura, PhD.[2] [1]*Cardiology, Cincinnati Childrens Hospital and Medical Center, Cincinnati, OH, USA,* [2]*Radiology, Cincinnati Childrens Hospital and Medical Center, Cincinnati, OH, USA.*

Introduction: Arrhythmogenic Right Ventricular Dysplasia (ARVD) has been implicated as an etiology of sudden cardiac death (SCD) in children, adolescents, and adults. For the past decade, cardiac MRI (CMR) has been used as an important means to help exclude ARVD via evaluation of right ventricular (RV) morphology and function. Recent published CMR protocols suggest that to exclude MRI criteria of ARVD, T1 weighted black blood fast spin echo (with and without fat suppression), and cine SSFP stacks in axial and oblique planes be performed.

Purpose: This pilot study sought to assess the reliability and potential decreased scanning time of a shortened ARVD CMR protocol, in which the T1 weighted fast spin echo stacks are replaced by a phase-sensitive SSFP imaging technique.

Methods: 7 juvenile patients (mean age 11.6 ± 1.7 years, 5 males) with a history of ventricular tachycardia of RVOT origin, near SCD, or significant family history of post-mortem, histopathologically proven ARVD were included in the study. All patients were scanned on a Siemens 3Tesla Trio Magnet with an 8 channel phased-array cardiac coil. Patients underwent localization with an SSFP sequence with following imaging parameters, TE/TR = 1.4/2.8 ms, inplane resolution = 1 × 1 mm^2, and slice thickness = 2.0 mm. Following this, T1 weighted turbo-spin (with and without fat saturation) and cine SSFP (TrueFISP) sequences including oblique axial 4 chamber views and oblique sagittal short axis and RVOT views were obtained. The SSFP sequence obtained for localization were post processed for fat suppression after the scan was completed. Fat-water separation was done using a technique described by Hargreaves et al. (2003). on a stand alone PC using customized in-house software.

Results: No patients had evidence of RV free wall fatty infiltration by post-processed phase-sensitive SSFP, a result confirmed by the combined standard fat supression spin echo technique. Of note, bright signal subcutaneous thoracic and epicardial fat, seen on the pre-processed SSFP images, were appropriately suppressed in the post-processed images (see Fig. 1).

Conclusion: This study suggests that post-processing fat-suppression may be a reliable alternative to spin echo sequences with and without standard fat suppression, and subsequently may decrease overall scanning time. This in turn

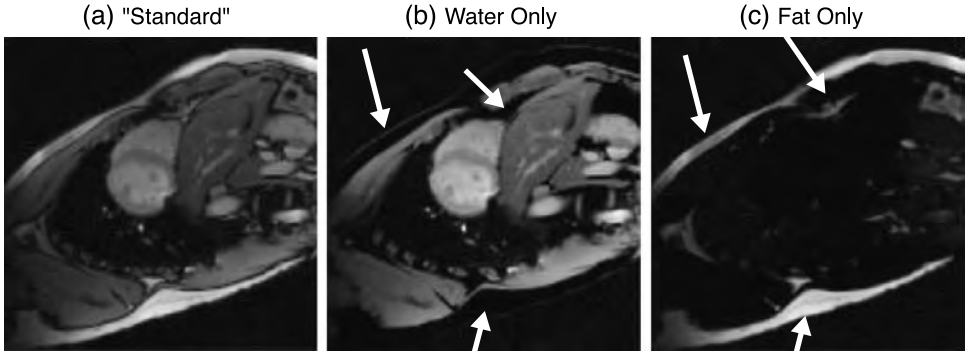

Figure 1. The standard SSFP image of the short axis (a) is separated into water-only (b) and fat-only (c) images by the phase-sensitive post processing technique. Fatty areas such as subcutaneous thoracic and epicardial fat (arrow in (b)) are retained in the fat-only image while suppressed in the water-only (c) image.

may prove helpful particularly for assessment of patients unable to perform long breath holds or unable to tolerate prolonged scanning time. Further study is warranted in patients with RV free wall fatty infiltration to determine the sensitivity and specificity of this novel method.

REFERENCE

Hargreaves, B. A., et al. (2003). *MRM* 50:210–213.

537. Improved Navigator Technique for the Assessment of Cardiac Function with Balanced SSFP during Free-Breathing

Bernd A. Jung, Maxim Zaitsev, Jürgen Hennig. *Department of Diagnostic Radiology, Medical Physics, University Hospital, Freiburg, Germany.*

Introduction: The assessment of ventricular function is typically based on on whole heart coverage using multiple breath-held 2D measurements with a balanced SSFP pulse sequences. Navigator echoes (NE) provide an efficient method to overcome limitations related to breath-holding. In cine imaging the acquisistion window typically covers the entire cardiac cycle and data may be acquired during significant motion of the rib cage and the heart if only a single NE per RR-interval is used. In this work we propose a prospective respiratory gating technique with multiple navigators for the assessment of the left ventricular function during free-breathing in combination with balanced SSFP imaging which is widely used in the clinical routine due to its high blood-tissue contrast and inherent high signal-to-noise ratio.

Material and Methods: For the tracking of the respiratory motion NE were periodically inserted into a continuously running balanced SSFP cine sequence. To avoid artifacts an $\alpha/2$ flip-back pulse was executed preceding the NE. Following the NE acquisition, a second $\alpha/2$ pulse restored the steady state and SSFP acquisition continued (Scheffler, 2001). Improved navigator gating was performed using two NE per cardiac cycle in combination with real-time acceptance criteria based on signal from successive navigator echo pairs, in the center and at the end of the cardiac cycle (Fig. 1b). Data acceptance or rejection was based on the combined information from both navigators for the two resulting data blocks independently treated. The total time for two NE including the evaluation following the second NE was 56 ms. Image acquisition parameters were as follow: 5-mm acceptance window in end-expiration, TR = 3 ms, data matrix 144 × 256, temporal resolution = 47 ms, slice thickness = 8 mm, flip angle 35–50°.

Prospective NE respiratory gating during free breathing was compared to breath-hold imaging in 4 volunteers and 1 patient with heart failure. For all measurements, ejection fraction, left ventricular volumes and mass were determined (Argus, Siemens Medical Solutions, Erlangen, Germany). For comparison of image quality and scan efficiency, additional images were acquired with previously described navigator-guided techniques using one NE per cardiac cycle (with and withot pre-and post navigator) (Bellenger, 2000; Keegan, 2004) (Fig. 1a) (Fig. 2).

Results: Figure 3 shows short axis images in a normal volunteer, a) one NE per cardiac cyle, b) one NE per cardiac cycle with pre-and post navigator, c) two NE per cardiac cycle, d) breath-hold. Left column: diastolic frame. Right column: systolic frame. Due to significant breathing motion during data acquisition, artifacts occurred in some cardiac frames in Fig. 3a. Images in Fig. 3b demonstrate good quality but strongly decreased scan efficiencies.

Excellent agreement was found between free-breathing and breath-hold ejection fraction, volumes and mass while image quality was comparable for both techniques (Table 1). Scan efficiency using two navigator echoes per cardiac cycle was superior (mean 37,8%) compared to data acceptance based on two navigator echoes in successive cardiac cycles (mean 20,5%).Compared to a single navigator echo per cardiac cycle, scan efficiency was inferior (mean 40,4%), but image quality was improved.

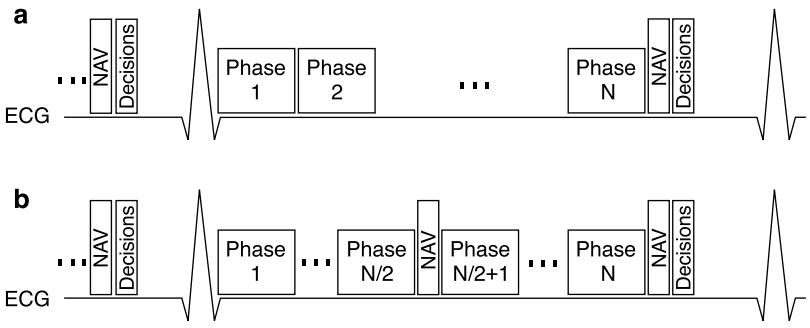

Figure 1.

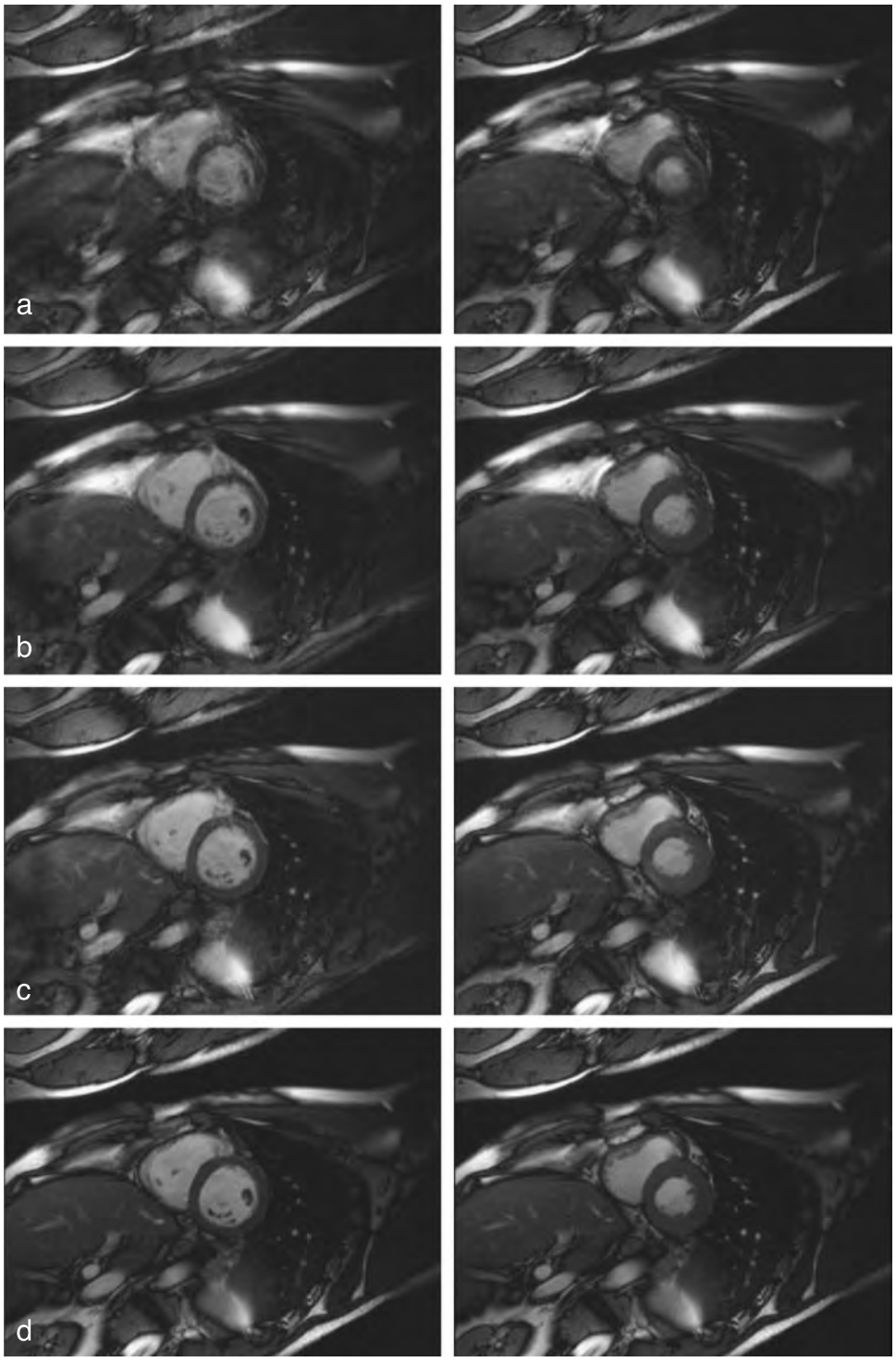

Figure 2.

Discussion: In this study, an efficient strategy for the combination of NE based respiratory gating and analysis of cardiac function with cine balanced SSFP imaging was demonstrated. In addition to improved scan efficiency with image quality comparable to breath-hold measurements, excellent agreement was found for derived functional parameters. The demonstrated navigator technique provides a useful tool for applications in pediatric cardiac MRI. In addition, other techniques for the quantification of myocardial function may benefit from an efficient free-breathing

Table 1. Comparison of Breath-Hold (BH) and Free-Breathing (FB) analysis in the five scanned subjects

	1		2		3		4		5	
	BH	FB	BH	FB	BH	FB	BH	FB	BH	FB
EF [%]	64.9	64.3	65.7	64.4	57.4	56.6	58.2	55.6	61.8	57.2
EDV [ml]	145.3	153.2	111.9	113.8	136.8	124.0	94.5	98.7	110.3	95.2
ESV [ml]	51.0	54.6	38.4	40.6	58.2	53.8	39.5	43.9	42.1	40.8
Mass [g]	139.4	137.3	94.2	92.5	111.7	102.9	96.7	102.7	147.5	132.7

technique, namely Phase Contrast Velocity Mapping, DENSE and tagging.

REFERENCES

Bellenger (2000). *JMRI* 11:411–417.
Keegan (2004). *JMRI* 9:40–49.
Scheffler (2001). *MRM* 45:1075–1080.

538. Inter Observer Variability in the Evaluation of Left Ventricular Segmental Function Can Be Reduced By Combining Visual Assessment of MRI Cine Sequences and Analysis of Corresponding Parametric Images of Myocardial Contraction

Alban Redheuil, MD,[1] Xavier Lyon, MD,[2] Arshid Azarine, MD,[1] Remi Laporte, MD,[1] Nadia Kachenoura,[3] Frédérique Frouin, PhD,[3] Elie Mousseaux, MD, PhD.[1] [1]*Department of Radiology, European Hospital, Paris, France,* [2]*University Hospital, Service of Cardiology, Lausanne, Switzerland,* [3]*INSERM U494-Quantitative Imaging Research Unit, Pitié-Salpétrière, Paris, France.*

Introduction: Segmental left ventricular (LV) function is usually evaluated by visual examination of cine sequences. This method is readily available but lack of reproducibility is a major drawback. Factorial analysis of medical image sequences (FAMIS) method summarizes-on a single static image-ventricular wall motion during the cardiac cycle by a three color code (green: no motion, red: inward motion, blue: outward motion). Parametric images can be automatically generated during the exam for immediate analyzis. This method has been described in echocardiography and isotopic ventriculography but was never reported in a MRI study. Furthermore it has never been validated if it confers any added value to subjective visual evaluation of wall motion alone.

Purpose: The aim of this study was to evaluate if adding objective parameters in images could help subjective visual analysis and improve inter and intra observer agreement.

Methods: Short axis LV cine loops (3 levels: basal, mid-ventriclar and apical) were obtained by MRI in 33 patients (18 with known myocardial infarction, 15 control) and 528 segments were analyzed. From each native sequence a single synthetic static parametric image was generated. Three independent observers scored LV wall motion using the 16 segments model (1: normal, 2: hypokinesia, 3: akinesia, 4: dyskinesia) initially by visual assessment of native cine loops alone then by combining native cine loop with the corresponding parametric image. Reference segmental scores were obtained by consensus for each modality. A global wall motion index (WMI) was calculated for each patient and observer in each modality. Segmental intra and inter observer agreement was assessed using raw agreement (%) and Cohen's Kappa unweighted coefficients and WMI were compared using linear correlation coefficients.

Results: Intra observer agreement for native cine loops was-respectively for observers 1, 2 and 3–: 80% ($\kappa = 0.56$), 81% ($\kappa = 0.65$) and 85% ($\kappa = 0.67$). When the parametric image was combined with visual assessment, agreement with the consensus was significantly higher for the 3 observers (Table 1) and inter observers agreement, when considering wall motion indexes, was also enhanced (Table 2).

Conclusions: Adding a single color-coded static parametric image to subjective visual assessment of segmental motion reduces inter observer variability and enhances diagnostic performance. Factorial analysis is an easy, fast and automatic therefore reproducible way to display static parametric images resuming the ventricular motion information

Table 1. Segmental score, agreement with the consensus

Agreement %/κ: κappa	Cine loops alone		Cine loops + parametric images	
Observer 1	89%	$\kappa = 0,76$	91%	$\kappa = 0,80$
Observer 2	84%	$\kappa = 0,69$	87%	$\kappa = 0,74$
Observer 3	93%	$\kappa = 0,84$	94%	$\kappa = 0,86$

Table 2. Wall motion index, inter observers agreement

R^2	Cine loops alone	Cine loops + parametric images
Obs 1 vs. 2	0.73	0.83
Obs 2 vs. 3	0.83	0.91
Obs 3 vs. 1	0.83	0.95

contained in an MRI contraction cine loop. It is an interesting self-evaluation and teaching tool to help in the understanding and diagnosis of complex segmental motion abnormalities and, furthermore, a synthetic visual communication tool.

539. Parametric Analysis of Main Motion (PAMM): An Objective Method to Quantify Myocardial Segmental Time-to-Contraction and Mean Velocity. Application in MRI to the Evaluation of Coronary Heart Disease (CHD): Feasibility Study

Nadjia Kachenoura[1], Alban B. Redheuil, MD, MSc.[2], Xavier Lyon, MD[3], Frédérique Frouin, PhD[1], Elie Mousseaux, MD, PhD[2]. [1]*Quantitative Imaging- Cardiovascular Imaging, INSERM U494, Paris, France,* [2]*Cardiovascular Imaging, European Hospital Georges Pompidou- Hôpitaux de Paris, Paris, France,* [3]*Cardiology, CHUV, Lausanne, Switzerland.*

Background: CMR is a reference method for the assessment of segmental wall thickness and thickening using contraction cine loops but also torsion, strain and strain rates thanks to tagging techniques. Nonetheless, routine analysis remains mostly visual since quantification techniques require long and fastidious post-processing. To accurately distinguish mild from severe hypokinesia at basal state or under stress is sometimes a challenge and interobserver variability remains a drawback. Parametric analysis of main motion (PAMM) is a fast and automatic method (few seconds on a PC) to extract, quantify and display as static color-coded parametric images both temporal and motion information contained in multislice MRI contraction cine loops. It is a multimodality technique that has been described in echocardiography but never reported as a potential quantification tool in MRI.

Aim: To evaluate the feasibility of extracting accurate segmental time-to-contraction and velocity parameters in normal subjects and test their potential usefulness in the evaluation of Coronary Heart Disease (CHD).

Methods: Short axis LV cine loops (3 slice levels: apical, mid-ventricular and basal) were obtained by MRI in 12 patients (6 control, 6 with myocardial infarction). Segmental wall motion was assessed using the 16 segment model and scored in 5 classes (normal, mild hypokinesia, severe hypokinesia, akinesia, dyskinesia) by consensus of 2 experts. End-diastolic and end-systolic LV endocardial contours were traced. For each slice level, corresponding to a cardiac cycle, we applied a fast processing method, PAMM, which fits a model of variation of the MRI amplitude on each pixel p. It estimates two temporal parameters: $T_b(p)$ and $T_e(p)$, which are respectively the time of the beginning and the end of the contraction movement over the pixels. The T_b map was combined with an Euclidian distance map computed from the endocardial contour to estimate for each segment two quantitative parameters: V_m: the mean velocity and T_{fc}: time-to-contraction corresponding to the electro-mechanical delay. All temporal data were normalized to the heart rate (RR interval).

Table 1.

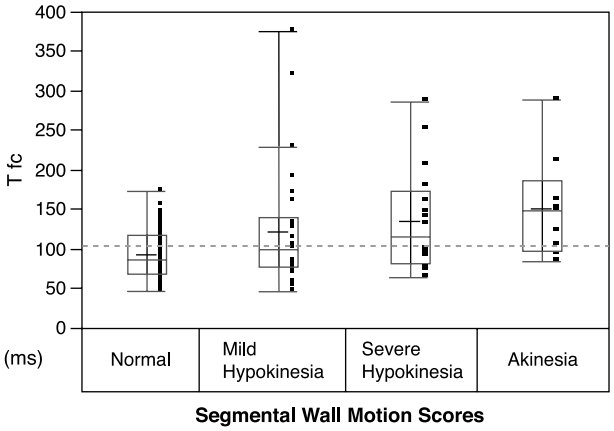

Results: In normal patients, the mean T_{fc} (time-to-contraction) considering all segments was 87 ms (SD: 13.5 ms) and we found an increasing delay in contraction from base to mid-wall to apex with respective mean values of 72 ms, 82 ms and 103 ms. The mean velocity (Vm) in all segments was 4.9 cm/s (SD: 0.9 cm/s). The interventricular septum showed a mean time-to-contraction delay compared to the other walls of 11 ms (SD: 6 ms). These data are consistent with physiology.Considering all subjects (normal and with myocardial infarction), we observed the following T_{fc} mean values according to the visual contraction consensus scores: normal motion: 93 ms, mild hypokinesia: 122 ms, severe hypokinesia: 137 ms and akinesia: 153 ms. No segment was scored dyskinetic. Distribution of data is resumed in Table 1.

Conclusion: These data suggest that a fast and automatic image processing method such as PAMM, allowing to quantify both time and velocity of motion information from MRI multislice contraction cine loops could be an interesting objective help to subjective visual analysis of segmental contraction. In particular it seems to be of potential interest in the exploration and diagnosis of mild or severe hypokinesia, especially if applied to stress studies to enhance sensitivity and specificity or in the measurement of ventricular asynchronism, as a tool to compare diseased segments to normal segments for a given patient. Larger scale studies are needed to confirm and validate this approach.

540. Improved Quantification of Left Ventricular Volumes and Mass Using Endocardial and Epicardial Surface Detection from Cardiac Magnetic Resonance Images

Cristiana Corsi, PhD[1], Claudio Lamberti, M.S.[1], Oronzo Catalano, MD[2], Serena Antonaci, MD[2], Peter MacEneaney, MD[3], Roberto M. Lang, MD[4], Enrico G. Caiani, PhD[5], Victor

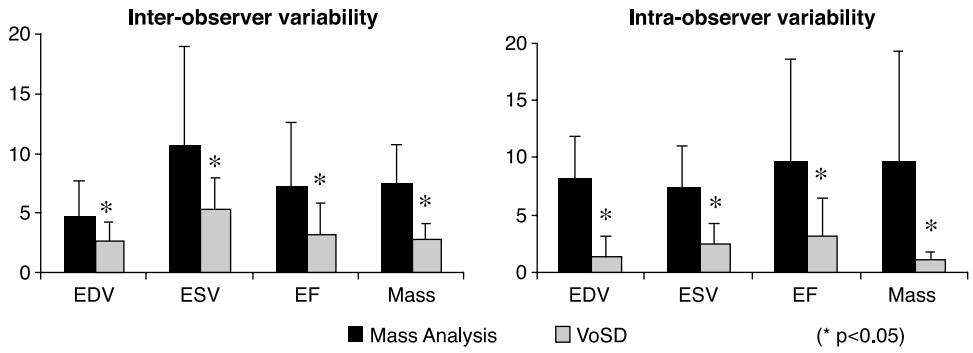

Figure 1.

Mor-Avi, PhD[4]. [1]*Electronics, Computer Science and Systems, University of Bologna, Bologna, Italy,* [2]*Salvatore Maugeri Foundation, Pavia, Italy,* [3]*Radiology, University of Chicago, Chicago, IL, USA,* [4]*Medicine/Cardiology, University of Chicago, Chicago, IL, USA,* [5]*Biomedical Engineering, Politecnico di Milano, Milan, Italy.*

Introduction: Cardiac magnetic resonance imaging (CMRI) is the standard for left ventricular (LV) volume, ejection fraction (EF) and mass measurements. However, LV volumes are obtained using semi-automated tracing of LV borders on multiple 2D slices and computations based on disk area summation approximation. This methodology is subjective and experience dependent and is known to suffer from limited reproducibility when applied to images of suboptimal quality. In addition, the use of fixed slice thickness for disk summation in segments where the endocardium is not perpendicular to imaging planes and the use of fixed number of slices throughout the cardiac cycle without taking into account systolic longitudinal shortening, may bias volume measurements. We developed a technique for detection of endocardial and epicardial surfaces, from which LV volumes and mass can be measured directly without any geometric approximation.

Purpose: This study was designed to test the hypothesis that this volumetric surface detection (VoSD) technique could provide accurate and more reproducible LV volume and mass estimates than the conventional methodology.

Methods: Twenty-four consecutive patients referred for CMRI were studied. Images (GE 1.5 T, FIESTA) were obtained during 12-second breath-holds in 6–10 short-axis slices from base to apex (9 mm thickness, no gaps) and reconstructed at 20 frames/cardiac cycle. Custom software was used to reconstruct from the short axis slices the volumetric data, from which endocardial and epicardial surfaces at end-systole (ES) and end-diastole (ED) were automatically detected following manual initialization using the level set approach. LV volume was obtained from voxel counts inside the endocardial surface at ES and ED, and EF was calculated. The LV mass was computed at end-diastole as the difference between epicardial and endocardial volumes times the mass density constant (1.05 g/cc). To obtain a reference for comparison, LV volumes and mass were also measured by an experienced investigator using the conventional technique based on semi-automated tracing with manual corrections (MASS Analysis, GE). Linear regression, correlation and Bland-Altman analyses were performed to test the accuracy of VoSD technique against the reference values. Reproducibility was tested in a subset of 12 patients by studying the inter-and intra-observer variability of each, the standard reference technique and the VoSD technique. Inter-observer variability was studied by blindly reanalyzing the images by a second observer. Intra-observer variability was studied by blindly reanalyzing the images by the same observer 1 week later. In both cases, variability index was calculated as the difference between repeated measurements in percent of their mean.

Results: In every patient, VoSD measurements were completed in < 5 min and correlated highly with the reference values (EDV: $r = 0.96$, $y = 0.95 \times + 12$; ESV: $r = 0.98$, $y = 1.1 \times - 2$; EF: $r = 0.91$, $y = 1.1 \times - 0.04$; mass: $r = 0.98$, $y = 0.91 \times + 5$). We found: 1) no significant biases for EDV, ESV, EF and mass (4 ml, 3 ml, 0.2% and − 9 g) and 2) narrow limits of agreement (SD: 16 ml, 12 ml, 6% and 9 g, respectively) between the two methods. Both inter-and intra-observer variability of the VoSD technique were significantly lower than those of the standard reference technique (Fig. 1).

Conclusions: Automated detection of endo-and epicardial surfaces from CMR images provides accurate measurements of LV volumes, EF and mass, in excellent agreement with the conventional methodology. In addition, this new technique is more reproducible than the standard reference technique.

541. Detecting BOLD Signal Changes with 2D-Balanced SSFP Imaging

Rohan Dharmakumar, PhD, Xiuling Qi, PhD, Juimiin Hong, MSc, Graham A. Wright, PhD. *Imaging Research, Sunnybrook & Women's College HSC, University of Toronto, Toronto, ON, Canada.*

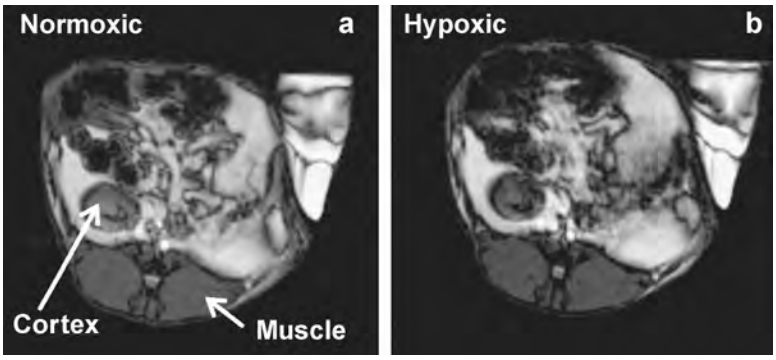

Figure 1.

Introduction: Microcirculatory changes in blood oxygen saturation ($\%O_2$), reflected as MR signal changes, can be useful in detecting and/or staging pathological processes such as ischemia. Recently, we reported that fast measurements of changes in $\%O_2$ (3–5 seconds) in whole blood can be achieved with 2D-balanced steady state free precession imaging (SSFP) (Dharmakumar et al., 2004). We hypothesize that the mechanism responsible for oxygen-sensitive contrast, defined as $O_2^{contrast}$ = % change in signal/change in $\%O_2$, in whole blood with SSFP can be exploited for rapid detection of microcirculatory $\%O_2$ changes.

Methods: We conducted both experimental and theoretical studies aimed at exploring the potential utility of SSFP imaging for tissue characterization.

A. Experimental Methods: We studied the effect of changing $\%O_2$ on the SSFP signal in 5 healthy New Zealand white rabbits, inducing temporary systemic arterial hypoxia by varying the partial pressure of O_2 in breathing gases. The systemic $\%O_2$ was varied from $\sim$ 88% at normoxic state to $\sim$ 65% at hypoxic state. Heart rate (HR) and $\%O_2$ were monitored with a pulsed oximeter. Once the desired $\%O_2$ was reached, $\%O_2$ was held relatively constant ($\pm$ 4%). Subsequently, SSFP was prescribed on one slice containing the dorsal muscle of the animal and the cortex of the kidney. The scan parameters were: flip angle = 60°, acquisition matrix = 256 × 256, TR = 8 ms, TE = 4 ms, number of pulses to reach steady-state = 1000, field of view = 22 cm, and slice thickness = 10 mm. This experiment was repeated 5 times on each animal at two different field strengths (1.5 T and 3.0 T).

B. Theoretical Method: We also performed numerical simulations using a set of modified Bloch equations, modeling the extravascular and intravascular space with known relaxation constants as a two-pool system (Dharmakumar et al., 2004). Spins in the different pools were allowed to exchange between the two compartments while phase-cycled RF pulses were applied every TR (8 ms) with a flip angle of 60° until the magnetization reached steady state. Oxygen-related changes at 1.5 T and 3.0 T were implemented as changes in intravascular transverse relaxation constant (T_{2vasc}) values given by the following equation: $1/T_{2vasc} = 1/T_{2o} + K(1-\%O_2/100)^2$, where K and T_{2o} are parameters that depend on field strength, TR, and flip angle as previously reported (Dharmakumar et al., 2004).

Results: The results showed the presence of $O_2^{contrast}$ in the MR images of the dorsal muscle and the cortex of the kidney. Typical SSFP images for normoxic and hypoxic states are shown below as Fig. 1a and Fig. 1b respectively. The cortex showed nearly a 10 fold increase in $O_2^{contrast}$ relative to the skeletal muscle of the rabbit, which is expected based on the relative blood volume. It was also found that doubling the field strength leads to nearly a 12 fold increase in $O_2^{contrast}$ in both the muscle and cortex which is also expected based on

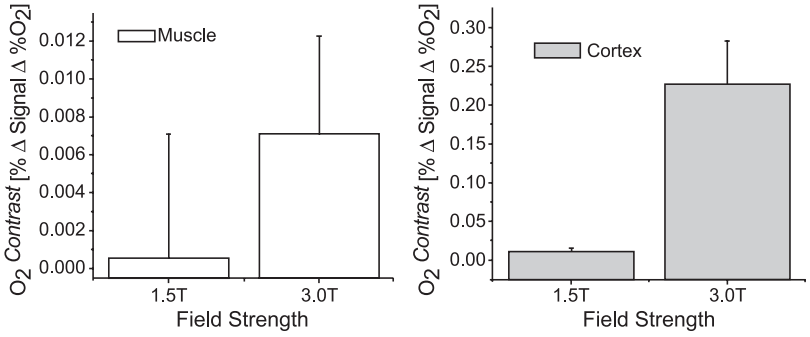

Figure 2.

blood signal changes with field. Refer to Fig. 2. These experimental results also agreed well with the predictions of the theoretical model.

Conclusion: The results confirmed our hypothesis that microcirculatory changes in $\%O_2$ can be detected with SSFP-based MRI. Based on our findings, we anticipate that changes in $\%O_2$ in other tissues, including the myocardium, may be detected with improved sensitivity using SSFP.

REFERENCE

Dharmakumar, R., et al. (2004). *2004 ISMRM Conference Proceedings*. 185.

542. Correcting Motion Artifacts in Stimulated Echo Mode (STEAM) Cardiac Imaging

Ahmed S. Fahmy, MSc,[1] Li Pan, MSc,[2] Matthias Stuber, PhD,[3] Nael F. Osman, PhD.[3] [1]*Electrical and Computer Engineering, Johns Hopkins University, Baltimore, MD, USA,* [2]*Biomedical Engineering, Johns Hopkins University, Baltimore, MD, USA,* [3]*Radiology, Johns Hopkins University, Baltimore, MD, USA.*

Introduction: STEAM imaging of the heart may be very useful for generating black blood images of the heart. However, its application for acquiring cine movies during cardiac cycle was hampered by non-uniform loss of signal intensity inside the myocardium.

Purpose: Developing a method to recover the signal loss caused by tissue deformation in STEAM sequences.

Theory: The STEAM sequence is based on modulating the longitudinal magnetization of the tissue with a sinusoidal pattern of frequency $f_m(x,y) = f_,$ where f_o is a constant determined by an applied modulation gradient. During image acquisition, a constant demodulation frequency, $f_d = f_o$, is used to refocus the magnetization and thus a stimulated echo is measured. Nevertheless, due to myocardial deformation, the modulation frequency $f_m(x,y)$ becomes spatially-variant as earlier described (Fischer et al., 1995), and $f_d = f_o$ cannot completely refocus the magnetization at all pixels; thus, loss of myocardial signal can be observed [Fig. 1(a), (d), and (g)].

Method: Two STEAM images (I_L and I_H) of the same anatomical slice are acquired with two different demodulation frequencies f_L and f_H. The frequencies f_L and f_H are selected such that $f_L<f_m(x,y)<f_H$. The selection of these two demodulation frequencies guarantees that the signal loss in one image is recovered by the other one. The summation (I_L+I_H) reduces the change of intensity due tissue deformation, but not completely. Further improvement is done by multiplying the summation by a spatially dependent map whose value at each pixel is determined by the amount

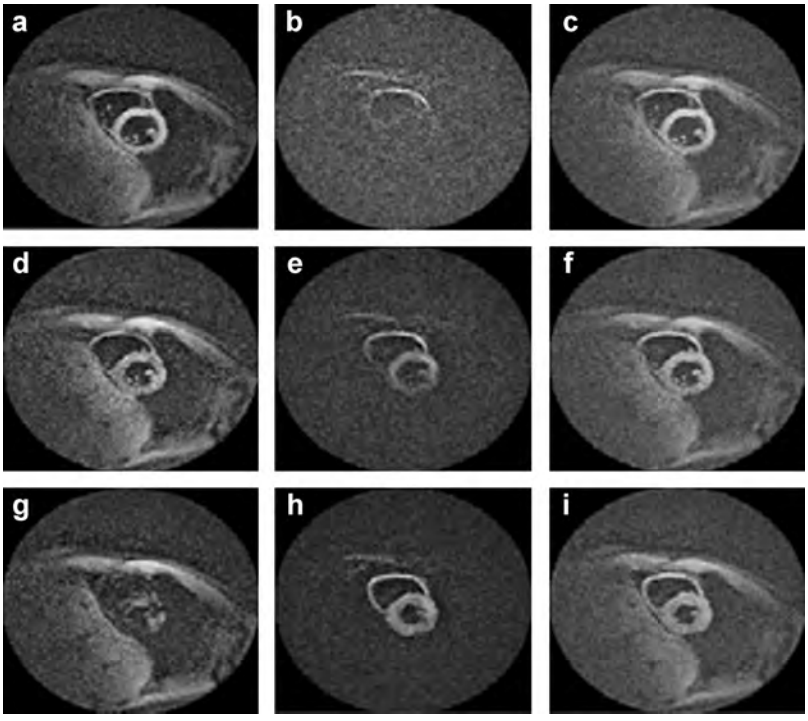

Figure 1. Short axis images of the human heart using a high-speed STEAM pulse sequence. Images in the left column were acquired with $f_L = f_o$, while images in the middle column were acquired with $f_H = 1.33\ f_o$. Images in the right columns are the result of combining the corresponding images in the other two columns as described in the text.

of tissue deformation [computed from the two intensity values of the pixel in the acquired images I_L and I_H (Osman et al., 2001].

Short axis images of a healthy volunteer's heart were obtained using fast STEAM sequence (Frahm et al., 1991). The images were acquired using spiral acquisition (12 interleaves) on an Intera 1.5 Tesla scanner (Phillips Medical Systems). The imaging parameters are slice thickness = 10 mm, 25 cardiac phases, FOV = 350 mm, flip angle = 40°, and modulation frequency $f_o = 0.3\ \text{mm}^{-1}$. Modulation of magnetization was applied at end diastole and thus $f_L = f_o$ was used since no further stretch of the myocardium was expected. Also, assuming a maximum contraction of the myocardium = 25%, a demodulation frequency $f_H = 1.33\ f_o$ was used.

Results: The rows of Fig. 1 show the acquired images at three time frames (at 58, 148, and 237 ms after ECG trigger). Images in the first and second columns were acquired with $f_d = f_L$ and $f_d = f_H$, respectively. Standard STEAM image acquisition (with $f_d = f_L$) suffers from signal loss in the myocardium originating from tissue contraction [Fig. 1(a), (d), and (g)]. In the images acquired with $f_d = f_H$, however, the situation is reversed and the myocardium signal increases with contraction [Fig. 1(b), (e), and (h)]. Combining the two images, as discussed above, compensates the loss of the myocardial signal and shows high contrast between the myocardium and the blood throughout the entire cardiac cycle [Fig. 1(c), (f), (i)].

Conclusion: The proposed method enables functional black-blood STEAM imaging of the heart without signal-loss due to tissue deformation.

ACKNOWLEDGMENTS

This research was supported by a grant from the National Heart, Lung, and Blood Institute (RO1 HL072704)

REFERENCES

Fischer, S. E., et al. (1995). *Magn. Reson. Med.* 22:133–142.
Frahm, J., et al. (1991). *Magn. Reson. Med.* 34:80–91.
Osman, N. F., et al. (2001). *Magn. Reson. Med.* 46:324–334.

543. Delineation of Myocardial Necrosis from Reperfused Infarction Using Extracellular and Necrosis-Specific Contrast Agents

Simon Schalla, Charles B. Higgins, MD, Maythem Saeed, PhD. *Radiology, University of California San Francisco, San Francisco, CA, USA.*

Introduction: Detection of acute myocardial infarction and assessment of the spatial extent are important for selecting therapeutic strategies and for prediction of patient outcome. Contrast enhanced magnetic resonance (MR) imaging was employed as a non-invasive method to delineate necrotic myocardium and several contrast agents have been studied such as extracelular, intravascular and necrosis-specific agents. Extracellular contrast agents are most important due to their approval for clinical use. However, extracellular contrast agents enhance both necrotic cells and interstitial edema including the peri-infarction zone. Since the enhanced area becomes smaller over time, it was proposed that at a certain point in this time course the contrast enhanced zone would match the true spatial extend of infarction. However, controversial findings were reported regarding the optimal imaging time after injection of extracellular contrast agent.

Purpose: The purpose of this study was to follow the time course of enhancement in infarcted myocardium with serial MR imaging using the extracellular contrast agent Gd-DTPA in comparison with baseline enhancement with the necrosis-specific contrast agent Gadophrin-3.

Methods: Myocardial infarction was produced in 10 rats by occluding the left coronary artery for 25 min followed by 3 hours reperfusion. At the beginning of reperfusion, the necrosis-specific agent Gadophrin-3 (Schering AG, Berlin, Germany) was intravenously injected (0.05 mmol/kg) to delineate infarcted myocardium. Three hours after injection, baseline MR imaging of Gadophrin-3 enhanced short axis slices covering the entire heart was performed. Two representative slices were selected for sequential follow up imaging (time course). The extracellular contrast agent Gd-DTPA (0.3 mmol/kg i.v., Schering AG, Berlin, Germany) was intravenously injected and serial MR imaging of the 2 selected slices was performed immediately after injection and subsequently every 5 minutes up to 45 minutes post-injection.

A 2.0 T CSI-II-system (Bruker Instruments, Fremont, CA) was used for image acquisition with the following parameter: slices thickness = 2 mm, field of view = 5 × 5 cm, TR = 30 ms, TE = 12 ms, image matrix = 256 × 128. After MR imaging, the left coronary artery was re-occluded and 0.7 ml of phthalocyanine blue dye was intravenously injected to define the area at risk. The LV was transversely sliced into 4–6 slices; each of 2 mm thickness corresponding to the MR images. Each slice was then incubated in 2% triphenyl-tetrazolium-chloride solution to define the necrotic myocardium. To define the value of Gadophrin-3-enhancement as a standard to measure the amount of necrotic tissue, the total size of necrosis in % of the LV mass determined with Gadophrin-3-enhanced MRI was compared with the size of necrosis determined at postmortem with histochemical staining. Subsequently, the time course of Gd-DTPA-enhancement was analysed in the 2 representative slices and compared with baseline images of Gadophrin-3 enhancement.

Results: Gadophrin-enhanced MR imaging was similar to post-mortem staining for the determination of infarction size. Infarction size was 9.3% of left ventricular mass determined with Gadophrin-enhanced MR imaging and 8.6% determined

with post-mortem staining (r = 0.97). On serial MR imaging, initial enhancement with Gd-DTPA directly after injection was up to 3.8-fold larger than baseline Gadophrin-enhancement (mean: 1.8 ± 0.8 fold). Within 15 min, the areas of enhancement were similar to baseline imaging in the majority of animals. However, in 2 animals, the time needed to observe a reduction of the size of the enhanced area to the baseline level was up to 22 min.

Conclusions: The spatial extend of myocardial necrosis after infarction can be precisely determined with Gadophrin-enhanced MR imaging. Thus, it can be used as a standard for comparisons with other methods in animal studies. Using extracellular contrast agents, contrast-enhanced MR imaging for the determination of necrosis can be performed approximately 25 min post-injection. The amount of viable myocardium and edema in the peri-infarction zone may vary individually.

544. In-Vivo Validation of Myocardial High-Resolution T_1 Mapping

Daniel R. Messroghli,[1] Sven Plein, MD,[1] David M. Higgins, MSc,[2] Kevin Walters, PhD,[3] Timothy Jones, MSc,[1] John P. Ridgway, PhD,[2] Mohan U. Sivananthan, MD.[1] [1]*Cardiac MRI Unit, Leeds General Infirmary, Leeds, UK,* [2]*Department of Medical Physics, Leeds General Infirmary, Leeds, UK,* [3]*Division of Genomic Medicine, University of Sheffield, Sheffield, UK.*

Background: The spin-lattice relaxation time (T_1) is used in magnetic resonance imaging (MRI) to generate tissue contrast. Conventional T_1-weighted imaging techniques such as delayed enhancement imaging only indicate relative signal differences. Quantification of true myocardial T_1 can serve to analyze areas of myocardial damage in a direct manner.

Purpose: To establish the reproducibility of myocardial T_1 as assessed by fast high-resolution T_1 mapping.

Materials and Methods: Single breath-hold T_1 mapping using Modified Look-Locker Inversion Recovery (MOLLI) was performed in 16 healthy volunteers (mean ± SD 35 ± 11 years, 9 male) before and repeatedly after administration of Gadolinium-DTPA on a 1.5 T MRI system. Image quality scores and myocardial T_1 values were derived for standard short-axis segments and slices. Results were compared with those from a second MRI study performed on the same day [native (= non-contrast) only, n = 16] and from a third study performed on a different day (native and contrast-enhanced, n = 8) in the same subjects. Intra-and inter-observer agreement were determined.

Results: Of 1362 myocardial segments, 1297 showed "good" (92.3%) or "satisfactory" (2.9%) image quality. Myocardial T_1 in short-axis slices was 982 ± 52 ms (mean ± SD; 95% confidence interval of mean: 966–997

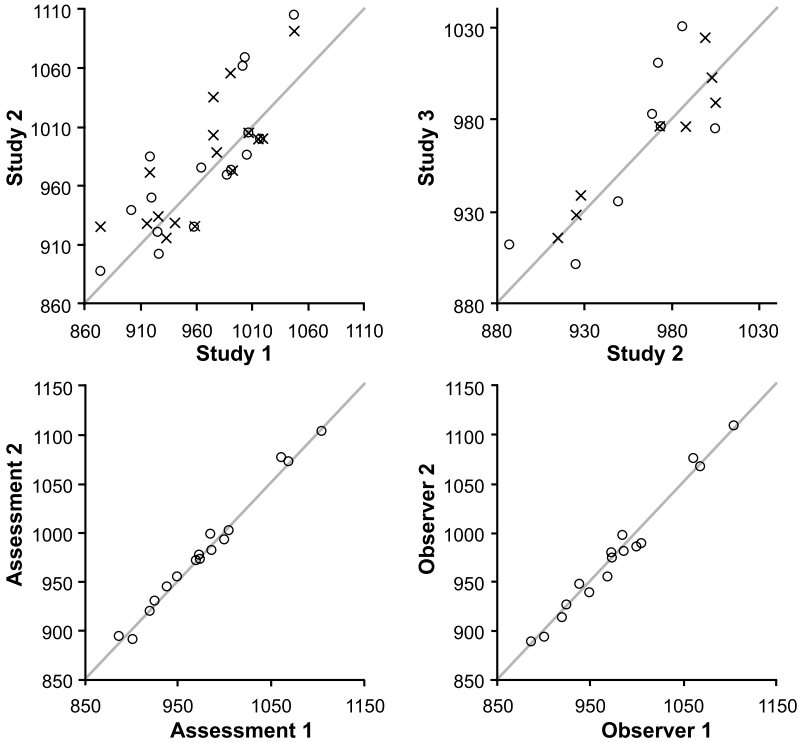

Figure 1. Scatter plots illustrating same-day inter-study (upper left), different-day inter-study (upper right), intra-observer (lower left), and inter-observer (lower right) agreement of native mid-cavity slice myocardial T_1 (ms). o = "raw" T_1; x = heart rate-corrected T_1; grey line = line of identity.

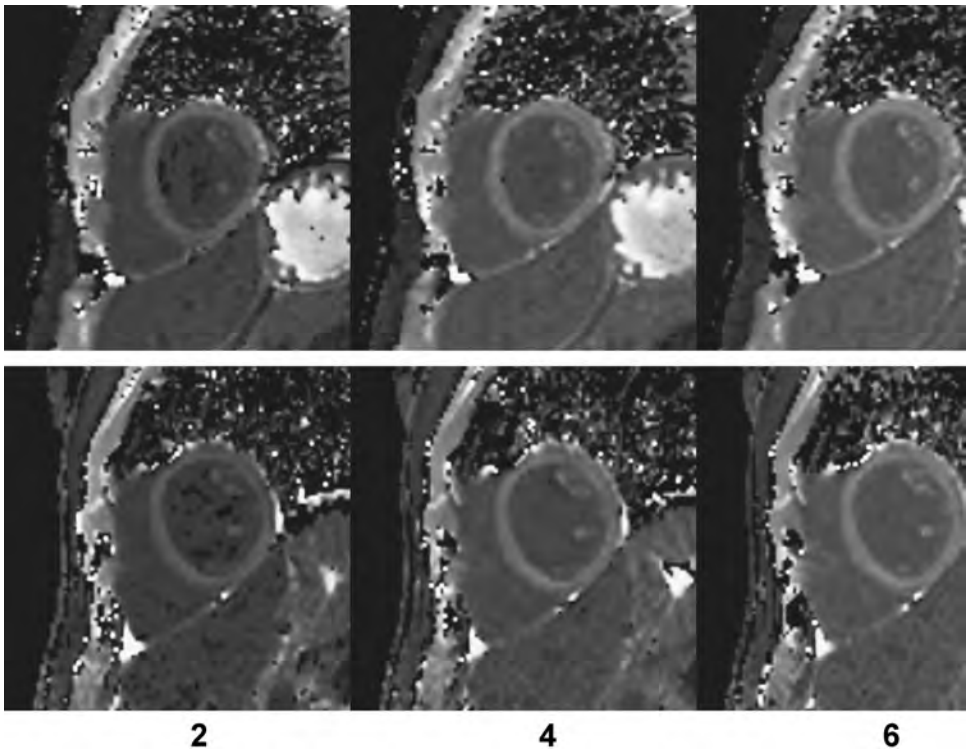

Figure 2. Short-axis post-contrast T_1 maps of the same subject acquired at 2 different days.

ms; n = 46). There was no significant difference in T_1 between basal, mid-cavity, and apical short-axis slices ($p = 0.35$, n = 14). Correlation and Bland-Altman bias analysis indicated good reproducibility for both native and post-contrast T_1 measurements. Intra-and inter-observer agreement in native T_1 measurements were very high. The spread of native myocardial T_1 could further be reduced by a simple heart rate correction (Figs. 1 and 2).

Conclusion: MOLLI T_1 mapping allows to rapidly obtain high-resolution myocardial T_1 maps in a robust and reproducible fashion. A normal range for native and post-contrast T_1 has been established. This technique is a promising tool to directly quantify tissue changes in ischemic and inflammatory myocardial diseases.

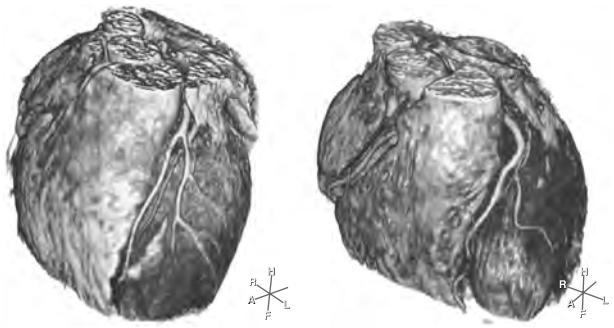

Figure 1. Examples of whole heart visualization.

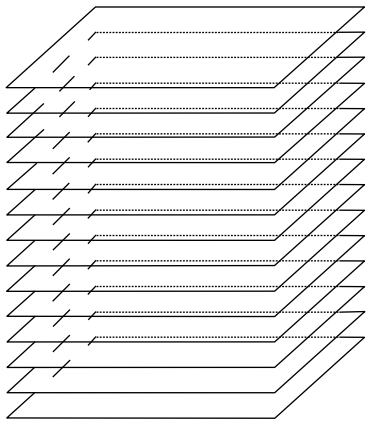

Figure 2. Contours are drawn on only a few slices. A 'paddle wheel' is automatically reformatted and the three-dimensional VOI is determined.

545. Fast and Easy Whole-Heart MRA Segmentation and Visualization

Hubrecht L. T. de Bliek, Steven Lobregt, Frans A. Gerritsen. *Medical IT-Advanced Development, Philips Medical Systems, Best, The Netherlands.*

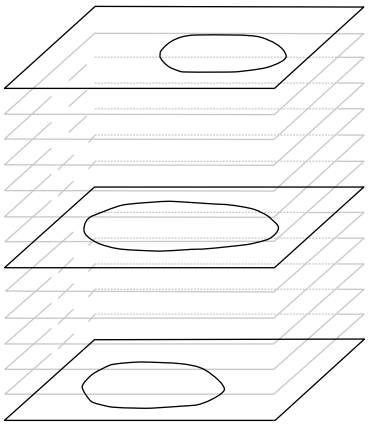

Figure 3. One of the interactively drawn contours.

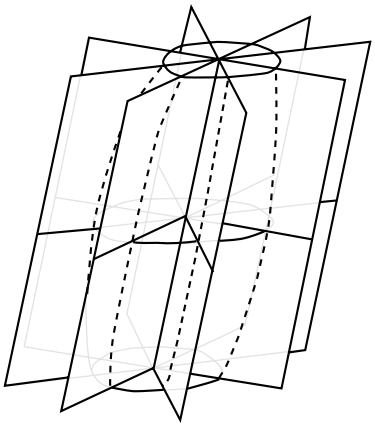

Introduction: Recent developments in MR acquisition techniques have led to the availability of high-resolution short-axis scans of the heart with sufficient contrast between tissues to allow high-quality visualizations that show heart and coronary artery tree as 3-D structures. In conventional systems such visualizations are unattractive for routine clinical use as they require elaborate interactive segmentation to isolate heart and coronaries from surrounding structures that disturb the visualization.

Purpose: Our goal is to provide tools that allow fast, simple and intuitive segmentation of the heart to facilitate visualization. User interaction is reduced to drawing a few contours from which a smooth surface is generated that delineates the Volume-Of-Interest (VOI) (see Fig. 1). Further interaction (such as modification of this VOI to remove structures blocking the view on coronaries) is done on VOI cross-sections while having a three-dimensional effect on its shape via a new segmentation concept called ''paddle wheel editing''. The segmentation result is visualized using predefined (interaction-free) settings for the transfer function (Fig. 2).

Methods: The whole-heart 3D scan (Ichikawa et al., 0000; Weber et al., 2003) is a free-breathing Balanced-TFE acquisition using respiratory navigators, VCG triggering and a resolution of 0.5 × 0.5 × 0.75 mm. The total scan time is 7–15 min on a Philips Intera 1.5 T Rel. 10.4. Usually the acquired volumes contain 150–180 slices. Our ''paddle wheel editor'' requires a minimum number of two drawn contours. Modification of the VOI to remove anatomy blocking the view on a coronary artery is simple, and a smooth, continuous shape of the VOI is ensured. See Figures 3–5.

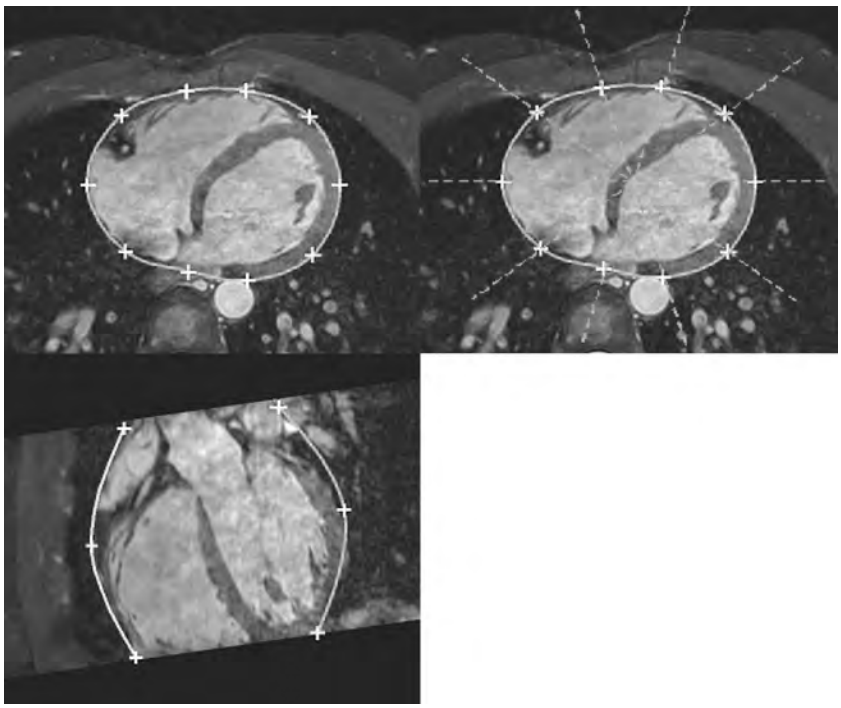

Figure 5. One of the paddle wheel planes.

A drawn or interpolated contour is shown on each slice, together with cross-sections of paddle wheel planes. The paddle wheel images show smooth curves that represent cross-sections of the plane and all contours. The contours in the slices and the curves in the paddle wheel planes are related through common control points. Convenient orientation is provided by linking the geometry of the three-dimensional visualization of the current VOI to the paddle wheel view. When a point on the 3-D image of the heart is selected, the nearest paddle wheel plane is activated. The Bézier spline closest to the selected point is then highlighted on the paddle wheel. Modifying curve or contour results in immediate update of the visualization. Visualization parameters can be loaded from presets and do not require expert knowledge.

Results: The time required for segmentation of a smooth, continuous three-dimensional VOI of the heart can be reduced to only a few minutes with a minimum of user interaction. Three different users evaluated the introduced ''paddle wheel'' segmentation approach on six datasets. The obtained results proved to be quite satisfactory and reproducible.

Conclusions: The proposed paddle wheel segmentation method offers a simple and intuitive tool for segmentation of three-dimensional anatomical structures. In this paper, we describe its application to segmentation of the whole heart for visualization. Other applications of the approach seem feasible and relevant.

REFERENCES

Ichikawa, Y., Sakuma, H., Suzawa, N., Nagata, M., Makino, K., Hirano, T., et al. Clinical feasibility of whole-heart coronary MRA using a navigator-gated 3D B-TFE, ISMRM2004 Proceedings Abstract #704.

Weber, O., Martin, A., Higgins, C. (2003). Whole-heart steady-state free precession coronary artery magnetic resonance angiography. *Magn. Reson. Med.* 50:1223–1228.

546. A New Approach to Subset Analysis of Global Left Ventricular Blood Flow

Ann Bolger,[1] Einar Heiberg, MSc,[2] Matts Karlsson, PhD,[2] Andreas Sigfridsson, MSc,[2] Jan Engvall, MD, PhD,[2] Lars Wigstrom, PhD.[2] [1]*University of California, San Francisco, San Francisco, CA, USA,* [2]*Linkoping University, Linkoping, Sweden.*

Introduction: Phase contrast magnetic resonance imaging (MRI) allows measurement of cardiac flow velocities in three dimensional (3D) space and time. Visualization of these dense data sets with particle trace pathlines can demonstrate the pathways that blood follows through the heart over the cardiac cycle, but the data density and the multiple simultaneous and confounding flows make useful quantification of specific flows very challenging.

Purpose: We hypothesized that the left ventricular (LV) inflow is inhomogeneous, and could be separated into discrete functional subsets according to expected flow behaviors. Further, once separated, we expected these subsets to be relatively homogeneous in their behavior over time and space, allowing quantification of velocity-based parameters and comparison between subsets without interference from other flows.

Methods: We used time-resolved phase contrast MRI (1.5 T scanner, TR = 18, TE = 6, VENC = 60 cm/s, spatial resolution of $1 \times 4 \times 4$ mm) to visualize diastolic LV inflow in a normal volunteer (age 50, heart rate 60 bpm). Eddy current and Maxwell corrections were applied. Groups of pathlines were emitted from a rectangular grid in the left atrium at every time step during diastole. The traces were sequentially separated into subgroups according to, first, whether or not they successfully entered the LV through the mitral vena contracta (Atrial versus Inflow traces), and, second, whether they exited the LV during the same cardiac cycle or not (Direct versus Delayed inflow). Each trace's volume was calculated based on the density of the emission grid, the velocity at the time of particle emission, and timestep duration in seconds. Velocities along the traces' routes were extracted and used to calculate their change in kinetic energy.

Results: Exclusion of Atrial traces yielded an anatomically correct distribution of emitters specific to LV inflow. Of the Inflow traces, Direct and Delayed flow subsets represented 59 and 41% of the total inflow, respectively. The inflow subsets followed distinct spatial routes through the LV, with different amounts of velocity change along their paths. The path of Direct inflow from mitral to aortic valves was homogenous and followed a smooth curving route in the base of the LV, with an average length of 8.4 ± 1.5 cm and change in kinetic energy from inflow to ejection of 0.9 mJ. In contrast, Delayed inflow was more varied in distribution and included the filling of the apical LV. The average path length from inflow to ejection was longer (15.3 ± 2.2 cm), and during its first diastole in the LV the Delayed inflow experienced less acceleration and deceleration than Direct inflow. The Delayed inflow's change in kinetic energy from inflow to its eventual ejection after two cardiac cycles was 8.1 mJ.

Conclusions: Division of complex intracardiac flows with subset analysis of particle trace pathlines allows highly targeted visualization of specific flows of interest. Separation from simultaneous confounding flows greatly improves quantitative analysis of the flow based on the underlying spatial, temporal and velocity data. In this example, this method demonstrates that the behavior of LV inflow comprises different components which are not uniform with respect to route, change in velocity along the path, or likelihood of successful ejection within a single cardiac cycle. Other flow characteristics could also have been used to separate out different flows of interest. This approach to

visualization and subgroup separation of complex and time-varying flow is a new and readily implemented approach to extracting meaningful quantitative information about flow-based aspects of cardiac function. As acquisition times improve, these analyses may provide new measures of normal cardiac physiology and pathophysiology, such as regional flow distribution and energy changes, that may assist in the design of devices and therapies for cardiovascular disease.

547. 3D Free-breathing Technique for High Spatial Resolution Myocardial Viability Imaging

Dana C. Peters, Rene M. Botnar, Evan A. Appelbaum, Kraig V. Kissinger, Warren J. Manning. *Cardiology, Beth Israel Deaconess Medical Center, Boston, MA, USA.*

Introduction: Imaging using the Gadolinium-DTPA delayed enhancement technique provides a spatial map of myocardial viability of the myocardium (Kim et al., 2000). However, the map's spatial resolution is generally low. High spatial resolution may have an important role in improving assessment of transmurality in quartiles; detecting and characterizing the presence of scar in the RV; and characterizing other cardiomyopathies. Therefore it is important to improve the spatial resolution for viability techniques. Here we present a 3D free-breathing, navigator-gated method with a goal of increasing spatial resolution. This approach is an adaptation of free-breathing coronary artery imaging methods (Botnar et al., 2003; Huber et al., 2003). 3D viability techniques have been employed by several investigators (Kuhl et al., 2004; Saranathan et al., 2004), mainly for imaging patients incapable of breath-holds, rather than to achieve increases in spatial resolution.

Purpose: To provide viability images at higher spatial resolution.

Methods: A 3D gradient echo acquisition, with an inversion prepulse is used. Navigator-gating is used for motion compensation. Diastole is chosen for imaging. Typical scan parameters were: 3D Cartesian, inversion recovery (180° RF applied every RR) spoiled gradient echo imaging, 16 views per segment, TR/TE/θ = 5.2/1.8/30°, elliptical centric acquisition order, 30 cm FOV, 224 × 224 × 13 Nz, 5 mm slice thickness (zero-filled to 2.5 mm), 120 Hz/pixel, fat saturation. Scan time was about 3 minutes for 50% navigator efficiency. Imaging was performed in 5 patients with scar (5 males, age 52 ± 9). Injection ranged from 0.1 to 0.2 mmol/kg, and imaging time post injection for the 2D and 3D spanned from 20 to 40 minutes. The TI was determined by using data from T1 of blood vs. time after injection (Goldfarb et al., 2004; Weinmann, 1984), and using trial 2D scans. An experienced reader compared the 2D and 3D data sets and matching slices, and graded on conspicuity of the infarct, contrast between myocardium, scar and blood pool, and level of spatial details observed (ratings of 1–4, 1 = worst, 4 = best).

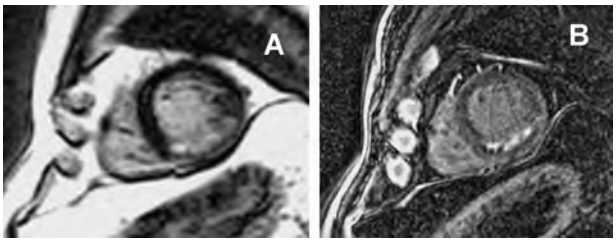

Figure 1. (A) 2D breath-held image (2 × 2 × 10 mm) compared to a (B) 3D free breathing image (1.5 × 1.5 × 5 mm).

Table 1. Subjective scoring of 5 patients on 3 criteria

	Overall	Spatial details	SNR	CNR
3D	2.8	3.2	2.2	2.8
2D	3.1	3.0	3	2.6

Results: Figure 1 shows a comparison between the 3D high spatial resolution method and 2D method. The improvement in scar demarcation is very clear in this example. The subjective grading is shown in Table 1. The SNR was lower, but the spatial resolution was slightly better.

Conclusions: The 3D scans provide higher spatial resolution images of viability, with good CNR, but lower SNR. In our experience, image quality of the 3D method is highly variable, due either to motion artifacts, imperfect nulling, etc. While further refinements are required for the pulse sequence and protocol, the improvement in spatial resolution achieved with our technique permits a new visualization of scar, with important potential applications in clinical cardiac imaging.

REFERENCES

Botnar, R. M., et al. (2003). *JMRI* 17:615–619.
Goldfarb, J. W., et al. (2004). *SCMR* 221.
Huber, M. E., et al. (2003). *MRM* 49:115–121.
Kim, R. J., et al. (2000). *N. Engl. J. Med.* 343:1445–1453.
Kuhl, H. P., et al. (2004). *Radiology* 230(2):576–582.
Saranathan, M., et al. (2004). *Magn. Reson. Med.* 51(5):1055–1060.
Weinmann, H. M. (1984). *Physiol. Chem. Phys. Med. NMR* 16:167–172.

548. Multi Coil Real Time Color Flow for Assessing Thoracoabdominal Aorta

Ajit Shankaranarayanan,[1] Andres Carrillo,[2] Jane Johnson,[1] Jean Brittain,[1] Bob Hu.[3] [1]*Applied Science Lab, West, GE Healthcare, Menlo Park, CA, USA,* [2]*Applied Science Lab, Central, GE Healthcare, Chicago, IL, USA,* [3]*Cardiology, Palo Alto Medical Foundation, Palo Alto, CA, USA.*

Introduction: The evaluation of the thoracoabdominal aorta is one of the most important challenges in the evaluation of

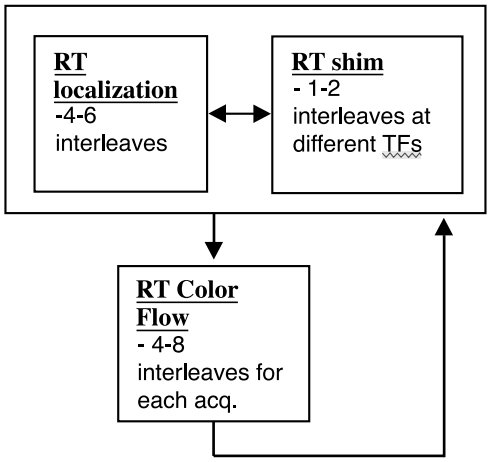

Figure 1. The schematic shows the workflow of the real time color flow tool. The unique imaging parameters for different modes are listed in each box.

patients with severe chest or abdominal pains or neurologic complaints. Magnetic resonance imaging of the aorta is potentially the best method for evaluating this condition because of its ability to examine both the anatomy and physiology of vascular lesions. CT angiography requires the use of nephrotoxic contrast agents while ultrasonography is frequently unable to examine the entire aorta. Magnetic resonance imaging of the aorta has not been adopted in the clinical setting due to the prolonged scan time that the patients have to endure.

Following the flexible architecture proposed in Santos et al. (2002), we have developed a dynamic real-time color flow system compatible with multi coil that allows us to scan the entire extent of the thoracic and abdominal aorta in real-time. The ability to perform real-time adjustment of slice location and sequence parameters increases the flexibility and efficiency in performing the aortic evaluation.

Methods: The real time multi coil color flow system is implemented on a GE 1.5 T Signa Twinspeed system (GE Healthcare Technologies, Waukesha, WI) that includes EXCITE technology running optimized sliding-window, gridding reconstruction software (Shankaranarayanan et al., 2003).

Figure 1 illustrates the three modes available in our real time color flow system: real time localizer, real time shim, and real time color flow mode.

The current implementation utilizes a spiral acquisition. However, the infrastructure can be easily combined with other imaging approaches. The imaging parameters common to all modes include a short 480 us sinc excitation pulse, 8 ms readout, 5 mm slice thickness, 30° flip angle. The minimum TR achieved was around 10 ms and minimum TE was 1.5 ms for a maximum velocity encoding (venc) of 200 cm/sec. Contextual information including slice location, prescan parameters, and shim values is automatically shared between the real time localization and color flow modes. The method described in Bernstein et al. (1994) was used to combine the phase images from the multi coil data set. A reconstruction frame rate of 15 frames/sec for the color over-layed images was achieved using sliding window reconstruction. The user was able to adjust the scan plane and FOV during the acquisition of real-time color flow images, thus increasing the efficiency of the assessment. An 8-channel torso phased array coil was used for signal reception. This ensured us the coverage of the entire aorta.

Results: Figure 2 shows coronal images of the aorta at different cardiac phases [(a) diastole, (b) mid-systole, (c) systole] acquired in real time. This application allowed us to examine the aorta from the aortic arch to the iliac vessels in as little as 8 minutes.

Conclusions: Rapid evaluation of the aortic anatomy and blood flow characteristics can be performed with real-time MRI in less than 10 minutes. This technique should provide a comprehensive evaluation of patients with suspected aortic pathologies without the current limitation of other imaging modalities.

REFERENCES

Bernstein, M., et al. (1994). *MRM*:330–334.
Santos, J. M., et al. (2002). *ISMRM*:738.
Shankaranarayanan, A., et al. (2003). *SCMR*:294–296.

549. Longitudinal Myocardial and Trans-mitral Velocities by Phase-Contrast (PC) MRI: Correlation with Doppler Echocardiography

Sriram Padmanabhan, MD,[1] Vandana Sachdev, MD,[2] Li-Yueh Hsu, DSc,[1] Sidenko Stanislav,[2] Andrew E. Arai, MD.[1]

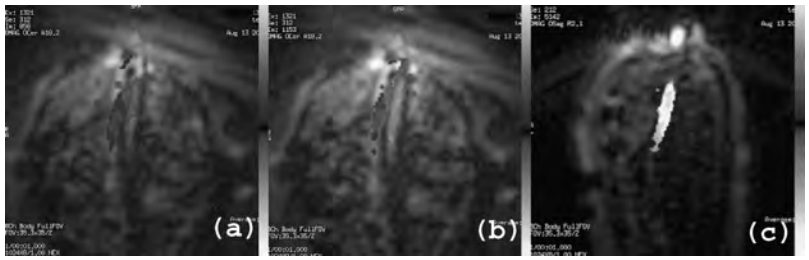

Figure 2. Coronal images of thoracoabdominal aorta and veins in different cardiac phases. (a) diastolic phase, (b) mid-systolic phase and (c) systolic phase.

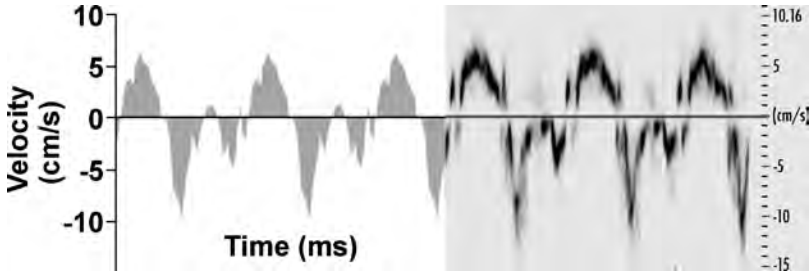

Figure 1. Longitudinal myocardial velocity by PC-MRI (left) and TDI (right) in the infero-septal wall of a normal volunteer.

[1]*Laboratory of Cardiac Energetics, NIH/NHLBI, Bethesda, MD, USA,* [2]*Echocardiography Laboratory, NIH/NHLBI, Bethesda, MD, USA.*

Introduction: Longitudinal myocardial velocity measurement has significance in assessing regional myocardial function and viability. Tissue Doppler Imaging (TDI) by echocardiography is well validated for measuring longitudinal myocardial velocities. PC MRI can provide quantifiable velocity measurements but has not been correlated with TDI derived velocities.

Purpose: To validate longitudinal myocardial and trans-mitral velocity measurements by PC MRI with Doppler echocardiography.

Methods: We recruited 17 patients with established myocardial infarction (MI) and 9 normal volunteers. Cardiac MRI and 2-D echocardiography with TDI were performed within 12 hours of each other. Basal myocardial tissue velocities and transmitral filling velocities were measured with PC MRI using a temporal resolution of 28 msecs. TDI measurements of systolic (S′), early diastolic (E′) and late diastolic (A′) myocardial velocities, and Doppler trans-mitral E and A velocities were measured by investigators blinded to the MRI data. Results are mean ± SD.

Results: Mean age of study participants was 62.9 ± 11.7. There was significant difference in the ejection fraction between normal and MI groups (60.1 ± 4.5 vs. 43.3 ± 7.4, $p < 0.001$). The MRI velocities ranged from 111.8 to − 15.4 cms/s. MRI velocity data showed strong linear correlation with echo-derived velocities (R = 0.98, $p < 0.001$). Bland-Altman analysis revealed that MRI overestimated longitudinal myocardial velocities by 0.47 ± 3.1 cm/s in all subjects. In patients with MI, MRI overestimated velocities by 0.19 ± 2.39 cms/s and in normal volunteers by 1.03 ± 4.09 cm/s. MRI underestimated trans-mitral flow by 10.3 + 10.02 cm/s (Fig. 1).

Conclusions: High temporal resolution PC MRI is feasible. Myocardial and trans-mitral velocities obtained by PC MRI strongly correlates with velocities by echo Doppler.

550. Time Continuous Full Cycle Contour Detection in Multi-Slice Multi-Phase Cardiac MR Studies

Mehmet Uzumcu, MSc,[1] Rob J. van der Geest, MSc,[1] Cory Swingen, PhD,[2] Johan H.C. Reiber, PhD,[1] Boudewijn P.F. Lelieveldt, PhD.[1] [1]*Division of Image Processing/Department of Radiology, Leiden University Medical Center, Leiden, The*

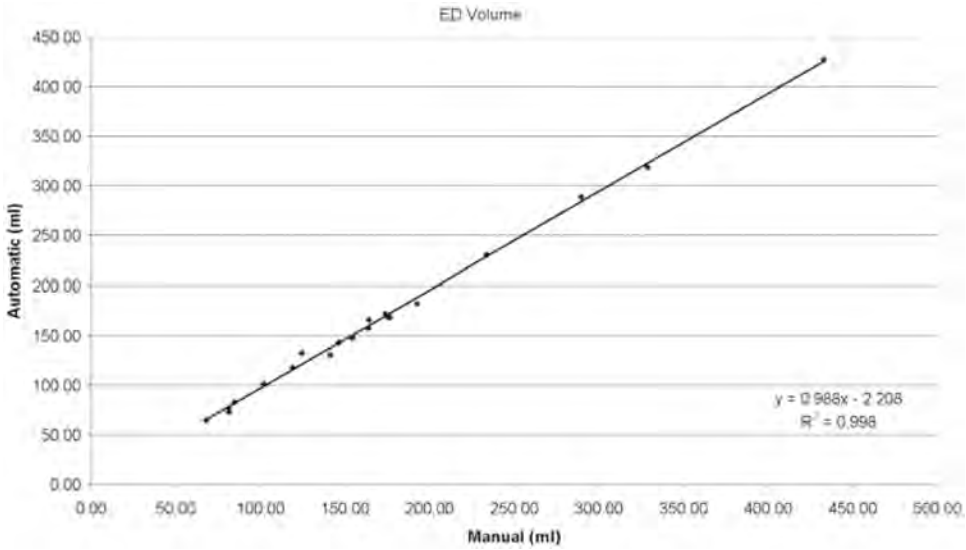

Figure 1.

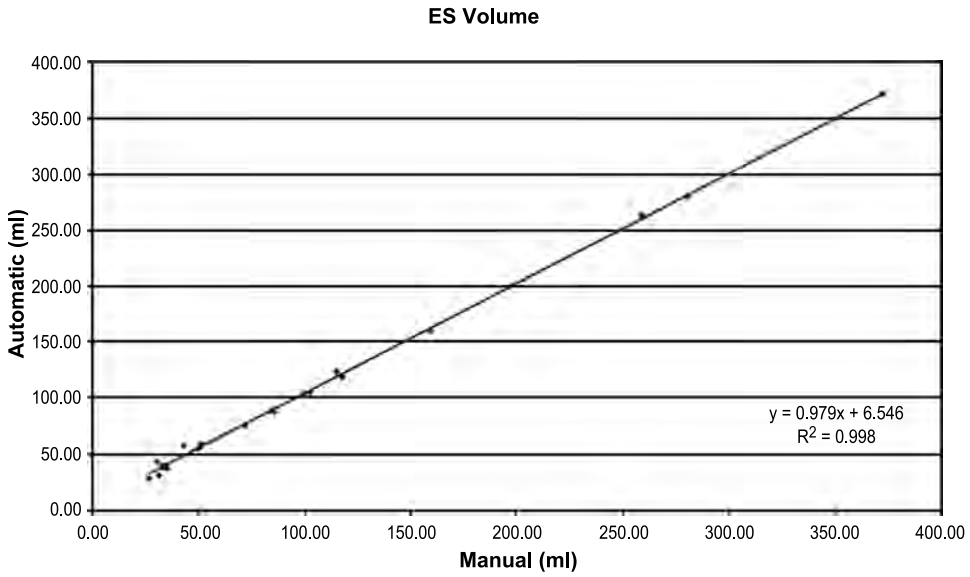

Figure 2.

Netherlands, [2]Department of Radiology, University of Minnesota, Minneapolis, MN, USA.

Introduction: For quantitative analysis of cardiac function, clinical parameters such as ED/ES volume, Ejection Fraction and Wall Motion are relevant. These parameters are usually obtained from short axis acquisitions. However, such a scan easily consists of more than 250 images. In these images endo- and epicardial contours of the cardiac left ventricle are needed to perform quantitative analysis. Many (semi-) automatic methods are available to automatically detect the contours. However, to our knowledge these methods generally do not yield time continuous contours over the full cardiac cycle. Time continuous segmentation of all frames yields more robust and consistent contours in ED and ES frames. Furthermore, other clinically relevant time dependent parameters can be derived this way, such as regional wall motion, rate of wall thickening and peak ejection/filling rate. We propose a semi-automatic method for detecting time continuous endo-and epicardial contours in all phases of the cardiac cycle.

Purpose: Full cycle contour detection in cardiac MR images using dynamic programming.

Methods: Our contour detection is based on dynamic programming. Initialization is performed manually by drawing one epi- and one endo-cardial contour in the mid-systolic phase for each slice level. These contours are resampled to 32 landmarks. In each landmark a mask is

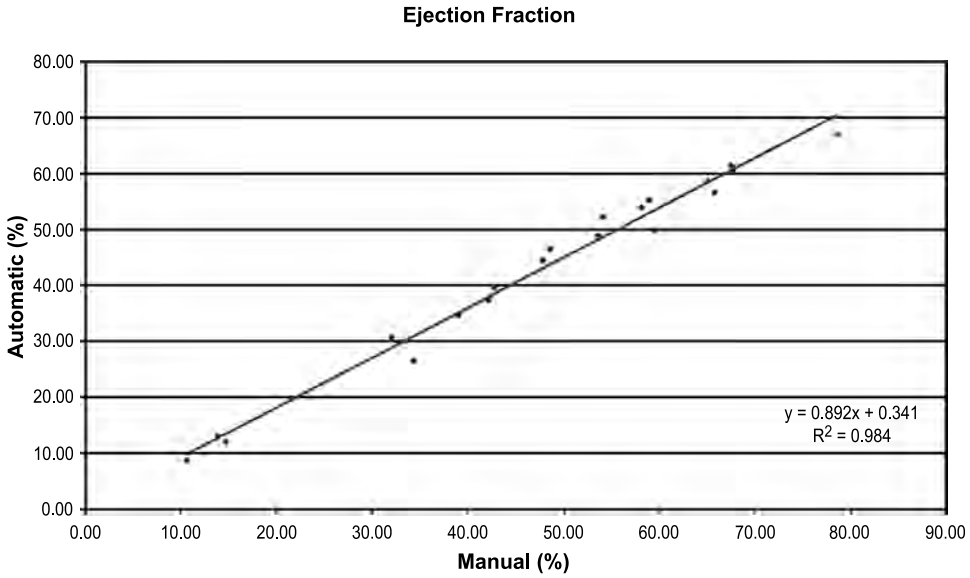

Figure 3.

positioned and a search space of possible mask positions around each landmark is defined. For each allowed position a cross-correlation is calculated between the shifted mask and the mask in the initialization frame. This is repeated for each phase, i.e. for all phases a cost matrix is filled with the correlation values. Per landmark, the cost matrices of all phases are stacked to create a 3D search space. The top and bottom slices of this cube are the cost matrix for the reference frame. The landmarks in the reference frame are fixed and not allowed to change position. Using dynamic programming, an optimal path through the 3D search space is found, yielding time continuous displacements for the landmarks over all phases.

Results: The method was evaluated on MR images of 20 subjects, i.e. 18 patients and 2 normals. Expert drawn epi- and endo-cardial contours were available in all phases and all slices. The following criteria were considered for the evaluation: border positioning error, ED volume, ES volume and Ejection Fraction. The average border positioning error over all slices, all phases and all studies was 1.77 ± 0.57 mm for epicardial contours and 1.86 ± 0.59 mm for endocardial contours. The average error in ED volumes over all studies was 4.24 ± 4.62 ml (average manual ED volume 171.68 ± 91.10) and for ES volumes − 4.36 ± 4.26 ml (average manual ES volume 103.96 ± 95.64). The average error in ejection fraction was 4.82 ± 3.01% on an average manual ejection fraction of 47.73 ± 19.20%. Figures 1–3 show the correlation between volumes and ejection fraction calculated from manually drawn contours and automatically detected contours.

Conclusions: The proposed method yields excellent border positioning errors (± 1 pixel), especially when considering that these are average errors over all slices, all phases and all studies. The ED and ES volumes and ejection fraction show a near perfect correlation ($R^2 > 0.98$). This underlines the potential of our method for obtaining a time continuous full cycle segmentation of the cardiac left ventricle with minimal user interaction.

551. Analysis of Myocardial Motion with Balanced SSFP-Tagging at 3 Tesla: Improved Tag-Fading and SNR at Small Flip Angles

Michael Markl, PhD, Bernd Jung, Jürgen Hennig, PhD. *Department of Diagnostic Radiology, Medical Physics, University Hospital Freiburg, Freiburg, Germany.*

Introduction: Application of SSFP-Tagging (combined SPAMM tagging and balanced CINE SSFP imaging) has proven to be useful for the study of myocardial performance and offers substantial improvement in tag-tissue contrast, tag-persistence and signal-to-noise ratio (*SNR*) when compared with conventional tagging methods. Tag-fading is influenced by tissue specific T_1-relaxation but the inverted longitudinal magnetization of the tags is also driven towards the steady state by repeated rf-excitation. Consequently, the SSFP imaging flip angle can be used to influence tag-persistence and *SNR*. Previous studies at a field strength of 1.5 T have shown that an ideal trade off between tag-persistence and *SNR* can be found at smaller flip angles at the order of 30° (Herzka et al., 2003; Markl et al., 2004).

MR Imaging at 3 T is ideally suited for the application of SSFP-Tagging. In addition to *SNR* improvements, imaging at 3 T offers prolonged T_1-relaxations times in myocardial tissue (867 ms at 1.5 T versus 1115 ms at 3 T, Schär et al., 2004). Thus, reduced tag-fading in combination with the feasibility of imaging at small flip angles to address SAR and resulting flip angle limitations associated with high field imaging is expected.

Materials and Methods: Measurements were performed on 3 T (TRIO, Siemens, Germany) and 1.5 T scanners (SONATA, Siemens, Germany) with equivalent gradient performance (G_{max} = 40 mT, risetime = 200 μs). On both systems, data were acquired using identical k-space segmented 2D balanced CINE SSFP pulse sequences with prospective ECG gating and the following parameters: TE = 1.43 ms, TR = 2.86 ms, BW = 890 Hz/pixel, FOV = (400 × 300)

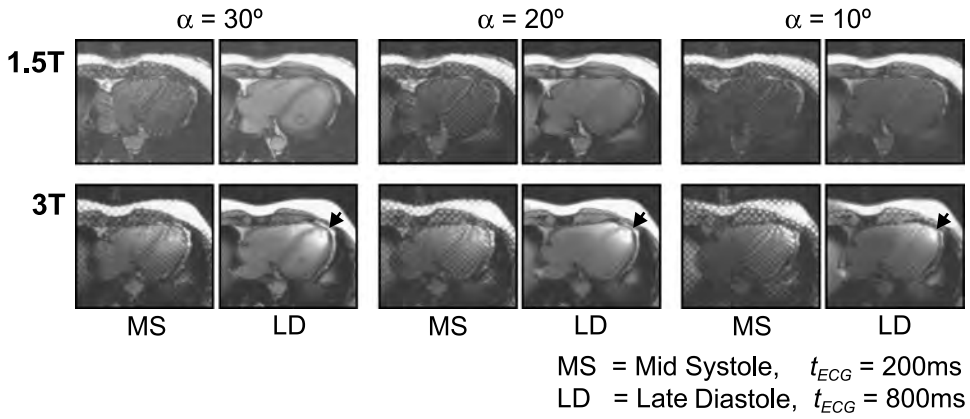

Figure 1.

Table 1. Relative late diastolic non-tagged SNR

	Flip angle = 30°	Flip angle = 20°	Flip angle = 10°
1.5 T	15.3	14.9	11.4
3 T	29.5	28.1	22.8

mm^2, slice thickness = 8 mm, matrix = 256 × 192, 20 time frames, 16 views per segment, temporal resolution = 45.8 ms, total acquisition time = 12 heart beats, and variable flip angles within SAR limits.

Tagging preparation (grid tag, spacing = 8 mm) was performed following R-wave detection and was embedded in a steady state storage scheme ($\alpha/2$ pulses separated from adjacent rf-excitation by TR/2) (Scheffler et al., 2001).

Results: Time resolved SSFP-Tagging images of a healthy volunteer for three different flip angles $\alpha = 10°$, 20° and 30° are shown in Fig. 1 and confirm the superior *SNR* and improved tag persistence of SSFP-Tagging at 3 T (bottom row) compared to 1.5 T (top row).

For both 1.5 T and 3 T, flip angle reduction results in improved tag persistence accompanied by SNR loss. For lower flip angles tags are clearly visibility even in late diastole (t_{ECG} = 800 ms in the RR-interval).

If images for individual flip angles are compared, the expected improvement in *SNR* and resulting increase in tag-tissue contrast is clearly visible in all 3 T images. In addition, 3 T imaging demonstrates improved late diastolic tag visibility along the entire left ventricular wall for all flip angles. Even at a flip angle of 30° tag lines can be identified in the late diastolic image while tags are almost faded for 1.5 T images. Analysis of relative non-tagged left ventricular *SNR* in late diastolic images displayed in Fig. 1 is summarized in Table 1.

Discussion: For SSFP-Tagging at 3 T, the combination of T_1 lengthening and superior *SNR* is highly promising and has the potential to improve the depiction of tagged myocardial function throughout the entire cardiac cycle. While higher flip angles are necessary at 1.5 T to maintain reasonable *SNR* levels, high field SSFP-Tagging can be performed at lower flip angles necessary for decreased tag-fading.

A potential drawback of SSFP-Tagging at 3 T is related to the sensitivity of SSFP imaging to off-resonance effects. Increased field inhomogeneity at 3 T may lead to artifacts such as signal oscillations from imperfect steady state storage or signal variations and/or flow artifacts (e.g., Fig. 1, small black arrows).

REFERENCES

Herzka, D. A., et al. (2003). *Magn. Reson. Med.* 49:329–340.
Markl, M., et al. (2004). *Radiology* 230:845–851.
Schär, M., et al. (2004). *Magn. Reson. Med.* 51:799–806.
Scheffler, K., et al. (2001). *Magn. Reson. Med.* 45:1075–1080.

552. Real Time Color Flow Imaging for Assessing Carotid Stenosis

Ajit Shankaranarayanan. *Applied Science Laboratory, GE Healthcare, Menlo Park, CA, USA.*

Introduction: The benefits of carotid endartrectomy are directly related to the degree of the existing stenosis. Because of the irregularity of carotid stenosis, the percentage narrowing is usually estimated based on velocity ratio of the unaffected to the affected vascular segments. Standard magnetic resonance angiography of the carotids also suffers from overestimation of the degree of stenosis.

We have developed a multi-coil, dynamic real-time color flow system that is capable of measuring the flow velocity of the carotid arteries in real-time. This allows a rapid screening of both carotids in their entirety along with the physiologic information in less than 10 minutes. We validated the velocity measurements up to 3 m/s and demonstrated its performance in normal volunteers.

Methods: The real-time multi-coil color flow system is implemented on a GE 1.5 Signa Twinspeed system (GE Medical Systems, Milwaukee, WI) with EXCITE technology running optimized sliding-window, gridding reconstruction software (Shankaranarayanan et al., 2003).

The current implementation of the real-time magnetic resonance flow imaging sequence utilizes a spiral acquisition. However, the infrastructure can be easily combined with other imaging trajectories. The imaging parameters common to all acquisition modes include a short 480 us sinc excitation pulse, 8 ms readout, 5 mm slice thickness, 30° flip angle. The minimum TR achieved was around 10 ms and minimum TE

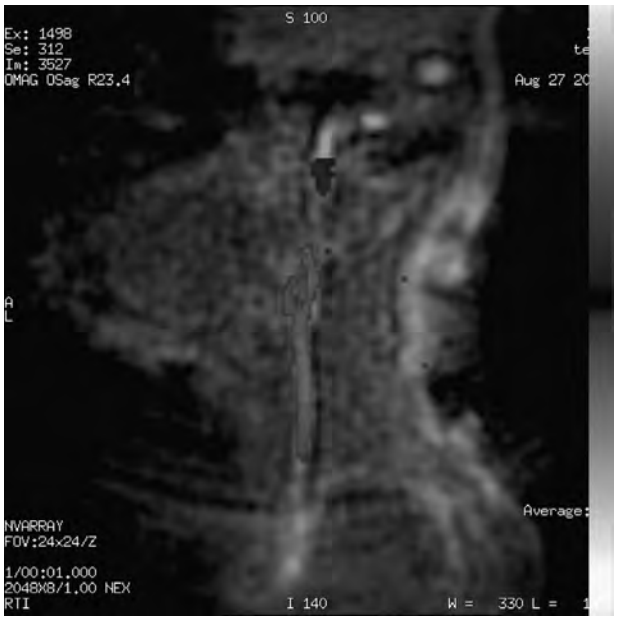

Figure 1. Longitudinal images of the carotid birufcation. Note that the bifurcation clearly depicted.

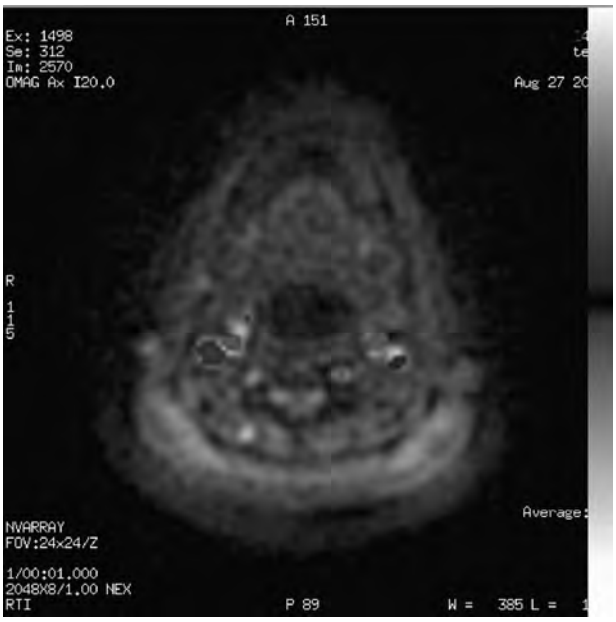

Figure 2. Axial image of the carotid arteries at a specific location.

was 1.5 ms for a maximum velocity encoding (venc) of 3 m/sec. Contextual information including slice location, prescan parameters, and shim values is automatically shared between the real time localization and color flow modes. The method described in Bernstein et al. (1994) was used to combine the phase images from the multi coil data set. A frame rate of 15 frames/sec for the color over-layed images was achieved using sliding window reconstruction. The user was able to adjust the scan plane and FOV during the acquisition of real-time color flow images, thus improving the efficiency of the study. A neurovascular phased array coil was used for signal reception. This ensured us the coverage of the entire carotids.

Results: Figure 1 shows coronal images of the carotid bifurcation acquired in real time. Figure 2 shows the axial views of the carotid arteries. This application allowed us to examine both the carotids in entirety in as little as 8 minutes.

Conclusion: Real-time flow velocity measurements can be used to rapidly quantify the degree of carotid stenosis without the limitation of ultrasound. Further clinical studies are needed to validate the impact of this technique.

REFERENCES

Bernstein, A., et al. (1994). *MRM*:330–334.
Shankaranarayanan, A., et al. (2003). *SCMR*:294–296.

553. Left Ventricular Morphology, Global and Longitudinal Function in Normal Elderly Individuals: a Cardiac Magnetic Resonance Study

Nikolay P. Nikitin, MD, PhD, Ramesh de Silva, MRCP, Poay Huan Loh, MRCP, Elena I. Lukaschuk, MSc, Lee Ingle, PhD, Anita Dunn, Alan Farnsworth, MD, Farqad Alamgir, MRCP, Andrew L. Clark, MA, MD, FRCP, John G. F. Cleland, MD, FRCP, FACC. *Academic Unit of Cardiology, University of Hull, Hull, UK.*

Introduction: The heart transforms structurally and functionally with age but the nature and magnitude of reported changes appear inconsistent. This study was designed to assess left ventricular (LV) morphology, global and longitudinal function in healthy elderly men and women using cardiac magnetic resonance (CMR).

Methods: 95 healthy subjects (age 62 ± 16 years, range 22 to 91 years) underwent breath-hold cine CMR. LV end-diastolic volume (EDV), end-systolic volume (ESV), myocardial mass, ejection fraction (EF), mass-to-volume ratio, mean midventricular wall motion, thickness and thickening were calculated from short-axis data sets. Average mitral annular displacement was measured to assess longitudinal LV function.

Results: Subjects were divided according to age (< 65 and ≥ 65 years) and sex. EDV and ESV indices (corrected for body surface area) decreased whilst EF increased with age. There was no difference in LV myocardial mass index between the age groups, but midventricular wall thickness was significantly higher in elderly people. Mass-to-volume ratio also increased with age. In contrast to EF, mitral annular displacement declined with age. Midventricular LV wall thickness, myocardial mass index and mass-to-volume ratio were higher in men than in women but there were no differences in measures of global and longitudinal LV systolic function.

Conclusions: Due to smaller LV volumes but higher wall thickness, myocardial mass remains unchanged with age. The age-related increase in EF and deterioration of longitudinal LV function may be essential when assessing elderly patients with heart failure and preserved LV systolic function. Men have higher myocardial mass then women due to thicker LV walls.

554. zHARP: Direct Three-Dimensional Motion Quantification in Myocardial Tagging

Khaled Z. Abd-Elmoniem,[1] Nael F. Osman, PhD,[2] Jerry L. Prince, PhD,[1] Matthias Stuber, PhD.[2] [1]*Electrical and Computer Engineering, Johns Hopkins University, Baltimore, MD, USA,* [2]*Radiology Department, Johns Hopkins University, Baltimore, MD, USA.*

Introduction: MRI is a powerful tool for the quantification of myocardial regional function in healthy and diseased states. Displacement encoding (Pelc, 1995), and velocity encoding, e.g. phase contrast (PC) (Aletras, 1999) techniques require the acquisition of two or more datasets for the computation of the three dimensional displacement or velocity information. Therefore, these methods suffer from long acquisition times

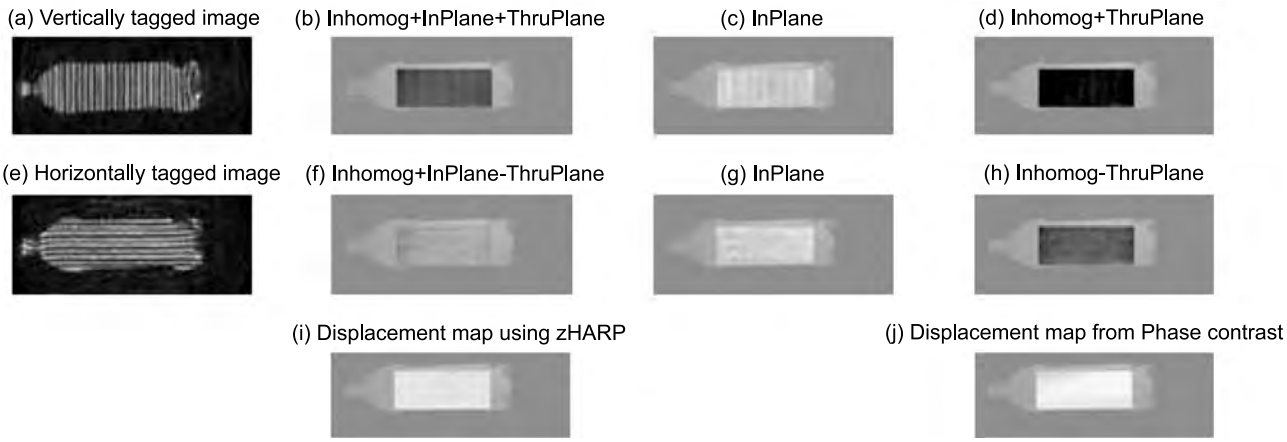

Figure 1. Algorithm steps applied to a water-filled bottle phantom. Results are shown in a rectangular ROI in the center of the bottle. Processing of the vertical and horizontal tag CSPAMM images in the 1st and 2nd rows, respectively. (a and e) Original data. (b and f) Harmonic phase of the CSPAMM images showing the phase contribution from the three components (Inhomogeneity, in-plane and through-plane displacement). (c and g) Harmonic phase of the |CSPAMM| images showing the in-plane displacement component. (d and h) are the subtraction (b−c) and (f−g), respectively. (i) Subtraction of (d−h); the through-plane displacement map using zHARP. (j) The through-plane displacement using the integration of the phase contrast image.

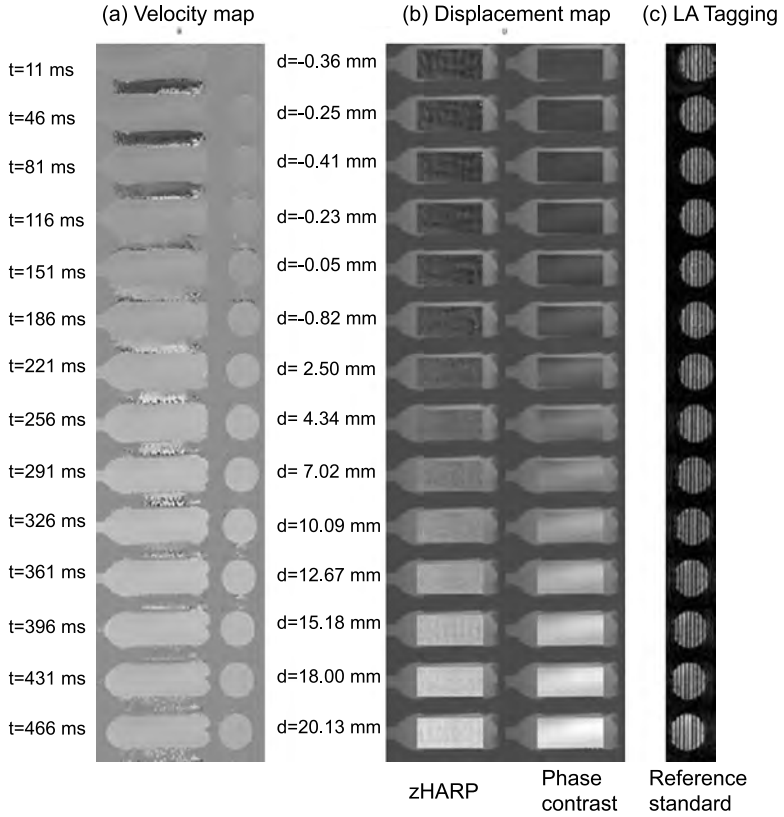

Figure 2. Displacement maps through the 14 CINE images. t: time, d: displacement. (a) Phase-contrast velocity maps in short-axis slices (left) and long-axis slices (eight). (b) Displacement maps using zHARP (left) and using phase contrast (right). (c) Reference standard dataset; tagged long axis slices that used for displacement calculations using cross correlation.

and sensitivity to misregistration. HARP is a fast automatic algorithm for tracking myocardial in-plane displacement and strain from MRI tagged datasets (Osman, 2000). However it only computes the apparent motion projected on the acquired plane.

Purpose: To design a pulse sequence that encodes both in-plane and through plane displacement information without sacrificing the acquisition speed. In addition, an automatic algorithm is proposed to directly track the 3-D displacement information from the acquired data. First results demonstrating the ability to directly extract trough-plane displacement from CSPAMM tagged images are presented.

Methods: Concept: The proposed technique (zHARP), is similar to the standard slice-following CSPAMM (SF-CSPAMM) (Fischer, 1994), except that during the imaging sequence, a small z-encoding gradient is applied immediately before the readout and again with opposite polarity to the second orthogonal CSPAMM acquisition. This gradient adds a z-position dependent phase to every material point in the acquired slice. This additional phase is linearly related to the distance of the point from the iso-center.

The algorithm runs on the two orthogonally tagged datasets. First, magnitude images are processed using HARP extracting the in-plane displacement. Second, HARP processing of the complex images yields a phase image that includes both the in-plane displacement and the phase originating from the distance to the iso-center. Unfortunately, susceptibility and general field inhomogeneities lead to an additional and artifactual phase accumulation. However, this erroneous phase is identical in both the horizontally and vertically tagged images. Therefore, the phase induced by in-plane displacement, and imperfections can be separated while the phase originating from through-plane motion can be isolated, see system of equations below

$$\phi^{\text{Vert.Tag}}_{\text{CSPAMM}} = \phi_{\text{Inhomogeniety}} + \phi^{\text{x-direction}}_{\text{InPlane}} + \phi^{\text{z-direction}}_{\text{Thru-Plane}}$$

$$\phi^{\text{Horz.Tag}}_{\text{CSPAMM}} = \phi_{\text{Inhomogeniety}} + \phi^{\text{y-direction}}_{\text{InPlane}} - \phi^{\text{z-direction}}_{\text{Thru-Plane}}$$

$$\phi^{\text{Vert.Tag}}_{|\text{CSPAMM}|} = \phi^{\text{x-direction}}_{\text{InPlane}}$$

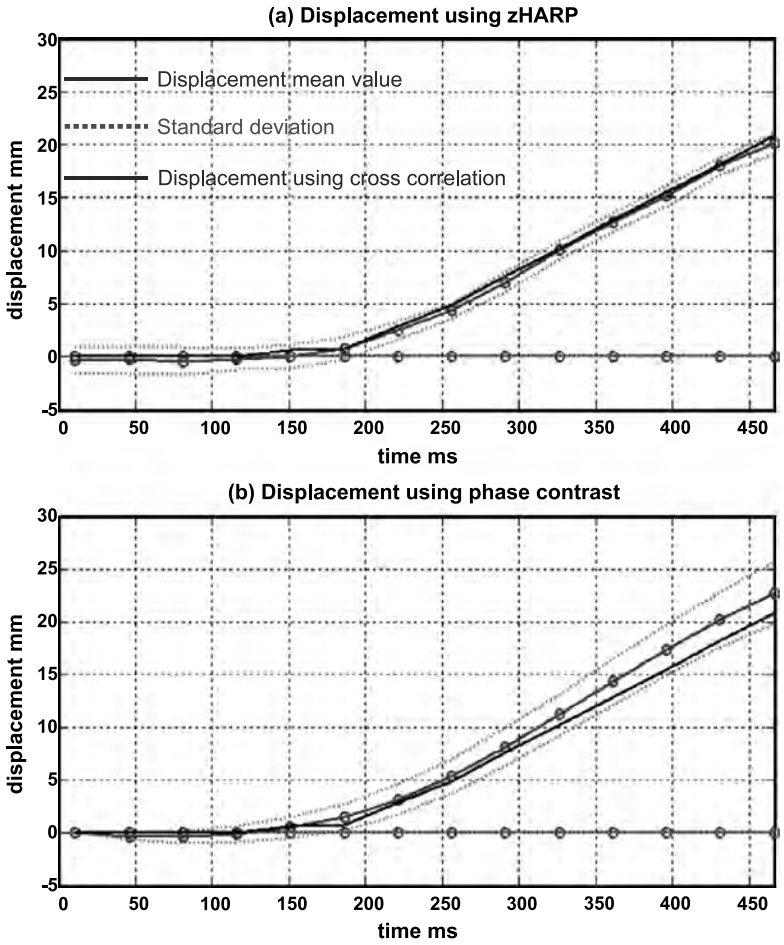

Figure 3. The displacement profile in the first 460 ms of the cycle. (a) Using zHARP. (b) Using phase contrast (PC). Notice the increasing standard deviation and the accumulation of error in PC and the deviation from the cross correlation values.

$$\phi^{\text{Horz.Tag}}_{|\text{CSPAMM}|} = \phi^{\text{y-direction}}_{\text{InPlane}}$$

Implementation: The pulse sequence was implemented on a Philips 3 T-Intera system. Image processing was performed off-line on a personal computer.

The pulse sequence and the algorithm were tested in a moving phantom experiment. The phantom was moving sinusoidally in parallel to the main magnetic field at a rate of 52 rpm. Fourteen cardiac phases were acquired during the first 466 ms of each cycle. Figure 1 shows the processing steps applied to the 14th frame and how through-plane and in-plane displacements were extracted.

For comparison, the phantom was also imaged using a conventional PC method, displacement was obtained thereafter by integration, Fig. 2-a. As a reference standard, displacement was also computed using cross correlation method (CC) applied to long-axis (LA) tagged dataset, Fig. 2-c.

Results: Figure 2-b visualizes the displacement maps over the dataset. Figure 3 compares the mean displacement value and the standard deviation obtained from PC, zHARP, and CC. Due to the integration and higher order motion terms, the accumulation of errors is dominant in the PC results. In comparison, direct displacement measures using zHARP had a consistent standard deviation throughout the entire cycle. Relative RMS error between PC and CC was 10.7% and between zHARP and CC was only 4.0% indicating good agreement of zHARP with the reference standard.

Conclusions: The proposed zHARP methodology supports the 3D quantification of myocardial motion by combining slice-following CSPAMM myocardial tagging and HARP. Hereby, an extra signal phase representing the position in the 3rd dimension is added to each material point. When compared to conventional PC method, no extra scanning time is needed and integration of the displacement over time is avoided, which adds to the robustness of the technique.

REFERENCES

Aletras (1999). *JMR*.
Fischer (1994). *MRM*.
Osman (2000). TMI.
Pelc (1995). *JMRI*.

555. Detection of Thrombus in the Left Atrial Appendage Using Contrast-Enhanced MRI

Oliver K. Mohrs,[1] Steffen E. Petersen,[2] Bernd Nowak,[1] Matthias Welsner,[1] Annett Magedanz,[1] Hans-Ulrich Kauczor,[3] Thomas Voigtlaender.[1] [1]*Department of MRI, Cardiovascular Center Bethanien, Frankfurt/Main, Germany,* [2]*University of Oxford Centre for Clinical MR Research, Oxford, UK,* [3]*Deutsches Krebsforschungszentrum DKFZ, Heidelberg, Germany.*

Introduction: The identification of left atrial thrombi is a critical and common clinical problem. Left atrial thombus is a frequent cause of cerebral stroke or peripheral embolism and anticoagulation is required to prevent further cerebral events. Furthermore, the exclusion of atrial thrombus is crucial before the conversion of atrial fibrillation into sinus rhythm to avoid embolisation. The main location for left atrial thrombus formation is the left atrial appendage possibly related to the phenomenon of atrial stunning. Diagnosis of a thrombus in the left atrial appendage could be challenging based on the complex anatomy with variable configuration of lobes and branches.

Purpose: Transesophageal echocardiography (TEE), the clinical reference, is semi-invasive and we thus aimed to assess the value of contrast-enhanced cardiovascular magnetic resonance (CMR) for detection of thrombus in the left atrial appendage.

Methods: A total of 25 patients with (19) and without (6) thrombi in the left atrial appendage as determined by TEE underwent two contrast-enhanced (Gadolinium-DTPA) CMR sequences (2D TrueFISP perfusion and 3D TurboFLASH). CMR data was analyzed by consensus of two blinded experienced observers for image quality (from grade 1 being not assessable to grade 5 being excellent), location, shape, and size thrombus.

Results: The image quality was good for both, 2D perfusion (grade 4 ± 1) and 3D TurboFlash (grade 4 ± 1). 2D perfusion, 3D TurboFlash and the combination of both techniques yielded sensitivities of 47/35/44%, specificities of 50/67/67%, positive predictive values of 73/75/80% and negative predictive values of 25/27/29%, respectively. The size of the thrombus was overestimated by 2D perfusion (66%) and by 3D TurboFlash (25%) and agreement for location and shape of thrombus was 88% and 50% for 2D perfusion and 50% and 83% for 3D TurboFlash, respectively. The thrombus size was significantly smaller in patients with false negative diagnoses by 2D perfusion (148%) and by 3D TurboFlash (151%) when compared to patients with true positive diagnoses ($p < 0.05$ for both). No such difference was found for image quality, time delay between TEE and CMR examination, location and shape of thrombi.

Conclusions: Contrast-enhanced CMR lacks diagnostic accuracy for the detection of thrombi in the left atrial appendage. Future technical improvements may help to establish this technique as a non-invasive alternative to TEE in the future.

556. Intramyocardial Lipid, 3D Structure and Function Measurement by Conventional 1.5 T Cardiac Magnetic Resonance Imaging in the Rat Heart; Is It Now Possible?

Hakki Bolukoglu, MD, June Yamrozik, Diane A. Vido, Ronald B. Williams, Teresa Hentosz, Richard P. Shannon, MD, Mark Doyle, PhD, Robert W. W. Biederman, MD. *Allegheny General Hospital, Pittsburgh, PA, USA.*

Introduction: Clinical whole body systems are widely available but, to date, their utility in performing detailed cardiac measurements in the rodent has not been assessed, particularly to image intramyocardial lipids. To date, there is substantial discord between the elegance of animal genomic models and the current echocardiographic ability to image them, typically limiting current measurements to 1D while necessitating a large 'n' due to the high variability required to achieve desired power.

Hypothesis: We hypothesize that a standard, non-modified, clinical 1.5 T cardiac MRI system could be used to assess LV function, mass and detect intramyocardial lipids in rodents.

Methods: A clinical 1.5 T GE CV/i scanner was used to image 6 Sprague-Dawley (NL, 20 wks), 10 spontaneously hypertensive heart failure (SHHF, 17 wks) and 9 Zucker Obese (Z, 17 wks) rats. EKG gated images were acquired using a quad knee coil with a gradient echo sequence: FOV 120^2 mm, matrix 256^2, 4 NEX, in 3D short axis. LV mass, volume and EF were calculated from 2 mm slices (10–12) with no gap. Lipid measurements were done using cine in/out phase images (Dixon method).

Results: High fidelity cine images (470^2 μ in-plane, 0.94 mm^3 voxel and 11 ms temporal resolution) were acquired at mean HR of 351 ± 45, (range 276–408 BPM). Significance difference was noted between NL, SHHF and Z for body weight (BW) (482 ± 55, 528 ± 48 and 678 ± 80 g, respectively, $p < 0.001$), EF (69.7 ± 6.3, 70.2 ± 5, 75.9 ± 5%, respectively, $p = 0.047$ between NL or SHHF vs. Z), and EDV was significantly different among groups (0.000844, 0.000783 and 0.000627 ml/g, respectively, $p = 0.002$). LV mass significantly increased across groups (0.62 ± 0.098, 0.71 ± 0.083, 0.76 ± 0.079 g, respectively, $p = 0.013$ for all), and intramyocardial lipid signal was different between NL or SHHF rats vs. Z (31 ± 28, 34 ± 40, 11 ± 30, respectively, $p < 0.05$)

Conclusion: Rodent heart imaging is possible using a standard clinical cardiac 1.5 T MRI scanner with conventional software and hardware at high heart rates (> 400 BPM) using an order of magnitude fewer subjects than typical by echocardiography. LV metrics, including EDV, EF and mass, are measurable in 3D. Importantly, differences between intramyocardial lipid levels were detectable between groups and demonstrate subtle, probably early accumulations prior to onset of CHF but manifested in LVH. Future translational application to lipid imaging in humans, previously not achievable, may now be possible.

557. Hardware-Dependent Sequence Optimization and Normal Values for Early Myocardial Contrast Enhancement

Petra Bock,[1] Hassan Abdel-Aty,[1] Stefan Dahm,[2] Andreas Greiser,[3] Philipp Boyé,[1] Andreas Kumar,[1] Ralf Wassmuth,[1] Rainer Dietz,[1] Matthias G. Friedrich,[4] Jeanette Schulz-Menger.[1] [1]*Cardiology, Franz-Volhard-Klinik, Helios-Klinikum, Charité Campus Buch, Universitätsmedizin Berlin, Berlin, Germany,* [2]*Department of Bioinformatics, Max Delbrück Center for Molecular Medicine, Berlin, Germany,* [3]*MR Application Development, Siemens AG Medical Solutions, Erlangen, Germany,* [4]*Cardiac Sciences, University of Calgary, Foothills Hospital, Calgary, AB, Canada.*

Background: Early contrast accumulation as defined by global relative enhancement (gRE) as opposed to delayed enhancement of the myocardium has been shown to be a reliable parameter for identification of acute myocarditis. Normal values for clinical application heavily depend on scanner hardware and the sequence used. For a new scanner setting we optimized a preexisting sequence and obtained normal values in healthy volunteers.

Purpose: We aimed at establishing an optimized T1-weighted turbo spin-echo sequence covering the first minutes after contrast-application and a database for definition of normal values of gRE. Such data could also be used as a reference guideline for centers with a similar scanner, when applying the same sequence.

Methods: We investigated 48 healthy volunteers including 21 males (37 ± 10 years) and 27 females (41 ± 13 years) on a 1.5 T MRI system (Sonata, Siemens, Germany) using the body coil for transmission and signal reception.

Before and immediately after an intravenous bolus of 0.1 mmol/kg Gd-DTPA (Magnevist, Schering AG) ECG-triggered T1 multislice turbo spin-echo imaging was performed in axial orientation (FOV: 284 × 350, matrix 208 × 512; 3 slices, slice thickness 8 mm spacing 4 mm, TR 278 ms, TE 14 ms; $\alpha = 160°$; bandwidth 110, nested multislice mode, turbo factor 5, 100% phase over sampling, mean acquisition time 4 ± 0.5 min, 5 averages) with identical parameters. By a suitable trigger delay, the acquisition window was positioned in end-diastole. In addition to parallel sat bands, we positioned a saturation band across the atria and the aorta to reduce the signal from slow-flowing blood in the left ventricle, which may influence signal intensity in the myocardium, especially after application of Gd-DTPA.

For calculation of global enhancement myocardial regions of interest were manually traced in the pre contrast image-set and copied in the post-contrast one using scanner-related analysis-software. In the same way skeletal muscle regions of interest in the same slice (Latissimus dorsi or Serratus anterior) were selected. Enhancement was calculated as the difference of signal before and after contrast divided by the signal before. gRE was calculated as a ratio of myocardial and skeletal muscle enhancement. The upper value of normal for a one-sided test was defined as gRE mean value + 1.68 × standard deviation.

Results: Image quality was sufficient for analysis in all cases. gRE ranged from 1.4 to 6.4 with mean 3.1 ± 1.1; leading to an upper value of normal of 4.95.

gRE showed no significant dependence to gender (males 3.4 ± 1.1; females 2.9 ± 1.1; t-test $p = 0.09$) or age ($p = 0.21$). The absolute myocardial enhancement was 48% ± 10% while the absolute skeletal muscle enhancement was 17% ± 5%.

Conclusion: We described an optimized sequence and provided normal values for gRE in a specific scanner setting. Using similar hardware and software conditions, these data could be used as a reference guideline for image acquisition and analysis of gRE as part of the diagnostic work-up of myocarditis patients. Standardization of the imaging procedures will facilitate CMR multi-center trials in acute myocarditis.

558. Automatic Contour Detection in Short-Axis Cardiac Cine MR Data

Gilion L.T.F. Hautvast,[1] Steven Lobregt,[2] Marcel Breeuwer,[2] Anna Vilanova,[1] Frans A. Gerritsen.[1] [1]*Biomedical Engineering, Technische Universiteit Eindhoven, Eindhoven, The Netherlands,* [2]*Medical IT-Advanced Development, Philips Medical Systems, Best, The Netherlands.*

Introduction: Short-axis cine cardiac MRI acquisitions usually consist of 15–25 phases at 10–15 slices (150–375 images) that are approximately perpendicular to the long axis of the heart. Segmentation of left ventricle, right ventricle and myocardium is required for quantification and diagnosis of the cardiac function (Fig. 1a). Current automatic segmentation methods usually ignore anatomical knowledge and already defined contours in adjacent images. Besides this, currently applied methods do not provide adequate contours in the presence of papillary muscles or trabeculae, requiring elaborate interaction of a skilled user.

Purpose: The purpose of our work was to develop and optimize an improved Active-Contour based segmentation method, which will provide correct contours also in areas where papillaries or trabeculae are present. User interaction is reduced to drawing only one initial contour, which is automatically propagated throughout the data set, resulting in a complete set of contours. During propagation, the 'drawing style' of the initial contour is imitated. As a result, the generated contours reflect the user's preferences (e.g., inclusion or exclusion of the papillary muscles).

Methods: The starting point for the new method was our existing Active Contour algorithm. The new algorithm optimizes the contour locally based on the matching of grayvalue profiles perpendicular to the contour path (Fig. 1b). The contour is propagated by repositioning a contour in neighboring phases in order to optimize the match between the grayvalue profiles. Consequently, the 'initial behaviour' of the contour is copied, until each phase in the dataset is segmented.

The result of contour propagation depends on a number of parameters such as resolution along the contour and the profiles, length of the profiles, and the number of steps in the iterative deformation process. The optimal parameter configuration was determined in an extensive search of the parameter space, including 4400 parameter configurations. Proper definition of a positioning error allowed Analysis of Variances to be used to determine main effects and interactions of the parameters. Ultimately, an optimal parameter configuration was concluded.

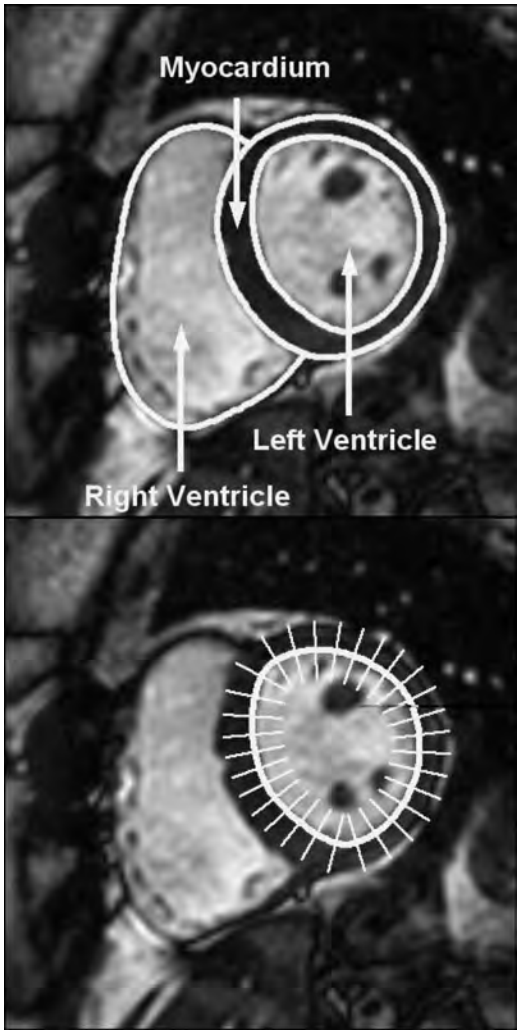

Figure 1. a) The anatom!ical structures of interest and related contours; b) Perpendicular orientation of grayvalue profiles for the LV endocardium contour.

The method was optimized and technically validated using 300 short axis ECG-triggered cine cardiac MR images, obtained in 4 acquisitions containing 25 phases in three slices which were imaged with slice thickness 8.0–10.0 mm, FOV 350 × 350 mm–410 × 410 mm; image size 256 × 256; flip angle 60°; TE 1.5–.6 ms; TR 3.1–3.2 ms. We are grateful to Eike Nagel of the Deutsches Herzzentrum, Berlin, for supplying image data.

Results: After optimization, the average border positioning RMS error observed throughout a complete heart cycle was 1.2 ± 0.48 mm for the LV endocardium contour, 0.88 ± 0.39 mm for the LV epicardium contour and 1.1 ± 0.55 mm for the RV endocardium contour, which is well below the values reported for other semi-automatic methods and within inter-user-variability of the manual segmentations. The algorithm segments the three cardiac

contours in all images of one slice of a dataset with 25 phases within 1.5 seconds, allowing complete segmentation including manual initiation within a minute, compared to the 60 minutes needed for manual segmentation. In an ongoing, more extensive clinical validation on a large number of patients, the algorithm proved to be robust towards the significant variation in image quality present in these datasets.

Conclusions: The presented algorithm for automatic propagation of cardiac contours demonstrated to be a robust and accurate method for the delineation of the LV endocardium, LV epicardium and RV endocardium contours. Additionally, the analysis time is reduced significantly.

559. Investigation of Cardiac Diseases in Conscious Animals Using Single-Shot FSE NMR Imaging: Preliminary Results

Elodie Parzy, PhD,[1] Yves Fromes, MD, PhD,[2] Jean-Michel Franconi, PhD,[3] Pierre G. Carlier, MD, PhD.[1] [1]*NMR Laboratory, AFM CEA, Institute of Myology, Paris, France,* [2]*INSERM U582, Paris, France,* [3]*RMSB U5536, Bordeaux, France.*

Introduction: Anaesthesia offsets part of the benefit of studying tissue function and/or metabolism non-invasively by NMR. Running NMR imaging protocols in conscious animals is an attractive alternative option. However, circumventing anesthetics is particularly challenging for cardiac imaging in small animals. In a feasibility study, we have previously shown that cardiac NMR imaging is possible in normal awaken hamsters.

Purpose: The goal of this study was to determine whether some degree of disease characterization was achievable with ultra-fast cardiac NMR imaging performed in conscious animals.

Methods: Conscious hamsters were slipped into a 4.6 cm diameter cylinder, with the neck and legs immobilized. Half-Fourier single-shot FSE imaging, with outer volume suppression to improve spatial resolution and with a double, selective and non-selective, inversion module to reinforce black-blood contrast provided motion artefact-free images and an excellent visualization of cardiac anatomy. Series of double oblique views were acquired with or without ECG gating. Image acquisition time was 53 ms, with an in-plane resolution of $470^{*}625$ μm^2. The ability of this protocol to detect alterations in cardiac anatomy and function and in myocardium texture was assessed in two pathological models. Cardiomyopathic hamsters and hamsters with LAD coronary ligation were compared to control animals.

Results: In cardiomyopathic hamsters (CM), left ventricular dilatation (short axis diastolic mid-ventricular area: CM: 53.0 ± 2.4 mm^2 vs. ctrls: 29.1 ± 5.3 mm^2; $p = 0.006$) and abnormal ejection fraction (CM: $37 \pm 7\%$ vs. ctrls: $83 \pm 4\%$; $p = 0.002$) were demonstrated. Confirming previous findings in anaesthetized animals, the NMR signal distribution was more heterogeneous in the myocardial wall of cardiomyopathic hamsters than in controls (2.21 ± 0.15 a.u. vs. 0.94 ± 0.16 a.u.; $p = 0.0006$ at TEeff = 45 ms).

After LAD coronary ligation, the course of infarct and scar formation was monitored during the next 3 weeks. Oedema-related myocardial signal intensity changes were detected on T2-weighed images at the acute phase. Segmental dysfunction was evidenced throughout the period of observation.

Conclusion: This study demonstrates for the first time that characteristic features of cardiac pathologies can be evaluated with ultra-fast NMR imaging in conscious rodents.

560. Real-Time Ex-Vivo Visualization of Cardiac Cryoablation Lesions

Girish Narayan, MD,[1] Juan Santos, PhD,[2] Sonal Josan, PhD,[1] Paul Wang, MD,[1] John Pauly, PhD,[2] Kim Butts, PhD,[3] Michael McConnell, MD.[1] [1]*Cardiology, Stanford University, Palo Alto, CA, USA,* [2]*Electrical Engineering, Stanford University, Palo Alto, CA, USA,* [3]*Radiology, Stanford University, Palo Alto, CA, USA.*

Introduction: Real-time guidance and visualization of cardiac ablation will improve the safety and efficacy of electrophysiologic procedures. MRI offers high quality anatomic delineation as well as post-ablation tissue characterization. Previous work has not demonstrated true real-time assessment during cardiac lesion formation using MRI. Given the unique MR appearance of frozen tissue and the increased use of cryoablation in electrophysiology, we imaged cardiac cryoablation in the MR environment.

Methods: MR imaging of cyroablation lesions was performed in a 0.5 T hybrid X-Ray/MR Interventional scanner (GE Medical Systems, Inc.). Both conventional Spin Echo (SE) (TE/TR 11/300 ms) and Real-time (RT) spiral

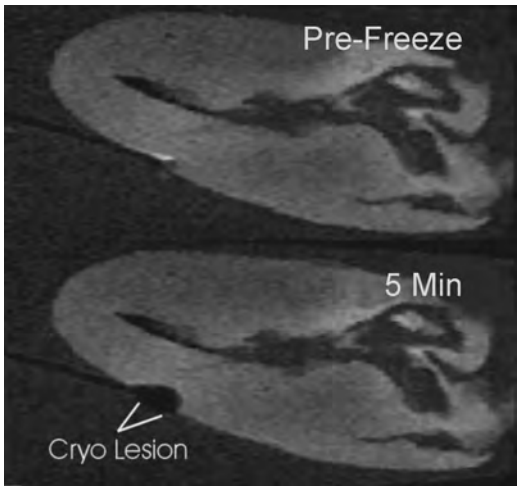

Figure 1.

imaging (resolution: 2.9 × 2.9 mm spatial, 400 ms temporal) was performed repetitively over the 5 min. duration of lesion formation in ex-vivo porcine myocardium using a MR safe cyroablation catheter. Photographs of lesions at the end of the freeze cycle were compared to SE images (n = 10 lesions, 4 hearts) for size comparison.

Results: RT imaging at 0.5 T demonstrated cryo lesion formation. However, catheter related artifacts prevented quantitative assessment of lesion volume. Lesions were clearly demarcated on the SE images (see Fig. 1). There was close correlation of measured lesion size by direct visualization vs. SE images (r = 0.75 for length, r = 0.70 for depth).

Conclusion: RT MR visualization of catheter tip position and lesion formation can be performed during cryoablation. SE techniques allow quantitation of cyrolesion size.

561. Atrial Function by Velocity Encoded-Magnetic Resonance Imaging

John F. Heitner, MD, Igor Klem, MD, Burkhard Sievers, MD, Jonathan W. Weinsaft, MD, Manesh Patel, MD, Anna Lisa Crowley, MD, Peter J. Cawley, MD, Michele Parker, MS, Robert M. Judd, PhD, Michael Elliott, MD, Raymond J. Kim, MD, Joseph C. Greenfield, Jr., MD. *Duke University, Durham, NC, USA.*

Introduction: Atrial function is an important parameter in cardiac hemodynamics contributing to both left ventricular (LV) function and thrombus formation. Velocity encoded magnetic resonance imaging (Ve-MRI) is a technique that can accurately determine blood volume through the mitral valve during diastole, thus be able to measure atrial function.

Purpose: 1) To assess the feasibility of using ve-MRI to determine atrial function in a select patient population. 2) To assess the variability of atrial function in a select patient population. 3) To assess the association of atrial function with other cardiac parameters (LV function and size, left atrial size, RR and PR intervals).

Methods: We evaluated the atrial function in 39 patients by obtaining 2 perpendicular in-plane ve-MRI images through the mitral valve. We then obtained a through plane ve-MRI image through the annulus of the mitral valve off these 2 in-plane images. Blood volume with respect to time was quantified using Argus analysis (Siemens) (Fig. 1). Atrial function is defined by the diastolic blood flow during the A wave divided by the total diastolic blood flow × 100.

Results: The atrial function was obtained in all 39 patients, mean age 56. The average ejection fraction was 58%Ã'Â± 11%, Two patients with atrial fibrillation acted as controls and were confirmed to have 0% atrial function. There was a wide range of variability (0%–51%) in atrial function. Four patients demonstrated no evidence of atrial mechanical

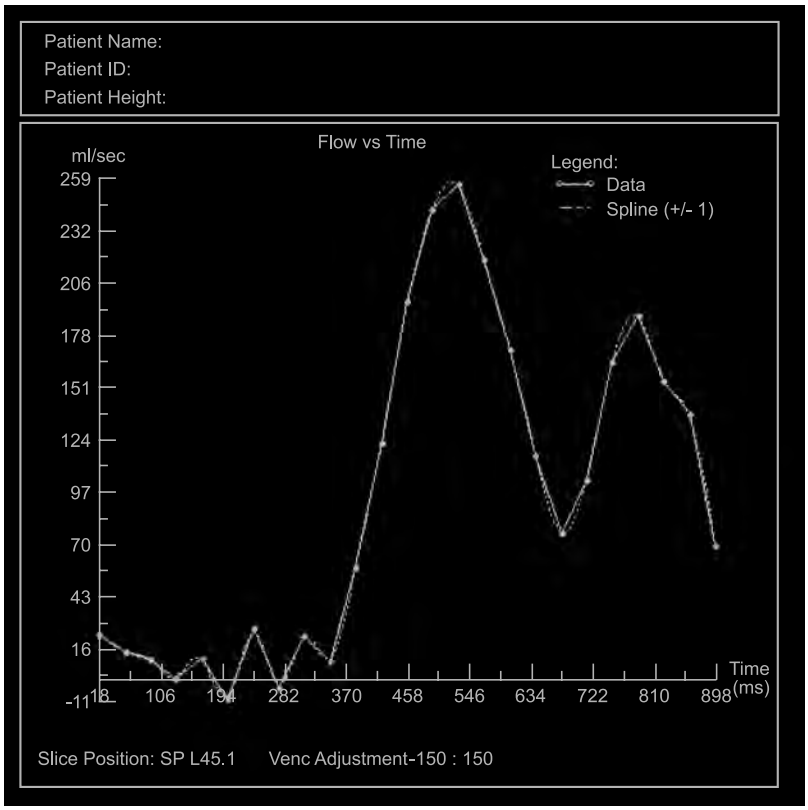

Figure 1.

function despite having normal sinus rhythm on ECG and no history of atrial arrythmias. There was a significant correlation between decrease atrial function and decrease LV systolic function ($p = 0.011$) and enlarged LV end systolic diameter ($p - 0.017$).

Conclusion: Ve-MRI is a technique that can be used to accurately quantify atrial function. There is a wide range of variability of atrial function among patients, with some patients having no evidence of atrial mechanical contraction despite normal atrial electrical activity.

562. Time Efficient CMR Flow Acquisition for Accurate Assessment of Left Ventricular Diastolic Function in Patients with Ischemic Heart Disease

Theodorus A. M. Kaandorp,[1] Joost Doornbos, PhD,[1] Jeroen J. Bax, MD,[2] Alexandra Wils, Msc,[1] Ernst E. van der Wall, MD,[2] Albert de Roos, MD,[1] Hildo J. Lamb, MD.[1] [1]*Radiology, Leiden University Medical Center, Leiden, The Netherlands,* [2]*Cardiology, Leiden University Medical Center, Leiden, The Netherlands.*

Introduction: Diastolic dysfunction is the earliest sign of myocardial ischemia. The pattern of flow across the mitral valve is commonly used to evaluate diastolic function. Important parameters for diastolic function obtained from the flow data are E/A peak and E/A volume ratios. Gradient-echo phase-contrast MRI (GRE-PC) has been widely used to measure blood flow. However, clinical application of this technique is hampered by the long data acquisition time. In contrast, echo-planar imaging (EPI) is a fast MRI technique and offers major advantages over conventional GRE-PC MRI.

Purpose: The purpose of this study is to validate the accuracy of flow measurements across the mitral valve obtained from multishot echo-planar imaging (EPI) compared to GRE-PC in patients with myocardial ischemia.

Methods: In contrast to GRE-PC, where acquisition of each line in *k*-space requires a new spin excitation, echo-planar imaging is an imaging technique, where several lines in *k*-space can be acquired after a single spin excitation.

Two multishot-EPI techniques were evaluated, one with a multishot factor of three (EPI 3), and one with a multishot factor of five (EPI 5), in 25 and 22 patients with myocardial ischemia, EPI 3 and EPI 5 respectively. Both techniques are compared with the gradient-echo phase-contrast imaging technique (GRE-PC) by evaluating flow across the mitral valve, E/A peak ratio and E/A volume ratio.

Results: Mean GRE-PC data acquisition time was 165 ± 29, EPI 3 acquisition time was 57 ± 10 and for EPI 5, acquisition time was 35 ± 6. There were no statistically significant differences between the three techniques according to the ANOVA-test, for both flow measurements ($p = 0.082$), and E/A peak ratio ($p = 0.859$), and E/A volume ratio ($p = 0.891$). E/A peak and E/A volume ratios with EPI correlated better with the values of GRE-PC than the flow volumes as is also evidenced by Bland-Altman plots and linear regression analysis. Flow volumes were consistently lower with EPI than with GRE-PC. But this error is less than 10%, which is acceptable for routine clinical use.

Conclusion: EPI has proven to be a robust method for a faster acquisition of flow measurements across the mitral valve and of important parameters of diastolic function in patients with myocardial ischemia.

563. Image Fusion of Cardiac MRI and Gated SPECT in the Assessment of Myocardial Function, Perfusion and Viability

Jolanta H. Misko,[1] Miroslaw Dziuk,[2] Ewa Skrobowska,[3] Norbert Szalus,[4] Agnieszka Warczynska,[3] Jacek Pietrzykowski.[4] [1]*Department of Nuclear Medicine, Central Rail Hospital, Warsaw, Poland,* [2]*Department of Internal Medicine and Cardiology, Medical Military Institute, Warsaw, Poland,* [3]*Department of Radiology, Medical Military Institute, Warsaw, Poland,* [4]*Department of Nuclear Medicine, Medical Military Institute, Warsaw, Poland.*

Introduction: The registration and fusion of electrocardiogram-gated myocardial perfusion single-photon emission computed tomography (SPECT) with structural information obtained by cardiac cine and delayed enhancement magnetic resonance (cine MRI and DE MRI) could allow the precise anatomical correlation of perfusion, function and viability images in patients with coronary artery disease.

Purpose: The aim of the study was to evaluate the 3-D image fusion cine MRI with rest gated SPECT (GSPECT) with technetium-99m sestamibi (MIBI) in the assessment of myocardial viability defined by MRI delayed enhancement study (DE MRI), myocardial function and perfusion.

Methods: We analysed 685 segments of the heart obtained as a result of MR and GSPECT studies performed in 18 patients (pts) (12 males, 6 females) with stable coronary artery disease. All pts were subjected to cine MRI + DE MRI study and rest GSPECT study. Cine MRI, DE MRI and normalized GSPECT images were fused using PMOD and HERMES Nuclear Diagnostics systems. Fused images were analysed using a 36–42 segment model (6–7 short axis slices; 6 segments per slice). Myocardial wall function was evaluated using fused images of diastolic and systolic phases of cine MRI. MIBI uptake per volume (MIV) (counts/mm3) in each myocardial segment was evaluated by fusion of diastolic phases of cine MRI and GSPECT images. Transmural extent of infarction was determined by fusion of DE MRI and diastolic phase of cine MRI. The segments were divided into normal (without dysfunction, without delayed enhancement) (n = 411), without dysfunction and with delayed enhancement below 50% transmural extension (n = 26), with dysfunction and without delayed enhancement

(n = 185), dysfunctional with delayed enhancement below 50% transmural extension (n = 45) and dysfunctional-nonviable (n = 18) (with DEMRI > 50% of wall thickness).

Results: Dysfunctional segments had significantly less MIV (MIV = 4,63 SD 1,58) than normal segments (MIV = 8,86 SD 2,77) ($p < 0.05$ for comparison in each wall). The Receiver-Operating-Characteristic curve showed that the MIV value between 5 and 6 (counts/mm3) discriminates between normal and dysfunctional segments with a 95% accuracy. There was no significance difference in MIV between viable and non-viable dysfunctional segments defined by DE MR.

Conclusion: 3-D image fusion of cardiac MRI and gated SPECT allows to determine the MIBI density in myocardial volume (MIV). MIV may help to diagnose the segmental dysfunction but myocardial viability could be diagnosed only by DE MRI. Fusion of cine MRI, DE MRI and GSPECT is useful for determination of myocardial function, perfusion and viability in patients with coronary artery disease.

564. Automated Left Ventricular Cardiac MRI Segmentation, Quantification and Visualisation Using a Radial-Ray Approach

Craig Prest, MSc,[1] Roger Phillips, PhD,[1] John G. F. Cleland, MD, FRCP, FACC,[2] Nikolay P. Nikitin, MD, PhD,[2] Chris M. Langton, PhD.[3] [1]*Department of Computer Science, University of Hull, Kingston Upon Hull, UK,* [2]*Academic Unit of Cardiology, University of Hull, Kingston Upon Hull, UK,* [3]*Department of Medical Physics, University of Hull, Kingston Upon Hull, UK.*

The search for a fast, accurate means of quantification of left ventricular volumes, myocardial mass and other cardiac indices has been the subject of much recent research. Most attempts at automating this process involve the registration and morphing of a ventricular model to the image data. This approach works well on well-defined data sets, but often falls short on problematic data sets and usually gives no consideration to the structures internal to the ventricle. Localised models provide the flexibility to segment and reconstruct structures within the ventricle, whilst also providing a locally accurate representation of the ventricular border (Fig. 1).

We propose a new segmentation technique allowing fully automated segmentation of the endocardium, epicardium and papillary muscles from short-axis cardiac MRI data sets. The technique is based on a method of image gradient analysis using higher order derivatives and local parameterisation to obtain reliable segmentation results. User interaction is minimised to the definition of centre points for the ventricle base, apex and papillary muscles. From the approximate centre of the ventricle, rays are cast and evaluated to find the extent of the ventricle wall. The segmentation algorithm parameterises three dynamic intersection tests to detect endocardium and epicardium intersections for each emitted ray, providing a high-resolution mesh describing both surfaces. Automated segmentation and reconstruction of the papillary muscles allows their exclusion from left ventricular volume calculations and their inclusion in myocardial mass calculations. A software package was created as a test-bed for the algorithm, which provides DICOM compatibility and user interaction for segmentation corrections. Full 3-dimensional visualisation of the segmentation results is also catered for, as both still and animated meshes, in mono or stereo vision. The algorithm has proved capable of detecting endocardium intersections with great accuracy on even very difficult data sets, along with providing separate reconstruction of the papillary muscles.

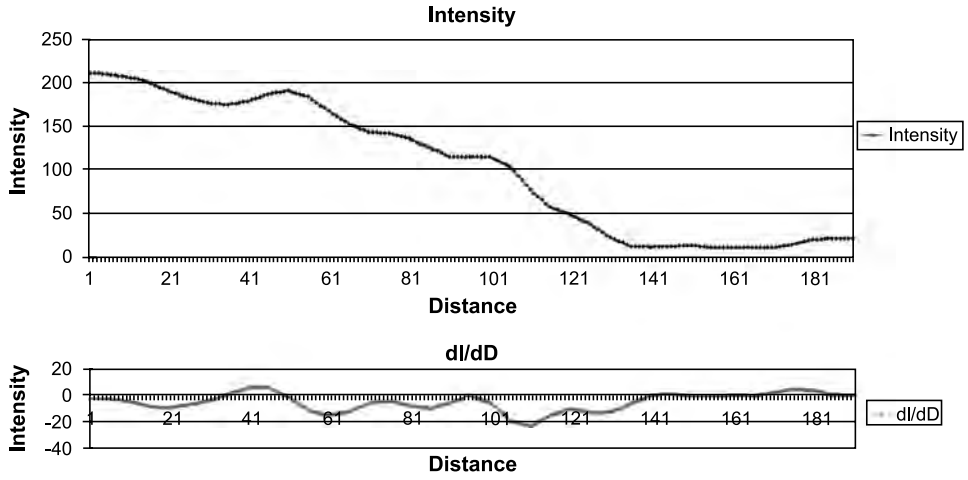

Figure 1. Intensity and 1st derivative graph for a single ray. Endocardium intersection identified as vertical line.